DISSERTATION

AIR QUALITY IMPLICATIONS FROM OXIDATION OF ANTHROPOGENIC AND BIOGENIC PRECURSORS IN THE TROPOSPHERE

Submitted by

Michael F. Link

Department of Chemistry

In partial fulfillment of the requirements

For the Degree of Doctor of Philosophy

Colorado State University

Fort Collins, Colorado

Fall 2019

Doctoral Committee:

Advisor: Delphine Farmer

Ellen R. Fisher
James R. Neilson
Shantanu H. Jathar
Akkihebbal R. Ravishankara

ABSTRACT

AIR QUALITY IMPLICATIONS FROM OXIDATION OF ANTHROPOGENIC AND BIOGENIC PRECURSORS IN THE TROPOSPHERE

Oxidation chemistry in the troposphere drives the formation of air pollutants, harmful to human health and the natural world. Emissions from both anthropogenic and biogenic sources control the ways in which air pollution is formed and thus understanding the chemistry of the oxidation of these emissions enhances our ability to predict how air quality evolves in the future. Experiments simulating tropospheric oxidation chemistry on anthropogenic point sources show that identifying unique chemical processes resulting in air pollution allow for a greater specificity in how to pursue strategies for pollution mitigation policy with regional and hemispheric implications. This thesis focuses on the implementation of advancements in instrumentation and experimental techniques to understand how tropospheric oxidation of anthropogenic and biogenic precursors can produce air pollution.

First, we subject vehicle exhaust to simulated tropospheric oxidation and quantify the formation of particulate matter and a toxic gas, isocyanic acid. We estimate how important oxidation of vehicle emissions are for these atmospheric pollutants for the South Coast Air Basin of California and the Seoul Metropolitan Region. Second, we investigate the propensity for isoprene to produce formic and acetic acid in laboratory oxidation experiments. We find that isoprene is likely a major source of formic acid in biogenically-influenced environments, however the exact mechanisms for formation remain unclear. Lastly, we use chemical ionization mass spectrometer measurements to quantify the fraction of oxidized carbon allocated to gas-

phase organic acids from isoprene oxidation in laboratory experiments. Through comparison with field measurements from a forest in Alabama to a forest in Colorado we determine high levels of isoprene in Alabama are responsible for high levels of organic acids compared to Colorado. We also observe that influences of anthropogenic NO_x suppress the formation of gas-phase organic acids suggesting as NO_x levels decrease throughout the US in the future organic acids produced from oxidation from isoprene are likely to increase.

ACKNOWLEDGEMENTS

The support of my friends and family has been critical to my success in graduate school. Thanks to the help of Mike Vannoy more than ten years ago I had the privilege of being able to participate in this educational experience. Without his intervention my life would look dramatically different than it does today. Others along the way including Steve Shertz from NCAR, folks from NOAA, and colleagues from the CSU atmospheric science department and CU Boulder have been instrumental in helping me develop a well-rounded analytical skill set. Friends, colleagues, and mentors I had through the NSR EAPSI program in Korea had an enormous impact on how I understand myself in the world and as a scientist. The Farmer group, through the years, has been a source of inspiration and many good times were had. Last, I could not imagine an advisor more constructive to my professional development than Delphine. Working under her counsel has been a gift.

DEDICATION

This work is dedicated to my dad.

TABLE OF CONTENTS

CHAPTER 1

INTRODUCTION TO TROPOSPHERIC OXIDATION AND REGULATION OF AIR QUALITY

1.1 Formation of Air Pollutants and Implications for Regulation of Air Quality

One of the most vital resources on Earth is air. The quality of air is defined by how much gases or particles, harmful to biological life or the natural world, are present in it. The lowest layer of the atmosphere is the troposphere extending approximately 12 km from the Earth's surface. In the troposphere gases and particles emitted from natural and human-derived sources undergo chemical reactions that ultimately influence air quality. Since the start of the industrial age humans have had a pronounced influence on air quality at times severely impacting human health and contributing to the deterioration of ecosystems.[1] In this modern age we study chemical reactions that occur in the troposphere to learn from mistakes of the past and inform future generations how to ensure an atmosphere optimal for sustaining biological life.

From a regulatory standpoint, air quality is characterized by the presence of criteria air pollutants. In the United States criteria air pollutants, as defined by the Environmental Protection Agency, include ozone (O_3), particulate matter ($PM_{2.5/10}$), sulfur oxides (SO_x), nitrogen oxides ($NO_x = NO + NO_2$), lead, and carbon monoxide (CO).[2] Most of these pollutants are emitted directly from human-derived, or anthropogenic, sources such as automobiles, manufacturing facilities, or through energy production. Regulation of SO_2 and NO_x from power plants has proven to be effective at decreasing harmful acid rain in the northeastern US and Canada.[3,4] Ozone and particulate matter, on the other hand, represent unique regulatory challenges because they are produced from oxidation chemistry in the troposphere and may not decrease in response to changes in emissions of criteria pollutants.

Oxidation of volatile organic compounds (VOCs) in the troposphere controls production of ozone and particulate matter. VOC oxidation mostly occurs through reaction with hydroxyl radical (OH) and when the products of VOC oxidation react with NO_x this can produce ozone or compounds that produce a subset of particulate matter, organic aerosol.[5,6] This complicates the issue of controlling air pollution because (1) VOC sources are diverse, (2) different VOCs produce air pollutants more efficiently than others, and (3) the production of air pollution from VOCs can be non-linear (i.e. decreases in emissions may not result in decreases in pollutant formation).[7]

Addressing the sources of air pollution effectively requires a detailed knowledge of VOC oxidation chemistry. VOCs emitted from forests are very reactive towards OH and can be very efficient sources of O_3 in the presence of low levels of NO_x.[8,9] Conversely, VOCs emitted from oil and natural gas operations are far less reactive towards OH than biogenic VOCs, but if emitted in high enough amounts, and accompanied by the appropriate levels of NO_x, can be important sources of O_3.[10–12] The complexity of pollutant source attribution is echoed when considering organic aerosol.[13,14] When VOCs react with OH they form oxidized organic gases that can condense to form organic aerosol and different types of VOCs produce organic aerosol with different efficiencies. For instance, recent work has shown that oxidation of volatile consumer products emitted to the outdoors from indoor environments is a larger source of organic aerosol to Los Angeles than automobile emissions.[15] Similar to O_3, organic aerosol production is highly dependent upon VOC type and NO_x levels.[16] Understanding this oxidation chemistry is critical for targeting the most important NO_x and VOC emission sources with regional specificity.

The importance of understanding the effects of oxidation chemistry on pollutant formation does not exclusively have regional implications, but also extends to how intra and trans-continental air quality policy is formed.[17] One example of this is shown by David and Ravishankara[18] (2019) who demonstrated that VOC precursors transported from central parts of the Indian subcontinent were responsible for ~30% of the boundary layer O_3 produced in Eastern India. They concluded reductions of VOC emissions in central India could decrease O_3 production in Eastern India. In slight contrast to the findings of the previous study, a paradigm shift in understanding air pollution sources has occurred in South Korea recently as the result of an extensive air sampling campaign.[19] Persistent challenges with aerosol pollution and severe haze events in Seoul, South Korea have often been attributed to transport of pollution from the east coast of China.[20] Recent measurements have demonstrated that most of the organic aerosol pollution observed in Seoul is produced from oxidation of locally emitted VOCs.[21] The study did find, however, that transport from China was still a major source of pollution to rural South Korea necessitating coordinated action from both China and South Korea to address the peninsula's air quality problem.

1.2 Understanding Tropospheric Chemistry Through Field and Laboratory Studies

Major advances in instrumentation over the past 20 years have enabled in situ investigations of tropospheric chemical processes on rapid timescales.[22] These advancements, complimented by numerous collaborative efforts between independent research groups, have allowed for holistic analyses of atmospheric chemical processes as observed over the ocean, in plumes from wildfire smoke, and in arctic expeditions, to name a few.[23–25] The level of detail provided by these studies has allowed for very specific identification of VOCs as sources of pollution in ambient

environments. For example, one study coupled ensemble VOC measurements, acquired from a remote oil and natural gas basin in Utah, to a detailed chemical model to identify carbonyl VOC photolysis as the major source of oxidants resulting in high O_3 production in the wintertime.[26] Another study coupled aircraft measurements and chemical modeling to identify toluene as a major precursor for organic aerosol on the Korean peninsula during the summer of 2016.[21] Extensive measurements of tropospheric chemistry in field environments have extended our ability to interpret ambient processes resulting in pollution beyond what could have been realized in laboratory settings.

Though field studies provide a holistic picture of tropospheric chemistry, the challenge of interpreting the complex results is often complimented with laboratory-based environmental chamber studies.[27] Environmental chambers are generally configured to simulate tropospheric oxidation of VOCs or inorganic gases for the purpose of measuring oxidation products of interest or aerosol.[28] Targeted studies of VOC oxidation in chambers, such as has been done with isoprene, have helped to elucidate explicit mechanisms of oxidation for VOCs of principle importance to O_3 and aerosol formation.[29] Chambers also have been used to measure ensemble organic aerosol production from oxidation of VOC mixtures like vehicle exhaust or biomass burning.[30,31] More recently chambers have ventured from laboratory settings and have performed oxidation of ambient air in forests, from aircraft, and from urban environments.[21,32,33] These field-based chamber studies have identified gaps in knowledge concerning our current understanding of sources of organic aerosol formation.[32] Expanding experimental capabilities that simulate tropospheric oxidation and measure oxidation products is a promising method to increase specificity when forming ideas on how to regulate air quality.[34]

1.3 Thesis Overview

This thesis presents measurements of tropospheric oxidation products from targeted laboratory studies and in the ambient environment.

Chapter 2 describes the measurement of a toxic gas-phase compound, isocyanic acid, from the OH oxidation of exhaust from an off-road diesel engine. We find oxidation enhances the magnitude of isocyanic acid produced from this source by factors of 2-3 over the course of an equivalent day of atmospheric oxidation. We conclude photochemical processing of off-road diesel exhaust could be an important source of isocyanic acid to urban areas such as the California South Coast Air Basin.

In Chapter 3 we measure ammonium nitrate aerosol primary emission and secondary production, from simulated OH oxidation in an environmental chamber, of exhaust from a passenger vehicle fleet representative for the Seoul Metropolitan Region. We find that though the levels of NO_x emitted from diesel vehicles far exceeded that of other vehicle types, the amount of ammonium nitrate formed, in response to OH oxidation, was higher in liquid petroleum gas and gasoline vehicles. These findings are consistent with high levels of ammonia emitted from LPG and gasoline vehicles coincident with low levels of NO_x that form ammonium nitrate aerosol. We find that vehicles may contribute significantly to localized secondary inorganic aerosol production in the Seoul Metropolitan Region.

In Chapter 4 we measure yields of formic and acetic acid from the oxidation of isoprene under a variety of experimental conditions. We use experimental evidence combined with detailed chemical modeling to identify missing sources of formic and acetic acid production in current isoprene oxidation mechanisms. Simple calculations, based on our results, suggest

isoprene oxidation is likely responsible for major discrepancies between model predictions and observational constraints of global formic acid production.

Chapter 5 presents measurements of total gas-phase organic acid yields from biogenic precursors and compares them to measurements from two forested field sites dominated by different biogenic VOC emissions. From the laboratory studies isoprene is identified as a major source of gas-phase organic acids whereas α-pinene oxidation produces much less. NO is observed to decrease the yield of organic acids from isoprene oxidation and we attribute this effect to isoprene-derived RO_2 + NO reactions as an inefficient source of gas-phase organic acids. Isoprene photochemistry is the dominant source of gas-phase organic acids at the forested site dominated by isoprene emissions. Patterns of organic acid abundance at the field site dominated by emissions of monoterpenes are distinctly different from the other forested site, but the sources of organic acids are not clear. Isoprene oxidation is likely a major source of organic acids in areas influenced by isoprene emissions globally.

REFERENCES

(1) Monks, P. S.; Granier, C.; Fuzzi, S.; Stohl, A.; Williams, M. L.; Akimoto, H.; Amann, M.; Baklanov, A.; Baltensperger, U.; Bey, I.; et al. Atmospheric Composition Change – Global and Regional Air Quality. *Atmos. Environ.* **2009**, *43* (33), 5268–5350. https://doi.org/10.1016/j.atmosenv.2009.08.021.

(2) Schmalensee, R.; Stavins, R. N. *Policy Evolution under the Clean Air Act*; National Bureau of Economic Research, 2018.

(3) Lehmann, C. M.; Bowersox, V. C.; Larson, R. S.; Larson, S. M. Monitoring Long-Term Trends in Sulfate and Ammonium in US Precipitation: Results from the National Atmospheric Deposition Program/National Trends Network. In *Acid Rain-Deposition to Recovery*; Springer, 2007; pp 59–66.

(4) Sullivan, T. J.; Driscoll, C. T.; Beier, C. M.; Burtraw, D.; Fernandez, I. J.; Galloway, J. N.; Gay, D. A.; Goodale, C. L.; Likens, G. E.; Lovett, G. M.; et al. Air Pollution Success Stories in the United States: The Value of Long-Term Observations. *Environ. Sci. Policy* **2018**, *84*, 69–73. https://doi.org/10.1016/j.envsci.2018.02.016.

(5) Monks, P. S.; Archibald, A. T.; Colette, A.; Cooper, O.; Coyle, M.; Derwent, R.; Fowler, D.; Granier, C.; Law, K. S.; Mills, G. E.; et al. Tropospheric Ozone and Its Precursors from the Urban to the Global Scale from Air Quality to Short-Lived Climate Forcer. *Atmospheric Chem. Phys.* **2015**, *15* (15), 8889–8973. https://doi.org/10.5194/acp-15-8889-2015.

(6) Volkamer, R.; Jimenez, J. L.; Martini, F. S.; Dzepina, K.; Zhang, Q.; Salcedo, D.; Molina, L. T.; Worsnop, D. R.; Molina, M. J. Secondary Organic Aerosol Formation from Anthropogenic Air Pollution: Rapid and Higher than Expected. *Geophys. Res. Lett.* **2006**, *33* (17). https://doi.org/10.1029/2006GL026899.

(7) von Schneidemesser, E.; Monks, P. S.; Allan, J. D.; Bruhwiler, L.; Forster, P.; Fowler, D.; Lauer, A.; Morgan, W. T.; Paasonen, P.; Righi, M.; et al. Chemistry and the Linkages between Air Quality and Climate Change. *Chem. Rev.* **2015**, *115* (10), 3856–3897. https://doi.org/10.1021/acs.chemrev.5b00089.

(8) Travis, K. R.; Jacob, D. J.; Fisher, J. A.; Kim, P. S.; Marais, E. A.; Zhu, L.; Yu, K.; Miller, C. C.; Yantosca, R. M.; Sulprizio, M. P.; et al. Why Do Models Overestimate Surface Ozone in the Southeast United States? *Atmospheric Chem. Phys.* **2016**, *16* (21), 13561–13577. https://doi.org/https://doi.org/10.5194/acp-16-13561-2016.

(9) Sanderson, M. G.; Jones, C. D.; Collins, W. J.; Johnson, C. E.; Derwent, R. G. Effect of Climate Change on Isoprene Emissions and Surface Ozone Levels. *Geophys. Res. Lett.* **2003**, *30* (18). https://doi.org/10.1029/2003GL017642.

(10) McDuffie, E. E.; Edwards, P. M.; Gilman, J. B.; Lerner, B. M.; Dubé, W. P.; Trainer, M.; Wolfe, D. E.; Angevine, W. M.; deGouw, J.; Williams, E. J.; et al. Influence of Oil and Gas Emissions on Summertime Ozone in the Colorado Northern Front Range. *J. Geophys. Res. Atmospheres* **2016**, *121* (14), 8712–8729. https://doi.org/10.1002/2016JD025265.

(11) Gilman, J. B.; Lerner, B. M.; Kuster, W. C.; de Gouw, J. A. Source Signature of Volatile Organic Compounds from Oil and Natural Gas Operations in Northeastern Colorado. *Environ. Sci. Technol.* **2013**, *47* (3), 1297–1305. https://doi.org/10.1021/es304119a.

(12) Abeleira, A.; Pollack, I. B.; Sive, B.; Zhou, Y.; Fischer, E. V.; Farmer, D. K. Source Characterization of Volatile Organic Compounds in the Colorado Northern Front Range Metropolitan Area during Spring and Summer 2015. *J. Geophys. Res. Atmospheres* **2017**, 2016JD026227. https://doi.org/10.1002/2016JD026227.

(13) Carlton, A. G.; Pinder, R. W.; Bhave, P. V.; Pouliot, G. A. To What Extent Can Biogenic SOA Be Controlled? *Environ. Sci. Technol.* **2010**, *44* (9), 3376–3380. https://doi.org/10.1021/es903506b.

(14) Carlton, A. M. G.; Pye, H. O. T.; Baker, K. R.; Hennigan, C. J. Additional Benefits of Federal Air Quality Rules: Model Estimates of Controllable Biogenic Secondary Organic Aerosol. *Environ. Sci. Technol.* **2018**. https://doi.org/10.1021/acs.est.8b01869.

(15) McDonald, B. C.; Gouw, J. A. de; Gilman, J. B.; Jathar, S. H.; Akherati, A.; Cappa, C. D.; Jimenez, J. L.; Lee-Taylor, J.; Hayes, P. L.; McKeen, S. A.; et al. Volatile Chemical Products Emerging as Largest Petrochemical Source of Urban Organic Emissions. *Science* **2018**, *359* (6377), 760–764. https://doi.org/10.1126/science.aaq0524.

(16) Xu, L.; Guo, H.; Boyd, C. M.; Klein, M.; Bougiatioti, A.; Cerully, K. M.; Hite, J. R.; Isaacman-VanWertz, G.; Kreisberg, N. M.; Knote, C.; et al. Effects of Anthropogenic Emissions on Aerosol Formation from Isoprene and Monoterpenes in the Southeastern United States. *Proc. Natl. Acad. Sci.* **2015**, *112* (1), 37–42. https://doi.org/10.1073/pnas.1417609112.

(17) Dentener, F.; Keating, T.; Akimoto, H. Hemispheric Transport of Air Pollution 2010: Part A: Ozone and Particulate Matter, Air Pollut. *Stud* **2011**, *17*, 305.

(18) David, L. M.; Ravishankara, A. R. Boundary Layer Ozone Across the Indian Subcontinent: Who Influences Whom? *Geophys. Res. Lett. 0* (0). https://doi.org/10.1029/2019GL082416.

(19) Huang, M.; Crawford, J. H.; Diskin, G. S.; Santanello, J. A.; Kumar, S. V.; Pusede, S. E.; Parrington, M.; Carmichael, G. R. Modeling Regional Pollution Transport Events During KORUS-AQ: Progress and Challenges in Improving Representation of Land-Atmosphere Feedbacks. *J. Geophys. Res. Atmospheres* **2018**, *123* (18), 10,732-10,756. https://doi.org/10.1029/2018JD028554.

(20) Kim, H. C.; Kim, E.; Bae, C.; Cho, J. H.; Kim, B.-U.; Kim, S. Regional Contributions to Particulate Matter Concentration in the Seoul Metropolitan Area, South Korea: Seasonal Variation and Sensitivity to Meteorology and Emissions Inventory. *Atmos Chem Phys* **2017**, *17* (17), 10315–10332. https://doi.org/10.5194/acp-17-10315-2017.

(21) Nault, B. A.; Campuzano-Jost, P.; Day, D. A.; Schroder, J. C.; Anderson, B.; Beyersdorf, A. J.; Blake, D. R.; Brune, W. H.; Choi, Y.; Corr, C. A.; et al. Secondary Organic Aerosol Production from Local Emissions Dominates the Organic Aerosol Budget over Seoul, South Korea, during KORUS-AQ. *Atmospheric Chem. Phys.* **2018**, *18* (24), 17769–17800. https://doi.org/https://doi.org/10.5194/acp-18-17769-2018.

(22) Farmer, D. K.; Jimenez, J. L. Real-Time Atmospheric Chemistry Field Instrumentation. *Anal. Chem.* **2010**, *82* (19), 7879–7884. https://doi.org/10.1021/ac1010603.

(23) Carlton, A. G.; de Gouw, J.; Jimenez, J. L.; Ambrose, J. L.; Attwood, A. R.; Brown, S.; Baker, K. R.; Brock, C.; Cohen, R. C.; Edgerton, S.; et al. Synthesis of the Southeast Atmosphere Studies: Investigating Fundamental Atmospheric Chemistry Questions. *Bull. Am. Meteorol. Soc.* **2018**, *99* (3), 547–567. https://doi.org/10.1175/BAMS-D-16-0048.1.

(24) Sullivan, A. P.; Guo, H.; Schroder, J. C.; Campuzano-Jost, P.; Jimenez, J. L.; Campos, T.; Shah, V.; Jaeglé, L.; Lee, B. H.; Lopez-Hilfiker, F. D.; et al. Biomass Burning Markers and Residential Burning in the WINTER Aircraft Campaign. *J. Geophys. Res. Atmospheres* **2019**, *124* (3), 1846–1861. https://doi.org/10.1029/2017JD028153.

(25) Mungall, E. L.; Abbatt, J. P. D.; Wentzell, J. J. B.; Lee, A. K. Y.; Thomas, J. L.; Blais, M.; Gosselin, M.; Miller, L. A.; Papakyriakou, T.; Willis, M. D.; et al. Microlayer Source of Oxygenated Volatile Organic Compounds in the Summertime Marine Arctic Boundary Layer. *Proc. Natl. Acad. Sci.* **2017**, *114* (24), 6203–6208. https://doi.org/10.1073/pnas.1620571114.

(26) Edwards, P. M.; Brown, S. S.; Roberts, J. M.; Ahmadov, R.; Banta, R. M.; deGouw, J. A.; Dubé, W. P.; Field, R. A.; Flynn, J. H.; Gilman, J. B.; et al. High Winter Ozone Pollution from Carbonyl Photolysis in an Oil and Gas Basin. *Nature* **2014**, *514* (7522), 351–354. https://doi.org/10.1038/nature13767.

(27) Burkholder, J. B.; Abbatt, J. P. D.; Barnes, I.; Roberts, J. M.; Melamed, M. L.; Ammann, M.; Bertram, A. K.; Cappa, C. D.; Carlton, A. G.; Carpenter, L. J.; et al. The Essential Role for

Laboratory Studies in Atmospheric Chemistry. *Environ. Sci. Technol.* **2017**, *51* (5), 2519–2528. https://doi.org/10.1021/acs.est.6b04947.

(28) Peng, Z.; Lee-Taylor, J.; Orlando, J. J.; Tyndall, G. S.; Jimenez, J. L. Organic Peroxy Radical Chemistry in Oxidation Flow Reactors and Environmental Chambers and Their Atmospheric Relevance. *Atmospheric Chem. Phys.* **2019**, *19* (2), 813–834. https://doi.org/https://doi.org/10.5194/acp-19-813-2019.

(29) Wennberg, P. O.; Bates, K. H.; Crounse, J. D.; Dodson, L. G.; McVay, R. C.; Mertens, L. A.; Nguyen, T. B.; Praske, E.; Schwantes, R. H.; Smarte, M. D.; et al. Gas-Phase Reactions of Isoprene and Its Major Oxidation Products. *Chem. Rev.* **2018**. https://doi.org/10.1021/acs.chemrev.7b00439.

(30) Koss, A. R.; Sekimoto, K.; Gilman, J. B.; Selimovic, V.; Coggon, M. M.; Zarzana, K. J.; Yuan, B.; Lerner, B. M.; Brown, S. S.; Jimenez, J. L.; et al. Non-Methane Organic Gas Emissions from Biomass Burning: Identification, Quantification, and Emission Factors from PTR-ToF during the FIREX 2016 Laboratory Experiment. *Atmos Chem Phys* **2018**, *18* (5), 3299–3319. https://doi.org/10.5194/acp-18-3299-2018.

(31) Robinson, A. L.; Donahue, N. M.; Shrivastava, M. K.; Weitkamp, E. A.; Sage, A. M.; Grieshop, A. P.; Lane, T. E.; Pierce, J. R.; Pandis, S. N. Rethinking Organic Aerosols: Semivolatile Emissions and Photochemical Aging. *Science* **2007**, *315* (5816), 1259–1262. https://doi.org/10.1126/science.1133061.

(32) Palm, B. B.; Campuzano-Jost, P.; Ortega, A. M.; Day, D. A.; Kaser, L.; Jud, W.; Karl, T.; Hansel, A.; Hunter, J. F.; Cross, E. S.; et al. In Situ Secondary Organic Aerosol Formation from Ambient Pine Forest Air Using an Oxidation Flow Reactor. *Atmos Chem Phys* **2016**, *16* (5), 2943–2970. https://doi.org/10.5194/acp-16-2943-2016.

(33) Ortega, A. M.; Hayes, P. L.; Peng, Z.; Palm, B. B.; Hu, W.; Day, D. A.; Li, R.; Cubison, M. J.; Brune, W. H.; Graus, M.; et al. Real-Time Measurements of Secondary Organic Aerosol Formation and Aging from Ambient Air in an Oxidation Flow Reactor in the Los Angeles Area. *Atmos Chem Phys* **2016**, *16* (11), 7411–7433. https://doi.org/10.5194/acp-16-7411-2016.

(34) Glasius, M.; Goldstein, A. H. Recent Discoveries and Future Challenges in Atmospheric Organic Chemistry. *Environ. Sci. Technol.* **2016**, *50* (6), 2754–2764. https://doi.org/10.1021/acs.est.5b05105.

CHAPTER 2

PHOTOCHEMICAL PROCESSING OF DIESEL FUEL EMISSIONS FORMS A LARGE SECONDARY SOURCE OF ISOCYANIC ACID (HNCO)[1]

2.1 Introduction

Atmospherically relevant levels of isocyanic acid (HNCO) are expected to be toxic at biological pH.[1] Toxic effects of HNCO are associated with cataracts, atherosclerosis, cardiovascular disease, renal failure and rheumatoid arthritis.[2] Roberts et al (2011) estimated exposure to only 1 ppb_v HNCO could produce aqueous isocyanate in the body, which can trigger harmful protein modifying processes.[3–5] Previous studies have recognized the occupational hazard of exposure to isocyanates, including HNCO, and have measured mixing ratios of HNCO near 1 ppb_v in different workplace environments underscoring the need to characterize its sources.[6–8] Observations of HNCO have been performed from direct sources such as light duty gasoline vehicle emissions, light duty diesel vehicle emissions, biomass burning and from secondary sources such as the photochemical oxidation of 2-aminoethanol and the aqueous dissociation of urea.[1,5,9–11] Studies in the ambient environment have correlated HNCO with photochemically produced species such as ozone, formic acid and nitric acid, which is consistent with a photochemical source of HNCO.[10,12–14] However, direct measurements of the photochemical production of HNCO have only been made in laboratory studies from isolated precursors such as 2-aminoethanol.[11] While modeled HNCO production from 2-aminoethanol

[1]Link, M.F., Friedman, B., Fulgham, R., Brophy, P., Galang, A., Jathar, S.H., Veres, P., Roberts, J.M., Farmer, D.K., 2016. Photochemical processing of diesel fuel emissions as a large secondary source of isocyanic acid (HNCO). Geophysical Research Letters, 43(8), pp.4033-4041.

oxidation only accounted for 14% of ambient measured HNCO in one study, ambient mixing ratios of formamide, can account for almost all observed HNCO in some rural environments.[12,15,16]

Emissions from non-road diesel engines have received less attention than emissions from on-road vehicles. Non-road diesel vehicles contributed 18% and 15% to PM10 and nitrogen oxide (NOx) emissions, respectively, in the United States in 2011. Previous studies have demonstrated that diesel exhaust is also a primary source of HNCO.[10,17] The most recent EPA Tier 4 standards of emissions reduction regulations have focused on the reduction of NOx by requiring all non-road diesel vehicles produced after 2015 to be equipped with selective catalytic reduction systems (SCR) in addition to particle reducing filters and hydrocarbon oxidation catalysts required by previous emission control mandates. The addition of SCR systems to diesel vehicles are known to produce HNCO as an intermediate in the NOx reduction process which has resulted in higher emission factors of HNCO observed than without the addition of the SCR system.[17] Wentzell et al (2013) measured HNCO emissions from light duty diesel engine exhaust, and concluded that diesel engine emissions in the greater Toronto area are smaller HNCO sources than biomass burning throughout Canada. They speculated, however, that HNCO emissions from heavy duty diesel vehicles and non-road use of diesel may be much larger as these sources are dominant contributors to total mobile source pollution.

Here, we investigate secondary production of HNCO by simulating photochemical oxidation (or aging) of diesel and biodiesel exhaust from a non-road diesel engine, and the extent to which this chemistry enhances the HNCO source from diesel exhaust. Despite regulatory controls in the US, urban air pollution remains a public health concern, particularly for highly sensitive groups.[18] Primary diesel particle emissions, and their resulting secondary chemistry,

have long been recognized as source of urban air pollution, but here we investigate the role of photochemically enhanced HNCO diesel engine emissions.[19]

2.2 Materials and Methods

2.2.1 Experimental Setup

The Diesel Exhaust Fuel and Control (DEFCON) experiment took place at the Colorado State University Engines and Energy Conversion Lab during June 3-11, 2015. A 4-cylinder, turbocharged, intercooled, heavy-duty diesel engine (John Deere 4045H), representative of those found in skid-steer loaders, tractors, etc., was run on an engine dynamometer under idle and 50% load operating conditions using both diesel (sulfur content 6-10 ppm) and biodiesel fuels to produce exhaust. No emissions control systems – including diesel oxidation catalyst, diesel particulate filter, nor SCR unit – were included in the experiments described herein. Raw exhaust was transferred through 4 m of heated Silcosteel© stainless steel line to a primary dilution system.[20] The exhaust was mixed with HEPA- and activated charcoal- filtered room air (Figure A1.1) to achieve dilution ratios of 45-110 (air:exhaust). The diluted exhaust was transferred to a 300 L stainless steel tank and had a residence time in the equilibration tank of 10 minutes before undergoing continuous sampling. Diluted engine exhaust is subsampled to the potential aerosol mass (PAM) reactor where oxidation occurs then this sample air is directed to both particle and gas-phase instruments on different sampling lines (Figure A1.1). Mixing ratios of CO_2, CO, total hydrocarbons (THC), NO, and NO_2 were measured by a 5-gas analyzer from the primary engine exhaust upstream of the dilution chamber (Table A1.1).[20]

The diluted sample exhaust was introduced into a potential aerosol mass (PAM) reactor to simulate atmospheric oxidation at a flowrate of 7 sLpm (residence time ~100 s).[21,22] The PAM reactor is a 13.1 L conductive aluminum chamber equipped with high pressure mercury lamps

(BHK Inc., Model # 82-9304-03) to simulate atmospheric HO_2 and OH oxidation chemistry. UV light is emitted at 185 and 254 nm in the reactor and initiates the production of hydroxyl radicals (OH) from the photolysis of O_2 and H_2O. The concentration of OH depends on the UV intensity emitted by the lamps and can simulate atmospheric aging of hours to weeks.[21]

The high reactivity (~5000 s^{-1}) of the diesel exhaust suppressed OH by a factor of two at the lowest UV light intensities and 14 at the highest intensities (see Supplemental Information for detailed calculations), comparable to the OH suppression observed during PAM experiments on biomass burning emissions.[23] The factor contributing most to variability in the estimated OH reactivity of the diesel exhaust in the PAM chamber was the dilution of the exhaust sample in the dilution chamber. The OH exposure in the PAM chamber is typically described in terms of equivalent days of OH exposure [Lambe et al., 2011; Li et al., 2015; Peng et al., 2015], which is calculated by dividing the OH exposure (molecules cm^{-3} s) by an average atmospheric OH concentration (1.5 x 106 molecules cm^{-3}, [Mao et al., 2008]).[22,24–26] The experiments described herein cover oxidative aging by OH of 0.2-1.5 (± 50%) equivalent days of OH exposure (OH_{exp}) (Figure A1.2).

2.2.2 Exhaust Experiments

We measured HNCO from engine emissions during six different experiments: two replicates of diesel fuel with engine at idle, two replicates of diesel fuel with engine at 50% load, one experiment with biodiesel fuel and engine at idle, and one experiment with biodiesel fuel and engine at 50% load. Each experiment consisted of six steps of increasing UV light voltage in the PAM chamber; each voltage step was held for 20 minutes. The 0V voltage step in the PAM represents the exhaust exposed to no UV light.

2.2.3 Acetate Chemical Ionization Mass Spectrometer (acetate-CIMS) Operation and Calibration

HNCO was detected by a high-resolution time-of-flight acetate-CIMS (Tofwerk AG and Aerodyne Research, Inc.). The ionization chemistry and instrument have been described extensively in previous literature.[9,10,27–29] Sample air for gas phase analytes was pulled through 3 m of PEEK tubing from the PAM chamber to the acetate-CIMS and diluted at the entrance to the instrument by 3.6 sLpm of ultra-high purity N_2 to maintain first order reactions of the analytes in the sample gas with the acetate reagent ion. The acetate-CIMS pulled sample air through a critical orifice (I.D. 0.067 cm) at a flowrate of 1.5 sLpm. Thus the emissions were diluted by a factor of 1200-3500 (air:exhaust) between the engine tailpipe and the instrument. Despite this large dilution, the reagent ion signal was titrated by large signals observed at m/z 45.99 (NO_2^-) and m/z 61.99 (NO_3^-) throughout the experiments, likely due to HONO and HNO_3, respectively. HNCO can be ionized through either a proton transfer or clustering reaction with acetate (Ac-),

$$Ac^- + HNCO \rightarrow HAc + CNO^- \qquad \text{(R1a)}$$

$$HAc(Ac^-) + HNCO \rightarrow HAc(CNO^-) + HAc \qquad \text{(R1b)}$$

The ion optics in the acetate-CIMS were tuned to minimize clustering in the observed spectra so that HNCO is detected as NCO^- at m/z 41.99.[29] No interfering species at same nominal mass as HNCO were observed through peak fitting procedures either during calibration or during the DEFCON experiments.

We calibrated the acetate-CIMS for HNCO with a stable source of HNCO that was produced by passing a stream of zero air at 50 sccm over the outlet of a diffusion cell containing heated cyanuric acid (250°C).[28] HNCO concentrations were determined with a custom-built analyzer that converts HNCO to NO on a heated platinum catalyst (750°C) followed by a molybdenum catalyst (450°C) and detects NO via chemiluminescence.[30] The acetate-CIMS had a sensitivity to HNCO of 47.5 normalized cps/ppt_v, and a detection limit (S/N = 3) for HNCO of 5 ppt_v at 1 second acquisition (Supplemental information for additional calibration details).

2.2.4 Calculation of Fuel Based Enhanced Emission Factors (EEF_t)

Fuel based emission factors have been recognized as a useful metric for comparing engines operating under different conditions but using similar fuels.[9] Emission factors (EF, mg-HNCO/kg-fuel) were first calculated by:

$$EF = \frac{[HNCO]}{\left(\frac{[CO_2]}{MW_{CO_2}}+\frac{[CO]}{MW_{CO}}\right)AW_c} C_i \qquad (1)$$

where concentrations are in mg cm^{-3} (HNCO) or g cm^{-3} (CO, CO_2); C_i is the carbon mass fraction of the fuel (850 and 770 gC/kg-fuel for diesel and biodiesel, respectively); and MW_{CO2}, MW_{CO}, and AW_C are the molecular weights of CO_2 and CO, and the atomic weight of carbon.[31] All concentration values used in the EF calculation were calculated from the dilution ratio in the dilution chamber to produce tailpipe exhaust emission concentrations. We define fuel based enhanced emission factors (EEF_t, mg-HNCO/kg-fuel) as the HNCO produced from a given amount of fuel via atmospheric aging of diesel exhaust. EEF_ts thus describe the extent of pollutant production from a given photochemical oxidation of engine exhaust originating from the combustion of a known amount of fuel. The EEF_t of a pollutant is a function of

photochemical exposure and will vary with time the pollutant spends in the atmosphere. EEF_ts were calculated to quantify the contribution of secondary production of HNCO from primary exhaust. EEF_ts were then calculated via equation (2):

$$EEF_t = EF_{voltage\ step} - EF_{0V\ step} \quad (2)$$

Where $EF_{voltage\ step}$ is the EF for HNCO at a given UV light voltage step and EF_{0V} step is the EF for HNCO at the UV light voltage step representative of diesel exhaust unperturbed by oxidation. The EEF_t is defined as a difference from the EF at the 0V step in order to separate the primary HNCO emission from the secondary HNCO formation.

2.3 Results and Discussion

2.3.1 Primary Emission of HNCO

EFs were within experimental error of one another for diesel and biodiesel under the same engine operating conditions (Table 2.1). EFs were, however, 3x larger for idle engine conditions (54 mg HNCO/kg diesel fuel) versus 50% load conditions (17 mg HNCO/kg fuel). EFs reported in the study herein are considerably higher than those reported in previous literature. EFs for HNCO reported by Heeb et al (2011) were similar between engine operating conditions at 4 mg HNCO/kg of diesel fuel for on-road light duty engines. Similarly, Brady et al (2014) measured EFs for HNCO on the order of 1-2 mg HNCO/kg of gasoline fuel for light duty gasoline vehicles. We note that Wentzell et al (2013) observed a difference in primary HNCO emission as a function of engine operating condition, but with higher EFs (4.0 mg HNCO/kg diesel fuel) during active engine operating conditions and lower EFs for idle conditions (0.7 mg HNCO/kg diesel fuel). Our data suggest that non-road diesel engines produce more primary HNCO than either the on-road light duty gasoline or diesel engines described in previous studies. Further, this type of engine produces much wider ranging primary HNCO emissions than

reported for other engine types. These comparisons suggest that similar engine operating conditions may produce different effects on the emissions between non-road diesel engines, such as the one used in this study, and on-road diesel engines like those used in previous studies.

Idle operating conditions generally result in less efficient combustion than more active engine operating conditions such as the 50% load conditions in this study as evidenced by the difference in THC concentration between operating conditions (Table A1.1). Our observations suggest that incomplete combustion can also be accompanied by increased primary HNCO emissions. This suggests that more precursors for HNCO could be available in the incompletely combusted exhaust under idle conditions than 50% load conditions.[32] Emissions of CO, NO_x, and THC measured from the engine in this study agree well with measurements reported from the same engine in another study suggesting the emissions from this engine are reproducible.[33] The CO mixing ratios measured in this study are nearly twice as high as those measured by Wentzell et al (2013) under similar (idle) engine operating conditions, consistent with our observations of higher primary HNCO. The lower bound of the variability of THC measured in this study under idle conditions captures the average THC mixing ratio measured by Wentzell et al (2013). In contrast, Wentzell et al (2013) reports NOx emissions that are larger by a factor of 6-7 than the NO_x measured in this study. Indeed, the HNCO/NO_x ratios measured in this study (Table A1.2) are much higher than the ratios reported in Wentzell et al (2013).

Previous studies have shown that steady-state engine cycles, such as those used in this study, can underestimate and misrepresent emissions of particles as well as pollutants such as HNCO.[34] For instance, Brady et al (2014) measured the highest emissions of HNCO during acceleration from gasoline exhaust. By measuring HNCO from steady-state engine conditions, we are providing a lower bound to what can be expected for real-world emissions of HNCO from

non-road diesel engines. Unlike on-road vehicles, non-road vehicles typically operate at steady-state, either idle or peak, engine loads. This suggests that the HNCO emissions presented herein are similar to what could be expected from real-world engine performance.

2.3.2 Secondary source of HNCO

We observe a strong secondary source of HNCO from diesel engine exhaust as a result of 0.4 to 1.5 days of photochemical aging for both biodiesel and diesel fuel and under both idle and high load operating conditions. Oxidation of diesel exhaust in the PAM chamber produced HNCO, enhancing observed concentrations by up to a factor of 4 (Figure 2.1, A1.5). All fuel types and engine operating conditions demonstrated similar behavior with photochemical enhancement of HNCO. Figure 1 shows an example of secondary HNCO production from diesel under idle and 50% load engine operating conditions. HNCO consistently increased with photochemical exposure.

Idle conditions produced consistently higher HNCO mixing ratios than 50% load operating conditions. EEFts of secondary HNCO from photochemical oxidation of diesel and biodiesel exhaust increase as a function of OH exposure under idle and 50% load conditions (Figure 2.2). EEFts of HNCO were higher under idle engine operating conditions than 50% load conditions for both fuels. Under idle conditions, HNCO emissions were enhanced by a factor of 4 after 1.5 OH equivalent days. This enhancement is the equivalent of 230 mg HNCO per kg of fuel, compared to primary emissions of 54 mg HNCO/kg of fuel (Figure S4.2). In contrast, the HNCO emissions were only enhanced by a factor of 1.5-3 after 1.5 OH equivalent days under 50% load conditions, or an increase of 26 mg HNCO/kg fuel. We hypothesize that HNCO EEFts are higher under idle conditions because there are more precursors for photochemical production available in incompletely combusted diesel exhaust (Figure S4.4).

2.3.3 Implications for Diesel Emission Reduction Technologies

Primary emissions of HNCO have been observed to be higher in the exhaust of diesel systems equipped with SCR (or de-NOx) systems. Heeb et al (2011) measured HNCO from diesel exhaust filtered through a de-NOx system and observed an increase in primary HNCO emissions by almost an order of magnitude under engine conditions similar to primary emissions observed in this study (from 3 to 79 mg HNCO/kg fuel). Krocher et al (2005) also reported tailpipe mixing ratios of HNCO much higher than those measured in this study (16-80 ppm_v) with the use of a de-NOx system. The decomposition of urea to HNCO and the subsequent hydrolysis of HNCO are temperature and catalyst dependent often resulting in emission of HNCO from the inefficient operation of the SCR system known as "HNCO slip".[35] Future studies should investigate the photochemical enhancement of HNCO from diesel exhaust treated with EPA Tier 4 emission abatement technologies such as diesel particle filters, oxidation catalysts, and SCRs.

Changing the composition of diesel fuel to biodiesel has been suggested to reduce emissions from older diesel vehicles that are not equipped with emissions control technologies.[36] While changing the composition of diesel fuel has been shown to be useful in reducing particle emissions, we demonstrate here that changing the composition of diesel fuel may not have a significant effect on reducing primary or secondary emissions of other pollutants such as HNCO.[37]

2.3.4 Atmospheric Relevance

We evaluate the relative contributions of primary vehicle emissions and secondary sources for the California South Coast Air Basin (SoCAB) as well as California statewide wildfire sources to total HNCO emissions in Table 2.2. Contributions of HNCO to this airshed

from different mobile sources include on-road light duty gasoline vehicles (using an average HNCO/CO ratio calculated from the work of Brady et al (2014)) and on-road light duty diesel vehicles, as well as contributions from non-road use of diesel (non-road diesel engines are assumed to be representative of the engine used in this study), using an average HNCO/CO measured in this study, were evaluated from emissions reports estimates published in 2013.[10,38] Inclusion of on-road light duty gasoline vehicles, non-road use of diesel and on-road light duty diesel accounts for 80% of total CO emissions from mobile sources reported by the California Air Resources Board (CARB) project emissions for 2015 totaling 1,505 tons/day. The largest sources of CO excluded from this calculation are from on-road medium duty trucks and recreational boats which accounts for ~17% of total reported CO emissions. Using HNCO/CO ratios for the respective vehicle types, HNCO is calculated to be emitted in the greatest abundance by the non-road use of diesel (Table 2.2).

Although light duty gasoline vehicles contribute >55% to the total CO emissions from mobile sources in this estimate, they contribute <2% of the HNCO directly emitted from mobile sources. Total mobile sources of HNCO emissions in SoCAB are less than statewide emissions from wildfires. If the HNCO emissions from mobile sources are assumed to be enhanced by a factor of 3, as measured in this study from 1.5 OH-equivalent days of atmospheric aging, then the secondary photochemical production of HNCO from mobile sources becomes several tons/day greater than primary contributions from wildfires. Previous modeling has suggested that the most important anthropogenic source of HNCO to the atmosphere is biomass burning, but here we provide evidence to suggest secondary production of HNCO, from anthropogenic sources, may be more important than primary sources in certain regions.[39] Further, we speculate that secondary production of HNCO from biomass burning precursors is likely to be a large

global source of HNCO due to the large amount of reduced nitrogen potentially released to the atmosphere during fire events.

The estimates of secondary production of HNCO presented in Table 2.2 may represent an upper bound for HNCO production from these sources because sinks for HNCO are not considered. The above estimate assumes that all the precursors leading to secondary HNCO production from these sources are oxidized to form HNCO as opposed to being lost through deposition or uptake to aerosol surfaces. Additionally, we assume that exhaust from all the emission sources included in this estimate experience photochemical enhancements of HNCO similar to the exhaust measured in this study. The above estimates, however, may represent a lower bound because our observations of photochemical production are limited to 1.5 days of equivalent OH exposure. Experiments that observe HNCO production within a greater range of OH_{exp} could provide insight into more realistic upper bounds of photochemical production. Other precursor compounds for photochemically produced HNCO, such as 2-aminoethanol and formamide, have been suggested to be important for contributing to ambient atmospheric HNCO and were not included in this estimate.[11,40] Possible precursors for secondary HNCO production include formamide and acetamide, which were observed during the diesel, but not biodiesel, experiments. A rough estimate of formamide and acetamide concentrations suggests that they could account for up to ~15% of the observed HNCO in the diesel experiments (A1.4.3 for further discussion of this analysis and uncertainties). Importantly, the nitrogen-containing organic species were observed to have clear secondary photochemical sources, suggesting that HNCO may be the result of multiple generations of oxidation; the precursors for formamide and acetamide in the diesel mixture are not known at this time. Other nitrogen-containing organic compounds must contribute to HNCO photochemical production in the biodiesel experiments,

and potentially to the diesel experiments as well. Further investigation into the emissions of such compounds and their chemistry is warranted. Studies focusing on the photochemical production of HNCO from biomass burning emissions as well as different vehicle sources would help clarify the precise contribution of secondary HNCO to the total atmospheric burden.

2.4 Conclusions

We present a direct observation of a photochemical source of HNCO from non-road diesel engine exhaust. This photochemical source is larger than the primary emission source, consistent with previous ambient HNCO observations.[12,14] Both primary emissions and secondary production of HNCO were observed to be higher under idle engine operating conditions compared to active conditions. No difference in primary emissions or secondary production of HNCO was observed through the use of diesel or biodiesel as a fuel source. While localized emissions of HNCO, either from biomass burning or mobile sources, greatly influence mixing ratios observed in ambient air, we suggest that photochemical production of HNCO could be a dominant contributor to regional HNCO budgets, and potentially to the global burden of HNCO.

An understanding of HNCO sources are essential for predicting human health effects, and for identifying controllable sources. This study demonstrates that compounds that are normally thought of as having primary sources from mobile combustion sources can be enhanced through secondary processing in the atmosphere. Inclusion of secondary pollutant sources in emissions regulation may lead to a more accurate portrayal of the potential impact of mobile sources or emissions control procedures on regional air quality.

2.5 Chapter 2 Figures

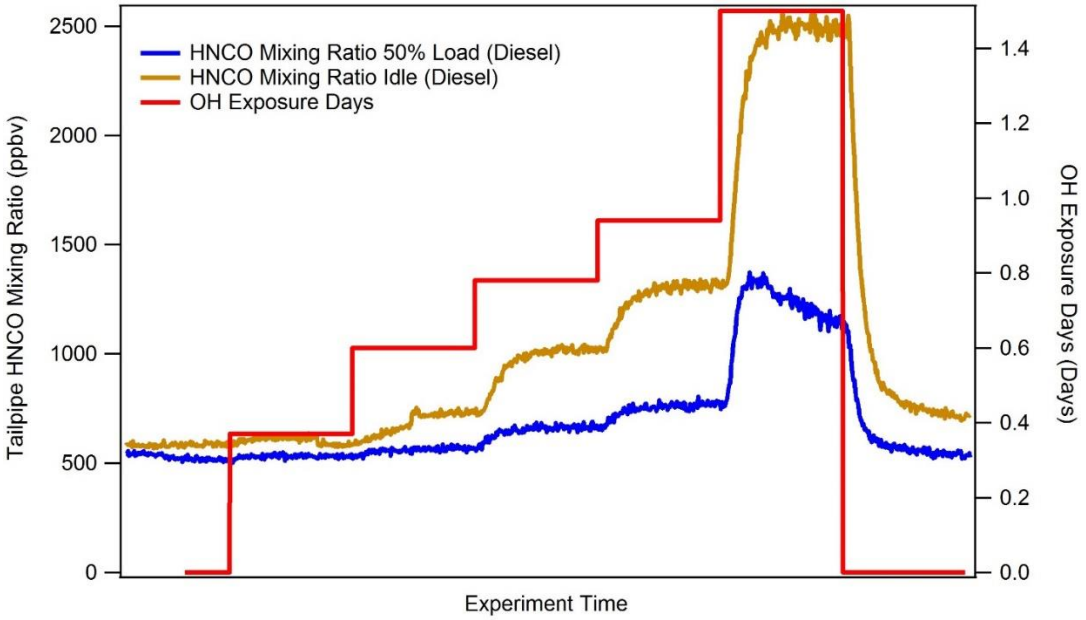

Figure 2.1. HNCO mixing ratio (ppb_v) during a typical PAM oxidation experiment under idle (orange) and 50% load (blue) engine operating conditions with diesel fuel. Increasing UV light voltage increases the OH_{exp} (red).

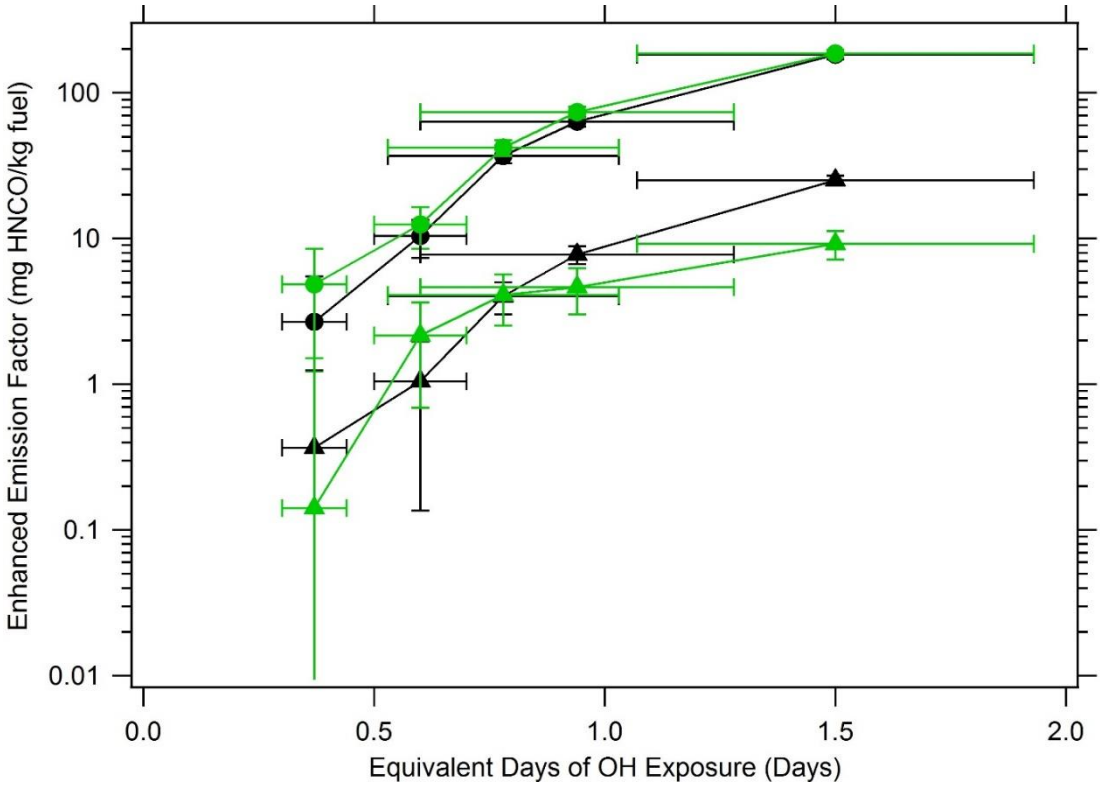

Figure 2.2. EEF_ts of HNCO plotted against OH_{exp} (assuming average [OH] = 1.5 x 10^6 molecules cm^{-3}) for biodiesel (green) and diesel (black) fuels under idle (circles) and 50% load (triangles) engine operating conditions. Vertical error bars represent the errors in measured mixing ratios of HNCO, CO_2, and CO propagated throughout the calculations of EFs and EEF_ts. Horizontal error bars are the ±1 standard deviation of the output from the OH_{exp} estimation model (Figure A1.2).

2.6 Chapter 2 Tables

Table 2.1. EFs and EEFs after 1.5 days of photochemical aging ($EEF_{1.5}$ days) for both fuel types and under both engine operating conditions. The EF describes primary emission of HNCO from the combustion of the fuel whereas the $EEF_{1.5}$ days describes how much HNCO is photochemically produced after 1.5 days of aging. The total emission of HNCO from the combustion of a given fuel source ($EF + EEF_t$) contributed from both primary emission and secondary formation of HNCO are shown in Figure A1.5.

	Idle		50% Load	
	EF (mg HNCO/kg fuel)	$EEF_{1.5}$ days (mg HNCO/kg fuel)	EF (mg HNCO/kg fuel)	$EEF_{1.5}$ days (mg HNCO/kg fuel)
Diesel	54 ± 3	183 ± 13	17 ± 1	26 ± 2
Biodiesel	54 ± 1	187 ± 17	17 ± 2	10 ± 2

Table 2.2. Comparison of mobile and statewide wildfire HNCO sources calculated from reported CO emissions by the CARB projected for 2015. Photochemically enhanced HNCO emissions describe total emissions of HNCO from mobile sources after ~1.5 equivalent days of atmospheric aging.

Emission Source	CO Emissions (tons/day)	HNCO Emissions (tons/day)	[d]Secondary HNCO Emissions (tons/day)
On-road light duty gasoline vehicles[a]	881	0.04	0.12
On-road light duty diesel vehicles[b]	5	0.02	0.06
Non-road use of diesel[c]	619	2.76	8.28
Total Mobile Sources and non-road sources	1505	2.82	8.46
Wildfires (statewide)[e]	4787	5.14	N/A

[a]HNCO emissions are calculated using an average HNCO/CO ratio of 0.028 mmol HNCO mol CO^{-1} calculated from the work of Brady et al (2014) measured from light duty gasoline vehicles.
[b]HNCO emissions are calculated using HNCO/CO ratio of 2.3 mmol HNCO mol CO^{-1} reported by Wentzell et al (2013) for a light duty diesel engine.
[c]HNCO emissions are calculated using an average HNCO/CO ratio of 2.9 mmol HNCO mol CO^{-1} measured in this study from a non-road diesel engine.
[d]Enhanced HNCO emissions are calculated by multiplying primary mobile source HNCO emissions by a photochemical enhancement factor of 3 based on our observations for 1.5 OH equivalent days of aging. While this represents a lower bound for oxidative production, as precursor molecules may have lifetimes longer than 1.5 days, we note that this estimate ignores the role of deposition, which may rapidly remove HNCO precursors from the atmosphere.
[e]HNCO emissions were calculated using an average HNCO/CO ratio of 0.7 mmol HNCO mol CO^{-1} reported in Veres et al (2010).

REFERENCES

(1) Roberts, J. M.; Veres, P. R.; Cochran, A. K.; Warneke, C.; Burling, I. R.; Yokelson, R. J.; Lerner, B.; Gilman, J. B.; Kuster, W. C.; Fall, R.; et al. Isocyanic Acid in the Atmosphere and Its Possible Link to Smoke-Related Health Effects. *Proc. Natl. Acad. Sci.* **2011**, *108* (22), 8966–8971. https://doi.org/10.1073/pnas.1103352108.

(2) Jaisson, S.; Pietrement, C.; Gillery, P. Carbamylation-Derived Products: Bioactive Compounds and Potential Biomarkers in Chronic Renal Failure and Atherosclerosis. *Clin. Chem.* **2011**, *57* (11), 1499–1505. https://doi.org/10.1373/clinchem.2011.163188.

(3) Wang, Z.; Nicholls, S. J.; Rodriguez, E. R.; Kummu, O.; Hörkkö, S.; Barnard, J.; Reynolds, W. F.; Topol, E. J.; DiDonato, J. A.; Hazen, S. L. Protein Carbamylation Links Inflammation, Smoking, Uremia and Atherogenesis. *Nat. Med.* **2007**, *13* (10), 1176–1184. https://doi.org/10.1038/nm1637.

(4) Mydel, P.; Wang, Z.; Brisslert, M.; Hellvard, A.; Dahlberg, L. E.; Hazen, S. L.; Bokarewa, M. Carbamylation-Dependent Activation of T Cells: A Novel Mechanism in the Pathogenesis of Autoimmune Arthritis. *J. Immunol.* **2010**, ji_1000075. https://doi.org/10.4049/jimmunol.1000075.

(5) Verbrugge, F. H.; Tang, W. H. W.; Hazen, S. L. Protein Carbamylation and Cardiovascular Disease. *Kidney Int.* **2015**, *88* (3), 474–478. https://doi.org/10.1038/ki.2015.166.

(6) Karlsson, D.; Dalene, M.; Skarping, G.; Marand, Å. Determination of Isocyanic Acid in Air. *J. Environ. Monit.* **2001**, *3* (4), 432–436. https://doi.org/10.1039/B103476F.

(7) Sennbro, C. J.; Lindh, C. H.; Östin, A.; Welinder, H.; Jönsson, B. a. G.; Tinnerberg, H. A Survey of Airborne Isocyanate Exposure in 13 Swedish Polyurethane Industries. *Ann. Occup. Hyg.* **2004**, *48* (5), 405–414. https://doi.org/10.1093/annhyg/meh034.

(8) Westberg, H.; Löfstedt, H.; Seldén, A.; Lilja, B.-G.; Nayström, P. Exposure to Low Molecular Weight Isocyanates and Formaldehyde in Foundries Using Hot Box Core Binders. *Ann. Occup. Hyg.* **2005**, *49* (8), 719–725. https://doi.org/10.1093/annhyg/mei040.

(9) Brady, J. M.; Crisp, T. A.; Collier, S.; Kuwayama, T.; Forestieri, S. D.; Perraud, V.; Zhang, Q.; Kleeman, M. J.; Cappa, C. D.; Bertram, T. H. Real-Time Emission Factor Measurements of Isocyanic Acid from Light Duty Gasoline Vehicles. *Environ. Sci. Technol.* **2014**, *48* (19), 11405–11412. https://doi.org/10.1021/es504354p.

(10) Wentzell, J. J. B.; Liggio, J.; Li, S.-M.; Vlasenko, A.; Staebler, R.; Lu, G.; Poitras, M.-J.; Chan, T.; Brook, J. R. Measurements of Gas Phase Acids in Diesel Exhaust: A Relevant Source of HNCO? *Environ. Sci. Technol.* **2013**, *47* (14), 7663–7671. https://doi.org/10.1021/es401127j.

(11) Borduas, N.; Abbatt, J. P. D.; Murphy, J. G. Gas Phase Oxidation of Monoethanolamine (MEA) with OH Radical and Ozone: Kinetics, Products, and Particles. *Environ. Sci. Technol.* **2013**, *47* (12), 6377–6383. https://doi.org/10.1021/es401282j.

(12) Roberts, J. M.; Veres, P. R.; VandenBoer, T. C.; Warneke, C.; Graus, M.; Williams, E. J.; Lefer, B.; Brock, C. A.; Bahreini, R.; Öztürk, F. New Insights into Atmospheric Sources and Sinks of Isocyanic Acid, HNCO, from Recent Urban and Regional Observations. *J. Geophys. Res. Atmospheres* **2014**, *119* (2), 1060–1072.

(13) Woodward-Massey, R.; Taha, Y. M.; Moussa, S. G.; Osthoff, H. D. Comparison of Negative-Ion Proton-Transfer with Iodide Ion Chemical Ionization Mass Spectrometry for Quantification of Isocyanic Acid in Ambient Air. *Atmos. Environ.* **2014**, *98*, 693–703. https://doi.org/10.1016/j.atmosenv.2014.09.014.

(14) Zhao, R.; Lee, A. K. Y.; Wentzell, J. J. B.; Mcdonald, A. M.; Toom-Sauntry, D.; Leaitch, W. R.; Modini, R. L.; Corrigan, A. L.; Russell, L. M.; Noone, K. J.; et al. Cloud Partitioning of Isocyanic Acid (HNCO) and Evidence of Secondary Source of HNCO in Ambient Air. *Geophys. Res. Lett.* **2014**, *41* (19), 6962–6969. https://doi.org/10.1002/2014GL061112.

(15) Karl, M.; Svendby, T.; Walker, S.-E.; Velken, A. S.; Castell, N.; Solberg, S. Modelling Atmospheric Oxidation of 2-Aminoethanol (MEA) Emitted from Post-Combustion Capture Using WRF–Chem. *Sci. Total Environ.* **2015**, *527–528*, 185–202. https://doi.org/10.1016/j.scitotenv.2015.04.108.

(16) Sarkar, C.; Sinha, V.; Kumar, V.; Rupakheti, M.; Panday, A.; Mahata, K. S.; Rupakheti, D.; Kathayat, B.; Lawrence, M. G. Overview of VOC Emissions and Chemistry from PTR-TOF-MS Measurements during the SusKat-ABC Campaign: High Acetaldehyde, Isoprene and Isocyanic Acid in Wintertime Air of the Kathmandu Valley. *Atmospheric Chem. Phys.* **2016**, *16* (6), 3979–4003. https://doi.org/https://doi.org/10.5194/acp-16-3979-2016.

(17) Heeb, N. V.; Zimmerli, Y.; Czerwinski, J.; Schmid, P.; Zennegg, M.; Haag, R.; Seiler, C.; Wichser, A.; Ulrich, A.; Honegger, P.; et al. Reactive Nitrogen Compounds (RNCs) in Exhaust of Advanced PM–NOx Abatement Technologies for Future Diesel Applications. *Atmos. Environ.* **2011**, *45* (18), 3203–3209. https://doi.org/10.1016/j.atmosenv.2011.02.013.

(18) Correia, A. W.; Pope, C. A.; Dockery, D. W.; Wang, Y.; Ezzati, M.; Dominici, F. The Effect of Air Pollution Control on Life Expectancy in the United States: An Analysis of 545 US Counties for the Period 2000 to 2007. *Epidemiol. Camb. Mass* **2013**, *24* (1), 23–31. https://doi.org/10.1097/EDE.0b013e3182770237.

(19) Robinson, A. L.; Donahue, N. M.; Shrivastava, M. K.; Weitkamp, E. A.; Sage, A. M.; Grieshop, A. P.; Lane, T. E.; Pierce, J. R.; Pandis, S. N. Rethinking Organic Aerosols:

Semivolatile Emissions and Photochemical Aging. *Science* **2007**, *315* (5816), 1259–1262. https://doi.org/10.1126/science.1133061.

(20) Quillen, K.; Bennett, M.; Volckens, J.; Stanglmaier, R. H. Characterization of Particulate Matter Emissions From a Four-Stroke, Lean-Burn, Natural Gas Engine. *J. Eng. Gas Turbines Power* **2008**, *130* (5), 52807-052807–5. https://doi.org/10.1115/1.2906218.

(21) Kang, E.; Root, M. J.; Toohey, D. W.; Brune, W. H. Introducing the Concept of Potential Aerosol Mass (PAM). *Atmos Chem Phys* **2007**, *7* (22), 5727–5744. https://doi.org/10.5194/acp-7-5727-2007.

(22) Lambe, A. T.; Ahern, A. T.; Williams, L. R.; Slowik, J. G.; Wong, J. P. S.; Abbatt, J. P. D.; Brune, W. H.; Ng, N. L.; Wright, J. P.; Croasdale, D. R.; et al. Characterization of Aerosol Photooxidation Flow Reactors: Heterogeneous Oxidation, Secondary Organic Aerosol Formation and Cloud Condensation Nuclei Activity Measurements. *Atmospheric Meas. Tech.* **2011**, *4* (3), 445–461. https://doi.org/https://doi.org/10.5194/amt-4-445-2011.

(23) Ortega, A. M.; Day, D. A.; Cubison, M. J.; Brune, W. H.; Bon, D.; de Gouw, J. A.; Jimenez, J. L. Secondary Organic Aerosol Formation and Primary Organic Aerosol Oxidation from Biomass-Burning Smoke in a Flow Reactor during FLAME-3. *Atmospheric Chem. Phys.* **2013**, *13* (22), 11551–11571.

(24) Li, R.; Palm, B. B.; Ortega, A. M.; Hlywiak, J.; Hu, W.; Peng, Z.; Day, D. A.; Knote, C.; Brune, W. H.; de Gouw, J. A.; et al. Modeling the Radical Chemistry in an Oxidation Flow Reactor: Radical Formation and Recycling, Sensitivities, and the OH Exposure Estimation Equation. *J. Phys. Chem. A* **2015**, *119* (19), 4418–4432. https://doi.org/10.1021/jp509534k.

(25) Peng, Z.; Day, D. A.; Stark, H.; Li, R.; Lee-Taylor, J.; Palm, B. B.; Brune, W. H.; Jimenez, J. L. HOx Radical Chemistry in Oxidation Flow Reactors with Low-Pressure Mercury Lamps Systematically Examined by Modeling. *Atmos Meas Tech* **2015**, *8* (11), 4863–4890. https://doi.org/10.5194/amt-8-4863-2015.

(26) Mao, J.; Ren, X.; Brune, W. H.; Olson, J. R.; Crawford, J. H.; Fried, A.; Huey, L. G.; Cohen, R. C.; Heikes, B.; Singh, H. B.; et al. Airborne Measurement of OH Reactivity during INTEX-B. *Atmos Chem Phys* **2009**, *9* (1), 163–173. https://doi.org/10.5194/acp-9-163-2009.

(27) Veres, P.; Roberts, J. M.; Warneke, C.; Welsh-Bon, D.; Zahniser, M.; Herndon, S.; Fall, R.; de Gouw, J. Development of Negative-Ion Proton-Transfer Chemical-Ionization Mass Spectrometry (NI-PT-CIMS) for the Measurement of Gas-Phase Organic Acids in the Atmosphere. *Int. J. Mass Spectrom.* **2008**, *274* (1–3), 48–55.

(28) Roberts, J. M.; Veres, P.; Warneke, C.; Neuman, J. A.; Washenfelder, R. A.; Brown, S. S.; Baasandorj, M.; Burkholder, J. B.; Burling, I. R.; Johnson, T. J.; et al. Measurement of HONO, HNCO, and Other Inorganic Acids by Negative-Ion Proton-Transfer Chemical-

Ionization Mass Spectrometry (NI-PT-CIMS): Application to Biomass Burning Emissions. *Atmospheric Meas. Tech.* **2010**, *3* (4), 981–990. https://doi.org/10.5194/amt-3-981-2010.

(29) Brophy, P.; Farmer, D. K. A Switchable Reagent Ion High Resolution Time-of-Flight Chemical Ionization Mass Spectrometer for Real-Time Measurement of Gas Phase Oxidized Species: Characterization from the 2013 Southern Oxidant and Aerosol Study. *Atmos Meas Tech* **2015**, *8* (7), 2945–2959. https://doi.org/10.5194/amt-8-2945-2015.

(30) Veres, P. R.; Roberts, J. M. Development of a Photochemical Source for the Production and Calibration of Acyl Peroxynitrate Compounds. *Atmospheric Meas. Tech.* **2015**, *8* (5), 2225–2231. https://doi.org/https://doi.org/10.5194/amt-8-2225-2015.

(31) Gordon, T. D.; Presto, A. A.; Nguyen, N. T.; Robertson, W. H.; Na, K.; Sahay, K. N.; Zhang, M.; Maddox, C.; Rieger, P.; Chattopadhyay, S.; et al. Secondary Organic Aerosol Production from Diesel Vehicle Exhaust: Impact of Aftertreatment, Fuel Chemistry and Driving Cycle. *Atmospheric Chem. Phys.* **2014**, *14* (9), 4643–4659. https://doi.org/https://doi.org/10.5194/acp-14-4643-2014.

(32) Chin, J.-Y.; Batterman, S. A.; Northrop, W. F.; Bohac, S. V.; Assanis, D. N. Gaseous and Particulate Emissions from Diesel Engines at Idle and under Load: Comparison of Biodiesel Blend and Ultralow Sulfur Diesel Fuels. *Energy Fuels* **2012**, *26* (11), 6737–6748. https://doi.org/10.1021/ef300421h.

(33) Drenth, A. C.; Olsen, D. B.; Cabot, P. E.; Johnson, J. J. Compression Ignition Engine Performance and Emission Evaluation of Industrial Oilseed Biofuel Feedstocks Camelina, Carinata, and Pennycress across Three Fuel Pathways. *Fuel* **2014**, *136*, 143–155. https://doi.org/10.1016/j.fuel.2014.07.048.

(34) Karjalainen, P.; Timonen, H.; Saukko, E.; Kuuluvainen, H.; Saarikoski, S.; Aakko-Saksa, P.; Murtonen, T.; Dal Maso, M.; Ahlberg, E.; Svenningsson, B.; et al. Time-Resolved Characterization of Primary and Secondary Particle Emissions of a Modern Gasoline Passenger Car. *Atmos Chem Phys Discuss* **2015**, *15* (22), 33253–33282. https://doi.org/10.5194/acpd-15-33253-2015.

(35) Kröcher, O.; Elsener, M.; Koebel, M. An Ammonia and Isocyanic Acid Measuring Method for Soot Containing Exhaust Gases. *Anal. Chim. Acta* **2005**, *537* (1), 393–400. https://doi.org/10.1016/j.aca.2004.12.082.

(36) Varatharajan, K.; Cheralathan, M. Influence of Fuel Properties and Composition on NOx Emissions from Biodiesel Powered Diesel Engines: A Review. *Renew. Sustain. Energy Rev.* **2012**, *16* (6), 3702–3710. https://doi.org/10.1016/j.rser.2012.03.056.

(37) Lapuerta, M.; Armas, O.; Rodríguez-Fernández, J. Effect of Biodiesel Fuels on Diesel Engine Emissions. *Prog. Energy Combust. Sci.* **2008**, *34* (2), 198–223. https://doi.org/10.1016/j.pecs.2007.07.001.

(38) California Environmental Protection Agency Air Resources Board. Almanac Emission Projection Data: 2015 Estimated Annual Average Emissions. 2013.

(39) Young, P. J.; Emmons, L. K.; Roberts, J. M.; Lamarque, J.-F.; Wiedinmyer, C.; Veres, P.; VandenBoer, T. C. Isocyanic Acid in a Global Chemistry Transport Model: Tropospheric Distribution, Budget, and Identification of Regions with Potential Health Impacts. *J. Geophys. Res. Atmospheres* **2012**, *117* (D10). https://doi.org/10.1029/2011JD017393.

(40) Barnes, I.; Solignac, G.; Mellouki, A.; Becker, K. H. Aspects of the Atmospheric Chemistry of Amides. *ChemPhysChem* **2010**, *11* (18), 3844–3857. https://doi.org/10.1002/cphc.201000374.

CHAPTER 3

ELEVATED PRODUCTION OF NH_4NO_3 FROM THE PHOTOCHEMICAL PROCESSING OF VEHICLE EXHAUST: IMPLICATIONS FOR AIR QUALITY IN THE SEOUL METROPOLITAN REGION[2]

3.1 Introduction

Measured fine particle burdens in the Seoul Metropolitan Region (SMR) are high despite ongoing efforts by the Korean Ministry of the Environment, including the enactment of the "Special Act on Metropolitan Air Quality Improvement" more than a decade ago. The particle burdens are similar to other large Asian cities such as Tokyo and Shanghai, and are responsible for low visibility and decreased air quality.[1–3] The SMR, which includes Incheon, Seoul, and parts of the Gyeonggi province, includes multiple pollution sources including biomass burning, industry, vehicles/transportation, and long-range transport. However, the exact contribution of each of these sources to observed fine particulate matter ($PM_{2.5}$) in the area is poorly understood.[1,4] Effective policy that reduces air pollution and human exposure to $PM_{2.5}$ in the SMR requires an understanding of how different sources contribute precursors to secondary $PM_{2.5}$ and thus local air pollution.[5,6]

Severe haze events in highly populated cities are dominantly due to secondary aerosol production.[7,8] In these events, the inorganic aerosol component often contributes to the total observed particle mass equally or greater than the organic fraction.[5,9,10] Vehicles in megacities can play an important role in these localized haze events by emitting nitrogen oxides (NO_x) that

[2]Link, M.F., Son, J., Kim, J., Park, G., Taehyun, P., Lim, H., Barbar, Z.B., Kim, P., Kang, S., Kim, J., Choi, Y., Lee, T., Farmer, D.K., 2017. Elevated Production of NH4NO3 from the photochemical processing of vehicle exhaust: Implications for air quality in the Seoul Metropolitan Region. Atmospheric Environment, 156, pp.95-101.

photochemically form nitric acid (HNO_3), leading to secondary inorganic ammonium nitrate (NH_4NO_3) through thermodynamic equilibrium with gas-phase ammonia (NH_3).[3,11] Introduction of stringent standards for vehicle emissions (such as the EURO 6 for diesel vehicles and California's non-methane organic gases fleet average system for gasoline-fueled vehicles; NMOG FAS) have been largely credited with reducing NO_x and non-methane volatile organic compounds throughout South Korea over the last twenty years.[9] However, ozone concentrations in the SMR have continued to increase, and visibility has continued to decrease, since 1989 (the start of the air quality monitoring network).[2] Previous studies suggest that a strong photochemical aerosol component contributes to localized air pollution in the SMR.[1,4]

Vehicles with a three-way catalyst system (TWC) produce NH_3 through a water gas-shift reaction on the catalyst involving carbon monoxide (CO), hydrogen gas and nitrogen monoxide (NO).[12–15] These TWCs are commonly used for gasoline and liquid petroleum gasoline (LPG) fuel types. In contrast, diesel vehicles are not equipped with TWCs and thus, unless equipped with modern NO_x-mitigating systems such as the selective catalytic reduction system, are unimportant sources of NH_3 to the urban atmosphere.[16,17] As of May 2016, vehicles equipped with the TWC system and powered by gasoline or LPG comprise over 60% of the total on-road vehicle fleet in Seoul and thus represent a potentially important source of NH_3 for NH_4NO_3 aerosol formation.[18] Evidence of high fractions of aerosol nitrate have been observed from particle pollution events in and around the SMR, as well as in air transported downwind of the SMR (>30% of particle mass) during times of morning traffic.[4,9,19,20] These observations suggest that photochemically processed vehicle emissions contribute to localized PM pollution from the SMR.[21] Here, we use a flow reactor study to investigate the hypothesis that NH_3 formed inside the catalytic converters of gasoline and LPG vehicles rapidly reacts with HNO_3 derived from

NO_x to act as the dominant source of NH_4NO_3 in the SMR. Additionally, we observe very low NH_4NO_3 formation from NO_x-saturated diesel exhaust, suggesting that NH_3 is the limiting reagent for NH_4NO_3 production from engine exhaust, and that controlling NH_3 emissions from gasoline and LGP vehicles may be key to reducing secondary inorganic aerosol in NO_x-dominant ambient environments, including the SMR.

3.2 Materials and Methods

3.2.1 Vehicle exhaust sampling

Vehicle exhaust sampling was conducted at the Transportation Pollution Research Center (TPRC) of the National Institute of Environmental Research (NIER), a certifying institute for vehicle exhaust emissions in Korea. The specifications for the vehicles tested are shown in Table 3.1. Four gasoline (G1-4), three diesel (D1-3), and three liquid petroleum gasoline (LPG; L1-3) vehicles were chosen as a representative fleet of SMR vehicles.

Testing for each vehicle required two days. Experiments took place between 18 November 2015 and 22 July 2016. Emissions were generated from vehicles operated under 20-minute constant speed driving conditions using a chassis dynamometer. Vehicle exhaust was diluted in a constant volume sampler with dilution ratios ranging from 10-60 (clean air/exhaust). Diluted air was pumped through 6 meters of stainless-steel tubing (3/8" O.D.) connected to a 1-meter length of stainless-steel tubing (1/4" O.D.) at a flowrate of 3 standard liters per minute (sLpm). During the 20-minute constant speed driving mode, the sampled air would pass through an oxidation flow reactor (KNU OFR) and either be transferred to the HR-AMS or transferred to a bypass every two minutes. This sampling design allowed the exhaust sample a greater opportunity to equilibrate in the flow reactor than if the diluted sample alternated through the KNU OFR and a bypass line. Primary emissions were measured by pumping undiluted exhaust through a separate line (2 meters of stainless-steel tubing) at a flowrate of 3 sLpm while the diluted air was diverted through the OFR bypass.

3.2.2 Emissions measurement information

Measurements of NO, NO_2, and NH_3 were acquired using a Horiba MEXA 1400QL-NX analyzer. NO_x was measured by chemiluminescence; CO and CO_2 were measured by non-dispersive infrared detectors. The authors note that measurements of NH_3 were only available for vehicles D1, G2, and L3 and were acquired several months after measurements were performed including the OFR. All emissions tests were performed in accordance with the World Forum for Harmonization of Vehicle Regulations, an international standard method used by the United Nations Economic Commission for Europe (UNECE). The Constant Volume Sampling method recommended by UNECE for hot-start was performed by running the engine until the engine temperature is the half of temperature gauge. This generally took 5-10 minutes. After the engine temperature reached the halfway point on the temperature gauge, the test vehicle was run for a distance of 4 km at a speed of 70 km/hr. The vehicle then would slow down to 30 km/hr (the first testing speed) and emissions measurements would then begin.

3.2.3 Flow reactor operation

We used a custom-built oxidation flow reactor (Kyungpook National University OFR; KNU OFR) to observe the formation of secondary inorganic aerosol from samples of vehicle exhaust.[22] The KNU OFR was similar in its design to previously described flow reactors, and consisted of a pyrex quartz tube 80 cm in length with an inner diameter of 14.3 cm.[23–26] OH radicals were produced by introducing O_3 to the sample flow which was photolyzed (λ = 254 nm) in the reactor to form OH radicals. An OH exposure calibration was performed over the range of lamp operating voltages; OH exposures ranged from 6.5×10^{10} to 6.5×10^{11} molecules cm^{-3} s, corresponding to 0.5-5 days of OH equivalent atmospheric processing (assuming an

average OH concentration of 1 x 10^6 molecules cm^{-3}). An analysis presented in the supporting information suggests the measurements from vehicles G2, L3, G7, L8, D9 and G10 should reflect OH exposures on the lower end of the calibrated range; approximately 0.5-1 days of OH equivalent atmospheric processing. The OH exposure for L6 may be higher than the other vehicles, and the OH exposure for D1 and D4 should be similar to or lower than the other vehicles.

The authors recognize recent modeling studies analyzing OFR oxidation chemistry as a function of relative humidity, photon flux, input ozone and externally added OH reactivity.[27–29] The conclusions of Peng, et al. (2016) define the interpretation of OFR results as "risky" when either the water vapor mixing ratio is <0.1% or when the externally added OH reactivity is >200 s^{-1}. Experiments using an OFR to explore the photochemical oxidation potential of vehicle exhaust and biomass burning commonly are operated under "riskier" conditions due to the presence of near-ppm levels of NO_x and/or high levels of reactive VOCs in the reactor.[30–34] Ultimately, the effect of high externally added OH reactivity in the OFR is that, particularly for VOCs, the potential effects of photolysis and non-OH oxidation chemistry become increasingly uncertain.[28] The analytical challenge of characterizing the photochemical oxidation of either vehicle exhaust or biomass burning as it occurs in the ambient environment through the use of OFRs remains and should be the subject of future study.

3.2.4 High Resolution Time-of-Flight Aerosol Mass Spectrometer (HR-AMS)

The Aerodyne HR-AMS has been described extensively in previous literature, and details of its operation will be briefly described here.[35–37] The exhaust sample passed through a diffusion drier and critical orifice, restricting the flow to 0.1 Lpm before entering the HR-AMS. Diffusion

dryers controlled sample humidity (< 40% RH), reducing uncertainties due to bounce-related changes in collection efficiency and reduced particle transmission through the aerodynamic lens.[35] The HR-AMS was calibrated weekly and the Composition-Dependent Collection Efficiency (CDCE) was calculated from observed chemical composition. Only low-humidity experiments were used for quantitative HR-AMS analysis. Data were collected at 10s resolution.

3.3 Results and Discussion

3.3.1 Trace gas and inorganic particle data

Here we present the primary emissions in terms of a distance-based emission factor. We express the inorganic aerosol produced from photochemical perturbation of the primary exhaust in terms of a photochemically enhanced (P.E.) distance-based emission factor. The P.E. emission factor is defined as the effective emission factor of a given compound after the vehicle exhaust has been exposed to 0.5-1 day of OH equivalent atmospheric aging. Throughout the sampling campaign, production of secondary inorganic aerosol in the form of NH_4NO_3 was most pronounced from vehicles fueled by gasoline and LPG (Figure 3.1).

The results indicate that relatively small amounts of photochemical perturbation can produce secondary aerosol from gaseous precursors in the exhaust. This secondary aerosol can be more than an order of magnitude greater than primary aerosol emissions. This is consistent with previous studies, including measurements of gasoline exhaust oxidation in a smog chamber.[38,39] Higher levels of CO were associated with higher NH_4NO_3 emission and production. In contrast, higher levels of NO_x were not correlated with higher levels of NH_4NO_3. Higher levels of CO emissions from gasoline vehicles often coincide with higher levels of NH_3 emissions.[12,13] In this study, we observe elevated NH_4NO_3 production corresponding to elevated CO emissions, suggesting that CO is an appropriate proxy measurement for NH_3 from gasoline and LPG vehicles in this study. The diesel particle filter (DPF) and diesel oxidation catalyst (DOC) are often used as exhaust aftertreatment technologies in diesel vehicles. However, these aftertreatments fail to remove NO_x, causing higher NO_x emissions from diesel than gasoline vehicles. The limiting reagent for NH_4NO_3 formation can be either NO_x or NH_3, depending on

the ambient environment. Both gasoline/LPG vehicles and diesel vehicles can act as a source of the limiting reactant, and spur secondary inorganic aerosol formation. The observations described herein demonstrate that in an NH_3-limited environment, gasoline and LPG vehicles can provide NH_3 and thus cause increased particulate matter loading, while in a NO_x-limited environment, diesel vehicles can provide the NO_x to produce particles.

Photochemically enhanced emission factors of inorganic aerosol from the gasoline and LPG fuel types vary widely by car brand (Figure 3.3). These differences can be attributed to engine design, combustion conditions and chemistry, as well as driving speed (e.g. Figure 3.2). Figure 3.3 shows the relationship between the different cars from which exhaust was sampled, and the production of aerosol nitrate.

Vehicles G2, L3, and G7 all have median values for secondary nitrate P.E. emission factors that are much higher than other vehicle brands. Vehicles G5 and L8 have median values for secondary nitrate production that are much lower than G2, L3 and G7, but still a factor of 5 or more higher than the diesel vehicles (D1, D4, and D9) as well as L6 and G10. The vehicles that were observed to have the highest secondary aerosol production rates were G2 and L3. Inconsistent patterns of aerosol nitrate production, as a function of speed, were observed between the different vehicles tested (Figure 3.2). The highest aerosol nitrate production rates were measured from some vehicles (e.g. G5 and G10) at the highest speeds (110 km/hr) when the highest values for NO_x were also observed (Figure A2.8). However, other vehicles (e.g. G2 and L3) produced the most aerosol nitrate at the lowest tested speed (30 km/hr). Although we observe variability in secondary inorganic aerosol production with speed across the different car brands, we do not observe any consistent trends.

Figure 3.4 shows a comparision between secondary nitrate production rate and NO, NO_2 and NH_3 emissions for three vehicles of the same brand - D1, G2, and L3 (i.e. Brand A) – that spanned the different fuel types. Emissions of NH_3 from G2 (gasoline) and L3 (LPG fuel) were much higher than emissions of NO or NO_2. In contrast, emissions of NH_3 were below the detection limit for D1. Elevated emissions of NH_3 from gasoline vehicles have been reported many times in the past.[12,13,40,41] Vehicles previously reported to emit high levels of NH_3 were medium-duty gasoline fueled vehicles that also emit high CO.[12] Here we present additional evidence that vehicles fueled by LPG can also emit NH_3 at similar levels as gasoline fueled vehicles. L3 also shows this pattern of high CO emission coupled with high NH_3 emission. Observations from previous studies show that high levels of CO and NH_3 are most often co-emitted when an engine is running under rich-fuel conditions.[42–44] The absence of the three-way catalyst in the diesel vehicles in this study explains why NH_3 emission was not observed for D1.

3.3.2 Vehicle fuel types and implications for air quality

We observe a direct relationship between the formation of NH_4NO_3 secondary aerosol and photochemical processing of exhaust from gasoline and LPG vehicles that use TWCs. In the KNU OFR, HNO_3 is formed rapidly when NO_2 reacts with OH. The HNO_3 can then react with NH_3 emitted directly from vehicle exhaust to form NH_4NO_3 aerosol.[45] NH_4NO_3 aerosol formation is limited (i) by NH_3 in the case of diesel vehicles, and (ii) by NO_2 in the case of gasoline and LPG vehicles (Figure 3.4). These two regimes of NH_3 and NO_x acting as limiting reagents for NH_4NO_3 formation have been observed in the ambient atmosphere.[6,10] In the San Joaquin Valley of California, NH_3 is more abundent than HNO_3 and limits NH_4NO_3 formation, while in the nearby South Coast Air Basin, local and transported sources of NH_3 may act as the limiting reagents for NH_4NO_3 formation.[40,46,47] The data presented herein is useful for studying

the impact of vehicles on NH_4NO_3 in NO_x- or NH_3-limited regimes.[10,48,49] Our results suggest that in an environment in which NH_3 is the limiting reagent for NH_4NO_3 aerosol formation, such as the SMR, emission of NH_3 from gasoline and LPG vehicle sources may be a large contributor to local air pollution.[50]

The contribution of on-road gasoline and LPG vehicles to localized NH_4NO_3 production in the SMR depends on many factors including vehicle age, meteorological conditions influencing mixing and stagnancy, driving patterns, and whether the vehicle is being run under rich-fuel conditions (i.e. low air-to-fuel ratio).[7,12,31,43,51–53] The relationship between NH_3 emission, resulting NH_4NO_3 particle formation, and age of the catalyst (i.e. the odometer reading) remains unclear. Previous studies had reported higher NH_3 emission for mid-age (~100,000 km) vehicles that tapered off as vehicle age increased (~200,000 km).[12] This is consistent with the pattern observed here, in which vehicles with the oldest catalysts (G2 and L3) also had the highest NH_4NO_3 production rates. The importance of aggressive stop-and-go driving conditions, characteristic of the SMR, to elevated levels of CO and NH_3 emissions has been reported previously.[43,51] The quantities and trends reported in this study, however, only reflect emission behavior from constant speed driving conditions, and thus potentially underestimate NH_4NO_3 precursor emissions and subsequent aerosol production. Previous studies have shown emission factors of NH_3 to be higher with more aggressive driving patterns, although the variability in reported emission factors is quite large.[12,13] Despite the complex patterns of NH_3 emission from vehicles using TWCs, this study demonstrates that these vehicle emissions have a potential for forming NH_4NO_3 aerosol rapidly and in high yields in response to photochemical perturbation.

A comparison of different NH_3 to CO emission ratios (NH_3:CO) from emission inventories in South Korea and Seoul demonstrates the importance of vehicles as a source of NH_3. From on-road sources in Seoul, annually averaged NH_3:CO emission ratios were 0.024 ppb_v/ppb_v, which is very close to a previously reported on-road emission ratio of 0.031 ± 0.005 ppb_v/ppb_v measured in the South Coast Air Basin.[51] The calculated NH_3:CO emission ratio from all inventoried sources in Seoul is 0.077 ppb_v/ppb_v suggesting that other sources of NH_3, in addition to on-road vehicle emissions, contribute to NH_3 in the SMR. Although mobile emissions are responsible for approximately 1/4th of the total NH_3 emissions in Seoul, a comparison of NO_x and NH_3 emissions (molar quantities) suggest that, since NO_x emissions are ~3.5x larger than NH_3 emissions, NH_4NO_3 formation in Seoul may be limited by the abundance of NH_3.[50] Because on-road vehicles are described as important sources of NH_3 to urban areas in some studies, but unimportant in others, [54,55] direct measurements of on-road NH_3 (e.g. Sun et al., 2014) are necessary for constraining the role of on-road gasoline and LPG vehicles as a NH_3 sources in the SMR.[3,41,54–56] Aircraft measurements have related observed enhancements of NH_4^+ (factor of ~4) above background levels in the South Coast Air Basin to elevated inputs of NH_3 from mobile sources downwind of the Los Angeles urban core.[40] These studies and the work described herein suggest that inputs of NH_3 from mobile sources are important to the formation of NH_4NO_3 in the SMR.

These experiments suggest that the chemical reactions that produce NH_3 in TWCs substantially increases the NH_3 available for formation of NH_4NO_3 aerosol. In the face of increasing vehicular emissions of NH_3, continued decreases in domestic emissions of sulfur dioxide (SO_2) would suppress $(NH_4)_2SO_4$ formation, and increase the availability of NH_3 for the formation of NH_4NO_3.[57] Further, adoption of selective catalyst reduction systems for NO_x

emissions control from diesel vehicles would add more vehicular NH_3 to the SMR, enhancing NH_4NO_3 production.[58,59] This study suggests that emission control strategies focused on reducing secondary inorganic aerosol pollution from NH_4NO_3 would be most effective by targeting a reduction of NH_3 from the exhaust of vehicles that have three-way catalyst systems.

3.4 Chapter 3 Figures

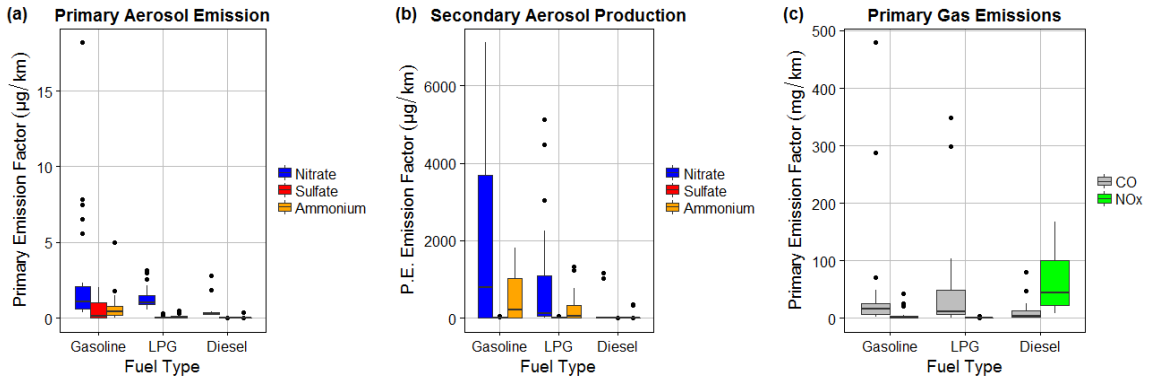

Figure 3.1. Inorganic aerosol and gas emission factors measured as (a) primary aerosol emission, (b) secondary aerosol production after oxidation in the KNU OFR and (c) primary gas emission. The edges of the boxplots represent the 25th and 75th quartiles and the whiskers represent the 10th and 90th quartiles. The median value is represented by the solid black lines in the boxes (N=21 for diesel, N=24 for LPG, and N=27 for gasoline). Outliers are shown as black dots.

In contrast, emissions of primary inorganic aerosol (PIA) were close to the HR-AMS detection limits for all fuel types. We observed higher levels of secondary aerosol ammonium and nitrate than sulfate across all fuel types. Some vehicles (e.g. D4 and G10) show elevated nitrate P.E. emission factors associated with influences of speed on engine performance (Figures 3.2 and A2.5).

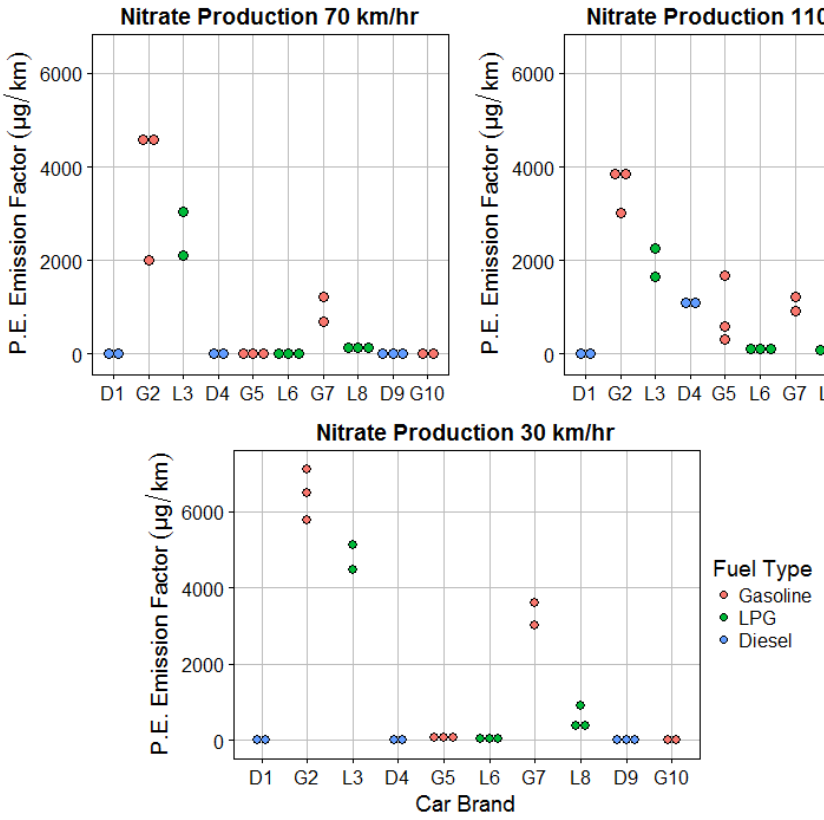

Figure 3.2. Aerosol nitrate P.E. emission factors (µg/km) as a function of car brand and speed. Individual measurements are represented by dots.

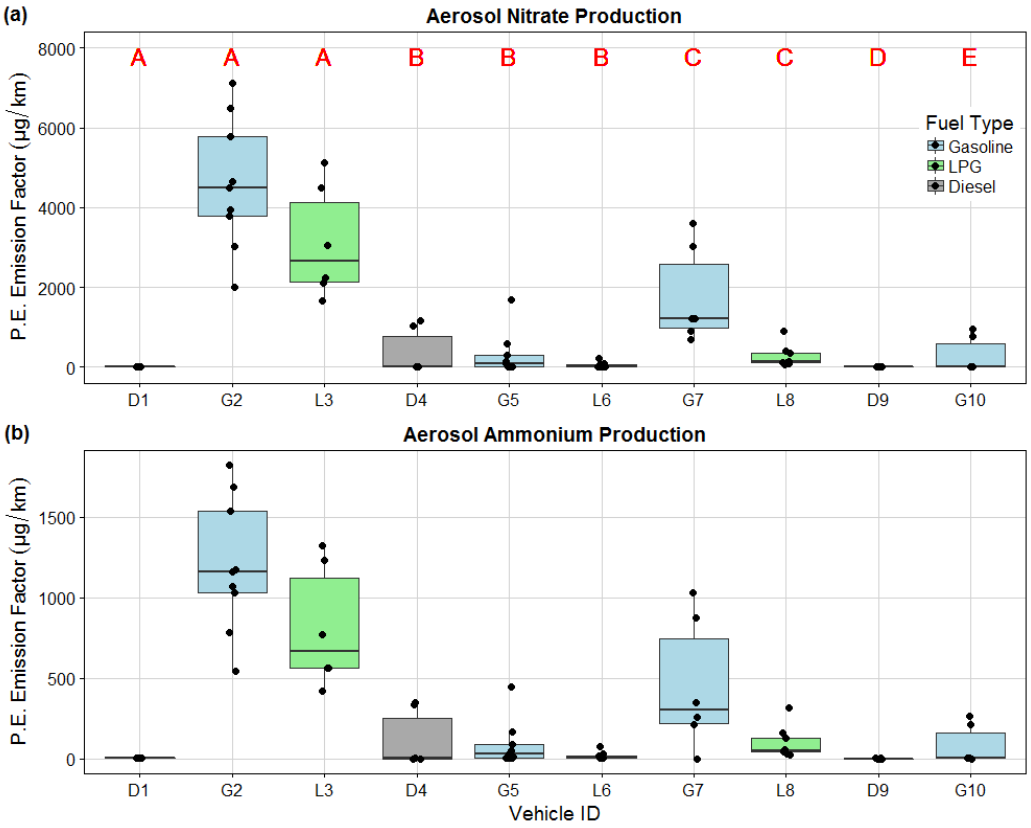

Figure 3.3. Secondary (a) aerosol nitrate and (b) aerosol ammonium P.E. emission factors (µg/km) as a function of vehicle ID and colored by fuel type. Additonally, car brand is indicated by the red letters in the top panel corresponding to the corresponding vehicle ID it is above on the x-axis. The edges of the boxplots represent the 25th and 75th quartiles and the whiskers represent the 10th and 90th quartiles. Individually measured data points are shown as black dots.

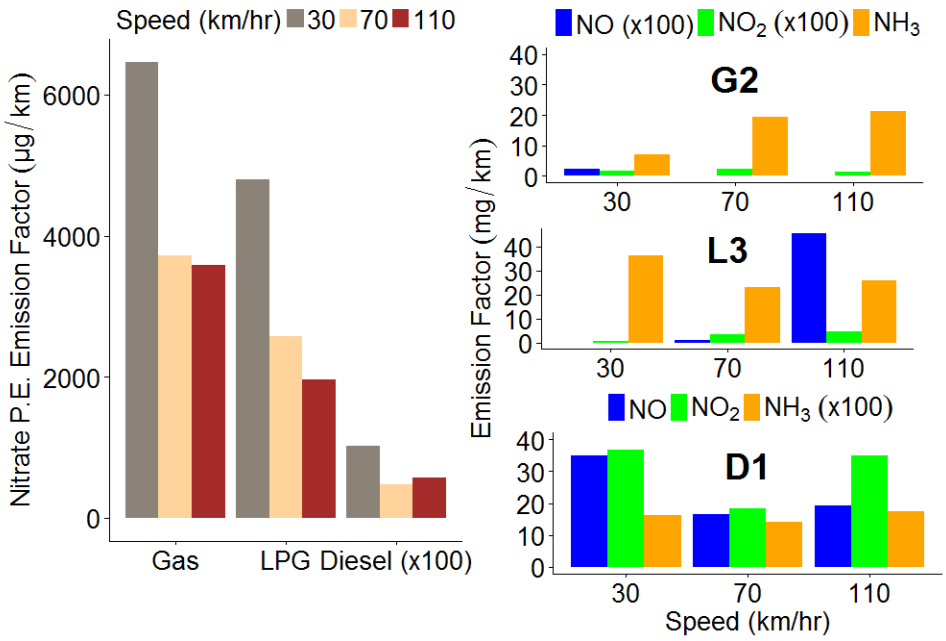

Figure 3.4. The (a) production rate of secondary aerosol nitrate from vehicles D1 (x100), G2, and L3 is shown as a function of speed and compared to (b) the emission rates of NO, NO_2, and NH_3 from the different vehicles as a function of speed (NO and NO_2 emission rates are multiplied by 100 for G2 and L3; emission rates of NH_3 are multiplied by 100 for D1).

3.5 Chapter 3 Table

Table 3.1 Specifications of the vehicle population tested at the TPRC separated by fuel type and brand.

[a]Vehicle ID	Brand	Fuel	After-treatment	Fuel Delivery	Engine Displacement (cc)	Odometer (km)	Emission Standard
D1	A	Diesel	[b]DOC +[c]DPF	[e]DI	1582	15396	Euro 6
G2	A	Gasoline	[d]TWC	[f]GDI	1591	71480	NMOG FAS
L3	A	LPG	TWC	[g]LPI	1591	54930	NMOG FAS
D4	B	Diesel	DOC +DPF	DI	2199	54060	Euro 6
G5	B	Gasoline	TWC	GDI	2999	26800	NMOG FAS
L6	B	LPG	TWC	LPI	2999	43784	NMOG FAS
G7	C	Gasoline	TWC	GDI	1999	29560	NMOG FAS
L8	C	LPG	TWC	LPI	1999	37268	NMOG FAS
D9	D	Diesel	DOC +DPF	DI	1956	17870	Euro 6
G10	E	Gasoline	TWC	GDI	998	51914	NMOG FAS

[a]Vehicle IDs beginning with G are for gasoline, D are for diesel and L are for LPG, [b]diesel oxidation catalyst (DOC), [c]diesel particle filter (DPF), [d]three way catalyst (TWC), [e]direct injection (DI), [f]gasoline direct injection (GDI), [g]liquid phase injection (LPI)

REFERENCES

(1) Heo, J.-B.; Hopke, P. K.; Yi, S.-M. Source Apportionment of PM2.5 in Seoul, Korea. *Atmos Chem Phys* **2009**, *9* (14), 4957–4971. https://doi.org/10.5194/acp-9-4957-2009.

(2) Shin, H. J.; Kim, J. C.; Lee, S. J.; Kim, Y. P. Evaluation of the Optimum Volatile Organic Compounds Control Strategy Considering the Formation of Ozone and Secondary Organic Aerosol in Seoul, Korea. *Environ. Sci. Pollut. Res.* **2012**, *20* (3), 1468–1481. https://doi.org/10.1007/s11356-012-1108-5.

(3) Chang, Y. H.; Zou, Z.; Deng, C. R.; Huang, K.; Collett Jr, J. L.; Lin, J.; Zhuang, G. S. The Importance of Vehicle Emissions as a Source of Atmospheric Ammonia in the Megacity of Shanghai. *Atmospheric Chem. Phys. Discuss.* **2015**, *15* (23), 34719–34763.

(4) Kim, Y. P. Trend and Characteristics of Ambient Particles in Seoul. *Asian J. Atmospheric Environ.* **2007**, *1* (1), 9–13.

(5) Huang, R.-J.; Zhang, Y.; Bozzetti, C.; Ho, K.-F.; Cao, J.-J.; Han, Y.; Daellenbach, K. R.; Slowik, J. G.; Platt, S. M.; Canonaco, F.; et al. High Secondary Aerosol Contribution to Particulate Pollution during Haze Events in China. *Nature* **2014**, *advance online publication*. https://doi.org/10.1038/nature13774.

(6) Aksoyoglu, S.; Ciarelli, G.; El-Haddad, I.; Baltensperger, U.; Prévôt, A. S. H. Secondary Inorganic Aerosols in Europe: Sources and the Significant Influence of Biogenic VOC Emissions Especially on Ammonium Nitrate. *Atmospheric Chem. Phys. Discuss.* **2016**, 1–27. https://doi.org/10.5194/acp-2016-739.

(7) Guo, S.; Hu, M.; Zamora, M. L.; Peng, J.; Shang, D.; Zheng, J.; Du, Z.; Wu, Z.; Shao, M.; Zeng, L.; et al. Elucidating Severe Urban Haze Formation in China. *Proc. Natl. Acad. Sci.* **2014**, *111* (49), 17373–17378.

(8) Wang, G.; Zhang, R.; Gomez, M. E.; Yang, L.; Zamora, M. L.; Hu, M.; Lin, Y.; Peng, J.; Guo, S.; Meng, J.; et al. Persistent Sulfate Formation from London Fog to Chinese Haze. *Proc. Natl. Acad. Sci.* **2016**, *113* (48), 13630–13635. https://doi.org/10.1073/pnas.1616540113.

(9) Park, S.-S.; Jung, S.-A.; Gong, B.-J.; Cho, S.-Y.; Lee, S.-J. Characteristics of PM2. 5 Haze Episodes Revealed by Highly Time-Resolved Measurements at an Air Pollution Monitoring Supersite in Korea. *Aerosol Air Qual. Res.* **2013**, *13* (3), 957–976.

(10) Petetin, H.; Sciare, J.; Bressi, M.; Gros, V.; Rosso, A.; Sanchez, O.; Sarda-Estève, R.; Petit, J.-E.; Beekmann, M. Assessing the Ammonium Nitrate Formation Regime in the Paris Megacity and Its Representation in the CHIMERE Model. *Atmos Chem Phys* **2016**, *16* (16), 10419–10440. https://doi.org/10.5194/acp-16-10419-2016.

(11) Wang, Y.; Yao, L.; Wang, L.; Liu, Z.; Ji, D.; Tang, G.; Zhang, J.; Sun, Y.; Hu, B.; Xin, J. Mechanism for the Formation of the January 2013 Heavy Haze Pollution Episode over Central and Eastern China. *Sci. China Earth Sci.* **2013**, *57* (1), 14–25. https://doi.org/10.1007/s11430-013-4773-4.

(12) Livingston, C.; Rieger, P.; Winer, A. Ammonia Emissions from a Representative in-Use Fleet of Light and Medium-Duty Vehicles in the California South Coast Air Basin. *Atmos. Environ.* **2009**, *43* (21), 3326–3333. https://doi.org/10.1016/j.atmosenv.2009.04.009.

(13) Suarez-Bertoa, R.; Zardini, A. A.; Astorga, C. Ammonia Exhaust Emissions from Spark Ignition Vehicles over the New European Driving Cycle. *Atmos. Environ.* **2014**, *97*, 43–53.

(14) Grenoble, D. C.; Estadt, M. M.; Ollis, D. F. The Chemistry and Catalysis of the Water Gas Shift Reaction. *J. Catal.* **1981**, *67* (1), 90–102. https://doi.org/10.1016/0021-9517(81)90263-3.

(15) Behera, S. N.; Sharma, M.; Aneja, V. P.; Balasubramanian, R. Ammonia in the Atmosphere: A Review on Emission Sources, Atmospheric Chemistry and Deposition on Terrestrial Bodies. *Environ. Sci. Pollut. Res.* **2013**, *20* (11), 8092–8131. https://doi.org/10.1007/s11356-013-2051-9.

(16) Suarez-Bertoa, R.; Zardini, A. A.; Lilova, V.; Meyer, D.; Nakatani, S.; Hibel, F.; Ewers, J.; Clairotte, M.; Hill, L.; Astorga, C. Intercomparison of Real-Time Tailpipe Ammonia Measurements from Vehicles Tested over the New World-Harmonized Light-Duty Vehicle Test Cycle (WLTC). *Environ. Sci. Pollut. Res.* **2015**, *22* (10), 7450–7460. https://doi.org/10.1007/s11356-015-4267-3.

(17) Suarez-Bertoa, R.; Astorga, C. Isocyanic Acid and Ammonia in Vehicle Emissions. *Transp. Res. Part Transp. Environ.* **2016**, *49*, 259–270. https://doi.org/10.1016/j.trd.2016.08.039.

(18) Ministry of Land, Infrastructure, and Transport. Total Registered Motor Vehicles. May 1, 2016.

(19) Geng, H.; Ryu, J. Y.; Maskey, S.; Jung, H.-J.; Ro, C.-U. Characterisation of Individual Aerosol Particles Collected during a Haze Episode in Incheon, Korea Using the Quantitative ED-EPMA Technique. *Atmos Chem Phys* **2011**, *11* (3), 1327–1337. https://doi.org/10.5194/acp-11-1327-2011.

(20) Choi, J. C.; Lee, M.; Chun, Y.; Kim, J.; Oh, S. Chemical Composition and Source Signature of Spring Aerosol in Seoul, Korea. *J. Geophys. Res. Atmospheres* **2001**, *106* (D16), 18067–18074. https://doi.org/10.1029/2001JD900090.

(21) Lee, Y. H.; Choi, Y.; Ghim, Y. S. Classification of Diurnal Patterns of Particulate Inorganic Ions Downwind of Metropolitan Seoul. *Environ. Sci. Pollut. Res.* **2016**, *23* (9), 8917–8928. https://doi.org/10.1007/s11356-016-6125-3.

(22) Babar, Z. B.; Park, J.-H.; Lim, H.-J. Influence of NH3 on Secondary Organic Aerosols from the Ozonolysis and Photooxidation of α-Pinene in a Flow Reactor. *Atmos. Environ.* **2017**, *164*, 71–84. https://doi.org/10.1016/j.atmosenv.2017.05.034.

(23) Lambe, A. T.; Ahern, A. T.; Williams, L. R.; Slowik, J. G.; Wong, J. P. S.; Abbatt, J. P. D.; Brune, W. H.; Ng, N. L.; Wright, J. P.; Croasdale, D. R.; et al. Characterization of Aerosol Photooxidation Flow Reactors: Heterogeneous Oxidation, Secondary Organic Aerosol Formation and Cloud Condensation Nuclei Activity Measurements. *Atmos Meas Tech* **2011**, *4* (3), 445–461. https://doi.org/10.5194/amt-4-445-2011.

(24) Lambe, A. T.; Chhabra, P. S.; Onasch, T. B.; Brune, W. H.; Hunter, J. F.; Kroll, J. H.; Cummings, M. J.; Brogan, J. F.; Parmar, Y.; Worsnop, D. R.; et al. Effect of Oxidant Concentration, Exposure Time, and Seed Particles on Secondary Organic Aerosol Chemical Composition and Yield. *Atmos Chem Phys* **2015**, *15* (6), 3063–3075. https://doi.org/10.5194/acp-15-3063-2015.

(25) Chhabra, P. S.; Lambe, A. T.; Canagaratna, M. R.; Stark, H.; Jayne, J. T.; Onasch, T. B.; Davidovits, P.; Kimmel, J. R.; Worsnop, D. R. Application of High-Resolution Time-of-Flight Chemical Ionization Mass Spectrometry Measurements to Estimate Volatility Distributions of α-Pinene and Naphthalene Oxidation Products. *Atmos Meas Tech* **2015**, *8* (1), 1–18. https://doi.org/10.5194/amt-8-1-2015.

(26) Friedman, B.; Brophy, P.; Brune, W. H.; Farmer, D. K. Anthropogenic Sulfur Perturbations on Biogenic Oxidation: SO2 Additions Impact Gas-Phase OH Oxidation Products of α- and β-Pinene. *Environ. Sci. Technol.* **2016**, *50* (3), 1269–1279. https://doi.org/10.1021/acs.est.5b05010.

(27) Li, R.; Palm, B. B.; Ortega, A. M.; Hlywiak, J.; Hu, W.; Peng, Z.; Day, D. A.; Knote, C.; Brune, W. H.; de Gouw, J. A.; et al. Modeling the Radical Chemistry in an Oxidation Flow Reactor: Radical Formation and Recycling, Sensitivities, and the OH Exposure Estimation Equation. *J. Phys. Chem. A* **2015**, *119* (19), 4418–4432. https://doi.org/10.1021/jp509534k.

(28) Peng, Z.; Day, D. A.; Ortega, A. M.; Palm, B. B.; Hu, W.; Stark, H.; Li, R.; Tsigaridis, K.; Brune, W. H.; Jimenez, J. L. Non-OH Chemistry in Oxidation Flow Reactors for the Study of Atmospheric Chemistry Systematically Examined by Modeling. *Atmos Chem Phys* **2016**, *16* (7), 4283–4305. https://doi.org/10.5194/acp-16-4283-2016.

(29) Peng, Z.; Day, D. A.; Stark, H.; Li, R.; Lee-Taylor, J.; Palm, B. B.; Brune, W. H.; Jimenez, J. L. HOx Radical Chemistry in Oxidation Flow Reactors with Low-Pressure Mercury

Lamps Systematically Examined by Modeling. *Atmos Meas Tech* **2015**, *8* (11), 4863–4890. https://doi.org/10.5194/amt-8-4863-2015.

(30) Jathar, S. H.; Friedman, B.; Galang, A. A.; Link, M. F.; Brophy, P.; Volckens, J.; Eluri, S.; Farmer, D. K. Linking Load, Fuel and Emission Controls to Photochemical Production of Secondary Organic Aerosol from a Diesel Engine. *Environ. Sci. Technol.* **2017**.

(31) Karjalainen, P.; Timonen, H.; Saukko, E.; Kuuluvainen, H.; Saarikoski, S.; Aakko-Saksa, P.; Murtonen, T.; Bloss, M.; Dal Maso, M.; Simonen, P.; et al. Time-Resolved Characterization of Primary Particle Emissions and Secondary Particle Formation from a Modern Gasoline Passenger Car. *Atmos Chem Phys* **2016**, *16* (13), 8559–8570. https://doi.org/10.5194/acp-16-8559-2016.

(32) Link, M. F.; Friedman, B.; Fulgham, R.; Brophy, P.; Galang, A.; Jathar, S. H.; Veres, P.; Roberts, J. M.; Farmer, D. K. Photochemical Processing of Diesel Fuel Emissions as a Large Secondary Source of Isocyanic Acid (HNCO). *Geophys. Res. Lett.* **2016**, *43* (8), 2016GL068207. https://doi.org/10.1002/2016GL068207.

(33) Ortega, A. M.; Day, D. A.; Cubison, M. J.; Brune, W. H.; Bon, D.; de Gouw, J. A.; Jimenez, J. L. Secondary Organic Aerosol Formation and Primary Organic Aerosol Oxidation from Biomass-Burning Smoke in a Flow Reactor during FLAME-3. *Atmospheric Chem. Phys.* **2013**, *13* (22), 11551–11571.

(34) Tkacik, D. S.; Lambe, A. T.; Jathar, S.; Li, X.; Presto, A. A.; Zhao, Y.; Blake, D.; Meinardi, S.; Jayne, J. T.; Croteau, P. L.; et al. Secondary Organic Aerosol Formation from in-Use Motor Vehicle Emissions Using a Potential Aerosol Mass Reactor. *Environ. Sci. Technol.* **2014**, *48* (19), 11235–11242. https://doi.org/10.1021/es502239v.

(35) Middlebrook, A. M.; Bahreini, R.; Jimenez, J. L.; Canagaratna, M. R. Evaluation of Composition-Dependent Collection Efficiencies for the Aerodyne Aerosol Mass Spectrometer Using Field Data. *Aerosol Sci. Technol.* **2012**, *46* (3), 258–271. https://doi.org/10.1080/02786826.2011.620041.

(36) Kuwayama, T.; Collier, S.; Forestieri, S.; Brady, J. M.; Bertram, T. H.; Cappa, C. D.; Zhang, Q.; Kleeman, M. J. Volatility of Primary Organic Aerosol Emitted from Light Duty Gasoline Vehicles. *Environ. Sci. Technol.* **2015**, *49* (3), 1569–1577.

(37) DeCarlo, P. F.; Kimmel, J. R.; Trimborn, A.; Northway, M. J.; Jayne, J. T.; Aiken, A. C.; Gonin, M.; Fuhrer, K.; Horvath, T.; Docherty, K. S.; et al. Field-Deployable, High-Resolution, Time-of-Flight Aerosol Mass Spectrometer. *Anal. Chem.* **2006**, *78* (24), 8281–8289.

(38) Liu, T.; Wang, X.; Hu, Q.; Deng, W.; Zhang, Y.; Ding, X.; Fu, X.; Bernard, F.; Zhang, Z.; Lü, S.; et al. Formation of Secondary Aerosols from Gasoline Vehicle Exhaust When Mixing with SO 2. *Atmospheric Chem. Phys.* **2016**, *16* (2), 675–689.

(39) Nordin, E. Z.; Eriksson, A. C.; Roldin, P.; Nilsson, P. T.; Carlsson, J. E.; Kajos, M. K.; Hellén, H.; Wittbom, C.; Rissler, J.; Löndahl, J.; et al. Secondary Organic Aerosol Formation from Idling Gasoline Passenger Vehicle Emissions Investigated in a Smog Chamber. *Atmos Chem Phys* **2013**, *13* (12), 6101–6116. https://doi.org/10.5194/acp-13-6101-2013.

(40) Liu, T.; Wang, X.; Deng, W.; Zhang, Y.; Chu, B.; Ding, X.; Hu, Q.; He, H.; Hao, J. Role of Ammonia in Forming Secondary Aerosols from Gasoline Vehicle Exhaust. *Sci. China Chem.* **2015**, *58* (9), 1377–1384. https://doi.org/10.1007/s11426-015-5414-x.

(41) Nowak, J. B.; Neuman, J. A.; Bahreini, R.; Middlebrook, A. M.; Holloway, J. S.; McKeen, S. A.; Parrish, D. D.; Ryerson, T. B.; Trainer, M. Ammonia Sources in the California South Coast Air Basin and Their Impact on Ammonium Nitrate Formation. *Geophys. Res. Lett.* **2012**, *39* (7), L07804. https://doi.org/10.1029/2012GL051197.

(42) Heeb, N. V.; Forss, A.-M.; Brühlmann, S.; Lüscher, R.; Saxer, C. J.; Hug, P. Three-Way Catalyst-Induced Formation of Ammonia—velocity- and Acceleration-Dependent Emission Factors. *Atmos. Environ.* **2006**, *40* (31), 5986–5997. https://doi.org/10.1016/j.atmosenv.2005.12.035.

(43) Bishop, G. A.; Peddle, A. M.; Stedman, D. H.; Zhan, T. On-Road Emission Measurements of Reactive Nitrogen Compounds from Three California Cities. *Environ. Sci. Technol.* **2010**, *44* (9), 3616–3620.

(44) Huai, T.; Durbin, T. D.; Miller, J. W.; Pisano, J. T.; Sauer, C. G.; Rhee, S. H.; Norbeck, J. M. Investigation of NH3 Emissions from New Technology Vehicles as a Function of Vehicle Operating Conditions. *Environ. Sci. Technol.* **2003**, *37* (21), 4841–4847.

(45) Meng, Z.; Seinfeld, J. H. Time Scales to Achieve Atmospheric Gas-Aerosol Equilibrium for Volatile Species. *Atmos. Environ.* **1996**, *30* (16), 2889–2900.

(46) Fraser, M. P.; Cass, G. R. Detection of Excess Ammonia Emissions from in-Use Vehicles and the Implications for Fine Particle Control. *Environ. Sci. Technol.* **1998**, *32* (8), 1053–1057.

(47) Markovic, M. Z.; VandenBoer, T. C.; Baker, K. R.; Kelly, J. T.; Murphy, J. G. Measurements and Modeling of the Inorganic Chemical Composition of Fine Particulate Matter and Associated Precursor Gases in California's San Joaquin Valley during CalNex 2010. *J. Geophys. Res. Atmospheres* **2014**, *119* (11), 2013JD021408. https://doi.org/10.1002/2013JD021408.

(48) Chen, D.; Liu, Z.; Fast, J.; Ban, J. Simulations of Sulfate–nitrate–ammonium (SNA) Aerosols during the Extreme Haze Events over Northern China in October 2014. *Atmos Chem Phys* **2016**, *16* (16), 10707–10724. https://doi.org/10.5194/acp-16-10707-2016.

(49) Mezuman, K.; Bauer, S. E.; Tsigaridis, K. Evaluating Secondary Inorganic Aerosols in Three Dimensions. *Atmos Chem Phys* **2016**, *16* (16), 10651–10669. https://doi.org/10.5194/acp-16-10651-2016.

(50) National Institute of Environmental Research. 2013 National Air Pollutants Emission Inventory. December 1, 2015.

(51) Burgard, D. A.; Bishop, G. A.; Stedman, D. H. Remote Sensing of Ammonia and Sulfur Dioxide from on-Road Light Duty Vehicles. *Environ. Sci. Technol.* **2006**, *40* (22), 7018–7022.

(52) Liu, X. G.; Li, J.; Qu, Y.; Han, T.; Hou, L.; Gu, J.; Chen, C.; Yang, Y.; Liu, X.; Yang, T.; et al. Formation and Evolution Mechanism of Regional Haze: A Case Study in the Megacity Beijing, China. *Atmos Chem Phys* **2013**, *13* (9), 4501–4514.

(53) Sun, K.; Tao, L.; Miller, D. J.; Khan, M. A.; Zondlo, M. A. On-Road Ammonia Emissions Characterized by Mobile, Open-Path Measurements. *Environ. Sci. Technol.* **2014**, *48* (7), 3943–3950.

(54) Yao, X.; Hu, Q.; Zhang, L.; Evans, G. J.; Godri, K. J.; Ng, A. C. Is Vehicular Emission a Significant Contributor to Ammonia in the Urban Atmosphere? *Atmos. Environ.* **2013**, *80*, 499–506. https://doi.org/10.1016/j.atmosenv.2013.08.028.

(55) Saylor, R. D.; Edgerton, E. S.; Hartsell, B. E.; Baumann, K.; Hansen, D. A. Continuous Gaseous and Total Ammonia Measurements from the Southeastern Aerosol Research and Characterization (SEARCH) Study. *Atmos. Environ.* **2010**, *44* (38), 4994–5004. https://doi.org/10.1016/j.atmosenv.2010.07.055.

(56) Li, Y.; Schwab, J. J.; Demerjian, K. L. Measurements of Ambient Ammonia Using a Tunable Diode Laser Absorption Spectrometer: Characteristics of Ambient Ammonia Emissions in an Urban Area of New York City. *J. Geophys. Res. Atmospheres* **2006**, *111* (D10).

(57) Lee, T.; Kreidenweis, S. M.; Collett Jr, J. L. Aerosol Ion Characteristics during the Big Bend Regional Aerosol and Visibility Observational Study. *J. Air Waste Manag. Assoc.* **2004**, *54* (5), 585–592.

(58) Li, Y.; Schichtel, B. A.; Walker, J. T.; Schwede, D. B.; Chen, X.; Lehmann, C. M.; Puchalski, M. A.; Gay, D. A.; Collett, J. L. Increasing Importance of Deposition of Reduced Nitrogen in the United States. *Proc. Natl. Acad. Sci.* **2016**, 201525736.

(59) Suarez-Bertoa, R.; Astorga, C. Unregulated Emissions from Light-Duty Hybrid Electric Vehicles. *Atmos. Environ.* **2016**, *136*, 134–143.

CHAPTER 4

LABORATORY STUDIES OF ISOPRENE OXIDATION CANNOT EXPLAIN AMBIENT OBSERVATIONS OF FORMIC AND ACETIC ACID

4.1 Introduction

Formic (HCOOH) and acetic (CH3COOH) acid are the two most abundant gas-phase organic acids in the atmosphere and control important atmospheric processes such as regulation of rainwater pH and gas-particle partitioning.[1,2] In fact, formic acid alone may contribute 30-50% to rainwater acidity in the southeastern United States in the summertime.[3] A recent surge in the interest in atmospheric organic acids is due in part to new instrumentation for both in situ and remote detection that have enabled multiple model-measurement comparisons.[3–6] These comparisons consistently show a missing source of formic and acetic acid, particularly over regions of heavy biogenic influence.[3,5,7,8] This gap in our understanding of organic acid sources is intriguing because organic acids represent a key fate of hydrocarbons emitted into the atmosphere, with potential impacts on aerosol formation.

Secondary chemistry of precursors from biogenically-dominated environments has been singled out as the principle source of formic and acetic acid to the global atmosphere.[5,7,9] Primary emission sources, such as soils or plants, have been repeatedly demonstrated to be insufficient to explain upward formic acid fluxes from forested environments, and instead upward fluxes have been associated with isoprene or monoterpene oxidation.[10–12] Isoprene, emitted mostly from deciduous trees in forested environments, is the most important source of reactive non-methane carbon to the atmosphere and is hypothesized to be a major source of formic acid.[3,13] Lack of targeted laboratory studies of formic and acetic acid formation from isoprene oxidation have

been cited as major reasons why model predictions have not constrained organic acid production from this source well.[7,11]

Extensive ambient measurements of isoprene and isoprene oxidation products were taken during the Southeastern Oxidant and Aerosol Study (SOAS) in the summer of 2013 in Talladega National Forest, an isoprene hotspot, in Alabama. High levels of formic acid were observed during SOAS and exhibited temporal behavior indicative of a rapid photochemical source and depositional sink.[14,15] To understand these observations, the Focused Isoprene eXperiment at the California Institute of Technology (FIXCIT) included a series of chamber experiments to study isoprene oxidation under a variety of SOAS-relevant environmental conditions and oxidants. Here, we present formic and acetic acid yields from these experiments and use models of isoprene oxidation to evaluate potential mechanisms leading to organic acid formation.

4.2 Experimental Methods

4.2.1 Gas-phase oxidation experiments

The FIXCIT study consisted of a series of chamber experiments from January 2-30, 2014 and focused on the OH, O3 and nitrate radical (NO_3) oxidation of isoprene, α-pinene and specific oxidation products of both precursors. A complete overview of the instrumentation suite, experimental design and facilities has been provided elsewhere.[16] The FIXCIT experiments used two 24 m^3 fluorinated ethylene propylene (FEP) Teflon chambers. One chamber was used for "low NO" experiments (< 100 parts-per-trillion (ppt_v)) and the other for "high NO" experiments (NO at parts-per-billion (ppb_v) levels). The primary source of OH was either photolysis of H_2O_2 (for "low NO" conditions) or methyl nitrite (CH_3ONO; for "high NO" conditions). The concentration of OH was ~10^6 molecules cm^{-3} for all OH oxidation experiments except for experiments where low levels of UV lights were used to generate OH. We analyzed OH oxidation experiments such that OH exposure ([OH] x experiment time; molecules s cm^{-3}) was comparable between experiments (Table A3.1). Ozonolysis experiments were initiated with an ozone-to-isoprene ratio between five and seven. Nitrate radical (NO_3) oxidation was performed in the presence of parts-per-million (ppmv) levels of formaldehyde (HCHO) to create conditions where the reaction of HO2 + RO2 would be competitive with NO3 + RO2 and RO2 + RO2.[17] The relative humidity (RH) in the chamber was ~50% for one OH oxidation and two ozonolysis experiments, otherwise experiments were performed in dry (RH < 5%) air. One OH oxidation experiment included the addition of deliquesced $(NH_4)_2SO_4$ seed aerosol (i.e. experiment 19). These experiments are summarized in Table A3.1.

4.2.2 Instrumentation

This study focuses on gas-phase formic acid and acetic acid. Two different chemical ionization mass spectrometers employing CF_3O^- as the reagent ion (CF_3O^- CIMS) measured organic acids during FIXCIT: a time-of-flight CIMS measured formic acid, while a triple-quad CIMS detected isobaric compounds including acetic acid from glycolaldehyde, and differentiated them by their unique fragmentation and ion-clustering patterns.[17–21] The CF_3O^- CIMS were calibrated for the organic acids using neat commercial standards (formic acid, HCOOH, and isotopically-labelled acetic acid, $^{13}CH_3{}^{13}COOH$, both Sigma Aldrich 95-99%) in permeation tubes that were gravimetrically analyzed and kept at a constant (50 °C) temperature. Known flows of the standard compounds were introduced into the CIMS with mass-flow controlled ultra high purity N_2. The sensitivity of formic and acetic acid to chamber relative humidity was corrected by application of a humidity-dependent calibration curve for each compound, performed by introducing known mixing ratios of water vapor into the CIMS flow region along with the commercial standards.

4.2.3 Chamber background subtraction of organic acids

Chamber studies demonstrate that formic and acetic acid are gas-phase oxidation products from biogenic precursors, but they also show that these acids have particularly high backgrounds in chamber experiments.[16,22–25] To minimize this background, the Teflon bags were flushed with purified air with the UV lights on to promote oxidation and desorption of material that had deposited on bags during previous experiments. Despite this overnight cleaning procedure, organic acid production was observed during the "blank" experiments in which clean air was introduced to the bag and the UV lights turned on. To account for these effects, we

consider organic acids produced during the three "blank" experiments as a background that is subtracted for other experiments. For example, most "low NO" OH experiments were conducted with all UV lights on and H_2O_2 photolysis as the OH precursor. To apply a background subtraction to the "low NO" OH experiments for formic acid, we subtract a timeseries of formic acid taken from the "low NO" blank experiment, normalized to start at the mixing ratio immediately before the UV lights were turned on during the actual experiment of interest (Figure 4.1). Backgrounds for "high NO" OH experiments were defined separately for experiments with UV lights at 50% (H_2O_2 OH precursor; Figure A3.1). We employ a regression-based background estimation method for experiments where low UV light intensity (i.e. 1%; CH_3ONO OH source) was used (i.e. "slow chemistry" experiments 7 and 16; Appendix 3.2.2; Figure A3.3).

Experiments with O_3 and NO_3 oxidants were simpler because very little, if any, organic acids were observed when oxidants (and humidified air if applicable) were mixed in the chamber for approximately an hour before introducing the hydrocarbon precursor, indicating negligible influence of chamber artifacts. For these oxidants, we simply subtracted the average organic acid mixing ratio before precursor was introduced from the organic acid timeseries for the entire experiment. Experiment 19 included deliquesced seed aerosol; we assume that the "low NO" OH blank best represents the experimental background for this experiment.

The size of the background subtraction (Figure 4.1) highlights the potential importance of photolysis of surface organic films as potential sources of volatile organic acids.[26]

4.3. Organic acid yields from chamber experiments

4.3.1 Organic acid yields and effects of experimental conditions on production

We define the molar yield of organic acids as the ratio of the background-subtracted mixing ratio of organic acid produced in the experiment with respect to the mixing ratio of hydrocarbon precursor that has been reacted (ppb_v/ppb_v x 100%). We report molar yields for a diverse set of experimental conditions defined by temperature, humidity, oxidant concentration, reaction time, and presence of other trace gases; however, these factors can influence organic acid production by themselves, as evidenced by previous studies.[23,27] We emphasize that yields calculated from laboratory experiments, such as ours, should be interpreted within the constraints of experimental conditions.

4.3.1.1 OH oxidation (experiments 2, 3, 10, 11 and 21)

Oxidation by OH radical is the dominant daytime sink for both isoprene ($\tau_{OH} \approx 2$ hours; 298 K; [OH] = 1.5 x 10^6 molecules cm^{-3}) and α-pinene ($\tau_{OH} \approx$ 3-4 hours; 298 K; [OH] = 1.5 x 10^6 molecules cm^{-3}). Several of the oxidation products from isoprene also have lifetimes with respect to OH oxidation on the order of hours, and we thus expect multiple generations of oxidation products to occur during the multiple hour-long chamber experiments. In the initial stages of OH oxidation, peroxyl radicals (ISOPOO) form from addition of oxygen to an allylic radical. The subsequent oxidation products are determined through specific bi- and uni-molecular RO_2 reaction pathways.

The chamber data clearly show that NO influences organic acid yields from isoprene oxidation. OH oxidation experiments encompassed a range of NO:HO_2 ratios to control the fate of RO_2. In the isoprene "low NO" experiments (i.e. NO:HO_2 ratio < 0.5), HO_2 preferentially

reacts with RO_2 to form characteristic products like isoprene hydroxy hydroperoxides (ISOPOOH) and isoprene epoxydiols (IEPOX). For reference, at NO:HO_2 ratios of ~1, the rate of RO_2 reaction with HO_2 should be approximately twice as fast as with NO. Three of the experiments (OH oxidation of IEPOX and "slow" OH oxidation of isoprene and α-pinene) were performed under conditions of "moderate NO" with NO:HO_2 ratios of 2-4. Under these conditions, NO reaction with RO_2 may be equal or slightly more competitive than HO_2, though this depends on the structure of the RO_2. For experiments where the ratio of NO:HO_2 was >100 ("high NO"), the fate of RO_2 is determined almost exclusively through reaction with NO. In the case of isoprene-derived RO_2, H-shift isomerization reactions have been shown to be competitive with RO_2 bimolecular reactions.

Increasing NO suppresses organic acid yields during OH oxidation of isoprene, suggesting that it is the RO_2 reaction pathways involving HO_2, RO_2 or H-shift isomerization that dominantly produce organic acids consistent with the findings of Paulot et al (2009). MACR oxidation is consistent, with higher formic acid yields under "low NO" than "high NO" conditions – and no acetic acid produced during high NO experiments. The "low NO" oxidation of 4,3-ISOPOOH produced a factor of four lower formic acid yields than the "low NO" isoprene oxidation experiment, suggesting that first generation isoprene products other than 4,3-ISOPOOH are the precursors for organic acids. There are two ISOPOOH isomers, and it is possible that the major isomer, the 1,2-ISOPOOH, is a substantial organic acid precursor, although the 4,3-ISOPOOH isomer is clearly not. Besides ISOPOOH, other first-generation products from isoprene + OH chemistry include hydroperoxy enals (HPALDs) from the isomerization pathway or products from RO_2 self-termination reactions. The relatively high yield

from the “moderate NO” oxidation of IEPOX suggests that IEPOX may be an important formic acid precursor under “high NO” conditions when all other sources of formic acid are low.

In contrast to isoprene, α-pinene does not show a substantial influence of NO on organic acid yields. However, organic acid production from OH oxidation of α-pinene is relatively low compared to isoprene, and we focus on isoprene sources of formic and acetic acids.

One intriguing pair of experiments subjected two different isoprene concentrations (42 vs 21 ppb_v) to otherwise identical “low NO” OH oxidation (i.e. identical amounts of OH exposure). Decreasing the hydrocarbon precursor concentrations increased the lifetime of RO_2 with respect to self-termination reactions. RO_2 termination pathways should thus be more influenced by reaction with HO_2 or isomerization pathways than RO_2 self-reaction. The experiment with half the isoprene precursor resulted in nearly double the formic acid yield (i.e. 12% vs 7%) – but acetic acid never exceeded background concentrations. These observations suggest that RO_2 + RO_2 are not sources of formic acid but are instead sources of acetic acid.

4.3.1.1.1 “Slow” OH oxidation (experiments 7 and 16)

When RO_2 bimolecular lifetimes are long (~100 s), recent modeling and measurement studies have determined that first-generation isoprene OH-adduct RO_2 (i.e. ISOPOO) can react through isomerization to produce isoprene hydroperoxy enals (HPALDs; $C_5H_8O_3$; yield = 25-40%), and other products, at a rate competitive with bimolecular reactions.[28–30] Extending RO_2 lifetimes in chamber studies to reach this regime is challenging.[16,31] Because of the reversible nature of oxygen addition to form ISOPOO, extending the ISOPOO lifetime likely brings this RO_2 population closer to the equilibrium distribution, thereby producing compounds more relevant to pristine ambient environments.[32]

Long RO_2 lifetimes were achieved during FIXCIT using very low levels of NO and HO_2 radicals for OH oxidation of isoprene (the "slow, moderate NO" experiment; low NO, low HO_2). Because ISOPOOH is exclusively produced from reaction of ISOPOO with HO_2, comparing the ratio of ISOPOOH to HPALD mixing ratios should demonstrate the efficacy of ISOPOO isomerization in this "slow" oxidation experiment relative to the standard "low NO" experiment. The average ratio of ISOPOOH to HPALD was lower for the "slow, low NO" experiment (1.5 ± 0.1) than for the standard "low NO" experiment (10.6 ± 1.8), suggesting that ISOPOO isomerization was indeed occurring. The yields of formic (17.5%) and acetic (4.3%) acids were much higher in this slow, low NO experiment compared to the standard "low NO" experiment (Figures 4.3 and A3.4). This highlights the importance of isomerization in isoprene oxidation and the subsequent production of organic acids. This result is consistent with observations of high concentrations of organic acids in forest environments with low anthropogenic influence, where RO_2 isomerization is considered important.[9,11,14]

Unimolecular processes representative of "slow" chemistry are poorly understood for monoterpenes compared to isoprene. Isomerization of monoterpene-derived RO_2 has been determined to be competitive with bimolecular reactions based on observations of highly oxidized molecules formed from autooxidation.[33,34] The rates of these reactions, however, have not been well quantified.[28,35] Xu et al[36] recently measured the isomerization rate of first-generation RO_2 resulting from the 4-member ring-opening of α-pinene to be $4 \pm 2\ s^{-1}$, suggesting that these processes are competitive or faster than other monoterpene-derived RO_2 fates. In one experiment, we oxidized α-pinene with OH under low UV light intensity to extend RO_2 lifetimes and explore the effects of isomerization on RO_2 termination ("slow, moderate NO α-pinene"). In this experiment, we also observed high yields of formic (14.5%) and acetic (5.5%) acid (Figure

A3.4). Isomerization of α-pinene RO_2 could be an important source of organic acids in monoterpene-dominated environments, though further experiments with appropriate controls are essential.

4.3.1.2 O_3 oxidation (experiments 6, 14, 23, and 29)

The lifetime of isoprene with respect to ozonolysis in the atmosphere is ~22 hours at [O_3] = 40 ppb_v, longer than for OH radicals. However, ozonolysis is an important source of HO_x in forested environments and accounts for ~10% isoprene removal from the atmosphere globally.[37–39] Isoprene ozonolysis produces formic acid through the reaction of the stabilized Criegee intermediate (sCI; Figure 4.4) with water vapor monomers and dimers to form hydroxymethylhydroperoxide (HMHP), which either heterogeneously decomposes or reacts with OH to produce formic acid.[19,40] However, recent studies reevaluated the role of HMHP as an intermediate in the production of formic acid, finding that less formic acid is produced from the direct reaction of sCI with water than previously thought.[19,41] In contrast to formic acid, sCIs have been suggested to be an inefficient source of acetic acid though the kinetics of this reaction pathway are still uncertain.[42]

During FIXCIT, isoprene was oxidized with ozone in both the presence and absence of an OH scavenger (cyclohexane), and under both dry and humid conditions. In the experiments without the OH scavenger, OH concentrations were ~10^6 molecules cm^{-3} and were comparable to levels observed during OH oxidation experiments. Including the cyclohexane scavenger decreased yields of both formic and acetic acid relative to comparable experiments without the scavenger. This result is consistent with the findings of a recent study by Sheps et al.[41] showing that the sole products of the simplest sCI (CH_2OO) with water were formaldehyde and HMHP (<

10% yield of formic acid) which reacts with OH ($k_{HMHP+OH}$ = 7.1 x 10^{-12} cm^3 s^{-1}) to produce formic acid in high yield (45%).[19] Previous studies attributed formic acid produced in ozonolysis experiments to heterogenous decomposition of ozonolysis products on chamber walls or within sampling apparatus.[40,43] Laser induced florescence (LIF) detection of formaldehyde noted an interference during HMHP oxidation, presumably due to surface chemistry on instrument walls.[19] We hypothesize that if formic acid was formed as an instrumental artifact from HMHP, it would form from homolytic cleavage of the peroxy bond in HMHP catalyzed by the metals of the instrument surface in a mechanism similar to that proposed by Rivera-Rios et al.[20] However, the resulting alkoxy radical might be expected to decompose to formaldehyde and an OH radical, so decomposition of HMHP on the walls may not be a source of formic acid. Further work should characterize peroxide decomposition on instrument surfaces to investigate whether this is a source of formic acid.

Formic acid yields were six times higher (and acetic acid two times higher) in humid experiments relative to dry (<5% RH) conditions, consistent with sCI reacting with water molecules to produce formic acid. Rate constants for the reaction of water vapor monomers and dimers with sCI vary across three orders of magnitude in the literature, resulting in very different estimates of the importance of water monomers versus dimers in determining the fate of sCI in the atmosphere.[9,41,44–46] Nonetheless, the FIXCIT experiments demonstrate that organic acid production from ozonolysis of isoprene may be competitive with OH oxidation in many areas of the world where daytime humidity levels can be close to or exceed 50%.

4.3.1.3 NO_3 oxidation (experiment 9)

Reaction with NO_3 radical comprises ~5-6% of the chemical sink for isoprene globally.[44] Despite its potential importance, there are no reported yields for organic acids from NO_3 oxidation of isoprene or α-pinene, to the best of our knowledge. After estimating the contribution of O_3 oxidation of isoprene to organic acid yields (section A3.3.2; Figure 4.5)—and subtracting out the modeled contribution from the reaction of HO_2 with HCHO for formic acid—we observed a yield of 1.9% of acetic acid and no significant formic acid production from the Isoprene + NO_3 experiment.

4.3.1.4 Oxidation through photolysis (experiments 7 and 16)

HPALDs and dihydroperoxy carbonyls (DHP) are potentially important sources of formic acid in the "low NO" and "slow" isoprene oxidation experiments. These oxidation products are formed from the 1,6-H shift isomerization of isoprene hydroxyperoxyl radicals (ISOPOO). If the rate to form HPALDs and DHPs is competitive with the bimolecular lifetime of ISOPOO, then decomposition, photolysis or OH-reaction of these isomerization products could be a source of organic acids. The rates of formation of HPALDs are uncertain – in part because of the strong temperature dependences in both the 1,6-H shift and the equilibrium between allylic radicals and ISOPOO, and because the propensity for isoprene to form HPALDs depends on whether OH addition occurs at the C1 or C4.[44] Additionally, several other major oxidation products have been observed to be formed from the 1,6-H shift isomerization of ISOPOO, in addition to HPALDs, however, the branching ratios and identities of these products are still an active area of research.[30,47]

After ~1.5 ppb_v of HPALDs were formed in the "slow" isoprene experiment, the UV intensity was increased and combined photolysis and OH reaction of the resulting HPALD compounds occurred over the course of two hours (OH exposure ~3 x 10^{10} molecules s cm^{-3}). Despite the OH exposure being a little less than half of the exposure determined for the standard "low NO" experiment, combined photolysis and OH reaction of HPALDs, and associated compounds, produced high mixing ratios of formic and, albeit to a lesser extent, acetic acid (Figure 4.3) in this HPALD photolysis experiment. This observation indicates that photolysis and OH reaction of HPALDS, and compounds produced from the ISOPOO H-shift isomerization pathway, are likely important contributors to formic acid production from OH oxidation of isoprene.

While 10 ppb_v of isoprene was still present when the UV lights were turned on to high intensity, this isoprene is likely only a minor source of formic acid from the HPALD + photolysis experiment. Assuming a 7% yield of formic acid from isoprene, based on the standard low NO experiment, oxidation of isoprene would only produce ~0.7 ppb_v formic acid. The final mixing ratio of formic acid produced in this slow HPALD experiment would then be 5.3 ppb_v. This implies that 70% of the carbon associated with HPALDs would have to be converted to formic acid. This is highly unlikely since there are no reactions currently known that produce this high of a carbon-equivalent yield of formic acid. It's likely that including isomerization co-products such as $C_5H_8O_4$ and $C_4H_8O_5$ into the carbon-balance described here would decrease the estimated yield of formic acid from HPALDs though because HPALDs are the major product the yield would likely still be unusually high. An uncertain influence on the results from this experiment are the potential oxidation reactions involving vapors lost on the walls of the chamber during the "slow chemistry" portion of the experiment. Oxidation of organic films on

chamber walls are likely sources of persistent formic and acetic acid backgrounds and could artificially enhance observed formic acid production in this experiment. Controlling for this experimental artifact is necessary for accurate interpretation of results from future experiments. Taking this into consideration we hypothesize that oxidation and/or photolysis of isomerization products of ISOPOO are important sources of formic acid in these experiments.

High mixing ratios of organic acids were also observed from the combined photolysis and OH oxidation of "slow chemistry" products from α-pinene (Figure A3.6). Isomerization products from α-pinene OH oxidation are potentially important precursors of organic acids. The products of first-generation α-pinene RO_2 are expected to be multi-functional compounds containing peroxide, carbonyl and nitrate functionalities.[36] These oxidation products are subject to competitive fates between particle partitioning, oxidation and photolysis. In the ambient, where isomerization processes are competitive with bimolecular RO_2 fates, daytime oxidation of monoterpene isomerization products could be a source of organic acids.

4.3.1.5 Influence of seed aerosol (experiment 19)

Studies attempting to modify existing gas-phase chemical mechanisms to improve model-measurement agreement for formic acid in the ambient atmosphere consistently fail to capture the daytime source.[48–50] Heterogenous reactions – reactions between the gas and condensed phase surface —produce organic acids in the lab, and have been invoked to explain elevated formic and acetic acid levels in the Arctic.[51–53] Indeed, the challenge of background subtraction in the FIXCIT chamber experiments must be the result of heterogeneous reactions or photolysis of organic films![26] In one FIXCIT experiment, isoprene was oxidized in the presence of deliquesced ammonium sulfate aerosol ('seed aerosol experiment'). Because the conditions of

the ‘seed aerosol experiment’ closely mimic the conditions of the “low NO” isoprene + OH experiment, we can compare organic acid yields from the two experiments. Seed aerosol clearly induces much higher organic acid yields (estimated yield from isoprene, 19% for formic acid and 7% for acetic acid), suggesting that heterogenous or aqueous processes involving either the aerosol or the walls of the chamber are important organic acid sources. However, we note that background subtraction was only done in the absence of seed aerosol, so this effect may be due, at least in part, to residual organics on the walls. Accounting for gas-phase OH oxidation of isoprene and ISOPOOH to form organic acids from the isoprene + OH “low NO” and ISOPOOH + OH “low NO” experiments, we calculate that gas-phase OH oxidation accounts for only 40% of the observed mixing ratios (Figure A3.7). We caution that the high (~2 ppm_v) levels of H_2O_2 included in the experiment serving as the gas-phase OH source could also partition into the aqueous aerosol and photolyze to produce OH. This would artificially enhance OH oxidation processes in the aqueous phase that are likely not relevant for the ambient atmosphere. Oxidation processes mediated by deliquesced aerosol or humidified chamber walls must contribute the remaining organic acid production but require further experiments to quantify and isolate specific sources or mechanisms.

4.3.2 Investigating missing sources of organic acid production

The chamber experiments enable identification of specific points in the isoprene oxidation mechanism where organic acids must be produced in significant quantities. In particular, we focus on the experiments where MACR, ISOPOOH and IEPOX were oxidized by OH to help inform how organic acid production from these oxidation products influenced organic acid production from the parent hydrocarbon isoprene.

We investigate organic acid formation chemistry using the Framework for 0-D Atmospheric Modeling (F0AM) v3.1 (MATLAB R2018b) equipped with three different isoprene oxidation mechanisms: (1) the Master Chemical Mechanism v3.3.1 (MCM), (2) the Wennberg Reduced+ semi-explicit mechanism (WR+), and (3) the Model of Atmospheric composition at Global and Regional scales using Inversion Techniques for Trace gas Emissions (MAGRITTE v1.1).[44,54,55] This setup allows us to test the sensitivity of organic acid production to reported mechanistic differences in isoprene oxidation. MCM is based on the work of Jenkin, et al[55] and contains 610 species and 1974 reactions. MCM is a near-explicit, comprehensive mechanism that includes reactions that are very slow (on atmospherically relevant timescales) and very fast (i.e. alkoxy radical decomposition) and reactions with low product yields. Importantly, MCM groups RO_2 as a single species that reacts indiscriminately with other RO_2 to simulate the effects of peroxy radical self-termination pathways. Wennberg, et al[44] summarized most of the theoretical and laboratory work on isoprene oxidation into the WR+.[28] The WR+ mechanism contains 155 species and 429 reactions and builds upon the mechanistic architecture presented in the MCM by modifying RO_2 + NO branching ratios, updating H-shift isomerization reactions, and explicitly including reaction products with ≥1% overall yield from isoprene. The MAGRITTE mechanism builds upon the Leuven Isoprene Mechanism, the Wennberg mechanism and the MCM. Unique features of MAGRITTE include incorporation of findings from recent laboratory work analyzing OH-oxidation of isoprene under conditions of low NO and HO_2 mixing ratios, photolysis of hydroperoxycarbonyls to produce enols and keto-enols that rapidly react with OH, and a reassessment of the influence of stabilized Criegee intermediates (sCI) in the formation of formic acid.[19,30,41,56,57] Specific differences between the mechanisms relevant to these experiments are in the supplemental information (section A3.4).

Below, we describe model experiments in which we modify the "base case" mechanisms to account for likely important sources of formic and acetic acid. These modifications include addition of the reaction of HCHO + HO_2 that forms formic acid, updates to the quantum yield for the photo-tautomerization of acetaldehyde to vinyl alcohol, and inclusion of OH oxidation of vinyl alcohol to formic acid with a 14% yield.[39,48,50,58,59] We follow the findings of Assaf et al (2017) who determined the reaction of OH with CH_3O_2 produced a Criegee intermediate with <5% yield and thus this reaction is not included in the mechanisms as a potential source of formic acid.[60,61] Base case model simulations of organic acids during the isoprene oxidation experiments predicted yields orders of magnitude lower than observed (Table A3.2). Some mechanisms performed better than others for different experiments. We increased organic acid yields on specific RO_2 reactions to improve organic acid model-measurement agreement, first working with MACR, then IEPOX, then ISOPOOH. We do not retain carbon-balance when applying modifications to the mechanisms, so the yields applied here are only to test the sensitivity of various oxidation pathways to organic acid production from isoprene and how that reflects on the potential importance of isoprene as an organic acid source in the ambient atmosphere.

4.3.2.1 MACR + OH

The lifetime of MACR with respect to OH oxidation is ~9 hours (T = 298K; [OH] = 1.5 x 10^6 molecules cm^{-3}). OH oxidation via OH-addition to the double bond and H-abstraction occur at nearly the same rate. The dominant fate (for ambient and chamber conditions) of the major (MACRO2) and minor (MACROHO2) yield RO_2 from OH addition is H-shift isomerization (Figure 4.5), which produces OH, CO, hydroxyacetone and hydroperoxyacetone. The RO_2 produced from H-abstraction of the aldehydic hydrogen (MACO3) mostly undergoes reaction

with HO_2 or NO, although the mechanisms and kinetics of RO_2 self-reactions are not well constrained.[44]

4.3.2.1.1 MACR + OH "low NO"

In the "low NO" OH-oxidation of MACR the MACRO2 radical undergoes fast isomerization (>90% MCM predicted) and the MACO3 radical is mostly terminated by reaction with HO_2.[62] Because the isomerization of MACRO2 is so rapid, we predict the likely pathway for both formic and acetic acid production in this experiment is from HO_2 reaction with MACO3. We note, however, if formic acid was a minor co-product of the isomerization channel this could also be a contributing source. For the mechanisms considered here, the kinetics of the reaction of MACO3 with HO_2 follows the IUPAC recommendation and the mechanism is modeled after the reaction of $CH_3C(O)O_2$ radical with HO_2.[63] The products of that reaction are predicted to be an acid, a peroxy acid and an acyl oxy radical in a proportion of 0.13:0.37:0.60 (Figure 4.5).[44] The acyl oxy radical that is produced rapidly decomposes to formaldehyde, CO, CH_3O_2 and $C_2H_3O_3$.

To improve model-measurement agreement for organic acid production from this pathway we prescribe variable molar yields (mechanism dependent, Table A3.3) for the organic acids from the MACO3 + HO_2 pathway (Figure A3.8) and assert this is likely associated with decomposition of the acyl oxy radical. These changes account for 15-20% of formic and acetic acid predicted from the isoprene + OH "low NO" experiment.

4.3.2.1.2 MACR + OH "high NO"

The primary fate of MACR-derived RO_2 in the "high NO" experiment is reaction with NO. Through these reactions RO_2 form alkoxy radicals that then rapidly decompose to products such as hydroxyacetone, CH_3O_2, and CH_3CO_3 radicals.

We prescribe yields of formic acid to the MACRO2 + NO pathway to bring model prediction into agreement with measurements (mechanism dependent, Table A3.3) from the MACR + OH "high NO" experiment (Figure A3.10). No acetic acid was measured in mixing ratios that exceeded the background for this experiment. Accordingly, we did not modify any mechanism to include a yield of acetic acid. Some acetic and formic acid production predicted from the mechanism is associated with low levels of HO_2 production and the associated MACO3 termination by HO_2 (see section 4.3.3.1.1). These changes account for ~30% of the measured formic acid from the isoprene + OH "high NO" experiment (Figure A3.10).

4.3.2.2 IEPOX + OH "moderate NO"

The lifetime of IEPOX with respect to OH oxidation is 24 hours (T = 298K; [OH] = 1.5 x 10^6 molecules cm^{-3}).[22] Oxidation of IEPOX by OH occurs via H-abstraction at the 1, 3 or 4 carbon (Figure 4.6). Oxygen adds to the alkyl radicals producing three RO_2, two of which produce ring-retaining isoprene carbonyl hydroxy epoxide species as minor yield products (~10-20% yield from IEPOX oxidation).[22,64] The primary fate for the RO_2 is isomerization resulting in the opening of the epoxide ring to form dihydroxy carbonyl peroxyl radicals. The fate of these radicals is highly uncertain because of varied observations from only a few studies. The IEPOX + OH experiment from FIXCIT was performed under condition where the NO:HO_2 ratio was ≈ 5, and thus we assume that organic acid production originates from termination of these RO_2 by NO.

Formic acid was produced with a yield of 14% (wall-loss corrected) from the IEPOX + OH experiment whereas acetic acid was not observed in levels that exceeded background. Because IEPOX was being lost to the wall during the experiment we cannot rule out

heterogenous wall-processes as a potential source of formic acid, however here we assume that all the formic acid was produced from gas-phase oxidation of IEPOX. Potentially due to the challenges in quantifying IEPOX, no models could reproduce the experimentally observed decay of IEPOX from oxidation (Figure A3.11). To match observed formic acid yields to model predictions we adjust formic acid yields in the model such that the model-predicted yields match the experimentally observed yield (Figure A3.12).

We attribute variable yields of formic acid to the RO_2 + NO reaction channel associated with one of the first generation RO_2 produced in the highest yield from IEPOX oxidation. Many bimolecular reactions of the IEPOX first generation RO_2 produce molecules reactive to OH and subject to photolysis such as glycolaldehyde, glyoxal, and methylglyoxal that are potential sources of organic acids. Dihydroxy butanone is also a high yield product from IEPOX + OH oxidation that itself reacts with OH and produces dicarbonyls that are likely sources of organic acids from photolysis analogous to the case of pyruvic acid photolysis.[24,65] The uncertainties associated with the kinetics and mechanisms of gas-phase oxidation of IEPOX prevent us from determining exactly where in the oxidation ladder formic acid is produced, but we assign the yields (mechanism dependent, Table A3.3) to test the sensitivity of formic acid production from isoprene to the IEPOX + OH source.

4.3.2.3 ISOPOOH + OH "low NO"

ISOPOOH reacts with OH (lifetime ~3 hours; T = 298K; [OH] = 1.5 x 10^6 molecules cm^{-3}) through a major OH-addition channel (~85% yield) and a minor H-abstraction channel (~15% yield) (Figure 4.7). The major product of the OH-addition channel is IEPOX. Minor products from the OH-addition channel are produced from bimolecular and isomerization reactions of the non-IEPOX forming RO_2. Yields and product distributions resulting from reactions of these RO_2

have been mostly characterized in complementary studies by Paulot et al and St Clair et al.[66,67] Neither study reported significant yields of organic acids. St. Clair et al note that ~15% of the OH-addition yield from ISOPOOH + OH under conditions of "low NO" results in a variety of low-volatility products whose likely fates include photolysis. Photolysis of these compounds likely result in fragmentation processes that potentially could be a source of organic acids.

During FIXCIT 4,3-ISOPOOH was oxidized with OH under conditions of "low NO". Similar to the difficulties experienced in modeling IEPOX decay, the models could not reproduce the experimentally observed decay of ISOPOOH from oxidation (Figure A3.13). We modified ISOPOOH oxidation mechanisms such that the model-predicted formic acid yields match the experimentally observed yield.

Formic acid was produced with a yield of 2% from the ISOPOOH + OH experiment whereas acetic acid was not observed in levels that exceeded background (Figure 4.2). Both the MCM and WR+ mechanisms predict very low mixing ratios of formic acid produced from the ISOPOOH + OH reaction (Figure A3.14; Table A3.2). The MAGRITTE mechanism predicts that, upon abstraction of the hydroxy-α-H, an unsaturated hydroxy aldehyde forms whose primary fate is rapid photolysis to form an enol that then reacts with OH to form formic acid. The MAGRITTE mechanism over-predicts formic acid production by almost 50% but is still within the bounds of error for the measurement. We follow the suggestions of Müller et al[9] and apply yields of formic acid in the MCM and WR+ mechanisms to the ISOPOOH + OH H-abstraction reaction to bring model prediction into agreement with the measurement. We don't apply an experimentally-determined formic acid yield to ISOPOOH oxidation in the MAGRITTE mechanism.

4.3.2.4 Isoprene + OH

The OH oxidation of isoprene occurs via OH-addition to carbons 1 and 4 in a ratio of 63:37 with addition to the central carbons making uncertain, but minor contributions to the total reactivity to OH. Upon OH addition a pool of allyic radicals are formed that then produce six major RO_2 (ISOPOO). Because of the reversibility of oxygen addition to ISOPOO, it has been suggested that the distribution of the six major ISOPOO is different in laboratory studies compared to the population in the atmosphere which is expected to be closer to thermal equilibrium.[68,69] Here we apply the modified isoprene oxidation mechanisms to two experiments of OH + isoprene performed under conditions of "low" and "high NO" (experiments 2 and 3, respectively).

4.3.2.4.1 Isoprene + OH "low NO"

The primary fate (>90%) of ISOPOO in the isoprene + OH "low NO" experiment was reaction with HO_2 and formed ISOPOOH as a major product. Subsequent reactions of isoprene oxidation products in the "low NO" environment promote the formation of multi-functional compounds, such as peroxy or hydroxy carbonyls, that are reactive towards OH or susceptible to photolysis. As discussed in section 4.3.2.1, during FIXCIT the "low NO" OH-oxidation experiments produced higher yields of organic acids from isoprene oxidation compared to the "high NO" pathways. This observation suggests oxidation of compounds formed from this isoprene + OH pathway is likely the most important source of organic acids from isoprene oxidation in the atmosphere.

All the mechanisms tested predict that formic and acetic acid mixing ratios from the isoprene + OH "low NO" experiment that fall within 50% of one another (Figure 4.8; Table

A3.2). The MAGRITTE mechanism predicts mixing ratios that most closely agree with observations from the experiment. More than 50% of the formic acid predicted in all mechanisms comes from the modified yields to MACR and ISOPOOH informed by the FIXCIT experiments. The rest of the formic acid predicted from WR+ and the MCM comes from chemistry involving sCIs. In contrast, the MAGRITTE mechanism is informed by work that does not support a high direct yield of formic acid from the reaction of sCIs with water and thus predicts low contributions of formic acid from this pathway.[41] MAGRITTE does, however, predict significant yields (20% for 4,1-ISOPOOH and 32% for 4,3-ISOPOOH) of formic acid from photolysis and OH oxidation of products formed from the H-abstraction channel of ISOPOOH OH oxidation. All the mechanisms predict that more than 50% of the acetic acid produced comes from the termination of the $CH_3C(O)O_2$ radical by HO_2 with significant contributions from the termination of MACO3 by HO_2. The MAGRITTE mechanism predicts more acetic acid than the other two mechanisms because of the inclusion of reactions that form methyl vinyl alcohol that reacts with OH to form acetic acid.

Few studies have looked at formic or acetic acid production from OH oxidation of isoprene, so we don't have reported literature values to apply modified yields of acids to major isoprene oxidation products that were not part of experiments performed during FIXCIT such as methyl vinyl ketone. To close the gap between measurement and model predictions, we apply a yield of formic acid to the photolysis of the HPALD compounds. High yields of both formic and acetic acid were observed during the HPALD photolysis experiment (section 4.3.2.3) and provide experimentally-determined justification for applying yields to the reactions in the models to test the sensitivity of formic acid production from isoprene from the "low NO" oxidation pathway. We emphasize that the yields applied to this HPALD photolysis pathway in the model

are applied to only close the gap between modeled formic acid and measured formic acid in the isoprene + OH "low NO" experiment. We apply a yield of formic acid from HPALD photolysis reflecting the production of three moles of formic acid per mole of HPALD photolyzed (Table A3.3) which is likely not realistic (Figures A3.15 and A3.16). Further detailed mechanistic studies are needed to accurately quantify organic acid production from isoprene oxidation products.

4.3.2.4.2 Isoprene + OH "high NO"

In the isoprene + OH "high NO" experiment, ISOPOO termination was dominated by reaction with NO. Major products from the reaction of ISOPOO with NO include isoprene hydroxy nitrates, unsaturated isoprene hydroxy carbonyls, MACR and MVK. Peeters et al.[69] note, however, that the population of ISOPOO produced in chamber experiments is kinetically determined by the decrease in the bimolecular lifetime of ISOPOO as a result of very high levels of NO in the experiments. Accordingly, the yields of products from the termination of ISOPOO by NO are very sensitive to the ISOPOO distribution. Extracting mechanistic detail from chamber experiments of the OH oxidation of isoprene using high levels of NO are challenged by this chemistry.

The yields of formic and acetic acid observed from the "high NO" oxidation of isoprene were approximately half of those observed in the "low NO" oxidation experiment. All the mechanisms used to model the "high NO" experiment predict similar levels of production of formic and acetic acid (Figure 4.8). All the mechanisms capture ~50% of the formic acid, but < 5% of the acetic acid. The WR+ predicts significant formic acid production from OH oxidation of an MVK hydroxy nitrate, and all the models predict only minor contributions from

termination of the first-generation IEPOX RO_2 by NO. MAGRITTE predicted the highest levels of acetic acid mostly because of the reaction of methyl vinyl alcohol with OH, which is unique to the mechanism.

The study of Paulot et al.[17] observed high yields of formic and acetic acid (10% and 3%, respectively) compared to this study. However, Paulot et al's yields agree very well with the yields observed in this study before background subtraction was applied – suggesting that Paulot et al's yields were overestimates. Most of the observed formic acid in that previous work was attributed to decomposition of a first-generation isoprene hydroxy nitrate (ISOPN) and OH oxidation of glycolaldehyde. 4,3-ISOPN was oxidized with OH during FIXCIT, but the experiment does not provide clear evidence for a source of formic acid. Additionally, modeling OH oxidation experiments with modifications to include formic acid production from glycolaldehyde show small (<5%) contributions from this source to predicted formic acid production. Unlike Paulot et al's study, the results from the FIXCIT experiments do not support the conclusion that the major source of acetic acid in the OH oxidation of isoprene under "high NO" conditions is hydroxyacetone. In the MACR + OH "high NO" experiment, acetic acid was not produced in levels that convincingly exceeded background. The modeling of acetic acid production from this "high NO" experiment included an acetic acid yield from hydroxyacetone. The model overpredicted acetic acid production (Figure A3.10), suggesting hydroxyacetone might not be an important source of acetic acid – a conclusion similar to Butkovskaya et al.[70] In light of these discrepancies between literature reports and this work, we do not at add any modifications to the isoprene oxidation mechanisms to close the gap between model predicted and measured formic and acetic acid for the isoprene + OH "high NO" experiment.

4.3.2.5 Effects of including formic acid source from hydroxyacetone and glycolaldehyde

The above experiments from FIXCIT demonstrated that organic acids are produced within the ensemble of reactions that occur from OH oxidation of major isoprene oxidation products. Millet et al. (2015) reported that the magnitude of formic acid produced in global simulations was reduced by one third when removing a formic acid source from OH oxidation of hydroxyacetone and glycolaldehyde originating from isoprene oxidation. We added in specific modifications to the unadulterated chemical mechanisms to assess the importance of hydroxyacetone and glycolaldehyde as primary sources of organic acids.

Hydroxyacetone is a major later-generation oxidation product from isoprene oxidation. The lifetime of hydroxyacetone with respect to OH oxidation (T= 298K; [OH] = 10^6 molecules cm^{-3}) is 2 days. The reaction of hydroxyacetone with OH produces methylglyoxal in high yield at 298K; yields of formic and acetic acid increase at lower temperatures.[70] Previous work has not observed formic acid production from hydroxyacetone at atmospherically relevant concentrations of NO_x, although these results have not been formally published.[71] To estimate the importance of this primary source of organic acids, we apply a yield of 20% for both formic and acetic acid to the hydroxyacetone + OH reaction. This 20% yield is at the upper end of yields reported by Butkovskaya et al.[70] For the MACR + OH "low NO" experiment, hydroxyacetone was a major (> 60%) contributor to the modeled production of both formic and acetic acid. On the other hand, all the mechanisms overpredicted hydroxyacetone production by more than 100% (Figure A3.9). We do not include the yields of formic and acetic acids from hydroxyacetone oxidation in the final iterations of mechanisms used for modeling in this study, but more studies measuring oxidation products from oxidation of hydroxyacetone are warranted.

A companion study from Butkovskaya, et al[72] reported a yield of 18 ± 6% formic acid from OH oxidation of glycolaldehyde. The lifetime of glycolaldehyde with respect to OH oxidation is 1.2 days. We apply a yield of 15% to the glycolaldehyde + OH reaction to test the sensitivity of formic acid production from this reaction. In the modeling of the reaction of isoprene + OH the production of formic acid from OH oxidation of glycolaldehyde accounts for <1% of the predicted yield of formic acid. We also note that glycolaldehyde undergoes photo-tautomerization to 1,2-ethenediol which reacts with OH to produce formic acid with a predicted yield of 4%.[73] The lifetime of 1,2-ethenediol with respect to OH oxidation is ~68 hours so we also do not expect this to be a major source of formic acid. Based on these results we do not consider OH oxidation of glycolaldehyde, or the associated photo-tautomerization source, to be a significant source of formic acid in these experiments or the atmosphere.

4.4 Modeling chemical source of formic and acetic acid measured during SOAS

We simulate organic acid production during SOAS using the modified MAGRITTE mechanism with yields determined above from the FIXCIT experiments. We use the MAGRITTE mechanism here because of the specific consideration of the OH oxidation of various enols as organic acid sources. The model includes the dry deposition scheme developed in Nguyen et al.[15] for oxidized organic compounds. Following the method of Kaiser et al.,[74] the model constrains a suite of VOCs and inorganic trace gases to their campaign median measured values. If absent from MAGRITTE, VOC reactions followed the MCM v3.3.1. Further details of the ambient simulation are in Appendix 3.

Campaign median mixing ratios varied between 0.35-2.3 ppb_v for formic acid and between 0.01-0.5 ppb_v for acetic acid in the afternoon and early morning (Figure 4.9). Measured

mixing ratios of both acids are characterized by a rapid increase in the morning (~8 am local time) and reaching maximum values in the afternoon (~2 pm) lasting until the early evening (~8 pm). At night, formic acid mixing ratios remain between 0.5-1 ppb_v, indicative of competitive sources and sinks. In contrast, acetic acid mixing ratios are controlled by a nighttime sink. Brophy and Farmer[14] suggested that the high temporal correlation of formic acid with nitric acid ($r^2 = 0.78$) observed during SOAS implied that formic acid had a rapid secondary photochemical source coupled to a rapid sink such as dry deposition. Millet et al.[49] arrived at a similar conclusion using GEOS-Chem to model formic acid production during SOAS.

Modeled formic and acetic acid mixing ratios are generally underpredicted by 85% and 35%, respectively (Figure A3.17). The modeled temporal distribution of formic acid is reasonably represented by the model ($r^2 = 0.82$) – but the rapid morning increase in both organic acid mixing ratios is not. However, we acknowledge that this model does not include known – but expected to be minor – formic acid sources such as primary emissions from plants or soils, nor does it consider advection from other regions. In addition, the model only considers limited monoterpene oxidation sources. The good agreement between predicted and measured acetic acid mixing ratios suggest that the most important gas-phase production reactions are well-represented in the chemical mechanism used here. Significant source contributions to formic acid mixing ratios still appear to be missing from the chemical mechanism even with the speculated sources added to the mechanism. For both acids, the major model sink is dry deposition. However, if additional source mechanisms are added to match the observations, additional sink terms may be required to maintain the diel profiles. Most of the production of acetic acid is controlled by reactions of the $CH_3C(O)O_2$ radical with HO_2 and RO_2 with some contributions from the reaction of methyl vinyl alcohol with OH. Approximately 25% of the production

originates from other sources, such as the MACO3 + HO_2 reaction modified with a yield determined from the MACR + OH “low NO” FIXCIT experiment.

The dominant source of formic acid from the model is from the addition of the source from HPALD photolysis. This source was added to the mechanism to force model predictions of formic acid to agree with measured mixing ratios from the isoprene + OH “low NO” FIXCIT experiment, but this source is only loosely supported from the HPALD photolysis experiment. Other important source contributions include vinyl alcohol (produced from photo-tautomerization of acetaldehyde) with OH, the reaction of isoprene with O_3 and MACO3 + HO_2 (from the MACR + OH “low NO” FIXCIT experiment).

4.5. Conclusions

Despite recent updates to isoprene oxidation mechanisms, that include novel pathways for organic acid formation, global simulations continue to provide estimates too low to explain high ambient levels of formic and acetic acid.[3,9,75] The high yields of formic and acetic acid measured from the FIXCIT experiments suggest oxidation of isoprene could be a major source of these acids globally. A recent GEOS-Chem simulation estimated the magnitude of the global chemical sinks of isoprene and differentiated the effect of reaction with OH by quantifying the fate of the first-generation isoprene OH-adduct peroxy radical (ISOPOO). Applying the yields measured from the FIXCIT experiments to the isoprene chemical sink distribution from this study provides a global annual production rate of 78 and 15 Tg a^{-1} of formic and acetic acid, respectively (Table A3.4). This estimation of acetic acid production is similar to other studies, but this estimated formic acid source is a factor of ~3 higher than other studies. The formic acid estimate here also falls below the satellite-constrained values of 100-120 Tg a^{-1}.[3] Major contributions to this estimate are from isoprene ozonolysis (~55%) and production from the ISOPOO isomerization pathway (~24%). While this estimate does not consider the complexities inherent in global modeling or the uncertainties in our results it does emphasize the potential importance of isoprene oxidation as a global source of formic acid.

Despite the modified model's ability to capture FIXCIT chamber data, the model-measurement discrepancy in ambient formic acid data at SOAS persists. However, the chemical mechanism employed in this study captures observed ambient acetic acid reasonably well. Aside from the addition of the HPALD photolysis source, the FIXCIT experiments did not provide evidence for substantial production of formic and acetic acid directly from gas-phase OH oxidation of isoprene oxidation products. Targeted studies of organic acid formation from other

isomers of ISOPOOH and IEPOX, methyl vinyl ketone, and isoprene isomerization products would help to inform the results from this study. Several conclusions can be drawn from the FIXCIT experiments that may help inform uncertainties that still exist with understanding organic acid formation during SOAS:

- Creating conditions in oxidation experiments where RO_2 lifetimes are similar to the atmosphere is likely necessary for accurately quantifying organic acid production from isoprene and monoterpenes (i.e. "slow" OH oxidation experiments)
- Compounds associated with the 1,6-H shift isomerization reactions of ISOPOO, such as HPALDs or DHPs, are a potentially important source of formic acid
- The influence of NO reactions of RO_2 from isoprene appear to suppress formation of formic and acetic acid
- The high formic acid backgrounds during chamber experiments highlight the potential for surface chemistry sources of these acids; ecosystem or aerosol surfaces may be relevant formic acid sources in the ambient atmosphere

The biggest challenge we faced assessing the experimental and atmospheric relevance of our results was reconciling "background" production of formic and acetic acids with chemical production from VOCs in the chamber experiments. As observed from the blank experiments, it is clear these acids are produced from oxidation in the absence of injected VOC and their production can be on the order of several ppb_v. Background subtraction is necessary to accurately quantify formic and acetic acid production from chamber experiments. The mechanism for the "background" production, however, is unclear. We hypothesize oxidation of vapors lost to the walls of the chamber are the most likely explanation for acid production. Because wall loss is reversible for some gases and because oxidation of gases lost to the walls

likely happens simultaneously with VOC oxidation during an experiment, there does not seem to be a robust way to account for the background acid production for this experimental configuration. For future studies quantifying organic acid production from chamber experiments we recommend performing “blank” experiments between regular experiments, measuring organic acids, and tracking how the backgrounds change in time. This would help to inform future studies how best to account for organic acid backgrounds.

Chapter 4 Figures

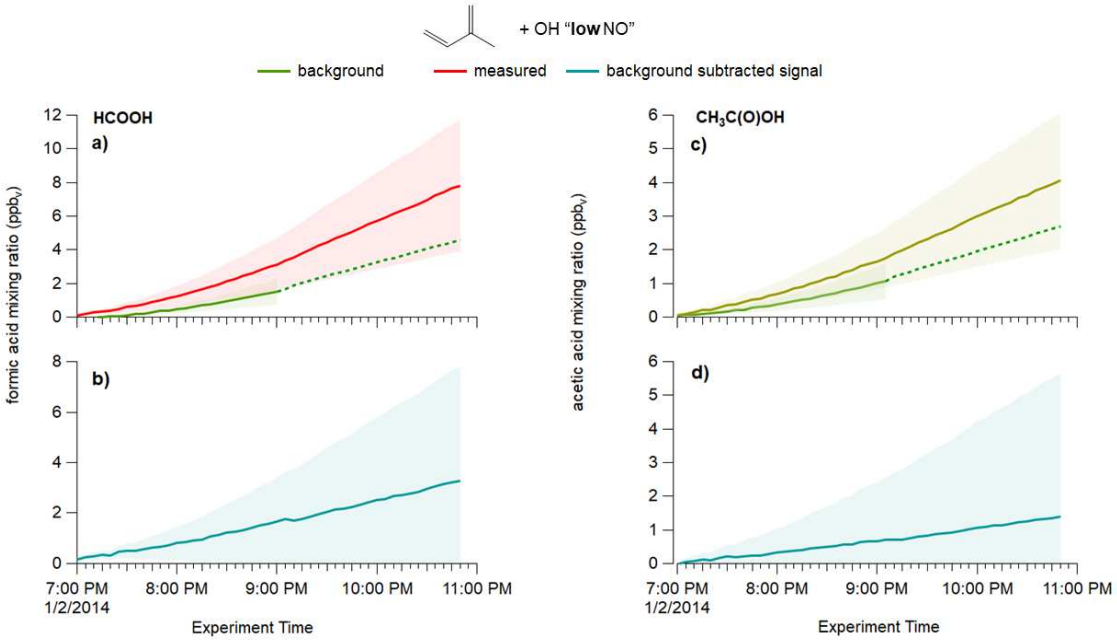

Figure 4.1. An example of background subtraction of formic (panels a and b; "HCOOH") and acetic (c and d; "CH3C(O)OH") acid from isoprene + OH "low NO" experiment. (a) The raw formic acid mixing ratio (red) is shown with the estimated mixing ratio from background (green). The solid portion of the background is the mixing ratio that was measured directly, and the dashed portion of the line is the interpolated mixing ratio. The shaded regions represent the uncertainty of measurements (top) and calculated background-subtracted mixing ratios (bottom). (b) Subtracting the green background mixing ratio from the red mixing ratio produces the blue line which is the background-subtracted formic acid mixing ratio for the isoprene + OH "low NO" experiment. (c) Same as panel (a) except acetic, instead of formic, acid is shown. (d) Same as panel (b) except acetic, instead of formic, acid is shown.

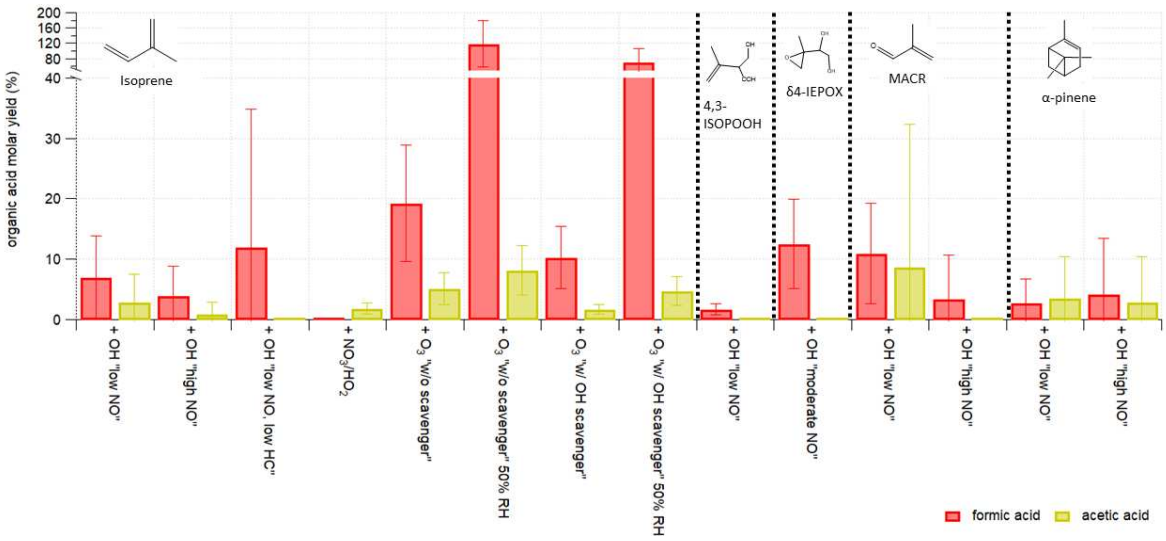

Figure 4.2. Formic (red bars) and acetic (yellow bars) acid molar yields (ppb_v/ppb_v) are separated by precursor (black dotted lines) and experiment (x-axis). Experiments on the x-axis are defined by oxidant, presence of NO, humidity and/or presence of an OH scavenger. Errors on the yields are propagated from the uncertainty in the precursor and organic acid background-subtracted measurements.

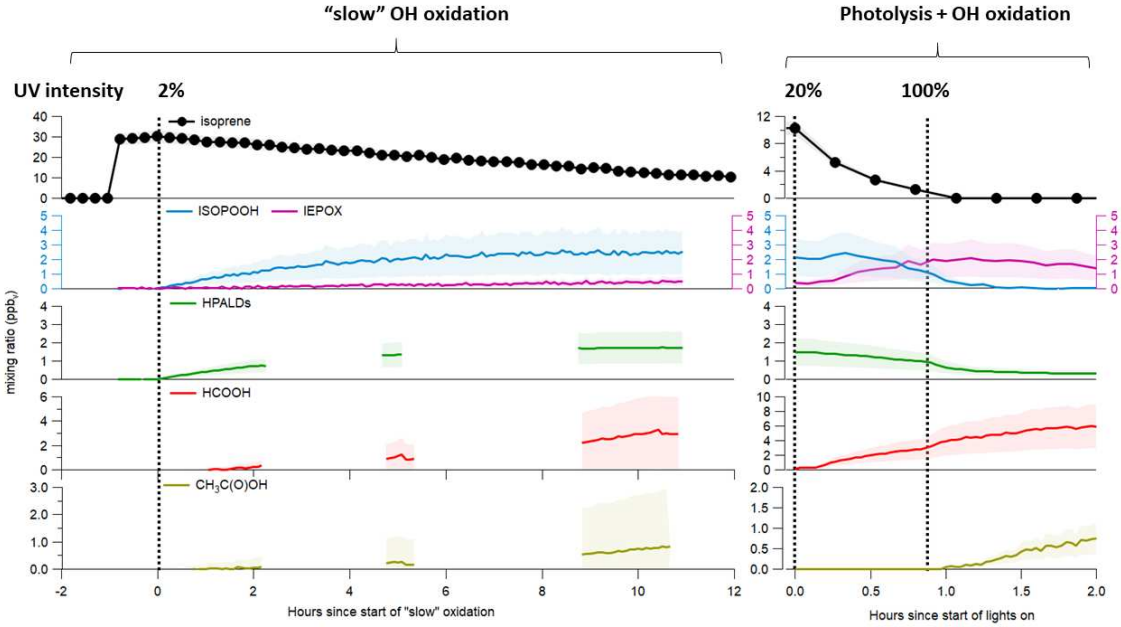

Figure 4.3. Isoprene (top panels; black trace) was oxidized with OH under conditions of low UV intensity (2% intensity "slow" oxidation; left panels) to promote the formation of HPALD compounds. High mixing ratios of formic (red trace) and acetic (yellow trace) acids were produced. After the period of "slow" oxidation the UV intensity was increased to 20% and then 100% (right panels) to promote photolysis of HPALD compounds.

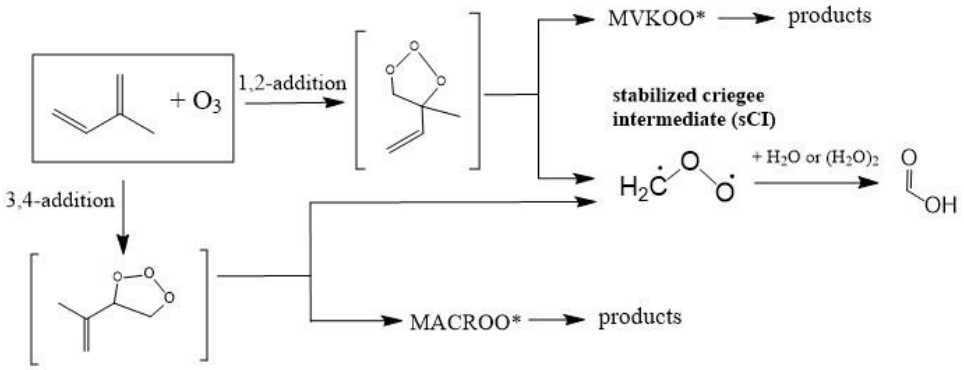

Figure 4.4. Simplified representation of isoprene ozonolysis producing formic acid. Two primary ozonides form from reaction of O_3 across the double bond of the 1 or 4 carbon. Both ozonides rapidly decompose to form C1 and C4 carbonyl oxides. The C1 carbonyl oxides undergo collisional stabilization to produce a stabilized Criegee intermediate. Through reactions involving monomeric and/or dimeric water vapor formic acid is produced.

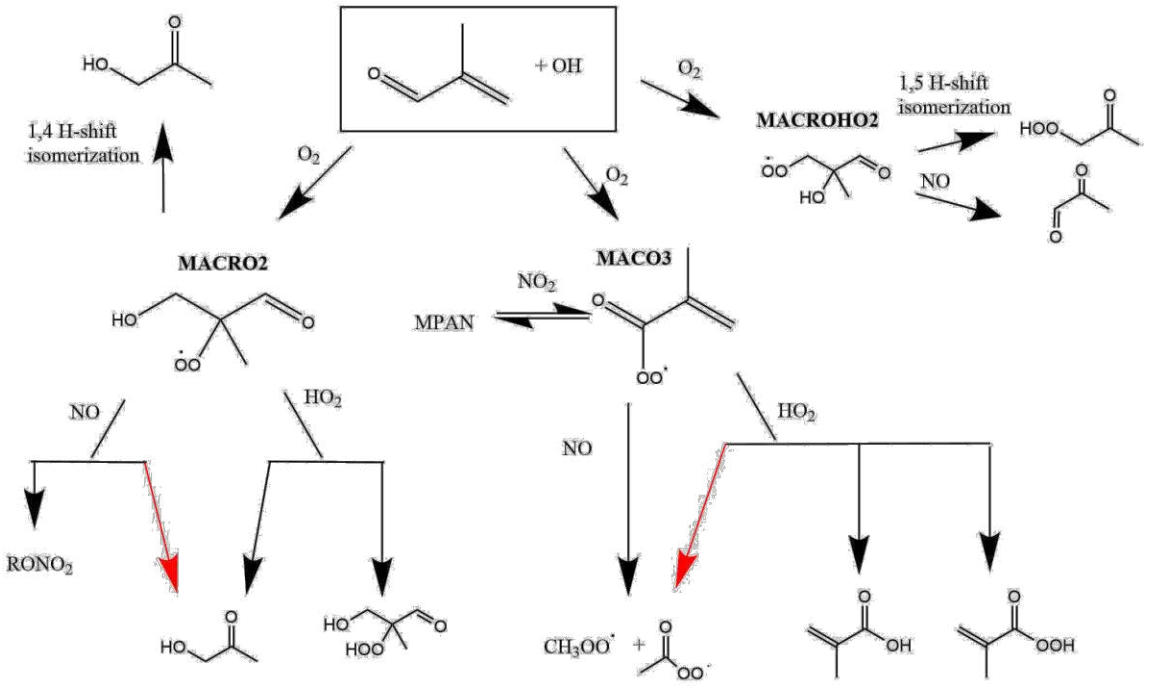

Figure 4.5. OH oxidation mechanism for MACR. For simplicity, some oxidation products such as OH or CO are not shown. In some cases, only major products (i.e. MACRO2 + NO results in alkoxy radical, with 94% yield, that decomposes to hydroxyacetone with 86% yield) or major reaction pathways (i.e. MACO3 with HO_2, NO, or NO_2). Peroxy radical self-reactions are excluded from this figure but are included in the MCM and MAGRITTE. The red arrows show where organic acid yields were attributed in the models to bring model prediction into agreement with measurements. Formic acid yields were assigned to the reaction of MACO3 with HO_2 and MACRO2 with NO. A yield of acetic acid was applied to the reaction of MACO3 with NO.

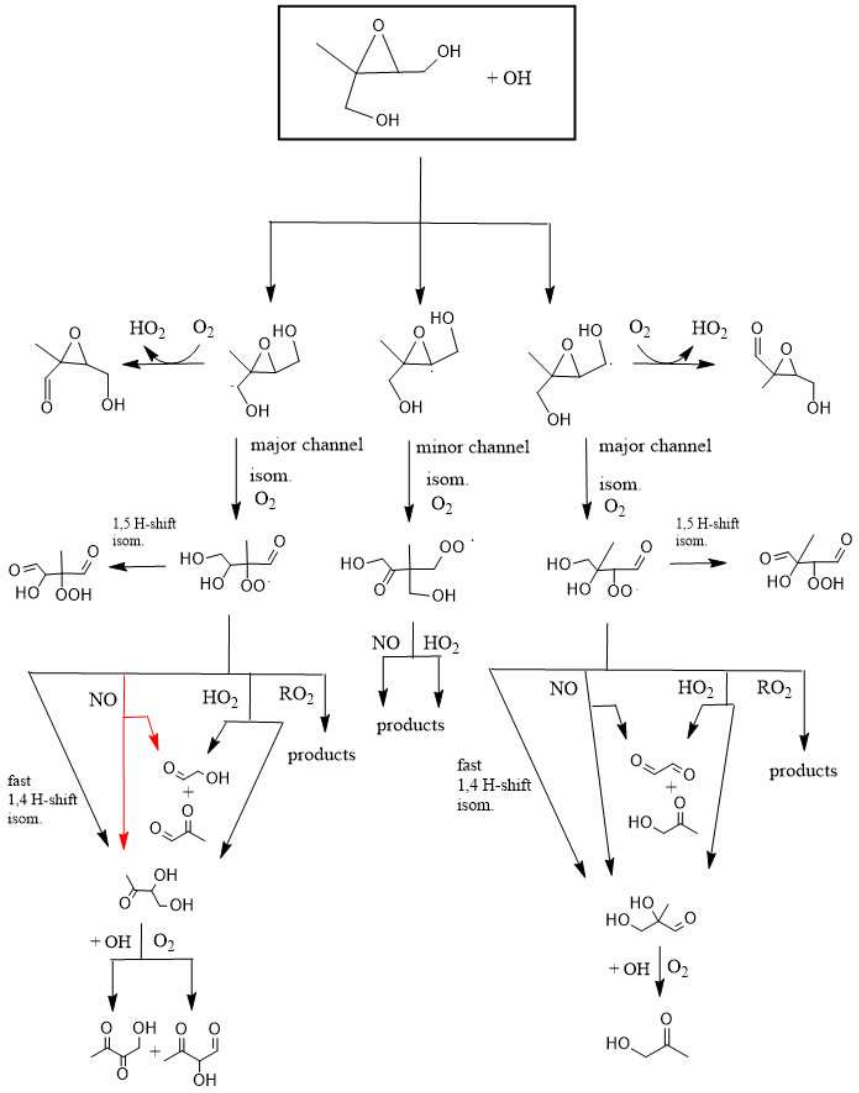

Figure 4.6. OH oxidation mechanism for trans-β-IEPOX. For simplicity, some oxidation products such as OH or CO are not shown. The red arrows show where formic acid yields were attributed in the models to bring model prediction into agreement with measurements. We assign a yield of formic acid to the reaction of the first-generation RO_2, produced from H-abstraction at C1 of IEPOX, with NO.

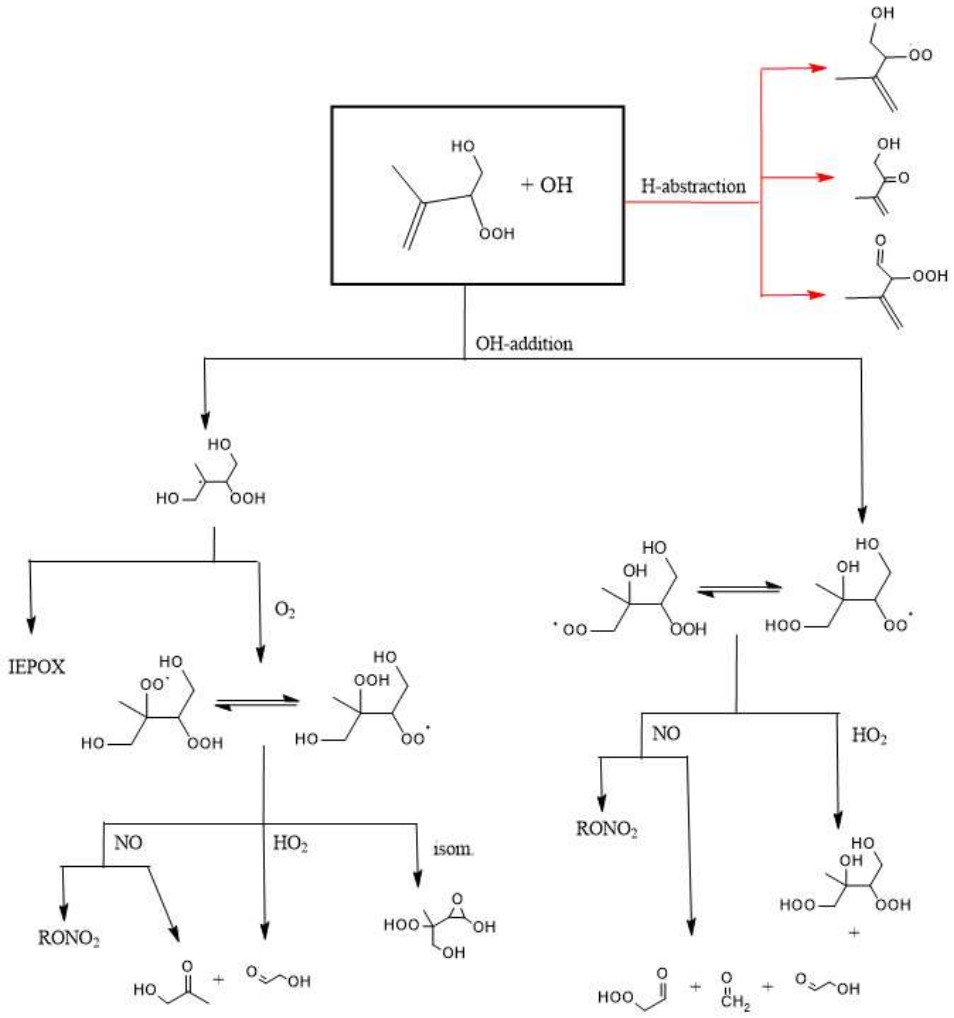

Figure 4.7. OH oxidation mechanism for 4,3-ISOPOOH. For simplicity, some oxidation products such as OH or CO are not shown. The isomerization channels corresponding OH-addition channels to the right that produce dihydroxy-hydroperoxy-epoxides and dihydroxy-hydroperoxy-carbonyls are not shown for simplicity. The red arrows show where formic acid yields were attributed in the models to bring model prediction into agreement with measurements. Because of simplifications used in the different models, we assign a yield of formic acid to the general H-abstraction mechanism for the OH + ISOPOOH reaction. The MAGRITTE mechanism specifically assigns a formic acid yield to reaction for the abstraction of the hydroxy-α-H.

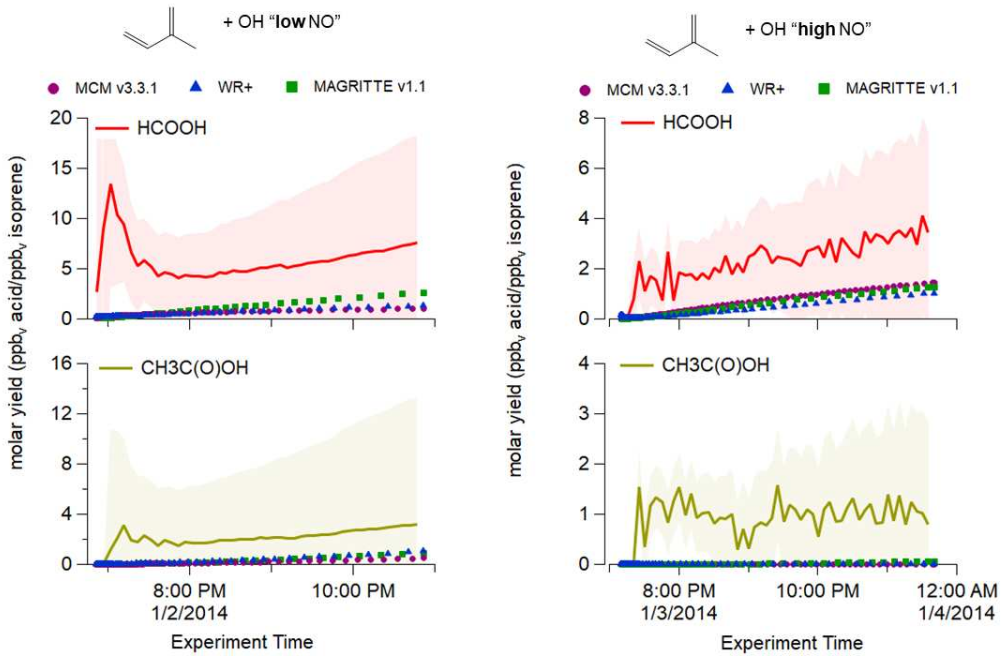

Figure 4.8. The measured production (solid lines) of formic (red) and acetic (yellow) acids are shown for the isoprene + OH experiments performed under conditions of "low NO" (left) and "high NO" (right). The organic acid production predicted from each of the three isoprene oxidation mechanisms, modified to include estimated yields of acids from other FIXCIT experiments, is shown by markers. Shaded regions represent propagated uncertainty in yields of organic acids.

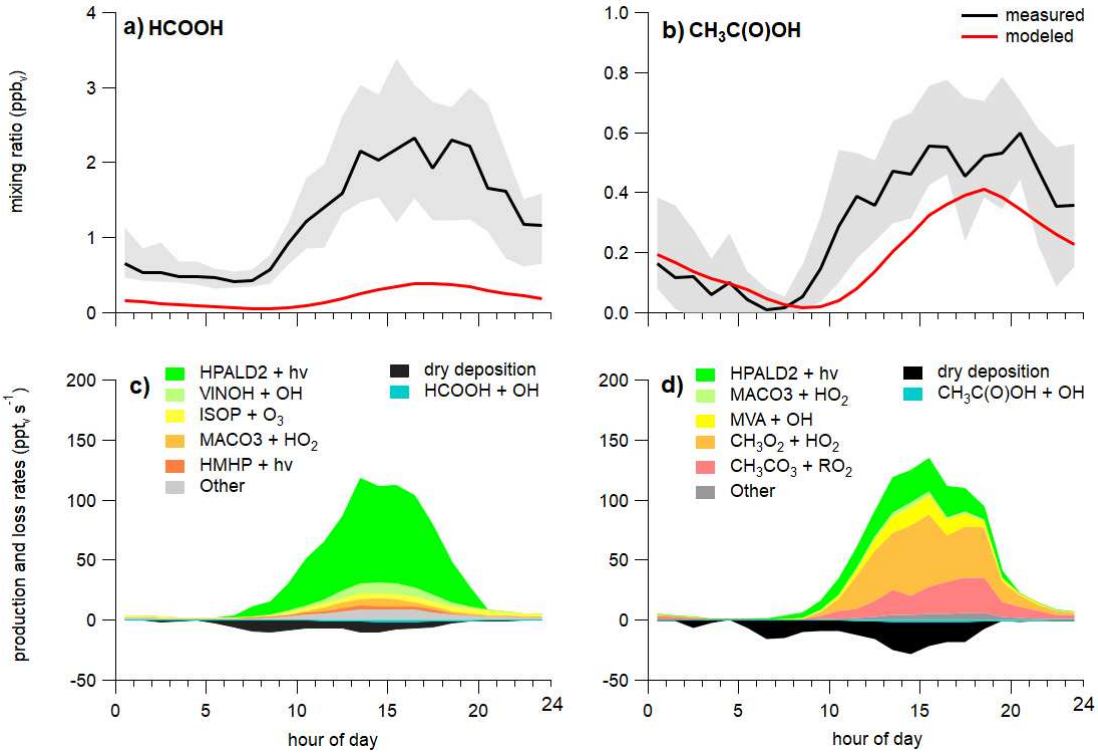

Figure 4.9. Formic (panel a) and acetic (panel b) acid mixing ratio measured during SOAS (black line) and mixing ratio prediction from FIXCIT-modified MAGRITTE model (red line). Shaded regions represent the 25th and 75th percentiles. Rates of production and loss of formic (panel c) and acetic (panel d) acid contributing to modeled organic acid mixing ratios at SOAS. The five most important production reactions are shown in the colored shaded regions and other minor reactions are grouped together and indicated by gray shades.

REFERENCES

(1) Millet, D. B. Atmospheric Chemistry: Natural Atmospheric Acidity. *Nat. Geosci.* **2012**, *5* (1), 8–9. https://doi.org/10.1038/ngeo1361.

(2) Metzger, S.; Mihalopoulos, N.; Lelieveld, J. Importance of Mineral Cations and Organics in Gas-Aerosol Partitioning of Reactive Nitrogen Compounds: Case Study Based on MINOS Results. *Atmospheric Chem. Phys.* **2006**, *6* (9), 2549–2567.

(3) Stavrakou, T.; Müller, J.-F.; Peeters, J.; Razavi, A.; Clarisse, L.; Clerbaux, C.; Coheur, P.-F.; Hurtmans, D.; De Mazière, M.; Vigouroux, C.; et al. Satellite Evidence for a Large Source of Formic Acid from Boreal and Tropical Forests. *Nat. Geosci.* **2012**, *5* (1), 26–30. https://doi.org/10.1038/ngeo1354.

(4) Bannan, T. J.; Booth, A. M.; Breton, M. L.; Bacak, A.; Muller, J. B. A.; Leather, K. E.; Khan, M. A. H.; Lee, J. D.; Dunmore, R. E.; Hopkins, J. R.; et al. Seasonality of Formic Acid (HCOOH) in London during the ClearfLo Campaign. *J. Geophys. Res. Atmospheres* **2017**, *122* (22), 12,488-12,498. https://doi.org/10.1002/2017JD027064.

(5) Paulot, F.; Wunch, D.; Crounse, J. D.; Toon, G. C.; Millet, D. B.; DeCarlo, P. F.; Vigouroux, C.; Deutscher, N. M.; González Abad, G.; Notholt, J.; et al. Importance of Secondary Sources in the Atmospheric Budgets of Formic and Acetic Acids. *Atmos Chem Phys* **2011**, *11* (5), 1989–2013. https://doi.org/10.5194/acp-11-1989-2011.

(6) Chaliyakunnel, S.; Millet, D. B.; Wells, K. C.; Cady-Pereira, K. E.; Shephard, M. W. A Large Underestimate of Formic Acid from Tropical Fires: Constraints from Space-Borne Measurements. *Environ. Sci. Technol.* **2016**, *50* (11), 5631–5640. https://doi.org/10.1021/acs.est.5b06385.

(7) Millet, D. B.; Baasandorj, M.; Farmer, D. K.; Thornton, J. A.; Baumann, K.; Brophy, P.; Chaliyakunnel, S.; de Gouw, J. A.; Graus, M.; Hu, L.; et al. A Large and Ubiquitous Source of Atmospheric Formic Acid. *Atmospheric Chem. Phys.* **2015**, *15* (11), 6283–6304. https://doi.org/https://doi.org/10.5194/acp-15-6283-2015.

(8) Chen, X.; Millet, D. B.; Singh, H. B.; Wisthaler, A.; Apel, E. C.; Atlas, E. L.; Blake, D. R.; Bourgeois, I.; Brown, S. S.; Crounse, J. D.; et al. On the Sources and Sinks of Atmospheric VOCs: An Integrated Analysis of Recent Aircraft Campaigns over North America. *Atmospheric Chem. Phys.* **2019**, *19* (14), 9097–9123. https://doi.org/https://doi.org/10.5194/acp-19-9097-2019.

(9) Müller, J.-F.; Stavrakou, T.; Peeters, J. Chemistry and Deposition in the Model of Atmospheric Composition at Global and Regional Scales Using Inversion Techniques for Trace

Gas Emissions (MAGRITTE v1.1) – Part 1: Chemical Mechanism. *Geosci. Model Dev.* **2019**, *12* (6), 2307–2356. https://doi.org/https://doi.org/10.5194/gmd-12-2307-2019.

(10) Schobesberger, S.; Lopez-Hilfiker, F. D.; Taipale, D.; Millet, D. B.; D'Ambro, E. L.; Rantala, P.; Mammarella, I.; Zhou, P.; Wolfe, G. M.; Lee, B. H.; et al. High Upward Fluxes of Formic Acid from a Boreal Forest Canopy. *Geophys. Res. Lett.* **2016**, *43* (17), 2016GL069599. https://doi.org/10.1002/2016GL069599.

(11) Alwe, H. D.; Millet, D. B.; Chen, X.; Raff, J. D.; Payne, Z. C.; Fledderman, K. Oxidation of Volatile Organic Compounds as the Major Source of Formic Acid in a Mixed Forest Canopy. *Geophys. Res. Lett.* **2019**, *46* (5), 2940–2948. https://doi.org/10.1029/2018GL081526.

(12) Fulgham, S. R.; Brophy, P.; Link, M.; Ortega, J.; Pollack, I.; Farmer, D. K. Seasonal Flux Measurements over a Colorado Pine Forest Demonstrate a Persistent Source of Organic Acids. *ACS Earth Space Chem.* **2019**. https://doi.org/10.1021/acsearthspacechem.9b00182.

(13) Gu, D.; Guenther, A. B.; Shilling, J. E.; Yu, H.; Huang, M.; Zhao, C.; Yang, Q.; Martin, S. T.; Artaxo, P.; Kim, S.; et al. Airborne Observations Reveal Elevational Gradient in Tropical Forest Isoprene Emissions. *Nat. Commun.* **2017**, *8*, 15541. https://doi.org/10.1038/ncomms15541.

(14) Brophy, P.; Farmer, D. K. A Switchable Reagent Ion High Resolution Time-of-Flight Chemical Ionization Mass Spectrometer for Real-Time Measurement of Gas Phase Oxidized Species: Characterization from the 2013 Southern Oxidant and Aerosol Study. *Atmos Meas Tech* **2015**, *8* (7), 2945–2959. https://doi.org/10.5194/amt-8-2945-2015.

(15) Nguyen, T. B.; Crounse, J. D.; Teng, A. P.; Clair, J. M. S.; Paulot, F.; Wolfe, G. M.; Wennberg, P. O. Rapid Deposition of Oxidized Biogenic Compounds to a Temperate Forest. *Proc. Natl. Acad. Sci.* **2015**, *112* (5), E392–E401. https://doi.org/10.1073/pnas.1418702112.

(16) Nguyen, T. B.; Crounse, J. D.; Schwantes, R. H.; Teng, A. P.; Bates, K. H.; Zhang, X.; St. Clair, J. M.; Brune, W. H.; Tyndall, G. S.; Keutsch, F. N.; et al. Overview of the Focused Isoprene eXperiment at the California Institute of Technology (FIXCIT): Mechanistic Chamber Studies on the Oxidation of Biogenic Compounds. *Atmos Chem Phys* **2014**, *14* (24), 13531–13549. https://doi.org/10.5194/acp-14-13531-2014.

(17) Paulot, F.; Crounse, J. D.; Kjaergaard, H. G.; Kroll, J. H.; Seinfeld, J. H.; Wennberg, P. O. Isoprene Photooxidation: New Insights into the Production of Acids and Organic Nitrates. *Atmospheric Chem. Phys.* **2009**, *9* (4), 1479–1501. https://doi.org/https://doi.org/10.5194/acp-9-1479-2009.

(18) St. Clair, J. M.; McCabe, D. C.; Crounse, J. D.; Steiner, U.; Wennberg, P. O. Chemical Ionization Tandem Mass Spectrometer for the in Situ Measurement of Methyl Hydrogen Peroxide. *Rev. Sci. Instrum.* **2010**, *81* (9), 94102. https://doi.org/10.1063/1.3480552.

(19) Allen, H. M.; Crounse, J. D.; Bates, K. H.; Teng, A. P.; Krawiec-Thayer, M. P.; Rivera-Rios, J. C.; Keutsch, F. N.; St. Clair, J. M.; Hanisco, T. F.; Møller, K. H.; et al. Kinetics and Product Yields of the OH Initiated Oxidation of Hydroxymethyl Hydroperoxide. *J. Phys. Chem. A* **2018**, *122* (30), 6292–6302. https://doi.org/10.1021/acs.jpca.8b04577.

(20) Rivera-Rios, J. C.; Nguyen, T. B.; Crounse, J. D.; Jud, W.; St. Clair, J. M.; Mikoviny, T.; Gilman, J. B.; Lerner, B. M.; Kaiser, J. B.; de Gouw, J.; et al. Conversion of Hydroperoxides to Carbonyls in Field and Laboratory Instrumentation: Observational Bias in Diagnosing Pristine versus Anthropogenically Controlled Atmospheric Chemistry. *Geophys. Res. Lett.* **2014**, *41* (23), 2014GL061919. https://doi.org/10.1002/2014GL061919.

(21) Clair, J. M. S.; Spencer, K. M.; Beaver, M. R.; Crounse, J. D.; Paulot, F.; Wennberg, P. O. Quantification of Hydroxyacetone and Glycolaldehyde Using Chemical Ionization Mass Spectrometry. *Atmospheric Chem. Phys.* **2014**, *14* (8), 4251–4262. https://doi.org/https://doi.org/10.5194/acp-14-4251-2014.

(22) Bates, K. H.; Crounse, J. D.; St. Clair, J. M.; Bennett, N. B.; Nguyen, T. B.; Seinfeld, J. H.; Stoltz, B. M.; Wennberg, P. O. Gas Phase Production and Loss of Isoprene Epoxydiols. *J. Phys. Chem. A* **2014**, *118* (7), 1237–1246.

(23) Friedman, B.; Farmer, D. K. SOA and Gas Phase Organic Acid Yields from the Sequential Photooxidation of Seven Monoterpenes. *Atmos. Environ.* **2018**, *187*, 335–345. https://doi.org/10.1016/j.atmosenv.2018.06.003.

(24) Reed Harris, A. E.; Cazaunau, M.; Gratien, A.; Pangui, E.; Doussin, J.-F.; Vaida, V. Atmospheric Simulation Chamber Studies of the Gas-Phase Photolysis of Pyruvic Acid. *J. Phys. Chem. A* **2017**, *121* (44), 8348–8358. https://doi.org/10.1021/acs.jpca.7b05139.

(25) Schnitzhofer, R.; Metzger, A.; Breitenlechner, M.; Jud, W.; Heinritzi, M.; De Menezes, L.-P.; Duplissy, J.; Guida, R.; Haider, S.; Kirkby, J.; et al. Characterisation of Organic Contaminants in the CLOUD Chamber at CERN. *Atmospheric Meas. Tech.* **2014**, *7* (7), 2159–2168. https://doi.org/https://doi.org/10.5194/amt-7-2159-2014.

(26) Malecha, K. T.; Nizkorodov, S. A. Photodegradation of Secondary Organic Aerosol Particles as a Source of Small, Oxygenated Volatile Organic Compounds. *Environ. Sci. Technol.* **2016**. https://doi.org/10.1021/acs.est.6b02313.

(27) Friedman, B.; Brophy, P.; Brune, W. H.; Farmer, D. K. Anthropogenic Sulfur Perturbations on Biogenic Oxidation: SO2 Additions Impact Gas-Phase OH Oxidation Products of α- and β-Pinene. *Environ. Sci. Technol.* **2016**, *50* (3), 1269–1279. https://doi.org/10.1021/acs.est.5b05010.

(28) Møller, K. H.; Bates, K. H.; Kjaergaard, H. G. The Importance of Peroxy Radical Hydrogen-Shift Reactions in Atmospheric Isoprene Oxidation. *J. Phys. Chem. A* **2019**, *123* (4), 920–932. https://doi.org/10.1021/acs.jpca.8b10432.

(29) Müller, J.-F.; Stavrakou, T.; Peeters, J. Chemistry and Deposition in the Model of Atmospheric Composition at Global and Regional Scales Using Inversion Techniques for Trace Gas Emissions (MAGRITTEv1.0). Part A. Chemical Mechanism. *Geosci. Model Dev. Discuss.* **2018**, 1–59. https://doi.org/https://doi.org/10.5194/gmd-2018-316.

(30) Berndt, T.; Hyttinen, N.; Herrmann, H.; Hansel, A. First Oxidation Products from the Reaction of Hydroxyl Radicals with Isoprene for Pristine Environmental Conditions. *Commun. Chem.* **2019**, *2* (1), 21. https://doi.org/10.1038/s42004-019-0120-9.

(31) Peng, Z.; Lee-Taylor, J.; Orlando, J. J.; Tyndall, G. S.; Jimenez, J. L. Organic Peroxy Radical Chemistry in Oxidation Flow Reactors and Environmental Chambers and Their Atmospheric Relevance. *Atmospheric Chem. Phys.* **2019**, *19* (2), 813–834. https://doi.org/https://doi.org/10.5194/acp-19-813-2019.

(32) Peeters, J.; L. Nguyen, T.; Vereecken, L. HO X Radical Regeneration in the Oxidation of Isoprene. *Phys. Chem. Chem. Phys.* **2009**, *11* (28), 5935–5939. https://doi.org/10.1039/B908511D.

(33) Bianchi, F.; Garmash, O.; He, X.; Yan, C.; Iyer, S.; Rosendahl, I.; Xu, Z.; Rissanen, M. P.; Riva, M.; Taipale, R.; et al. Insight into Naturally-Charged Highly Oxidized Molecules (HOMs) in the Boreal Forest. *Atmos Chem Phys Discuss* **2017**, *2017*, 1–20. https://doi.org/10.5194/acp-2017-481.

(34) Ehn, M.; Thornton, J. A.; Kleist, E.; Sipilä, M.; Junninen, H.; Pullinen, I.; Springer, M.; Rubach, F.; Tillmann, R.; Lee, B.; et al. A Large Source of Low-Volatility Secondary Organic Aerosol. *Nature* **2014**, *506* (7489), 476–479. https://doi.org/10.1038/nature13032.

(35) Berndt, T.; Richters, S.; Jokinen, T.; Hyttinen, N.; Kurtén, T.; Otkjær, R. V.; Kjaergaard, H. G.; Stratmann, F.; Herrmann, H.; Sipilä, M.; et al. Hydroxyl Radical-Induced Formation of Highly Oxidized Organic Compounds. *Nat. Commun.* **2016**, *7*. https://doi.org/10.1038/ncomms13677.

(36) Xu, L.; Møller, K. H.; Crounse, J. D.; Otkjær, R. V.; Kjaergaard, H. G.; Wennberg, P. O. Unimolecular Reactions of Peroxy Radicals Formed in the Oxidation of α-Pinene and β-Pinene by Hydroxyl Radicals. *J. Phys. Chem. A* **2019**, *123* (8), 1661–1674. https://doi.org/10.1021/acs.jpca.8b11726.

(37) Malkin, T. L.; Goddard, A.; Heard, D. E.; Seakins, P. W. Measurements of OH and HO_2 Yields from the Gas Phase Ozonolysis of Isoprene. *Atmospheric Chem. Phys.* **2010**, *10* (3), 1441–1459. https://doi.org/https://doi.org/10.5194/acp-10-1441-2010.

(38) Paulson, S. E.; Orlando, J. J. The Reactions of Ozone with Alkenes: An Important Source of HOx in the Boundary Layer. *Geophys. Res. Lett.* **1996**, *23* (25), 3727–3730. https://doi.org/10.1029/96GL03477.

(39) Atkinson, R.; Baulch, D. L.; Cox, R. A.; Crowley, J. N.; Hampson, R. F.; Hynes, R. G.; Jenkin, M. E.; Rossi, M. J.; Troe, J.; IUPAC Subcommittee. Evaluated Kinetic and Photochemical Data for Atmospheric Chemistry: Volume II – Gas Phase Reactions of Organic Species. *Atmospheric Chem. Phys.* **2006**, *6* (11), 3625–4055. https://doi.org/https://doi.org/10.5194/acp-6-3625-2006.

(40) Neeb, P.; Sauer, F.; Horie, O.; Moortgat, G. K. Formation of Hydroxymethyl Hydroperoxide and Formic Acid in Alkene Ozonolysis in the Presence of Water Vapour. *Atmos. Environ.* **1997**, *31* (10), 1417–1423. https://doi.org/10.1016/S1352-2310(96)00322-6.

(41) Sheps, L.; Rotavera, B.; J. Eskola, A.; L. Osborn, D.; A. Taatjes, C.; Au, K.; E. Shallcross, D.; H. Khan, M. A.; J. Percival, C. The Reaction of Criegee Intermediate CH 2 OO with Water Dimer: Primary Products and Atmospheric Impact. *Phys. Chem. Chem. Phys.* **2017**, *19* (33), 21970–21979. https://doi.org/10.1039/C7CP03265J.

(42) Khan, M. A. H.; Lyons, K.; Chhantyal-Pun, R.; McGillen, M. R.; Caravan, R. L.; Taatjes, C. A.; Orr-Ewing, A. J.; Percival, C. J.; Shallcross, D. E. Investigating the Tropospheric Chemistry of Acetic Acid Using the Global 3-D Chemistry Transport Model, STOCHEM-CRI. *J. Geophys. Res. Atmospheres* **2018**, *123* (11), 6267–6281. https://doi.org/10.1029/2018JD028529.

(43) Orzechowska, G. E.; Paulson, S. E. Photochemical Sources of Organic Acids. 1. Reaction of Ozone with Isoprene, Propene, and 2-Butenes under Dry and Humid Conditions Using SPME. *J. Phys. Chem. A* **2005**, *109* (24), 5358–5365. https://doi.org/10.1021/jp050166s.

(44) Wennberg, P. O.; Bates, K. H.; Crounse, J. D.; Dodson, L. G.; McVay, R. C.; Mertens, L. A.; Nguyen, T. B.; Praske, E.; Schwantes, R. H.; Smarte, M. D.; et al. Gas-Phase Reactions of Isoprene and Its Major Oxidation Products. *Chem. Rev.* **2018**. https://doi.org/10.1021/acs.chemrev.7b00439.

(45) Nguyen, T. B.; Tyndall, G. S.; Crounse, J. D.; Teng, A. P.; Bates, K. H.; Schwantes, R. H.; Coggon, M. M.; Zhang, L.; Feiner, P.; Milller, D. O.; et al. Atmospheric Fates of Criegee Intermediates in the Ozonolysis of Isoprene. *Phys. Chem. Chem. Phys.* **2016**, *18* (15), 10241–10254. https://doi.org/10.1039/C6CP00053C.

(46) Chao, W.; Hsieh, J.-T.; Chang, C.-H.; Lin, J. J.-M. Direct Kinetic Measurement of the Reaction of the Simplest Criegee Intermediate with Water Vapor. *Science* **2015**, *347* (6223), 751–754. https://doi.org/10.1126/science.1261549.

(47) Teng, A. P.; Crounse, J. D.; Wennberg, P. O. Isoprene Peroxy Radical Dynamics. *J. Am. Chem. Soc.* **2017**, *139* (15), 5367–5377. https://doi.org/10.1021/jacs.6b12838.

(48) Yuan, B.; Veres, P. R.; Warneke, C.; Roberts, J. M.; Gilman, J. B.; Koss, A.; Edwards, P. M.; Graus, M.; Kuster, W. C.; Li, S.-M.; et al. Investigation of Secondary Formation of Formic Acid: Urban Environment vs. Oil and Gas Producing Region. *Atmos Chem Phys* **2015**, *15* (4), 1975–1993. https://doi.org/10.5194/acp-15-1975-2015.

(49) Millet, D. B.; Baasandorj, M.; Farmer, D. K.; Thornton, J. A.; Baumann, K.; Brophy, P.; Chaliyakunnel, S.; de Gouw, J. A.; Graus, M.; Hu, L.; et al. A Large and Ubiquitous Source of Atmospheric Formic Acid. *Atmos Chem Phys* **2015**, *15* (11), 6283–6304. https://doi.org/10.5194/acp-15-6283-2015.

(50) Shaw, M. F.; Sztáray, B.; Whalley, L. K.; Heard, D. E.; Millet, D. B.; Jordan, M. J. T.; Osborn, D. L.; Kable, S. H. Photo-Tautomerization of Acetaldehyde as a Photochemical Source of Formic Acid in the Troposphere. *Nat. Commun.* **2018**, *9* (1), 2584. https://doi.org/10.1038/s41467-018-04824-2.

(51) Vlasenko, A.; George, I. J.; Abbatt, J. P. D. Formation of Volatile Organic Compounds in the Heterogeneous Oxidation of Condensed-Phase Organic Films by Gas-Phase OH. *J. Phys. Chem. A* **2008**, *112* (7), 1552–1560. https://doi.org/10.1021/jp0772979.

(52) Molina, M. J.; Ivanov, A. V.; Trakhtenberg, S.; Molina, L. T. Atmospheric Evolution of Organic Aerosol. *Geophys. Res. Lett.* **2004**, *31* (22). https://doi.org/10.1029/2004GL020910.

(53) Mungall, E. L.; Abbatt, J. P. D.; Wentzell, J. J. B.; Wentworth, G. R.; Murphy, J. G.; Kunkel, D.; Gute, E.; Tarasick, D. W.; Sharma, S.; Cox, C. J.; et al. High Gas-Phase Mixing Ratios of Formic and Acetic Acid in the High Arctic. *Atmospheric Chem. Phys.* **2018**, *18* (14), 10237–10254. https://doi.org/https://doi.org/10.5194/acp-18-10237-2018.

(54) Wolfe, G. M.; Marvin, M. R.; Roberts, S. J.; Travis, K. R.; Liao, J. The Framework for 0-D Atmospheric Modeling (F0AM) v3.1. *Geosci. Model Dev.* **2016**, *9* (9), 3309–3319. https://doi.org/https://doi.org/10.5194/gmd-9-3309-2016.

(55) Jenkin, M. E.; Young, J. C.; Rickard, A. R. The MCM v3.3.1 Degradation Scheme for Isoprene. *Atmospheric Chem. Phys.* **2015**, *15* (20), 11433–11459. https://doi.org/https://doi.org/10.5194/acp-15-11433-2015.

(56) Liu, Z.; Son Nguyen, V.; Harvey, J.; Müller, J.-F.; Peeters, J. The Photolysis of α-Hydroperoxycarbonyls. *Phys. Chem. Chem. Phys.* **2018**, *20* (10), 6970–6979. https://doi.org/10.1039/C7CP08421H.

(57) Liu, Z.; Son Nguyen, V.; Harvey, J.; Müller, J.-F.; Peeters, J. Theoretically Derived Mechanisms of HPALD Photolysis in Isoprene Oxidation. *Phys. Chem. Chem. Phys.* **2017**, *19* (13), 9096–9106. https://doi.org/10.1039/C7CP00288B.

(58) Jenkin, M. E.; Hurley, M. D.; Wallington, T. J. Investigation of the Radical Product Channel of the CH3OCH2O2 + HO2 Reaction in the Gas Phase. *J. Phys. Chem. A* **2010**, *114* (1), 408–416. https://doi.org/10.1021/jp908158w.

(59) Lei, X.; Wang, W.; Cai, J.; Wang, C.; Liu, F.; Wang, W. Atmospheric Chemistry of Enols: Vinyl Alcohol + OH + O2 Reaction Revisited. *J. Phys. Chem. A* **2019**, *123* (14), 3205–3213. https://doi.org/10.1021/acs.jpca.8b12240.

(60) Assaf, E.; Sheps, L.; Whalley, L. K.; Heard, D. E.; Tomas, A.; Schoemaecker, C.; Fittschen, C. The Reaction between CH3O2 and OH Radicals: Product Yields and Atmospheric Implications. *Environ. Sci. Technol.* **2017**.

(61) Assaf, E.; Schoemaecker, C.; Vereecken, L.; Fittschen, C. Experimental and Theoretical Investigation of the Reaction of RO2 Radicals with OH Radicals: Dependence of the HO2 Yield on the Size of the Alkyl Group. *Int. J. Chem. Kinet.* **2018**, *50* (9), 670–680. https://doi.org/10.1002/kin.21191.

(62) Crounse, J. D.; Knap, H. C.; Ørnsø, K. B.; Jørgensen, S.; Paulot, F.; Kjaergaard, H. G.; Wennberg, P. O. Atmospheric Fate of Methacrolein. 1. Peroxy Radical Isomerization Following Addition of OH and O2. *J. Phys. Chem. A* **2012**, *116* (24), 5756–5762. https://doi.org/10.1021/jp211560u.

(63) Hasson, A. S.; Tyndall, G. S.; Orlando, J. J. A Product Yield Study of the Reaction of HO2 Radicals with Ethyl Peroxy (C2H5O2), Acetyl Peroxy (CH3C(O)O2), and Acetonyl Peroxy (CH3C(O)CH2O2) Radicals. *J. Phys. Chem. A* **2004**, *108* (28), 5979–5989. https://doi.org/10.1021/jp048873t.

(64) Jacobs, M. I.; Darer, A. I.; Elrod, M. J. Rate Constants and Products of the OH Reaction with Isoprene-Derived Epoxides. *Environ. Sci. Technol.* **2013**, *47* (22), 12868–12876. https://doi.org/10.1021/es403340g.

(65) Bates, K. H.; Nguyen, T. B.; Teng, A. P.; Crounse, J. D.; Kjaergaard, H. G.; Stoltz, B. M.; Seinfeld, J. H.; Wennberg, P. O. Production and Fate of C4 Dihydroxycarbonyl Compounds from Isoprene Oxidation. *J. Phys. Chem. A* **2016**, *120* (1), 106–117. https://doi.org/10.1021/acs.jpca.5b10335.

(66) Paulot, F.; Crounse, J. D.; Kjaergaard, H. G.; Kürten, A.; Clair, J. M. S.; Seinfeld, J. H.; Wennberg, P. O. Unexpected Epoxide Formation in the Gas-Phase Photooxidation of Isoprene. *Science* **2009**, *325* (5941), 730–733. https://doi.org/10.1126/science.1172910.

(67) St. Clair, J. M.; Rivera-Rios, J. C.; Crounse, J. D.; Knap, H. C.; Bates, K. H.; Teng, A. P.; Jørgensen, S.; Kjaergaard, H. G.; Keutsch, F. N.; Wennberg, P. O. Kinetics and Products of the Reaction of the First-Generation Isoprene Hydroxy Hydroperoxide (ISOPOOH) with OH. *J. Phys. Chem. A* **2016**, *120* (9), 1441–1451. https://doi.org/10.1021/acs.jpca.5b06532.

(68) Peeters, J.; Müller, J.-F. HOx Radical Regeneration in Isoprene Oxidation via Peroxy Radical Isomerisations . II: Experimental Evidence and Global Impact. *Phys. Chem. Chem. Phys.* **2010**, *12* (42), 14227–14235. https://doi.org/10.1039/C0CP00811G.

(69) Peeters, J.; Müller, J.-F.; Stavrakou, T.; Nguyen, V. S. Hydroxyl Radical Recycling in Isoprene Oxidation Driven by Hydrogen Bonding and Hydrogen Tunneling: The Upgraded LIM1 Mechanism. *J. Phys. Chem. A* **2014**, *118* (38), 8625–8643. https://doi.org/10.1021/jp5033146.

(70) Butkovskaya, N. I.; Pouvesle, N.; Kukui, A.; Mu, Y.; Le Bras, G. Mechanism of the OH-Initiated Oxidation of Hydroxyacetone over the Temperature Range 236−298 K. *J. Phys. Chem. A* **2006**, *110* (21), 6833–6843. https://doi.org/10.1021/jp056345r.

(71) Orlando, J. J.; Tyndall, G. S.; Taraborrelli, D. Atmospheric Oxidation of Two Isoprene By-Products, Hydroxyacetone and Glycolaldehyde. *AGU Fall Meet. Abstr.* **2012**, *33*, A33L–0315.

(72) Butkovskaya, N. I.; Pouvesle, N.; Kukui, A.; Le Bras, G. Mechanism of the OH-Initiated Oxidation of Glycolaldehyde over the Temperature Range 233−296 K. *J. Phys. Chem. A* **2006**, *110* (50), 13492–13499. https://doi.org/10.1021/jp064993k.

(73) So, S.; Wille, U.; da Silva, G. A Theoretical Study of the Photoisomerization of Glycolaldehyde and Subsequent OH Radical-Initiated Oxidation of 1,2-Ethenediol. *J. Phys. Chem. A* **2015**, *119* (38), 9812–9820. https://doi.org/10.1021/acs.jpca.5b06854.

(74) Kaiser, J.; Skog, K. M.; Baumann, K.; Bertman, S. B.; Brown, S. B.; Brune, W. H.; Crounse, J. D.; de Gouw, J. A.; Edgerton, E. S.; Feiner, P. A.; et al. Speciation of OH Reactivity above the Canopy of an Isoprene-Dominated Forest. *Atmos Chem Phys* **2016**, *16* (14), 9349–9359. https://doi.org/10.5194/acp-16-9349-2016.

(75) Bates, K. H.; Jacob, D. J. A New Model Mechanism for Atmospheric Oxidation of Isoprene: Global Effects on Oxidants, Nitrogen Oxides, Organic Products, and Secondary Organic Aerosol. *Atmospheric Chem. Phys.* **2019**, *19* (14), 9613–9640. https://doi.org/https://doi.org/10.5194/acp-19-9613-2019.

CHAPTER 5

LABORATORY AND FIELD STUDIES OF ORGANIC ACIDS TO IDENTIFY BIOGENIC PRECURSORS AND ANTHROPOGENIC INFLUENCE

4.1 Introduction

Gas-phase organic acids have been, until recently, a broad class of molecules in the atmosphere that have mostly evaded quantitative measurement.[1] Early studies recognized the importance of organic acids to new particle formation through the observation of new particle formation events in forested environments coincident with elevated levels of formic and acetic acid suggestive of a common formation mechanism.[2] We now understand gas-phase organic acids are key indicators of atmospheric oxidation, are critical to the growth and formation of organic aerosol (OA), and regulate aerosol and rainwater pH, yet our understanding of their sources is still highly uncertain.[3,4,5,6]

Unlike atmospheric organic molecules such as peroxides (formed generally through hydroperoxy radical (HO_2) reaction with peroxy radicals (RO_2)) or alcohols (largely formed from OH-addition to alkenes) the formation mechanisms for gas-phase organic acids are not as clear. It is generally thought that the specific mechanisms involve several oxidation reactions (multiple generations) before resulting in the formation of a carboxylic acid moiety through functionalization of a precursor carbon backbone or fragmentation of the backbone to produce lower molecular weight products.[7,8] In fact, the carboxylic acid moiety is so important for determining the extent of oxidation that a molecule has undergone that OA oxidation is often characterized by the amount of CO_2^+ ion that is detected from aerosol samples as measured by aerosol mass spectrometers.[3,9] Most chemical models used to predict OA formation circumvent the uncertainties in the mechanisms of gas-phase OA components by assuming the key reactions controlling the extent of OA formation are $RO_2 + NO$ or $RO_2 + HO_2$.[10] It is assumed, in some

instances, these reactions result in oxygenated species—such as hydroperoxides or organic acids—that partition to aerosol. As demonstrated in one study, different representations of the reactions controlling the concentration of HO_2 radicals can dramatically influence predicted OA production mechanisms (i.e. shifting between HO_2 and NO-dominated RO_2 termination control) and magnitudes.[11] Reducing the uncertainties in how organic acids are formed is one approach for constraining the extent to which we can use simplified chemical schemes to predict OA formation and other processes.

Recently developed techniques for the measurement of gas-phase organic acids have revealed two major findings; (1) organic acids are ubiquitous and (2) our ability to explain their atmospheric presence is poor. Organic acids have been observed in ppb_v-level concentrations from a diversity of environments including forests, cities, the arctic mainland, the arctic ocean, classrooms and oil and natural gas-producing regions complicating a holistic understanding of where they come from and how they are formed.[1,12–21] Several modeling studies have pointed to a 'missing source' of organic acids not adequately explained by current chemical mechanisms or emissions estimates. In particular, attempts to model the simplest organic acids, formic and acetic acid, on the global and regional scales do not capture their abundance or diel variability.[13,22–24] Some studies have suggested interesting, yet uncertain, organic acid formation processes such as heterogenous reactions on snow surfaces and aerosol, and reactions of ozone on soil to help explain observed 'missing sources'.[12,13,17] Recent studies have pointed to the importance of enol—produced from photolysis of aldehydes—OH oxidation in the gas phase and ketone photolysis in the aqueous phase as important sources of organic acids.[24–26] Other organic acid chemical production pathways that would be particularly difficult to observe as isolated processes in the ambient environment—but none the less have been suggested to be

important sources—include reactions of Criegee biradicals at gas-liquid interfaces of aerosol and photolysis of organic aerosol.[27,28] In addition to all of this—like most oxidation products of hydrocarbons by OH—organic acid production is likely affected by cycles of RO_2 reaction with NO and HO_2. Characterization and quantification of a wide variety of organic acids in different environments is necessary to determine the importance of speculated mechanisms for organic acid formation.

Areas dominated by biogenic influence are observed to be major sources of organic acids.[23,29] We focus our study on the characterization and quantification of a wide variety of gas-phase organic acids in a forest with mixed deciduous and coniferous vegetation, during the Southeastern Aerosol and Oxidant Study (SOAS), and a ponderosa pine forest, during the Seasonal Particles in Forest Fluxes study (SPiFFY). We use acetate reagent ion chemical ionization mass spectrometry (acetate CIMS) to measure and quantify organic acids with a high enough time resolution to capture timescales relevant for rapid chemical change. We use the results of targeted laboratory studies of isoprene and α-pinene oxidation to aid in understanding the secondary sources of organic acids during SOAS and SPiFFY. From these measurements we evaluate the importance of various potential mechanisms responsible for organic acid levels observed from both forests.

5.2. Experimental Methods

5.2.1 acetate CIMS

Gas-phase oxygenated VOCs were measured using an Aerodyne high resolution time-of-flight chemical ionization mass spectrometer equipped with the acetate ($C_2H_3O_2^-$) reagent ion (hereafter referred to as acetate CIMS). Details of the acetate reagent ion chemistry and CIMS

operation have been described elsewhere.[30–35] Briefly, the acetate reagent ions are generated by flowing 40 sccm of ultra high purity nitrogen through a stainless-steel reservoir containing acetic anhydride (Fischer Scientific, 99.5%) which is then diluted with 2 SLPM nitrogen and introduced to the ion molecule reactor through a radioactive ^{210}Po (NRD, Inc.) ionizer. Acetate reagent ions selectively ionize organic acids through a gas-phase proton-transfer reaction so that mostly deprotonated analytes ($[M]^-$) are detected. However, if the instrument is operated such that cluster ion transmission is efficient, then reagent ion clusters ($[C_2H_3O_2 \cdot M]^-$) enable measurements of additional species including peroxides.[36,37] Details of data filtering processes and artifact identification procedures are presented in Appendix 4. Below, we occasionally provide chemical names to measured elemental formulae from the acetate CIMS based on atmospheric or experimental relevance. However, we do not employ an isomer separation technique, and every observed ion should be considered the sum of possible isomers with carboxylic acid functionality.

5.2.2 Laboratory measurements: Focused Isoprene Experiments at the California Institute of Technology (FIXCIT)

FIXCIT included multiple chamber studies in January 2014, described in detail by Nguyen et al.[38] (2014). We focus on FIXCIT experiments investigating the influence of OH, O_3, and nitrate (NO_3) oxidation of isoprene and α-pinene and investigate the relative importance of RO_2 reaction with NO versus HO_2 on the production of organic acids. Additional relevant experimental details are in Appendix 4.

5.2.3 Southeastern Oxidant and Aerosol Study (SOAS)

The SOAS campaign took place at the Centerville (CTR) Southeastern Aerosol Research and Characterization (SEARCH) site in Brent, AL (32.903016°N, -87.250104°W) in the summer of 2013.[19,39–41] The site is located on a hill surrounded by Talladega National Forest, which consists of mixed deciduous and coniferous vegetation. VOC emissions are dominated by isoprene with median daytime mixing ratios ~5 ppb_v with significant contributions from monoterpenes (Figure A4.1). We consider the SOAS measurements to represent organic acid chemistry from mixed monoterpene and isoprene precursors. Ambient NO_x and SO_2 at the site indicate anthropogenic influence on atmospheric chemical processes in the area.[41,42] The acetate CIMS was operated from 22 June to 16 July with a 7.5 m inlet (2 liter per minute (lpm) flowrate) 6 m above ground level. The CalTech CIMS operated throughout this period with an inlet 22 m above ground level.[40] Gas-phase organic acid data was filtered to remove precipitation events, thus minimizing the effects of wet deposition on diel trends.

5.2.4 Seasonal Particles in a Forest Flux Study (SPiFFY)

The SPiFFY campaign took place 2-14 August 2016 at the Manitou Experimental Forest Observatory (MEFO), which is ~40 km west of Colorado Springs, CO (39.102140 N, -105.108630 W). MEFO is a Ponderosa pine plantation and is described in detail by Ortega et al.[43] (2014). Fulgham et al. (2019) describe CIMS measurements in detail. Briefly, ambient air was sampled from the top of the 30 m tower at ~40 lpm through a 35 m inlet into a trailer below the tower where the CIMS subsampled at 2 lpm.

5.2.5 Quantification of organic acids from acetate CIMS measurements

We observe hundreds of unique species with the acetate CIMS. Direct calibrations were only performed for select compounds during the different campaigns so we utilized a previously

published parameterization of instrument sensitivity as a function of number of carbons and average carbon oxidation state (OSc; OSc ≈ 2 x O/C – H/C) of organic acid analytes.[1] During FIXCIT, SOAS, and SPiFFY the field-based acetate CIMS was operated under a different set of voltage settings, extraction frequencies, and inlet flowrates compared to the laboratory-based CIMS on which the sensitivity parameterization was developed. For instance, the voltage configuration of the instrument during FIXCIT and SOAS was such that transmission of clusters between the reagent ion and neutral analytes was efficient. The potential influence of reagent-analyte clusters on the analysis is discussed in greater detail in Appendix 4. Laboratory calibrations with the laboratory-based acetate CIMS provided key transformations to relate the calibrations in lab to the measurements from the acetate CIMS used during FIXCIT, SOAS, and SPiFFY (Figure 5.1; left side panels).

Briefly, the sensitivities of 12 different organic acids were measured offline in lab under a specific set of instrument operating conditions and voltages. We typically configure the acetate CIMS to collisionally dissociate clustered species as they travel from the ionization region to the detector, resulting in a mass spectrum of deprotonated ions (i.e. $m/z_M = MW_M - 1.00794$).[30,31] However, during FIXCIT, the CIMS was configured to retain reagent-analyte clusters. This configuration allowed us to sensitively detect peroxides as clusters with acetate (e.g. [ISOPOOH + acetate]; sensitivity = 0.5 ncps ppb_v^{-1}).[36,37] The sensitivities of the 12 organic acids were corrected for the different voltage settings used during FIXCIT and SOAS (Figure 5.1; panel a) using the reagent self-clustering ratio ($[C_2H_4O_2 \cdot C_2H_3O_2]^-/[C_2H_3O_2]^-$) as an indicator of the instrument low voltage configuration. The sensitivities were then corrected for the influence of extraction frequency (Figure 5.1; panel b). In the case of SPiFFY the sensitivities were also corrected for the influence of inlet flowrate (Figure 5.1; panel c). These corrected sensitivities

were then used as parameters along with observed elemental formulae to perform a multiple linear regression (Figure 5.1; right side panel d) used to estimate sensitivities, as described in detail by Liu et al. (2017). A detailed discussion of detection limit filtering, elemental formula categorization and filtering, and characterization of clustering and instrumental artifacts is in Appendix 4.

During SPiFFY online calibrations were performed for four different acids—formic, propanoic, butanoic and methacrylic acid—providing a population to compare the sensitivity parameterization against actual calibrations (Figure 5.2). The results of these comparisons suggest that the bulk C_{eq} mixing ratios of organic acids are likely a lower bound for their actual mixing ratios. However, it is encouraging that after several instrumental corrections to sensitivities and then a regression to calculate a sensitivity to these acids based on properties of the elemental formula there is still reasonably good agreement between estimated formic acid mixing ratios and calibrated formic acid mixing ratios. The discrepancy between estimated and calibrated mixing ratios for some of the other acids serve as examples to demonstrate the potential pitfalls using bulk quantification methods and further support the assertion that an online calibration is always the preferred method when pursuing quantification.[30]

As an additional point of comparison, we compare our results to those of Yatavelli et al.[44] (2014) and Hunter et al.[45] (2017), who used slightly different methods to measure gas-phase organic acids at the MEFO site from August 20-28 in 2011. Those studies found mixing ratios of total gas-phase organic acids of 0.8 ± 0.3 ppb_v (assuming 1.2 µg m^{-3} of particle-phase organic acids, an average organic acid molecular weight of 150 g mol^{-1} and 48% of total gas and particle organic acids partitioned to particle mass), similar to our measurement of 1.5 ± 0.4 ppb_v gas-phase organic acid mixing ratios (SPiFFY campaign average).

Our reagent ion selection prevents us from detecting acetic acid, one of the most abundant atmospheric organic acids. We use measurements of acetic acid from a triple quad CIMS to contribute to organic acid bulk analyses from the FIXCIT chamber experiments and SOAS.[40,46] We use previous measurements of acetic acid (measured as acetic acid + glycolaldehyde), measured by proton-transfer time-of-flight mass spectrometry (PTR-ToF), in the summer of 2008 at the Manitou Experimental Forest site to estimate acetic acid during SPiFFY.[47] Without subtraction of the glycolaldehyde contribution, we consider this acetic acid estimate at Manitou to be an upper-bound.

5.2.6 Positive Matrix Factorization (PMF) analyses of SOAS and SPiFFY UMR measurements

Positive Matrix Factorization (PMF) is a statistical method often used in atmospheric chemistry to group a population of time-varying signals from VOCs or aerosol into factors that represent physically-meaningful sources or processes.[48,49] PMF assumes that a factor's chemical composition (in this case, mass spectral composition) is constant over the time of analysis. This has been relatively useful for describing primary source contributions and effects of chemical processing on organic aerosol measured by aerosol mass spectrometers (AMS).[50] In contrast to aerosol factors, VOC data is often more challenging to interpret.[48,51] Yuan et al. (2012) found that PMF resolved two VOC factors representing photochemical processing and transport of anthropogenic primary emissions with indistinguishable source contributions. This observation was replicated by Abeleira et al.[52] (2017), who found VOCs associated with oil and natural gas produced two separate factors, one with more reactive (i.e. larger rate constants with OH) VOCs and the other with less reactive species. Koss et al. (2019) found that PMF factors from chamber VOC data represented the average chemical composition at a specific time during the experiment

(i.e. beginning, middle, and end), and did not provide any information on the kinetics of the oxidation experiment. Thus, to date, PMF is unable to separate specific chemical processes (e.g. OH versus O_3 oxidation), generations of oxidation (i.e. first-generation versus late-generation), or precursor contribution (e.g. isoprene oxidation versus toluene oxidation products) for VOC data. Nonetheless, correlating VOC data from laboratory and ambient experiments provides one method for inferring chemical sources of oxidized VOCs.[53] However, the success of this example was likely enhanced by the highly selective nature of the measurement technique complimented by low background signals.

We perform PMF on the acetate CIMS unit mass resolution (UMR) mass spectral data collected during SOAS and SPiFFY to explore the general time-varying trends observed from the population of species observed. We circumvent challenges associated with quantifying error related to limited-resolution peak fitting by performing PMF on UMR data.[54] Following Yan et al.[53] (2016), we then qualitatively identify specific species from high-resolution data with trends that match the temporal behavior of the PMF factors. Similar to other studies, we use correlations of the resulting factors with time series of ancillary chemical data to help aid identification of physical or chemical processes contributing to the variability of the organic acids associated with the factors.[48,55] We use unique species in the mass spectra from the FIXCIT experiments (Figures A4.2-A4.8) to elucidate factors from SOAS. We note that UMR data can include signals from molecules other than organic acids such as organic and inorganic sulfur and nitrogen containing species (e.g. SO_2^-, SO_3^-), as well as fragment ions (e.g. $C_2H_3O^-$, $C_3H_5O^-$). Multiple PMF solutions contained factors that reflected the influence of complex background processes in the acetate CIMS, such as reagent contamination, sample tubing off-gasing, and

reagent-ion chemistry artifacts. To reduce complexity, we excluded numerous ions representing known artifacts from the PMF analysis (Table A4.4).

5.3. Results and discussion

5.3.1 Organic acid production observed from the FIXCIT experiments

5.3.1.1 Oxidation of isoprene and α-pinene oxidation produced compositionally diverse organic acids during FIXCIT

We observe many different products from α-pinene and isoprene oxidation in the CIMS mass spectra as either clusters with the acetate reagent ion ($[M + C_2H_3O_2]^-$) or deprotonated species ($[M-H]^-$) (Figure 5.3). Figures A4.2-A4.8 show the diversity of species, represented in the difference mass spectra, produced for each experiment analyzed in this study during FIXCIT. Some clustered species observed in the experiments are useful markers, in the ambient atmosphere, for isoprene oxidation such as isoprene hydroxy hydroperoxide or isoprene epoxydiol (ISOPOOH/IEPOX; $C_5H_{10}O_3$) and a dihydroperoxide compound ($C_5H_{12}O_4$; Krechmer et al., 2015)—indicative of $HO_2 + RO_2$ influenced reactions. Similarly, isoprene nitrates, $C_4H_7NO_5$ and $C_5H_{11}NO_4$, were observed in the "high NO" experiment (Figure A4.3) and indicate $NO + RO_2$ influenced reactions. Organic acids were mostly observed as deprotonated species and varied in production and diversity depending on experimental conditions.

Many similar organic acids were produced across experiments though with some important differences. The isoprene + OH "low NO" experiment produced more unique acids with appreciable signal than the "high NO" experiment, which suggests NO generally suppresses organic acid formation from biogenic precursors. Formic acid was produced with relatively high signal in each experiment and, therefore, is a poor tracer for specific types of oxidation chemistry

involving isoprene and α-pinene. Many acids, in fact, shared common oxidation sources including propionic ($C_3H_6O_2$), 3-oxobutyric acid ($C_4H_6O_3$), glycolic ($C_2H_4O_3$), glyoxylic acid ($C_2H_2O_3$), pyruvic ($C_3H_4O_3$), and malonic acid ($C_3H_4O_4$). Some of these acids have been previously observed from isoprene oxidation [57] and have implications atmospheric aqueous production of organic radicals and secondary organic aerosol [58–60]. Oxidation of α-pinene produced more higher molecular weight acids, such as pinalic ($C_9H_{14}O_3$), pinonic ($C_{10}H_{16}O_3$), and pinic ($C_9H_{12}O_4$), with minor contributions from smaller (<C6) acids. This difference demonstrates the potential effectiveness of isoprene versus monoterpene oxidation as a source of gas-phase organic acids.

5.3.1.2 Organic acid carbon-equivalent (C_{eq}) yields

The FIXCIT experiments show that gas-phase organic acids are important multi-generation oxidation products that account for 4-28% of the reacted carbon in the isoprene experiments. Isoprene ozonolysis at high RH ("50% RH with OH scavenger") produced the highest carbon-equivalent (C_{eq}) yield (ppbC organic acid/ppbC of precursor) of organic acids, with C_{eq} yield = 28% (Figure 5.4). Interestingly, the NO_3 radical experiment produced a C_{eq} yield of 11% (corrected for coincident ozonolysis; Appendix 4) which is larger than from both isoprene + OH experiments. This suggests both ozonolysis and NO_3 oxidation could be important nighttime chemical sources of organic acid production. Though OH oxidation produced the lowest yields of organic acids, compared to NO_3 and O_3, this route of oxidation is likely the most important source of acids to the atmosphere because it accounts for ~88% of the isoprene sink globally.[61]

The distribution of organic acids organized by carbon number were different depending on how isoprene was oxidized. For instance, organic acids measured during the isoprene + OH oxidation experiments were almost equally distributed across C1 through C5 species. This observation suggests simultaneous fragmentation and functionalization processes influence the organic acid population. Both alkoxy radical decomposition and functionalization of the original isoprene carbon backbone (or portions of it) were equally important for producing the observed organic acid population in the OH oxidation experiments. In contrast, NO_3 oxidation produced mostly formic and acetic acids indicating important decomposition mechanisms.

In the isoprene + O_3 oxidation experiments, more C4 organic acids were produced than C5 acids, which we speculate is the result of unimolecular rearrangements from Criegee Intermediates. In the first generation of oxidation, ozonolysis of a terminal alkene in isoprene results in formaldehyde and a C4 Criegee intermediate (CI). Nguyen et al.[62] (2014) describes the fate of C4 CIs from isoprene ozonolysis and suggests that the primary fate of C4 CIs is decomposition with minor contributions from unimolecular rearrangement reactions. In that work methacrylic acid ($C_4H_6O_2$) may be produced from unimolecular rearrangement of the methacrolein CI, and, in our experiments, this acid constitutes most of the C4 organic acid yield from isoprene ozonolysis. Unimolecular rearrangement reactions of other CI isomers, and their respective conformers, likely also contribute to the population of C4 acids observed in these isoprene ozonolysis experiments (Figure A4.12). Interestingly, although the C4 organic acid C_{eq} yield increases from 2% to 6% going from < 5% to 50% humidity (in the presence of an OH scavenger), the distribution of C4 acid products is similar for the two experiments. This suggests that, similar to the hypothesized mechanism for the C1 CI producing formic acid, bimolecular reactions of C4 with water vapor potentially result in minor production of C4 organic acids.

The major sink for C4 CIs produced from isoprene ozonolysis is decomposition—thought to produce formaldehyde and an acylperoxy radical in high yield—though the chemistry at this stage of oxidation is highly uncertain. Acetic acid yields from ozonolysis increase from dry (< 5% RH) to humid (50% RH) conditions, potentially from HO_2 + acylperoxy radical reactions, or decomposition of α-hydroxy hydroperoxides on the humid chamber surface.[62] These surface decomposition reactions could follow mechanisms similar to hydroxy methyl hydroperoxide.[63] In contrast to C4 acids, humidity does not affect the C_{eq} yield of C3 acids. Thus, while wall effects may complicate chemistry producing organic acids under humid conditions from these chamber experiments, C4 CI decomposition to RO_2 and subsequent RO_2+HO_2 reactions remain a likely source of at least some organic acid production.

Organic acid yields were lowest during α-pinene oxidation. However, the amount of SOA produced from α-pinene oxidation is much higher than isoprene oxidation. This difference in SOA production is not a novel observation, but comparison of the gas-phase acids produced from each precursor shows that acids from α-pinene oxidation may simply be lower in vapor pressure and thus contribute more to aerosol growth compared to isoprene. This is consistent with the recent observations of Zhang et al. (2018) suggesting that, while isoprene mixing ratios are much higher than monoterpenes, at least 50% of summertime organic aerosol in the Southeastern US is derived from monoterpenes. Overall, these results suggest OH oxidation of α-pinene is not an important source of gas-phase organic acids to the ambient atmosphere.

Several key observations about gas-phase organic acid production are apparent from the FIXCIT chamber experiments; (1) diverse species of organic acids are produced from isoprene and α-pinene oxidation in carbon-equivalent yields similar in magnitude to formic and acetic acids, (2) RO_2 reaction with NO suppresses organic acid formation compared to reaction with

HO_2, (3) OH oxidation of isoprene yields more organic acids than α-pinene, and (4) water vapor increases organic acid production during isoprene ozonolysis. These experiments suggest that isoprene may be a more important source of gas-phase organic acids than monoterpenes during SOAS, but that monoterpenes may instead contribute more particle phase organic acids. Monoterpene-dominated environments such as the SPiFFY site, may have lower organic acid levels than isoprene-dominated environments, even if total reactive carbon levels are the same.

5.3.2 Ambient observations of organic acids from SOAS and SPiFFY

5.3.2.1 C_{eq} mixing ratios of organic acids measured during SOAS and SPiFFY

Total organic acid C_{eq} mixing ratios varied considerably, in abundance and diel variability, as shown in Figure 5.5. C_{eq} mixing ratios of organic acids are typically a factor of two to four higher during the day at SOAS than SPiFFY. Nighttime median organic acid mixing ratios are nearly identical during the two campaigns (Figure 5.5; top panel). These differences in mixing ratios may be due to surface exchange processes (emission or deposition) or chemical reactions. C_{eq} mixing ratios at both sites have diel trends similar to ozone, consistent with a strong photochemical source. During both campaigns, formic acid is the single largest contributor to C_{eq}, accounting for 30% of the total C_{eq} at SOAS (60% at SPiFFY) (Figure 5.6). The fractional importance of formic acid to total organic acid showed similar diel patterns (insets, Figure 5.6). A more diverse population of organic acids, distinguished by carbon number, contribute to the total C_{eq} mixing ratio at SOAS compared to SPiFFY (Figure 5.5; inset pie charts). We hypothesize most of the differences observed in total organic acid C_{eq} mixing ratios and acid diversity between the two sites is because of a strong photochemical source at SOAS that is not as influential at SPiFFY.

5.3.2.2 Diel variation of organic acids by carbon number and functionality

We analyze organic acids differentiated by carbon number and functional group composition (Figure 5.7) to understand site-specific processes influencing organic acid abundance throughout the day. Additionally, we follow the methods of Liu et al (2017) to categorize analytes as monoacids (saturated or unsaturated), carbonyl acids (saturated or unsaturated), diacids + hydroxycarbonyls (cannot be differentiated by this method), or hydroxyacids.

All organic acids measured during SOAS exhibit signatures of a daytime photochemical source regardless of carbon number. As the organic acid carbon number increases, however, the implied strength of the photochemical source decreases—as shown by the change in mixing ratio in Figure 5.7, panel a, relative to the mixing ratio observed at midnight. While saturated monoacids contribute to most of the organic acid C_{eq} mixing ratio (42%) during SOAS (mostly from formic acid), other types of acids, such as hydroxyacids (17%) and carbonyl acids (18%), make important contributions. Because the majority of the acids observed from SOAS contain between one and five carbon atoms (Figure 5.5; 86% of total C_{eq} mixing ratio) and exhibit a strong daytime source signature we hypothesize photochemical oxidation of isoprene likely also produces acids with diverse functionalities.

Organic acids at SPiFFY exhibit distinct diel patterns depending on how big they are. In contrast to the acids at SOAS, all the acids are at maximum levels around midnight. Except for the largest acids (i.e. C8-C10) most acids follow the pattern of going down in concentration in the morning and then increasing in concentration, at varying rates, throughout the day. The largest acids show a characteristic spike in concentration around 8 a.m. then decrease in

concentration during the day, similar to the diel signature of monoterpenes. This observation does not necessitate nighttime sources – instead, much like monoterpenes at the site, the loss mechanisms for these organic acids may be larger during the day. The lack of a strong photochemical influence at SPiFFY, like is observed at SOAS, is likely responsible for the decreased diversity of acids as indicated by the functional group distribution (Figure 5.7, panel d). In the absence of the strong influence from isoprene photochemical oxidation, minor chemical and physical organic acid sources are likely more observable influences on the organic acid population from SPiFFY such as monoterpene oxidation or emissions.

5.3.3 PMF analyses of ambient gas-phase organic acids

We use PMF to identify groups of ions that show similar temporal patterns, providing insight on the potential chemical or physical sources of organic acids. Unless explicitly stated, we perform correlations with campaign diel medians of PMF factors and ancillary data to understand the behavior of organic acids on average.

5.3.3.1 SOAS PMF factors show influence of NO and HO_2 reactions with isoprene-derived RO_2

A six-factor solution adequately represents the variability observed in the data from SOAS. Three factors associated with daytime chemical production, an anthropogenic sulfur factor, a biogenic oxidation factor and an interference factor from a co-located air conditioning (A/C) unit were identified (Figure 5.8).

Isoprene is the main precursor for organic acid formation at SOAS with likely important contributions from monoterpenes. Massoli et al. (2018) conducted a PMF analysis on NO_3 CIMS data at SOAS, identifying six factors, including three factors corresponding to isoprene oxidation

and three factors associated with terpene oxidation. In particular, we find that two of the factors from Massoli et al., the "isoprene afternoon" and the "isoprene nitrates II" factors, have good temporal correlation with two factors from our study. Below, we compare the factors we derived from acetate CIMS data at SOAS to two of Massoli et al's factors as well as the mass spectra observed during FIXCIT (described above) to understand the potential influence of NO on the organic acid population.

OH oxidation of isoprene OH and $RO_2 + HO_2$ reactions are the likely source of acids corresponding to the "isoprene $RO_2 + HO_2$" acetate CIMS factor. One of the most prominent peaks in the "isoprene $RO_2 + HO_2$" factor mass spectrum is ISOPOOH and/or isoprene epoxydiol (IEPOX), identified as a cluster with the acetate reagent (m/z 177). Both species are major products of isoprene-derived RO_2 reaction with HO_2. Several species from the mass spectra for this factor also overlap with FIXCIT experiments, consistent with "low NO" OH oxidation of isoprene. The diel pattern from the acetate CIMS "isoprene $RO_2 + HO_2$" factor is nearly identical to Massoli et al's "isoprene afternoon" factor (NO_3 CIMS). The "isoprene afternoon" factor from the Massoli et al. study is identified as isoprene-derived because it has a mass spectrum containing mostly C4 and C5 low-volatility species observed from the "low NO" OH oxidation of ISOPOOH as measured by the NO_3 CIMS during FIXCIT. We also observe a good correlation ($r = 0.67$) of this acetate CIMS factor with HO_2 (Figure 5.10) further suggesting the importance of $RO_2 + HO_2$ chemistry to this factor.

NO reaction with RO_2 from isoprene OH oxidation is the likely source of organic acids in the "isoprene RO_2 + NO" factor. The diel profile of the acetate CIMS "isoprene RO_2 + NO" factor correlates well with the Massoli et al. NO_3 CIMS "isoprene nitrate II" factor ($r = 0.88$). Massoli et al.'s "isoprene nitrate II" factor included C5 nitrates and dinitrates that had either been

observed in chamber studies of isoprene OH oxidation under "high NO" conditions or were hypothesized to be associated with second and third generation oxidation products of isoprene hydroxy nitrates. Several ions are prominent in the mass spectrum from the "isoprene RO_2 + NO" factor that were also observed in the mass spectra from isoprene and α-pinene OH oxidation during FIXCIT such as $C_4H_6O_2$ (methacrylic acid; isoprene oxidation), $C_4H_6O_3$ (isoprene oxidation), and $C_5H_8O_3$ (α-pinene oxidation). The close correlation between our acetate CIMS factor and the Massoli et al. isoprene nitrate factor suggests that this factor represents acids that are produced from, or associated with, reactions that produce isoprene nitrates during the day – that is, representing isoprene + OH and RO_2 + NO reactions.

Both the isoprene "RO_2 + HO_2" and "RO_2 + NO" factors identified in this study peak in the middle of the day, though the timeseries are different – making it clear that RO_2 simultaneously reacts with NO and HO_2 at SOAS, producing distinct suites of organic acids. Peroxy radical chemistry is often defined in terms of being merely in a 'high NOx' versus a 'low NOx' regime, but this factor analysis reaffirms the concept that RO_2 termination occurs simultaneously via reaction with NO and HO_2. The ratio of the isoprene "RO_2 + NO" to the "RO_1 + HO_2" PMF factor shows what times of the day these respective RO_2 reactions are most important (Figure 5.9). This factor ratio spikes shortly after a spike in NO in the morning on average at SOAS and the ratio decreases, relative to early morning and evening hours, throughout the day. These factors further demonstrate that the shift from RO_2 termination by NO to HO_2 as NO_x decreases has strong implications on the organic acid budget – and thus the mechanisms ultimately responsible for organic carbon fate and SOA formation in the atmosphere.

We identified four additional factors in the acetate CIMS data:

- We define the "biogenic" factor from the ions most prominent in the mass spectrum that were associated with monoterpene and isoprene oxidation the FIXCIT experiments. One of the strongest peaks in the factor spectrum, $C_5H_{12}O_4 \cdot (C_2H_3O_2)^-$, has been observed in organic aerosol samples from SOAS and from NO_3 CIMS measurements of 4,3-ISOPOOH oxidation during FIXCIT. [56,64] Additionally, the "biogenic" factor exhibits modest correlations with organic aerosol PMF factors (r = 0.60; MO-OOA and r=0.47; ISOPOOH-OA) at different times during SOAS.[41,56] We hypothesize this factor must reflect the gas-phase molecules associated with biogenic organic aerosol production – species produced during isoprene or monoterpene oxidation that did not appreciably condense to aerosol.
- Despite removing UMRs we knew to be associated with measurement artifacts, our six-factor solution still includes a sample tubing artifact factor. On average, this factor correlates well with solar radiation, and the factor time series correlates well (r = 0.68) with the high-resolution time series of CF_3O^-; a tubing artifact (Figure 5.10). We also note this factor includes $C_3H_4O_2$ (acrylic acid), $C_3H_4O_3$ (pyruvic acid), and $C_3H_4O_4$ (malonic acid), which suggests these species may be susceptible to tubing partitioning processes.
- The acetate CIMS "anthropogenic sulfur" factor includes SO_2^-, SO_3^-, SO_5^-, and two organosulfur compounds in the mass spectrum. SO_2^- signals in the acetate CIMS correlate well with observed $SO_{2\,(g)}$ (r^2 = 0.86). The time series of this factor is irregular, consistent with regional transport of sulfur to the site from anthropogenic sources (Figure 5.10).
- The cycling of the air-conditioning unit (A/C unit) co-located in the trailer with the CIMS created an oscillating CIMS signal resulting in the "A/C unit" factor (Figures A4.14 and

A4.15). This interference affected all ions in the mass spectrum, but most strongly impacted ions with low signal-to-noise and compounds expected to have a high affinity for partitioning to surfaces (e.g. lactic acid, $C_3H_5O_3$). Two processes may be producing the A/C factor: (i) wall-desorption processes on the tubing and instrument inlet and (ii) physical changes in the instrument (e.g. expansion/contraction of ToF region). On average, the A/C unit factor accounted for 26% of the total CIMS signal during SOAS (Figure A4.16), highlighting the potential importance of instrument interferences in affecting bulk analysis of instrument signals.

5.3.3.2 SPiFFY PMF factors show distinct daytime and nighttime features

We describe the SPiFFY campaign acetate CIMS data with a five-factor solution. Three factors showed daytime maxima ("daytime factor I", "daytime factor II", and "tubing artifact" factors), one nighttime maxima ("nighttime factor") and one factor ("anthropogenic sulfur") was more sporadic in nature (Figure 5.11).

The largest fraction of the UMR signal (33%) is allocated to the "daytime I" factor and the time series of this factor correlated with more high-resolution species than any other factor. Formic acid was not included in the PMF analysis but correlates well with the "daytime I" factor ($r = 0.78$; Figure 5.12). This indicates formic acid is not only the most abundant acid at the MEFO site but is influenced by production and loss processes that impact many other acids such as pyruvic, propanoic, and glycolic acid. The "daytime I" factor has a diel profile similar to other oxidized VOCs observed at the site from previous years including acetaldehyde, acetone, and methanol.[65] Kaser et al. (2013) measured light and temperature dependent fluxes for these oxidized VOCs indicative of emission sources. In contrast, Fulgham et al. (2019) measured weak

temperature dependencies of C1-C6 alkanoic acids and estimated primary emission sources to make minor contributions to observed summertime fluxes. The high temporal correlation of this "daytime I" factor with many organic acids underscores the importance of common sources and sinks for many of the acids measured by the acetate CIMS at the MEFO site.

The "daytime II" factor shows a strong time series correlation (r = 0.78) with ozone and we hypothesize this factor is associated with daytime OH oxidation. Organic acid concentrations frequently correlate with ozone in outdoor field studies, suggesting that photochemistry is a major source of organic acids.[16,66] Notably, NO_3^- and CNO^---presumably nitric and isocyanic acid—correlate well with this factor further supporting the conclusion that this factor represents acids with a photochemical source.[67] Isoprene mixing ratios are, on average, an order of magnitude lower at the SPiFFY site compared to SOAS while monoterpene mixing ratios are comparable (Figure A4.1).[68] Though less studied than isoprene and monoterpenes, 2-methyl-3-buten-2-ol (MBO) accounts for most of the OH reactivity at the SPiFFY site, but is not an expected source of organic acids.[45,69,70]

The "nighttime I" factor maximizes at midnight but shows an intriguing second peak in the mid-morning between 9-11 am that is similar to the diel behavior of total monoterpenes (measured by proton-transfer MS) observed in previous years.[65] Monoterpenes minimize in the middle of the day at Manitou due to their short lifetime against OH and O_3. Interestingly, the diel profile of the 'nighttime II' factor was similar (r = 0.83) to the "terpene nitrates" factor measured by the NO_3 CIMS during SOAS, though we acknowledge limitations to this comparison as the sites had very different meteorology and sources. While we do not observe any monoterpene nitrates in the acetate CIMS data—potentially due to the relatively long inlet lines—ions associated with monoterpene oxidation appear in the factor mass spectrum (i.e. $C_{10}H_{15}O_4^-$,

$C_9H_{15}O_3^-$). Additionally, the time series of this factor correlates well (r= 0.80) with the C10 group of acids indicating a likely oxidation source. We hypothesize this population of organic acids is influenced by oxidation of monoterpenes. Several of the acids present in this factor (i.e. $C_2H_3O_3^-$, $C_4H_7O_2^-$, $C_3H_5O_3^-$, ect.) would not be detected by the NO_3 CIMS and thus shows our measurements captures a subset of oxidation products potentially produced coincidentally with terpene nitrates.

We identified two additional factors:

- Similar to SOAS, we observe an "anthropogenic sulfur" factor associated with regional transport of pollutants. Transport of pollution from the neighboring cities of Denver and Colorado Springs has been reported in a previous study, and was determined to influence RO_2 termination through increased reaction with NO over HO_2.[43] However, SO_2 and its potential effects on RO_2 fate do not affect the organic acid distribution: similar to SOAS, the organic acid PMF factors do not correlate with this factor.
- Despite extensive filtering of the UMR data we identified a "tubing artifact" factor whose time series exhibited high correlation with tracers, in our instrument, for off-gasing of sampling lines such as CF_3O^- and $C_2F_3O_2^-$. Like SOAS, many acids exhibit reasonable correlations with this factor indicating that some acids measured during SPiFFY were susceptible to tubing wall partitioning processes.

5.4 Implications for gas-phase organic acids in biogenically-influenced environments

We quantified and characterized ~ 100 individual gas-phase organic acids from two forests and laboratory oxidation experiments of isoprene and α-pinene. FIXCIT shows that while individual organic acids are poor indicators of specific chemical processes such as HO_2 or NO

termination of RO_2, bulk analysis of the detected organic acids can provide some clear contrasts between chemical systems. Isoprene oxidation by OH under low NO conditions produced both the most diverse population of organic acids (i.e. the greatest number of individual organic acids contributing to the total C_{eq} yield) and highest organic acid yield. Where isoprene ozonolysis effectively produces select organic acids, OH oxidation of isoprene likely contributed to the diversity of organic acids at SOAS. NO suppresses the photochemical production of organic acids, resulting in much lower organic acid concentrations and a smaller array of organic acid products than low-NO conditions for both isoprene and α-pinene.

The major sink for OH at SOAS was isoprene compared to SPiFFY where the major sink was MBO and monoterpenes with only a minor (~5%) contribution from isoprene.[45,71] Daytime organic acid C_{eq} mixing ratios were 4x higher at SOAS than SPiFFY, emphasizing the important role of isoprene OH-initiated oxidation in producing organic acids. This conclusion is also supported when comparing the C_{eq} yields of organic acids produced from isoprene versus α-pinene OH oxidation. Though the two sites had important differences with respect to the presence of isoprene they showed similar levels of organic acid carbon in the evening. These similarities suggest that both sites potentially share a common chemical production source with similarly important sinks. For instance, monoterpene mixing ratios were similar between SOAS and SPiFFY so that might be an important nighttime chemical source and physical loss could also occur at similar rates.

The extent to which organic acids, as an entire class of gas-phase molecules, regulate the pH of atmospheric water or can act as predictors for atmospheric organic aerosol are questions that can be addressed through quantification of these species. Shifts in anthropogenic emissions of NO_x and SO_2 are predicted to have impacts on how organic aerosol is formed from biogenic

precursors and the levels of gas-phase organic acids will likely also respond to these changes with corresponding impacts on atmospheric processes.[72] Further quantification of these species could help characterize how environments with biogenic influence respond to ecosystem changes in the future and what impact those changes have on the atmosphere. In order to isolate the importance of specific chemical processes important for organic acid formation from biogenic precursors more laboratory oxidation studies are needed, particularly focusing on organic acid formation from isoprene.

5.5 Chapter 5 Figures

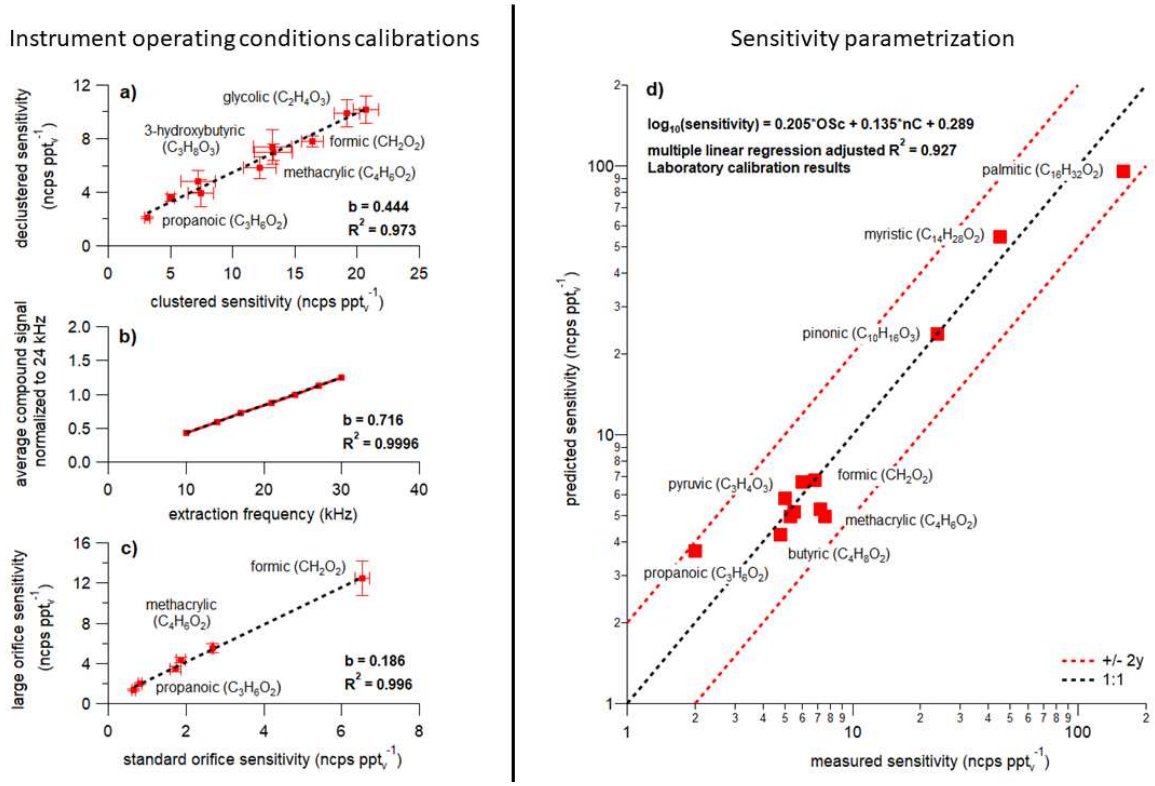

Figure 5.1. Acetate CIMS calibrations performed under different operating conditions (left side panels) defined by (a) voltage settings/cluster transmission efficiency, (b) extraction frequency, and (c) inlet orifice size. Laboratory-derived sensitivities for 12 different acids were corrected for the different operating conditions employed during FIXCIT, SOAS, and SPiFFY then used as inputs to the multiple linear regression (right side panel; d) to calculate predicted sensitivities for uncalibrated organic acids. The names and formulas of select acid calibrants are shown.

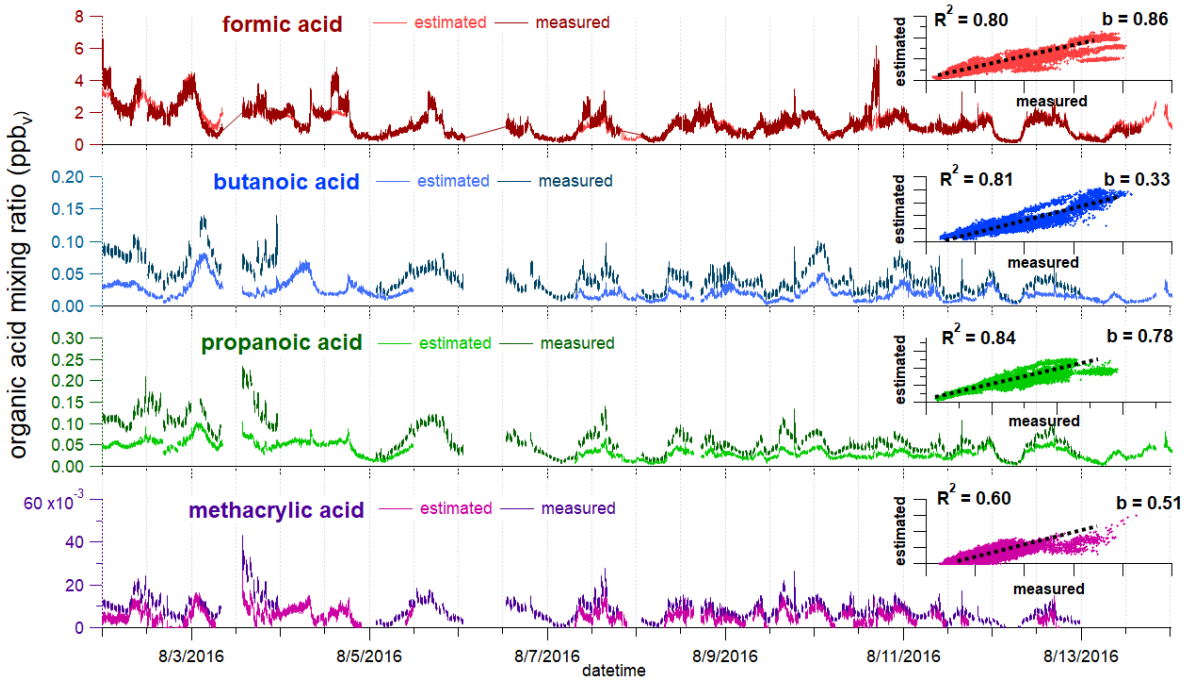

Figure 5.2. Comparison of select organic acid mixing ratios observed during SPiFFY calculated with sensitivities derived from using on-line hourly calibrations (measured) versus estimation from the sensitivity parameterization (estimation).

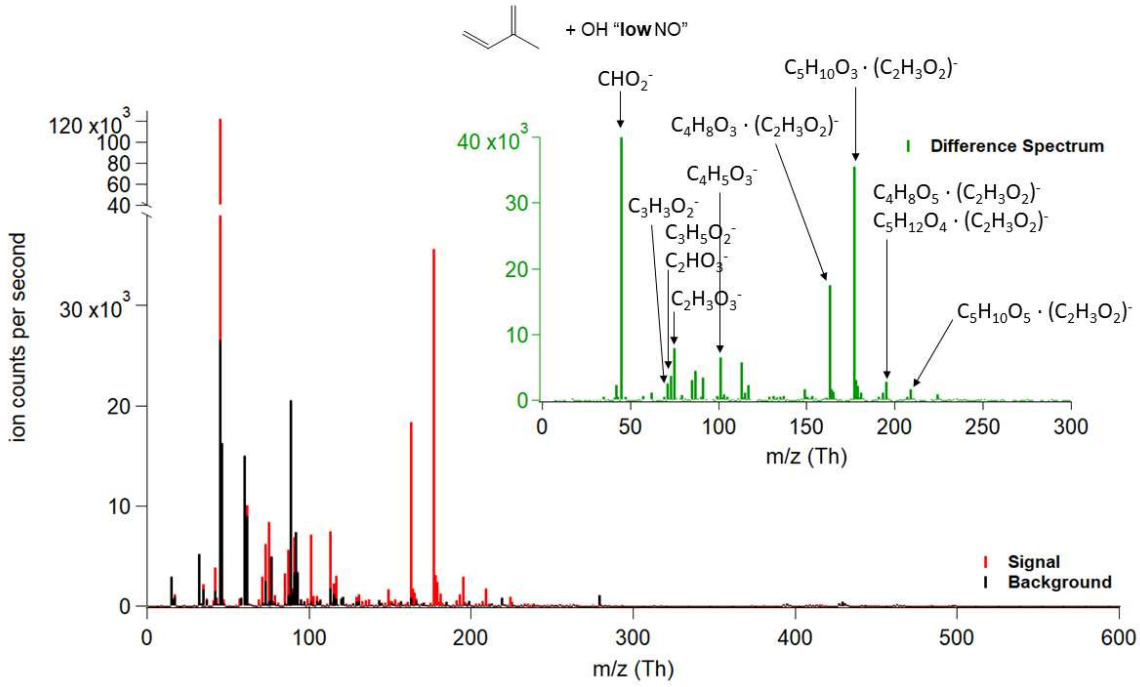

Figure 5.3. Mass spectra measured by the acetate CIMS from the end of the "low NO" isoprene + OH experiment (red) versus the background (black). Signals are shown in ion counts per second (normalized to the acetate reagent) in the main panel. The difference between the signal and background spectra are shown in the inset figure (green trace). Several organic acids observed in the mass spectrum are identified as their conjugate bases (i.e. $[M\text{-}H]^-$) and several suspected peroxide species are identified as clusters with the acetate reagent ion (i.e. $[M + C_2H_3O_2]^-$).

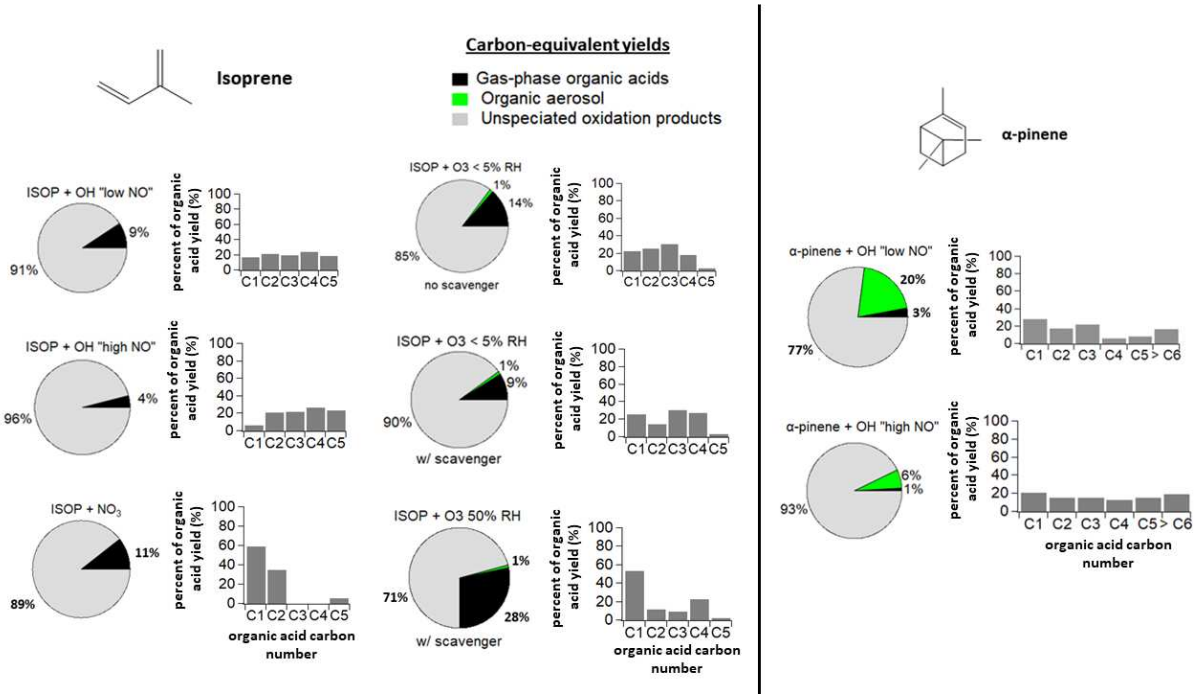

Figure 5.4. Summary of organic acid production from six isoprene and two α-pinene oxidation experiments observed during FIXCIT. The pie charts show the distribution of total carbon measured during each experiment and allocation to organic acids (black), SOA (green), or non-speciated oxidation products (light gray) as carbon reservoirs. The bar charts show the percent contribution of organic acids, sorted by carbon number, to the total measured organic acid yield from each experiment (i.e. represented as percentage of black slice). Organic acids measured during the isoprene oxidation experiments containing more than five carbons were not included in the quantitative analysis. Measured organic acids containing more than ten carbon atoms were not included in any of the quantitative analyses for α-pinene. Additionally, we neglect particle wall loss in the organic aerosol yield calculation as this effect should be similar between experiments and doesn't impact the conclusions of this work.

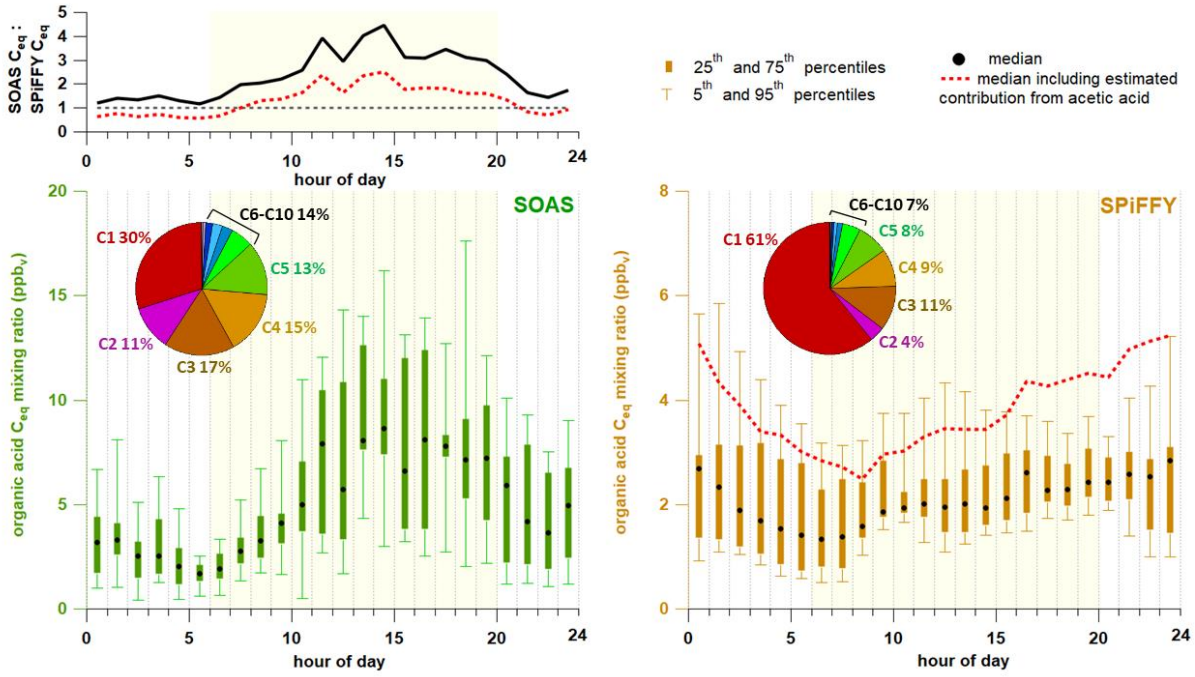

Figure 5.5. Diel boxplots showing the carbon equivalent (C_{eq}) mixing ratio of total measured organic acid carbon for SOAS (left panel) and SPiFFY (right panel). The bars represent the 5th and 95th percentiles and the boxes are the 25th and 75th percentiles. The black dots are medians. The shaded yellow area shows the daylight hours. Pie charts show the distribution of the organic acids by carbon number throughout the campaigns. The pie chart includes the contribution from acetic acid for SOAS, but not SPiFFY. The observed ratio of Ceq at SOAS (including acetic acid) versus SPiFFY (excluding acetic acid) is in black the top panel, while the red dashed lines include the estimated contribution of acetic acid to SPiFFY from acetic acid + glycolaldehyde measurements from Kim et al. (2010).[47]

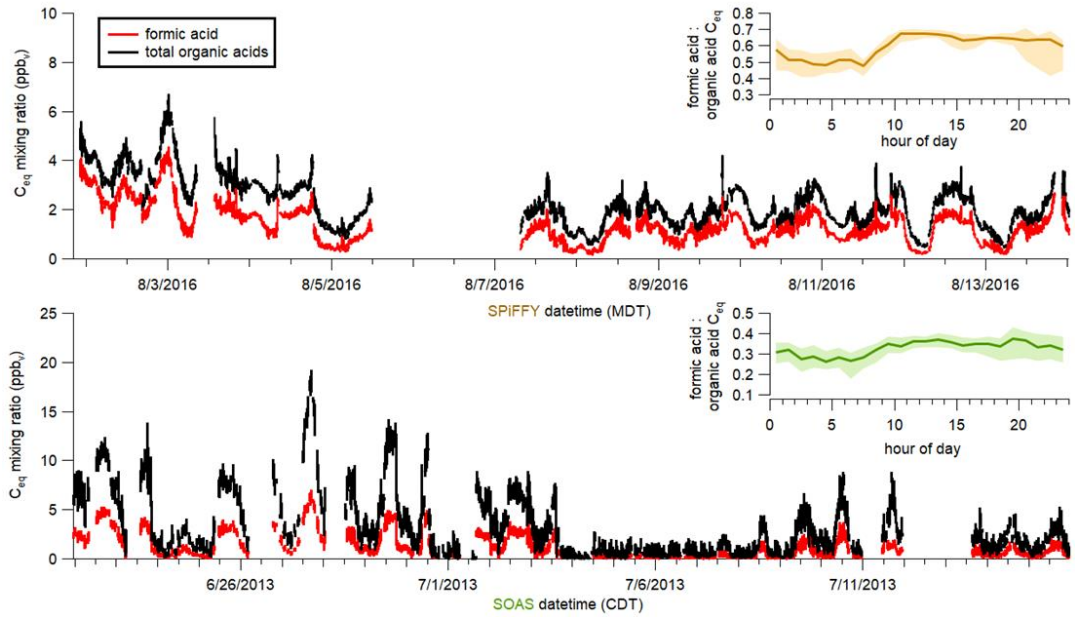

Figure 5.6. Time series of formic acid and C_{eq} mixing ratios for SPiFFY (top) and SOAS (bottom). The insets show the diel variation of the formic acid to C_{eq} ratio; the solid line represents the median and the shaded area the interquartile range.

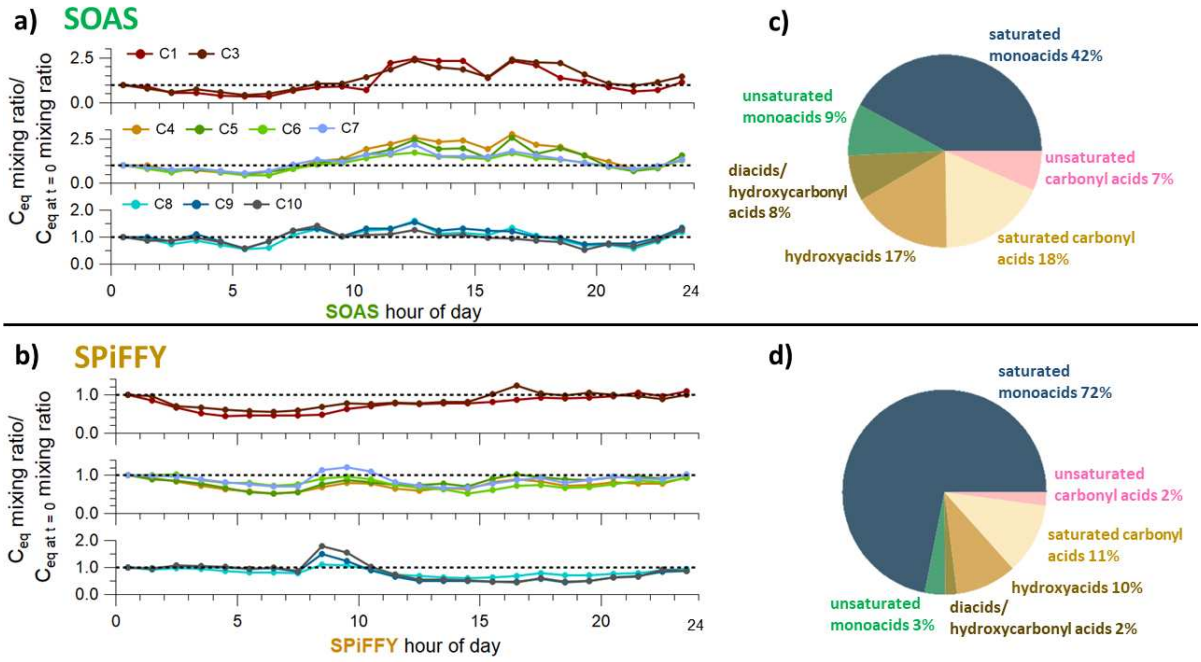

Figure 5.7. Analysis of organic acid carbon number diel variation and functionality distribution during SOAS (top) and SPiFFY (bottom). The carbon number diel plots (panels a and b) show C1 and C3 acids in the top panels, C4 through C7 acids in the middle panels, and C8 through C10 acids in the bottom panels. Carbon number diel traces are normalized by the mixing ratio at hour zero to show difference in day and nighttime levels. The distribution of organic acids classified by functional group are shown in panels c and d for each campaign. The contribution from acetic acid is not included in this analysis.

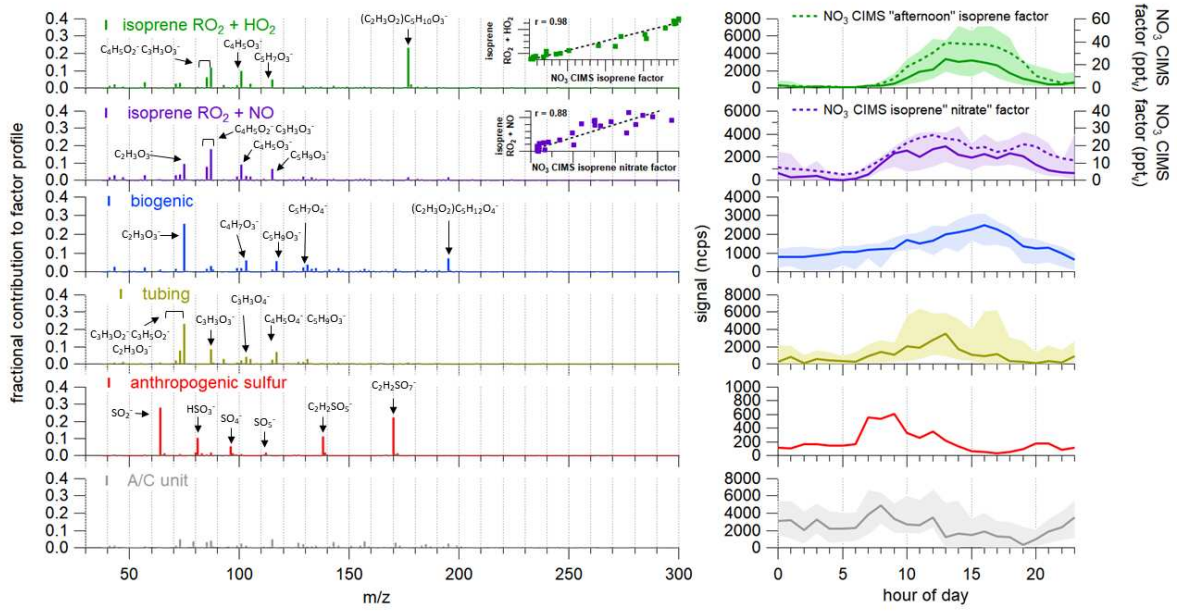

Figure 5.8. Mass spectra (right) and diel time series (left) for the six factors from the PMF solution for SOAS. The peaks in the factor mass spectra are presented as fractional contributions to the total composition of the factor (i.e. a peak with an intensity of 0.2 would represent 20% of the factor's signal). From top to bottom the identities of the factors are isoprene RO_2 + HO_2 factor (green), biogenic factor (blue), isoprene RO_2 + NO factor (purple), daytime factor (yellow), anthropogenic sulfur (red), and a factor associated with signal variation caused by the A/C unit (gray). Important species associated with the factors are identified with arrows in the mass spectra and described by the conjugate base of the organic acid analyte. Diel profiles represent campaign medians, and the shaded areas show the interquartile range. Correlation plots are shown as insets for two of the factors. The "isoprene nitrate II" factor, from the NO_3 CIMS PMF, diel time series is correlated with the "isoprene RO_2 + NO" factor (r = 0.88), and the "isoprene afternoon" factor, from the NO_3 CIMS PMF, diel time series is correlated with the "isoprene RO_2 + HO_2" factor (r = 0.98).[55] The corresponding diel time series from the NO_3 CIMS PMF factors are shown as dashed lines in the plots to the right of the corresponding factors.

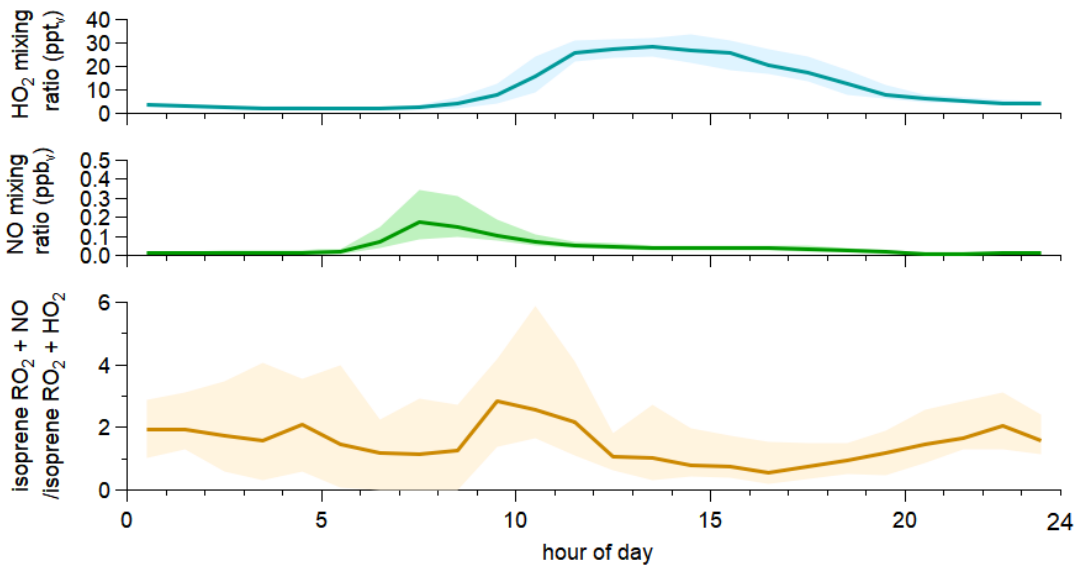

Figure 5.9. Diel profiles showing HO_2, NO, and the ratio of the time series from the isoprene "RO_2 + NO" factor to the isoprene "RO_2 + HO_2" factor (bottom panel). NO spikes in the morning around 8am and shortly after that around 10am the ratio of the isoprene "RO_2 + NO" to the "RO_2 + HO_2" factors spikes. The ratio of these factors decreases during the day.

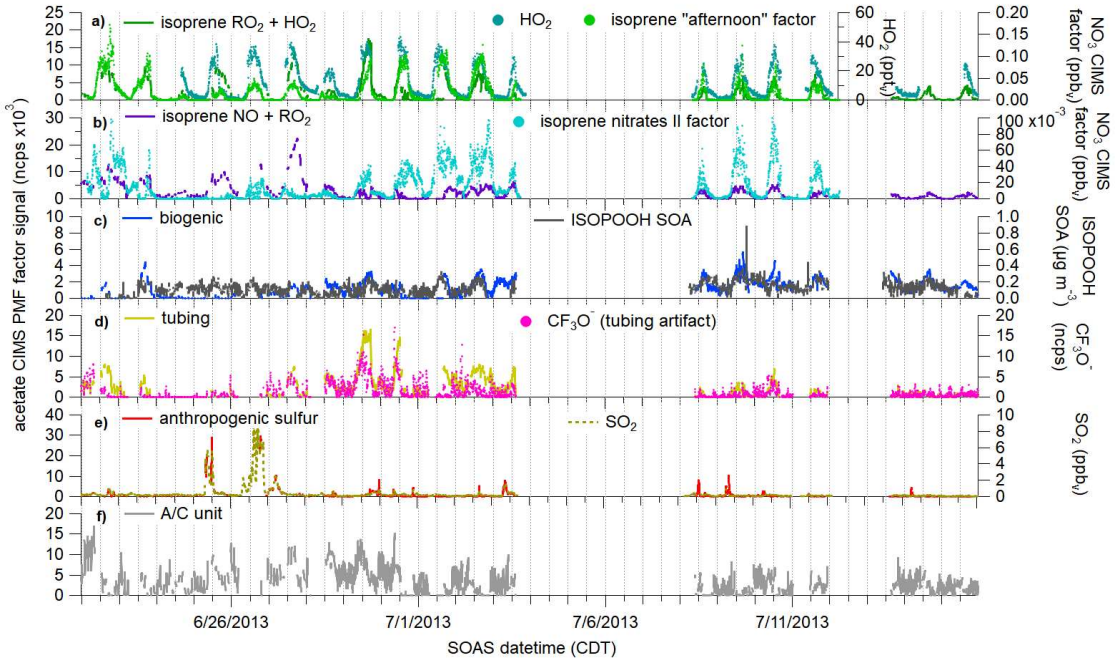

Figure 5.10. SOAS PMF factor time series. The traces shown in panels a and b were measured by the NO_3 CIMS (Massoli et al., 2018) and the ISOPOOH SOA PMF factor shown in panel c was measured by an AMS during SOAS.[56]

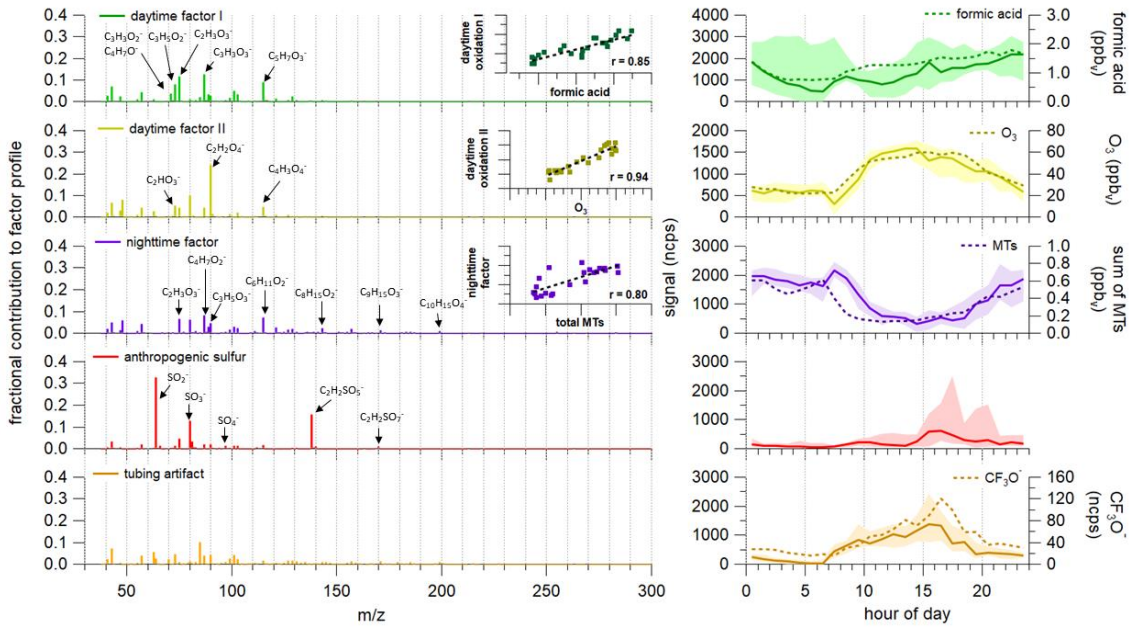

Figure 5.11. Mass spectra (left) and diel time series (right) for the five factors from the PMF solution for SPiFFY. From top to bottom the identities of the factors are daytime factor I (green), daytime factor II (yellow), nighttime factor (purple), anthropogenic sulfur (red), and a tubing artifact factor (orange). Inset correlation plots show diel profile measurements of formic acid correlated with daytime factor I (r = 0.85), O_3 is correlated with the daytime II factor (r = 0.94), and total monoterpenes (MTs) correlated with the nighttime factor (r = 0.80). Good correlation was also observed between the diel profiles of CF_3O^- and the tubing artifact factor.

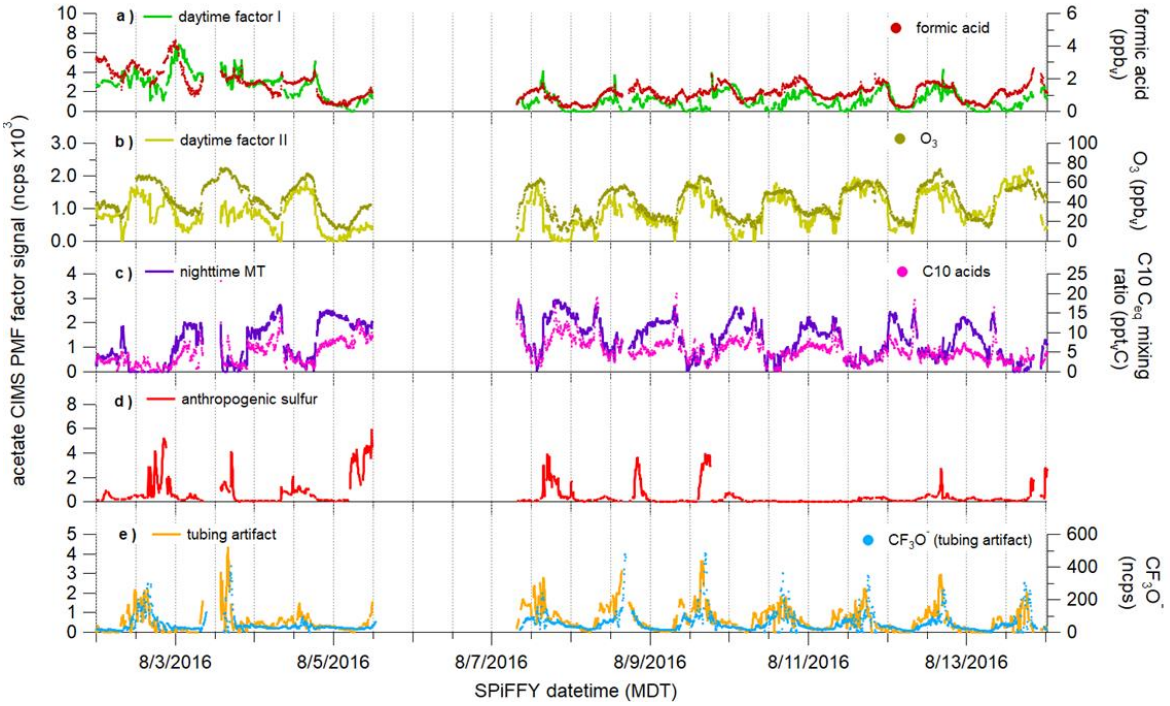

Figure 5.12. SPiFFY PMF factor time series. Species correlated with PMF factors—formic acid, C10 acids, and CF_3O^---were measured by the acetate CIMS.

REFERENCES

(1) Liu, S.; Thompson, S. L.; Stark, H.; Ziemann, P. J.; Jimenez, J. L. Gas-Phase Carboxylic Acids in a University Classroom: Abundance, Variability, and Sources. *Environ. Sci. Technol.* **2017**, *51* (10), 5454–5463. https://doi.org/10.1021/acs.est.7b01358.

(2) Kavouras, I. G.; Mihalopoulos, N.; Stephanou, E. G. Formation of Atmospheric Particles from Organic Acids Produced by Forests. *Nature* **1998**, *395* (6703), 683–686. https://doi.org/10.1038/27179.

(3) Yatavelli, R. L. N.; Mohr, C.; Stark, H.; Day, D. A.; Thompson, S. L.; Lopez-Hilfiker, F. D.; Campuzano-Jost, P.; Palm, B. B.; Vogel, A. L.; Hoffmann, T.; et al. Estimating the Contribution of Organic Acids to Northern Hemispheric Continental Organic Aerosol. *Geophys. Res. Lett.* **2015**, *42* (14), 2015GL064650. https://doi.org/10.1002/2015GL064650.

(4) Metzger, S.; Mihalopoulos, N.; Lelieveld, J. Importance of Mineral Cations and Organics in Gas-Aerosol Partitioning of Reactive Nitrogen Compounds: Case Study Based on MINOS Results. *Atmospheric Chem. Phys.* **2006**, *6* (9), 2549–2567.

(5) Millet, D. B. Atmospheric Chemistry: Natural Atmospheric Acidity. *Nat. Geosci.* **2012**, *5* (1), 8–9. https://doi.org/10.1038/ngeo1361.

(6) Liggio, J.; Moussa, S. G.; Wentzell, J.; Darlington, A.; Liu, P.; Leithead, A.; Hayden, K.; O'Brien, J.; Mittermeier, R. L.; Staebler, R.; et al. Understanding the Primary Emissions and Secondary Formation of Gaseous Organic Acids in the Oil Sands Region of Alberta, Canada. *Atmos Chem Phys* **2017**, *17* (13), 8411–8427. https://doi.org/10.5194/acp-17-8411-2017.

(7) R. Wilson, K.; D. Smith, J.; H. Kessler, S.; H. Kroll, J. The Statistical Evolution of Multiple Generations of Oxidation Products in the Photochemical Aging of Chemically Reduced Organic Aerosol. *Phys. Chem. Chem. Phys.* **2012**, *14* (4), 1468–1479. https://doi.org/10.1039/C1CP22716E.

(8) Barsanti, K. C.; Kroll, J. H.; Thornton, J. A. Formation of Low-Volatility Organic Compounds in the Atmosphere: Recent Advancements and Insights. *J. Phys. Chem. Lett.* **2017**, *8* (7), 1503–1511. https://doi.org/10.1021/acs.jpclett.6b02969.

(9) Ng, N. L.; Canagaratna, M. R.; Zhang, Q.; Jimenez, J. L.; Tian, J.; Ulbrich, I. M.; Kroll, J. H.; Docherty, K. S.; Chhabra, P. S.; Bahreini, R.; et al. Organic Aerosol Components Observed in Northern Hemispheric Datasets from Aerosol Mass Spectrometry. *Atmospheric Chem. Phys.* **2010**, *10* (10), 4625–4641. https://doi.org/https://doi.org/10.5194/acp-10-4625-2010.

(10) Jathar, S. H.; Cappa, C. D.; Wexler, A. S.; Seinfeld, J. H.; Kleeman, M. J. Multi-Generational Oxidation Model to Simulate Secondary Organic Aerosol in a 3-D Air Quality Model. *Geosci Model Dev* **2015**, *8* (8), 2553–2567. https://doi.org/10.5194/gmd-8-2553-2015.

(11) Akherati, A.; Cappa, C. D.; Kleeman, M. J.; Docherty, K. S.; Jimenez, J. L.; Griffith, S. M.; Dusanter, S.; Stevens, P. S.; Jathar, S. H. Simulating Secondary Organic Aerosol in a Regional Air Quality Model Using the Statistical Oxidation Model – Part 3: Assessing the Influence of Semi-Volatile and Intermediate-Volatility Organic Compounds and NO_x. *Atmospheric Chem. Phys.* **2019**, *19* (7), 4561–4594. https://doi.org/https://doi.org/10.5194/acp-19-4561-2019.

(12) Mattila, J. M.; Brophy, P.; Kirkland, J.; Hall, S.; Ullmann, K.; Fischer, E. V.; Brown, S.; McDuffie, E.; Tevlin, A.; Farmer, D. K. Tropospheric Sources and Sinks of Gas-Phase Acids in the Colorado Front Range. *Atmospheric Chem. Phys.* **2018**, *18* (16), 12315–12327. https://doi.org/https://doi.org/10.5194/acp-18-12315-2018.

(13) Yuan, B.; Veres, P. R.; Warneke, C.; Roberts, J. M.; Gilman, J. B.; Koss, A.; Edwards, P. M.; Graus, M.; Kuster, W. C.; Li, S.-M.; et al. Investigation of Secondary Formation of Formic Acid: Urban Environment vs. Oil and Gas Producing Region. *Atmos Chem Phys* **2015**, *15* (4), 1975–1993. https://doi.org/10.5194/acp-15-1975-2015.

(14) Archibald, A. T.; McGillen, M. R.; Taatjes, C. A.; Percival, C. J.; Shallcross, D. E. Atmospheric Transformation of Enols: A Potential Secondary Source of Carboxylic Acids in the Urban Troposphere. *Geophys. Res. Lett.* **2007**, *34* (21). https://doi.org/10.1029/2007GL031032.

(15) Bannan, T. J.; Murray Booth, A.; Le Breton, M.; Bacak, A.; Muller, J. B. A.; Leather, K. E.; Khan, M. A. H.; Lee, J. D.; Dunmore, R. E.; Hopkins, J. R.; et al. Seasonality of Formic Acid (HCOOH) in London during the ClearfLo Campaign. *J. Geophys. Res. Atmospheres* **2017**, *122* (22), 2017JD027064. https://doi.org/10.1002/2017JD027064.

(16) Veres, P. R.; Roberts, J. M.; Cochran, A. K.; Gilman, J. B.; Kuster, W. C.; Holloway, J. S.; Graus, M.; Flynn, J.; Lefer, B.; Warneke, C. Evidence of Rapid Production of Organic Acids in an Urban Air Mass. *Geophys. Res. Lett.* **2011**, *38* (17).

(17) Mungall, E. L.; Abbatt, J. P. D.; Wentzell, J. J. B.; Wentworth, G. R.; Murphy, J. G.; Kunkel, D.; Gute, E.; Tarasick, D. W.; Sharma, S.; Cox, C. J.; et al. High Gas-Phase Mixing Ratios of Formic and Acetic Acid in the High Arctic. *Atmospheric Chem. Phys.* **2018**, *18* (14), 10237–10254. https://doi.org/https://doi.org/10.5194/acp-18-10237-2018.

(18) Mungall, E. L.; Abbatt, J. P. D.; Wentzell, J. J. B.; Lee, A. K. Y.; Thomas, J. L.; Blais, M.; Gosselin, M.; Miller, L. A.; Papakyriakou, T.; Willis, M. D.; et al. Microlayer Source of Oxygenated Volatile Organic Compounds in the Summertime Marine Arctic Boundary Layer. *Proc. Natl. Acad. Sci.* **2017**, *114* (24), 6203–6208. https://doi.org/10.1073/pnas.1620571114.

(19) Brophy, P.; Farmer, D. K. A Switchable Reagent Ion High Resolution Time-of-Flight Chemical Ionization Mass Spectrometer for Real-Time Measurement of Gas Phase Oxidized Species: Characterization from the 2013 Southern Oxidant and Aerosol Study. *Atmos Meas Tech* **2015**, *8* (7), 2945–2959. https://doi.org/10.5194/amt-8-2945-2015.

(20) Fulgham, S. R.; Brophy, P.; Link, M. F.; Ortega, J.; Pollack, I.; Farmer, D. K. Seasonal Flux Measurements over a Colorado Pine Forest Demonstrate a Persistent Source of Organic Acids. *ACS Earth Space Chem.* **2019**. https://doi.org/10.1021/acsearthspacechem.9b00182.

(21) Schobesberger, S.; Lopez-Hilfiker, F. D.; Taipale, D.; Millet, D. B.; D'Ambro, E. L.; Rantala, P.; Mammarella, I.; Zhou, P.; Wolfe, G. M.; Lee, B. H.; et al. High Upward Fluxes of Formic Acid from a Boreal Forest Canopy. *Geophys. Res. Lett.* **2016**, *43* (17), 2016GL069599. https://doi.org/10.1002/2016GL069599.

(22) Millet, D. B.; Baasandorj, M.; Farmer, D. K.; Thornton, J. A.; Baumann, K.; Brophy, P.; Chaliyakunnel, S.; de Gouw, J. A.; Graus, M.; Hu, L.; et al. A Large and Ubiquitous Source of Atmospheric Formic Acid. *Atmos Chem Phys* **2015**, *15* (11), 6283–6304. https://doi.org/10.5194/acp-15-6283-2015.

(23) Paulot, F.; Wunch, D.; Crounse, J. D.; Toon, G. C.; Millet, D. B.; DeCarlo, P. F.; Vigouroux, C.; Deutscher, N. M.; González Abad, G.; Notholt, J.; et al. Importance of Secondary Sources in the Atmospheric Budgets of Formic and Acetic Acids. *Atmos Chem Phys* **2011**, *11* (5), 1989–2013. https://doi.org/10.5194/acp-11-1989-2011.

(24) Shaw, M. F.; Sztáray, B.; Whalley, L. K.; Heard, D. E.; Millet, D. B.; Jordan, M. J. T.; Osborn, D. L.; Kable, S. H. Photo-Tautomerization of Acetaldehyde as a Photochemical Source of Formic Acid in the Troposphere. *Nat. Commun.* **2018**, *9* (1), 2584. https://doi.org/10.1038/s41467-018-04824-2.

(25) So, S.; Wille, U.; da Silva, G. A Theoretical Study of the Photoisomerization of Glycolaldehyde and Subsequent OH Radical-Initiated Oxidation of 1,2-Ethenediol. *J. Phys. Chem. A* **2015**, *119* (38), 9812–9820. https://doi.org/10.1021/acs.jpca.5b06854.

(26) Eugene, A. J.; Guzman, M. I. Reactivity of Ketyl and Acetyl Radicals from Direct Solar Actinic Photolysis of Aqueous Pyruvic Acid. *J. Phys. Chem. A* **2017**, *121* (15), 2924–2935. https://doi.org/10.1021/acs.jpca.6b11916.

(27) Qiu, J.; Ishizuka, S.; Tonokura, K.; Colussi, A. J.; Enami, S. Reactivity of Monoterpene Criegee Intermediates at Gas–Liquid Interfaces. *J. Phys. Chem. A* **2018**, *122* (39), 7910–7917. https://doi.org/10.1021/acs.jpca.8b06914.

(28) Malecha, K. T.; Nizkorodov, S. A. Photodegradation of Secondary Organic Aerosol Particles as a Source of Small, Oxygenated Volatile Organic Compounds. *Environ. Sci. Technol.* **2016**. https://doi.org/10.1021/acs.est.6b02313.

(29) Stavrakou, T.; Müller, J.-F.; Peeters, J.; Razavi, A.; Clarisse, L.; Clerbaux, C.; Coheur, P.-F.; Hurtmans, D.; De Mazière, M.; Vigouroux, C.; et al. Satellite Evidence for a Large Source of Formic Acid from Boreal and Tropical Forests. *Nat. Geosci.* **2012**, *5* (1), 26–30. https://doi.org/10.1038/ngeo1354.

(30) Brophy, P.; Farmer, D. K. Clustering, Methodology, and Mechanistic Insights into Acetate Chemical Ionization Using High-Resolution Time-of-Flight Mass Spectrometry. *Atmos Meas Tech* **2016**, *9* (8), 3969–3986. https://doi.org/10.5194/amt-9-3969-2016.

(31) Veres, P.; Roberts, J. M.; Warneke, C.; Welsh-Bon, D.; Zahniser, M.; Herndon, S.; Fall, R.; de Gouw, J. Development of Negative-Ion Proton-Transfer Chemical-Ionization Mass Spectrometry (NI-PT-CIMS) for the Measurement of Gas-Phase Organic Acids in the Atmosphere. *Int. J. Mass Spectrom.* **2008**, *274* (1–3), 48–55.

(32) Aljawhary, D.; Lee, A. K. Y.; Abbatt, J. P. D. High-Resolution Chemical Ionization Mass Spectrometry (ToF-CIMS): Application to Study SOA Composition and Processing. *Atmos Meas Tech* **2013**, *6* (11), 3211–3224. https://doi.org/10.5194/amt-6-3211-2013.

(33) Bertram, T. H.; Kimmel, J. R.; Crisp, T. A.; Ryder, O. S.; Yatavelli, R. L. N.; Thornton, J. A.; Cubison, M. J.; Gonin, M.; Worsnop, D. R. A Field-Deployable, Chemical Ionization Time-of-Flight Mass Spectrometer. *Atmospheric Meas. Tech.* **2011**, *4* (7), 1471–1479. https://doi.org/https://doi.org/10.5194/amt-4-1471-2011.

(34) Lee, B. H.; Lopez-Hilfiker, F. D.; Mohr, C.; Kurtén, T.; Worsnop, D. R.; Thornton, J. A. An Iodide-Adduct High-Resolution Time-of-Flight Chemical-Ionization Mass Spectrometer: Application to Atmospheric Inorganic and Organic Compounds. *Environ. Sci. Technol.* **2014**, *48* (11), 6309–6317. https://doi.org/10.1021/es500362a.

(35) Yatavelli, R. L. N.; Lopez-Hilfiker, F.; Wargo, J. D.; Kimmel, J. R.; Cubison, M. J.; Bertram, T. H.; Jimenez, J. L.; Gonin, M.; Worsnop, D. R.; Thornton, J. A. A Chemical Ionization High-Resolution Time-of-Flight Mass Spectrometer Coupled to a Micro Orifice Volatilization Impactor (MOVI-HRToF-CIMS) for Analysis of Gas and Particle-Phase Organic Species. *Aerosol Sci. Technol.* **2012**, *46* (12), 1313–1327. https://doi.org/10.1080/02786826.2012.712236.

(36) Budisulistiorini, S. H.; Li, X.; Bairai, S. T.; Renfro, J.; Liu, Y.; Liu, Y. J.; McKinney, K. A.; Martin, S. T.; McNeill, V. F.; Pye, H. O. T.; et al. Examining the Effects of Anthropogenic Emissions on Isoprene-Derived Secondary Organic Aerosol Formation during the 2013 Southern Oxidant and Aerosol Study (SOAS) at the Look Rock, Tennessee Ground Site. *Atmos Chem Phys* **2015**, *15* (15), 8871–8888. https://doi.org/10.5194/acp-15-8871-2015.

(37) Inomata, S.; Hirokawa, J. Non-Radioactive Chemical Ionization Mass Spectrometry Using Acetic Acid–Acetate Cluster as a Reagent Ion for the Real-Time Measurement of Acids and Hydroperoxides. *Chem. Lett.* **2016**, *46* (1), 38–41. https://doi.org/10.1246/cl.160828.

(38) Nguyen, T. B.; Crounse, J. D.; Schwantes, R. H.; Teng, A. P.; Bates, K. H.; Zhang, X.; St. Clair, J. M.; Brune, W. H.; Tyndall, G. S.; Keutsch, F. N.; et al. Overview of the Focused Isoprene eXperiment at the California Institute of Technology (FIXCIT): Mechanistic Chamber Studies on the Oxidation of Biogenic Compounds. *Atmos Chem Phys* **2014**, *14* (24), 13531–13549. https://doi.org/10.5194/acp-14-13531-2014.

(39) Carlton, A. G.; de Gouw, J.; Jimenez, J. L.; Ambrose, J. L.; Attwood, A. R.; Brown, S.; Baker, K. R.; Brock, C.; Cohen, R. C.; Edgerton, S.; et al. Synthesis of the Southeast Atmosphere Studies: Investigating Fundamental Atmospheric Chemistry Questions. *Bull. Am. Meteorol. Soc.* **2018**, *99* (3), 547–567. https://doi.org/10.1175/BAMS-D-16-0048.1.

(40) Nguyen, T. B.; Crounse, J. D.; Teng, A. P.; Clair, J. M. S.; Paulot, F.; Wolfe, G. M.; Wennberg, P. O. Rapid Deposition of Oxidized Biogenic Compounds to a Temperate Forest. *Proc. Natl. Acad. Sci.* **2015**, *112* (5), E392–E401. https://doi.org/10.1073/pnas.1418702112.

(41) Xu, L.; Guo, H.; Boyd, C. M.; Klein, M.; Bougiatioti, A.; Cerully, K. M.; Hite, J. R.; Isaacman-VanWertz, G.; Kreisberg, N. M.; Knote, C.; et al. Effects of Anthropogenic Emissions on Aerosol Formation from Isoprene and Monoterpenes in the Southeastern United States. *Proc. Natl. Acad. Sci.* **2015**, *112* (1), 37–42. https://doi.org/10.1073/pnas.1417609112.

(42) Lee, B. H.; Mohr, C.; Lopez-Hilfiker, F. D.; Lutz, A.; Hallquist, M.; Lee, L.; Romer, P.; Cohen, R. C.; Iyer, S.; Kurtén, T.; et al. Highly Functionalized Organic Nitrates in the Southeast United States: Contribution to Secondary Organic Aerosol and Reactive Nitrogen Budgets. *Proc. Natl. Acad. Sci.* **2016**, *113* (6), 1516–1521. https://doi.org/10.1073/pnas.1508108113.

(43) Ortega, J.; Turnipseed, A.; Guenther, A. B.; Karl, T. G.; Day, D. A.; Gochis, D.; Huffman, J. A.; Prenni, A. J.; Levin, E. J. T.; Kreidenweis, S. M.; et al. Overview of the Manitou Experimental Forest Observatory: Site Description and Selected Science Results from 2008 to 2013. *Atmospheric Chem. Phys.* **2014**, *14* (12), 6345–6367. https://doi.org/https://doi.org/10.5194/acp-14-6345-2014.

(44) Yatavelli, R. L. N.; Stark, H.; Thompson, S. L.; Kimmel, J. R.; Cubison, M. J.; Day, D. A.; Campuzano-Jost, P.; Palm, B. B.; Hodzic, A.; Thornton, J. A.; et al. Semicontinuous Measurements of Gas–particle Partitioning of Organic Acids in a Ponderosa Pine Forest Using a MOVI-HRToF-CIMS. *Atmospheric Chem. Phys.* **2014**, *14* (3), 1527–1546. https://doi.org/https://doi.org/10.5194/acp-14-1527-2014.

(45) Hunter, J. F.; Day, D. A.; Palm, B. B.; Yatavelli, R. L. N.; Chan, A. W. H.; Kaser, L.; Cappellin, L.; Hayes, P. L.; Cross, E. S.; Carrasquillo, A. J.; et al. Comprehensive

Characterization of Atmospheric Organic Carbon at a Forested Site. *Nat. Geosci.* **2017**, *10* (10), 748–753. https://doi.org/10.1038/ngeo3018.

(46) Clair, J. M. S.; Spencer, K. M.; Beaver, M. R.; Crounse, J. D.; Paulot, F.; Wennberg, P. O. Quantification of Hydroxyacetone and Glycolaldehyde Using Chemical Ionization Mass Spectrometry. *Atmospheric Chem. Phys.* **2014**, *14* (8), 4251–4262. https://doi.org/https://doi.org/10.5194/acp-14-4251-2014.

(47) Kim, S.; Karl, T.; Guenther, A.; Tyndall, G.; Orlando, J.; Harley, P.; Rasmussen, R.; Apel, E. Emissions and Ambient Distributions of Biogenic Volatile Organic Compounds (BVOC) in a Ponderosa Pine Ecosystem: Interpretation of PTR-MS Mass Spectra. *Atmospheric Chem. Phys.* **2010**, *10* (4), 1759–1771. https://doi.org/https://doi.org/10.5194/acp-10-1759-2010.

(48) Yuan, B.; Shao, M.; Gouw, J. de; Parrish, D. D.; Lu, S.; Wang, M.; Zeng, L.; Zhang, Q.; Song, Y.; Zhang, J.; et al. Volatile Organic Compounds (VOCs) in Urban Air: How Chemistry Affects the Interpretation of Positive Matrix Factorization (PMF) Analysis. *J. Geophys. Res. Atmospheres* **2012**, *117* (D24). https://doi.org/10.1029/2012JD018236.

(49) Zhang, Q.; Jimenez, J. L.; Canagaratna, M. R.; Ulbrich, I. M.; Ng, N. L.; Worsnop, D. R.; Sun, Y. Understanding Atmospheric Organic Aerosols via Factor Analysis of Aerosol Mass Spectrometry: A Review. *Anal. Bioanal. Chem.* **2011**, *401* (10), 3045–3067. https://doi.org/10.1007/s00216-011-5355-y.

(50) Ulbrich, I. M.; Canagaratna, M. R.; Zhang, Q.; Worsnop, D. R.; Jimenez, J. L. Interpretation of Organic Components from Positive Matrix Factorization of Aerosol Mass Spectrometric Data. *Atmospheric Chem. Phys.* **2009**, *9* (9), 2891–2918. https://doi.org/https://doi.org/10.5194/acp-9-2891-2009.

(51) Keutsch, N.; Kroll, J. H. Dimensionality-Reduction Techniques for Complex Mass Spectrometric Datasets: Application to Laboratory Atmospheric Organic Oxidation Experiments.

(52) Abeleira, A. J.; Farmer, D. K. Summer Ozone in the Northern Front Range Metropolitan Area: Weekend–weekday Effects, Temperature Dependences, and the Impact of Drought. *Atmos Chem Phys* **2017**, *17* (11), 6517–6529. https://doi.org/10.5194/acp-17-6517-2017.

(53) Yan, C.; Nie, W.; Äijälä, M.; Rissanen, M. P.; Canagaratna, M. R.; Massoli, P.; Junninen, H.; Jokinen, T.; Sarnela, N.; Häme, S. A. K.; et al. Source Characterization of Highly Oxidized Multifunctional Compounds in a Boreal Forest Environment Using Positive Matrix Factorization. *Atmos Chem Phys* **2016**, *16* (19), 12715–12731. https://doi.org/10.5194/acp-16-12715-2016.

(54) Cubison, M. J.; Jimenez, J. L. Statistical Precision of the Intensities Retrieved from Constrained Fitting of Overlapping Peaks in High-Resolution Mass Spectra. *Atmospheric Meas. Tech.* **2015**, *8* (6), 2333–2345.

(55) Massoli, P.; Stark, H.; Canagaratna, M. R.; Krechmer, J. E.; Xu, L.; Ng, N. L.; Mauldin, R. L.; Yan, C.; Kimmel, J. R.; Misztal, P. K.; et al. Ambient Measurements of Highly Oxidized Gas Phase Molecules during the Southern Oxidant and Aerosol Study (SOAS) 2013. *ACS Earth Space Chem.* **2018**. https://doi.org/10.1021/acsearthspacechem.8b00028.

(56) Krechmer, J. E.; Coggon, M. M.; Massoli, P.; Nguyen, T. B.; Crounse, J. D.; Hu, W.; Day, D. A.; Tyndall, G. S.; Henze, D. K.; Rivera-Rios, J. C.; et al. Formation of Low Volatility Organic Compounds and Secondary Organic Aerosol from Isoprene Hydroxyhydroperoxide Low-NO Oxidation. *Environ. Sci. Technol.* **2015**, *49* (17), 10330–10339. https://doi.org/10.1021/acs.est.5b02031.

(57) Paulot, F.; Crounse, J. D.; Kjaergaard, H. G.; Kroll, J. H.; Seinfeld, J. H.; Wennberg, P. O. Isoprene Photooxidation: New Insights into the Production of Acids and Organic Nitrates. *Atmospheric Chem. Phys.* **2009**, *9* (4), 1479–1501. https://doi.org/https://doi.org/10.5194/acp-9-1479-2009.

(58) Carlton, A. G.; Turpin, B. J.; Lim, H.-J.; Altieri, K. E.; Seitzinger, S. Link between Isoprene and Secondary Organic Aerosol (SOA): Pyruvic Acid Oxidation Yields Low Volatility Organic Acids in Clouds. *Geophys. Res. Lett.* **2006**, *33* (6). https://doi.org/10.1029/2005GL025374.

(59) Liu, Y.; Monod, A.; Tritscher, T.; Praplan, A. P.; DeCarlo, P. F.; Temime-Roussel, B.; Quivet, E.; Marchand, N.; Dommen, J.; Baltensperger, U. Aqueous Phase Processing of Secondary Organic Aerosol from Isoprene Photooxidation. *Atmospheric Chem. Phys.* **2012**, *12* (13), 5879–5895. https://doi.org/https://doi.org/10.5194/acp-12-5879-2012.

(60) Otto, T.; Stieger, B.; Mettke, P.; Herrmann, H. Tropospheric Aqueous-Phase Oxidation of Isoprene-Derived Dihydroxycarbonyl Compounds. *J. Phys. Chem. A* **2017**, *121* (34), 6460–6470. https://doi.org/10.1021/acs.jpca.7b05879.

(61) Bates, K. H.; Jacob, D. J. A New Model Mechanism for Atmospheric Oxidation of Isoprene: Global Effects on Oxidants, Nitrogen Oxides, Organic Products, and Secondary Organic Aerosol. *Atmospheric Chem. Phys.* **2019**, *19* (14), 9613–9640. https://doi.org/https://doi.org/10.5194/acp-19-9613-2019.

(62) Nguyen, T. B.; Tyndall, G. S.; Crounse, J. D.; Teng, A. P.; Bates, K. H.; Schwantes, R. H.; Coggon, M. M.; Zhang, L.; Feiner, P.; Milller, D. O.; et al. Atmospheric Fates of Criegee Intermediates in the Ozonolysis of Isoprene. *Phys. Chem. Chem. Phys.* **2016**, *18* (15), 10241–10254. https://doi.org/10.1039/C6CP00053C.

(63) Allen, H. M.; Crounse, J. D.; Bates, K. H.; Teng, A. P.; Krawiec-Thayer, M. P.; Rivera-Rios, J. C.; Keutsch, F. N.; St. Clair, J. M.; Hanisco, T. F.; Møller, K. H.; et al. Kinetics and

Product Yields of the OH Initiated Oxidation of Hydroxymethyl Hydroperoxide. *J. Phys. Chem. A* **2018**, *122* (30), 6292–6302. https://doi.org/10.1021/acs.jpca.8b04577.

(64) Zhang, H.; Yee, L. D.; Lee, B. H.; Curtis, M. P.; Worton, D. R.; Isaacman-VanWertz, G.; Offenberg, J. H.; Lewandowski, M.; Kleindienst, T. E.; Beaver, M. R.; et al. Monoterpenes Are the Largest Source of Summertime Organic Aerosol in the Southeastern United States. *Proc. Natl. Acad. Sci.* **2018**, *115* (9), 2038–2043. https://doi.org/10.1073/pnas.1717513115.

(65) Kaser, L.; Karl, T.; Guenther, A.; Graus, M.; Schnitzhofer, R.; Turnipseed, A.; Fischer, L.; Harley, P.; Madronich, M.; Gochis, D.; et al. Undisturbed and Disturbed above Canopy Ponderosa Pine Emissions: PTR-TOF-MS Measurements and MEGAN 2.1 Model Results. *Atmospheric Chem. Phys.* **2013**, *13* (23), 11935–11947. https://doi.org/https://doi.org/10.5194/acp-13-11935-2013.

(66) Liu, J.; Zhang, X.; Parker, E. T.; Veres, P. R.; Roberts, J. M.; de Gouw, J. A.; Hayes, P. L.; Jimenez, J. L.; Murphy, J. G.; Ellis, R. A.; et al. On the Gas-Particle Partitioning of Soluble Organic Aerosol in Two Urban Atmospheres with Contrasting Emissions: 2. Gas and Particle Phase Formic Acid. *J. Geophys. Res. Atmospheres* **2012**, *117* (D21), D00V21. https://doi.org/10.1029/2012JD017912.

(67) Roberts, J. M.; Veres, P. R.; VandenBoer, T. C.; Warneke, C.; Graus, M.; Williams, E. J.; Lefer, B.; Brock, C. A.; Bahreini, R.; Öztürk, F. New Insights into Atmospheric Sources and Sinks of Isocyanic Acid, HNCO, from Recent Urban and Regional Observations. *J. Geophys. Res. Atmospheres* **2014**, *119* (2), 1060–1072.

(68) Karl, T.; Hansel, A.; Cappellin, L.; Kaser, L.; Herdlinger-Blatt, I.; Jud, W. Selective Measurements of Isoprene and 2-Methyl-3-Buten-2-Ol Based on NO^+ Ionization Mass Spectrometry. *Atmospheric Chem. Phys.* **2012**, *12* (24), 11877–11884. https://doi.org/https://doi.org/10.5194/acp-12-11877-2012.

(69) Chan, A. W. H.; Galloway, M. M.; Kwan, A. J.; Chhabra, P. S.; Keutsch, F. N.; Wennberg, P. O.; Flagan, R. C.; Seinfeld, J. H. Photooxidation of 2-Methyl-3-Buten-2-Ol (MBO) as a Potential Source of Secondary Organic Aerosol. *Environ. Sci. Technol.* **2009**, *43* (13), 4647–4652. https://doi.org/10.1021/es802560w.

(70) Novelli, A.; Kaminski, M.; Rolletter, M.; Acir, I.-H.; Bohn, B.; Dorn, H.-P.; Li, X.; Lutz, A.; Nehr, S.; Rohrer, F.; et al. Evaluation of OH and HO_2 Concentrations and Their Budgets during Photooxidation of 2-Methyl-3-Butene-2-Ol (MBO) in the Atmospheric Simulation Chamber SAPHIR. *Atmospheric Chem. Phys.* **2018**, *18* (15), 11409–11422. https://doi.org/https://doi.org/10.5194/acp-18-11409-2018.

(71) Kaiser, J.; Skog, K. M.; Baumann, K.; Bertman, S. B.; Brown, S. B.; Brune, W. H.; Crounse, J. D.; de Gouw, J. A.; Edgerton, E. S.; Feiner, P. A.; et al. Speciation of OH Reactivity

above the Canopy of an Isoprene-Dominated Forest. *Atmos Chem Phys* **2016**, *16* (14), 9349–9359. https://doi.org/10.5194/acp-16-9349-2016.

(72) Carlton, A. G.; Pinder, R. W.; Bhave, P. V.; Pouliot, G. A. To What Extent Can Biogenic SOA Be Controlled? *Environ. Sci. Technol.* **2010**, *44* (9), 3376–3380. https://doi.org/10.1021/es903506b.

(73) Massoli, P.; Stark, H.; Canagaratna, M. R.; Krechmer, J. E.; Xu, L.; Ng, N. L.; Mauldin, R. L.; Yan, C.; Kimmel, J.; Misztal, P. K.; et al. Ambient Measurements of Highly Oxidized Gas-Phase Molecules during the Southern Oxidant and Aerosol Study (SOAS) 2013. *ACS Earth Space Chem.* **2018**, *2* (7), 653–672. https://doi.org/10.1021/acsearthspacechem.8b00028.

CHAPTER 6

CONCLUSIONS

6.1 Scientific Outcomes and Air Quality Implications

This thesis used lab-based experiments to demonstrate the importance of oxidation chemistry for producing air pollutants.

In Chapter 2 it is shown OH oxidation of diesel exhaust can produce levels of a demonstrably toxic gas-phase compound, isocyanic acid (HNCO), on the timescale of a day. We approximate this source to be important for urban areas such as the California South Coast Air Basin (SoCAB). A follow-up modeling study by Jathar et al.[1] (2016) showed that, after implementing results from our study, daily averaged mixing ratios of HNCO in the SoCAB region were modeled to be approximately 10x lower than is expected to be harmful to humans. As noted in Jathar et al., further epidemiological studies producing estimates of harmful HNCO exposure limits would be useful for assessing the importance of this compound as a toxic gas-phase species in all parts of the world. However, the current body of literature supporting harmful biological action of the cyanate ion coupled with the estimate of Roberts et al.[2] (2011) suggesting 1 ppb_v of HNCO sufficient to promote protein carbamylation should be sufficient evidence to classify HNCO as a toxic air pollutant under the Clean Air Act.

In Chapter 3 we find that ammonia emitted from liquid petroleum gas (LPG) and gasoline vehicles, measured a representative fleet of passenger vehicles from the Seoul Metropolitan Region, acted as a limiting reagent to ammonium nitrate aerosol formation from OH oxidation of the exhaust. This contrasted with what we expected because LPG and gasoline vehicles are known for having low emissions of NO_x because of the specific exhaust aftertreatment used in

those types of vehicles. We expected low levels of NO_x would produce low levels of ammonium nitrate, in response to OH oxidation of the vehicle exhaust, but ammonia was the key reagent to forming the aerosol as demonstrated when we observed low levels of aerosol produced from oxidation of diesel vehicle exhaust. Our study suggests (1) LPG and gasoline vehicles could be important sources of ammonia, a precursor to aerosol formation, in the Seoul Metropolitan Region and (2) photochemical oxidation of vehicle exhaust is likely an important source of local aerosol pollution in Seoul.

In Chapter 4 we found that oxidation of isoprene in an environmental chamber, via reactions with OH and O_3, produced high yields of formic and acetic acid. The yield for formic acid from ozonolysis of isoprene in a humid chamber produced yields exceeding 100% suggesting that though the global isoprene sink, with respect to ozonolysis, is only ~11%[3] this pathway is an important source of formic acid in the ambient atmosphere. Through chemical box-modeling of the oxidation experiments of isoprene oxidation products—IEPOX, ISOPOOH and MACR—that accounting for formic and acetic acid production from these sources could only account for small amounts of organic acid yields from isoprene OH oxidation experiments and from the SOAS field study. We found that the "slow" OH oxidation experiment, that extended isoprene-derived RO_2 lifetimes towards realistic values observed during SOAS, nearly doubled the calculated formic acid yield. Additionally, photolysis of isoprene oxidation products formed during the "slow" OH oxidation experiment ox high levels of organic acids. We hypothesize that oxidation of products formed from the isoprene hydroxy peroxy radical autooxidation pathway are a major source of formic acid. When applying the experimentally determined yields to an estimation of global formic acid production from isoprene we find an annual production of 74 Tg an^{-1}, which closes the gap between a model prediction of formic acid

production and the observationally constrained value of 100-120 Tg an^{-1} to a greater extent than any previous study.[4]

In Chapter 5 we collected evidence from laboratory experiments and field measurements to suggest isoprene oxidation is an important source of gas-phase organic acids. Similar to the findings in Chapter 4 we find that ozonolysis of isoprene produced the highest yields of gas-phase organic acids and that the presence of NO suppressed the formation of organic acids in response to OH oxidation. Gas-phase organic acids accounted for ~10% of the oxidized carbon from isoprene oxidation whereas the share of gas-phase organic acid carbon was ~1% for experiments of α-pinene oxidation. In contrast, organic aerosol accounted for very low amounts of oxidized isoprene carbon (<1%) whereas 20% of the oxidized carbon was allocated to organic aerosol from OH oxidation of α-pinene under "low NO" conditions. The findings of the laboratory studies were supported by observations of gas-phase organic acids from a forest with mixed isoprene and monoterpene emissions, SOAS, compared to a forest with dominant monoterpene emissions, SPiFFY. Total gas-phase organic acid carbon was, on average, a factor of four higher during the day at SOAS compared to SPiFFY suggesting the importance of isoprene photooxidation as a source. A factor analysis of the organic acids showed that photooxidation of isoprene was likely the major source of many acids during SOAS, whereas the population of acids during SPiFFY showed more diverse diel signatures with the influence of specific sources remaining unclear. As NO_x levels continue to decrease throughout the United States in the future, we expect increases in gas-phase organic acids from isoprene oxidation.

6.2 Analytical Triumphs and Challenges for Atmospheric Chemistry

Like many areas in science, atmospheric chemistry has experienced a paradigm shift in the way scientists think about forming research questions and conducting research in response to

advances in computational power. Several decades ago many researchers earned their PhDs measuring rate constants for specific reactions or thermodynamic parameters for specific processes. Those things are still done today, but many researchers are now trying to understand how to use parameterizations and estimations of fundamental properties of reactions to simulate complex systems that lead to pollutant formation in the atmosphere. This information-based approach to understanding and predicting important phenomena related to air quality is the vehicle that drives our ability to inform public policy discussions. Laboratory and field-based studies fuel these information-based approaches to atmospheric chemistry, and the quality of our predictive capabilities are only as good as the measurements for which they are dependent upon.

Capturing atmospherically-relevant organic chemistry through measurements and laboratory experiments continues to be an area of research with significant analytical challenges. The level of insight and discovery brought by new advancements in instrumentation and experimental methods are often accompanied by problems that take years of research to characterize. One example of this is the realization that the inability of global chemical models to reproduce measured levels of organic aerosol was, in part, because measurements of organic aerosol production in laboratory experiments were biased low because of the vapor wall-loss phenomenon. After nearly 15 years of research on vapor wall-loss, significant progress in modeling organic aerosol on regional and global scales has been made. As findings from complex atmospheric measurements become increasing robust and policy-relevant, methods of quantification, experimental bias/artifact characterization, and method validation should accordingly become more standardized.

6.3 Embracing the "Unknown Unknowns"

One analytical method thoroughly employed in this thesis is non-targeted mass spectrometry without preseparation. In most studies we deployed mass spectrometers, in this way, without knowing with high certainty what we were going to measure. The amount of data collected using this measurement technique is rather large, and, to many people, nearly impossible to comprehend in its entirety. In addition to taking the measurement we also quantified every species we determined reasonable to quantify that appeared in the mass spectrum. The sentiment voiced recently in the atmospheric chemistry community has asked if it is necessary to quantify everything in the atmosphere.[5] The appropriate answer is that no one knows. Might we all have skin cancer or be dead if it wasn't for James Lovelock floating around on the ocean measuring whatever was in the air with his newfangled gas chromatograph equipped with an electron capture detector? I'd like to think not, but the discovery of the ozone hole, in part, was a result of scientists purely researching things they could measure. As the field of atmospheric chemistry evolves scientists should not only ask what is necessary or what is relevant, but not forget to ask, first and foremost, what does it mean.

CHAPTER 6 REFERENCES

(1) Jathar, S. H.; Heppding, C.; Link, M. F.; Farmer, D. K.; Akherati, A.; Kleeman, M. J.; Gouw, J. A. de; Veres, P. R.; Roberts, J. M. Investigating Diesel Engines as an Atmospheric Source of Isocyanic Acid in Urban Areas. *Atmospheric Chem. Phys.* **2017**, *17* (14), 8959–8970. https://doi.org/https://doi.org/10.5194/acp-17-8959-2017.

(2) Roberts, J. M.; Veres, P. R.; Cochran, A. K.; Warneke, C.; Burling, I. R.; Yokelson, R. J.; Lerner, B.; Gilman, J. B.; Kuster, W. C.; Fall, R.; et al. Isocyanic Acid in the Atmosphere and Its Possible Link to Smoke-Related Health Effects. *Proc. Natl. Acad. Sci.* **2011**, *108* (22), 8966–8971. https://doi.org/10.1073/pnas.1103352108.

(3) Bates, K. H.; Jacob, D. J. A New Model Mechanism for Atmospheric Oxidation of Isoprene: Global Effects on Oxidants, Nitrogen Oxides, Organic Products, and Secondary Organic Aerosol. *Atmospheric Chem. Phys.* **2019**, *19* (14), 9613–9640. https://doi.org/https://doi.org/10.5194/acp-19-9613-2019.

(4) Stavrakou, T.; Müller, J.-F.; Peeters, J.; Razavi, A.; Clarisse, L.; Clerbaux, C.; Coheur, P.-F.; Hurtmans, D.; De Mazière, M.; Vigouroux, C.; et al. Satellite Evidence for a Large Source of Formic Acid from Boreal and Tropical Forests. *Nat. Geosci.* **2012**, *5* (1), 26–30. https://doi.org/10.1038/ngeo1354.

(5) Glasius, M.; Goldstein, A. H. Recent Discoveries and Future Challenges in Atmospheric Organic Chemistry. *Environ. Sci. Technol.* **2016**, *50* (6), 2754–2764. https://doi.org/10.1021/acs.est.5b05105.

APPENDIX 1 - CHAPTER 2 SUPPORTING INFORMATION

A1.1 Experimental Design

A1.1.1 Sampling of Engine Exhaust

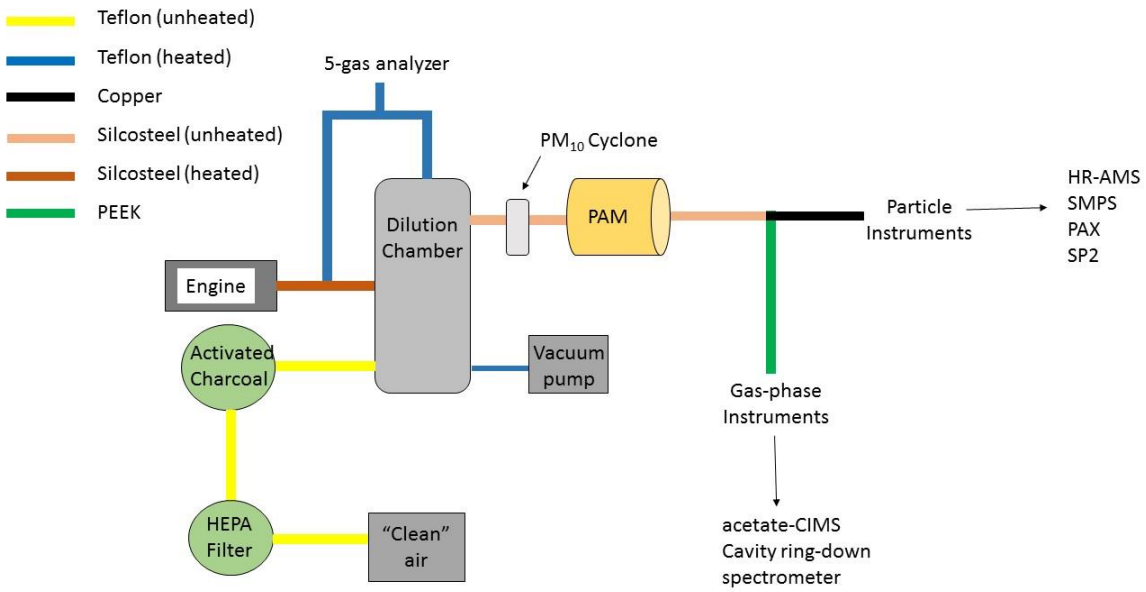

Figure A1.1. Experimental design for engine exhaust PAM experiments. Sample and dilution lines are colored by the material and heating regime. Engine exhaust is directed to a dilution chamber where it is diluted with compressed air that was filtered with activated charcoal and a HEPA filter. Diluted engine exhaust is subsampled to the PAM chamber, where oxidation occurs. Following oxidation, sample air is directed to particle and gas-phase instruments on different sampling lines. Gas-phase instrumentation included the acetate-CIMS and a cavity ring-down spectrometer. Particle-phase instrumentation included a high-resolution aerosol mass spectrometer (HR-AMS), a scanning mobility particle sizer (SMPS), a Photoacoustic Extinctiometer (PAX), and a Single Particle Soot Photometer (SP2).

Table A1.1. Summary statistics of engine emissions and operating parameters for both engine operating modes (± 1 standard deviation) measured from tailpipe exhaust.

Operating Mode	Power (kW)	Fuel Consumption (g min-1)	CO (ppm_v)	CO2 (%)	NOx (ppm_v)	THC (ppm_v)
Idle	0	21.9 (0.6)	428 (80)	1.7 (0.1)	130 (8)	85 (22)
50% Load	60	243 (5)	97 (11)	5.1 (0.1)	436 (43)	27 (12)

A1.2 Estimation of OH Exposure (OH_{exp}) in Potential Aerosol Mass (PAM) Chamber

A1.2.1 Effect of OH Suppression on OH_{exp}

The hydroxyl radical (OH) exposure (OH_{exp}) in the PAM is defined as the time a precursor gas spends exposed to a given steady-state mixing ratio of OH. If the OH reactivity of a sample or precursor gas is high enough, the OH/HO_2 ratio can be shifted to a point where reactions with OH are not pseudo first-order. This regime is termed "OH suppression" and complicates the calculation of OH_{exp}. Generally, OH_{exp} is determined by calculating the OH mixing ratio resulting from the decay of SO_2.[1] However, this method could not be used in this experiment because SO_2 was produced in response to applied UV light intensities in the PAM. OH suppression has been reported previously and has been corrected by different methods that approximate the link between the OH reactivity of the sample on the OH mixing ratio in the PAM.[2,3] No correction methods previously presented in the literature were suitable for use in this study to estimate OH_{exp} in the PAM. Li et al (2014) recently presented a model (improved upon by Peng et al (2015)) of the PAM system, and described the way in which OH reactivity of a sample affects OH mixing ratio in the PAM. In this study, we constructed a model like that

described by Peng et al. (2015) and calculated the OH mixing ratio expected from an estimated OH reactivity of our diesel exhaust samples.

A1.2.2 Estimation of OH Reactivity (OHR) of Diesel Exhaust

The OH reactivity (OHR) of a compound or sample is defined as the concentration of the compound or sample multiplied by the rate constant from reaction with OH. The OHR of the diesel exhaust sample entering the PAM was estimated by summing the dominant OH reactive species in sample as described by equation A.1.1:

$$OHR_{sample} = \sum(OHR_{NO} + OHR_{NO2} + OHR_{CO} + OHR_{THC}) \quad (A1.1)$$

Where OHR_{sample}, OHR_{NO}, OHR_{NO2}, OHR_{CO}, and OHR_{THC} is the OHR of the sample, NO, NO_2, CO, and total hydrocarbons (THC), respectively. The OHR of THC had to be estimated because the composition could not be measured. A speciated emissions profile for heavy duty diesel vehicle exhaust was used to approximate the volatile organic compound (VOC) composition of the diesel exhaust in this study.[4] Rate constants for each of the 26 VOCs listed in the profile were used to calculate an OHR_{THC} from the total THC concentration measured in the experiment.[5]

A1.2.3 Estimation of OH_{exp}

The calculated OHR of the sample, water, and ozone produced from the primary diesel exhaust was used as inputs into Equations (11) and (12) from the work of Peng et al. (2015) to obtain estimates of OH_{exp}. Quartz sleeves were placed over the lamps used in the PAM which blocked 145nm wavelengths and permitting operation of the PAM in "OFR254" mode. Operation of the PAM in "OFR254" mode makes applicable use of Equations (11) and (12) found in Peng et al (2015). The H_2O mixing ratio was calculated from relative humidity (RH) measurements acquired during the experiment (50% RH). Mixing ratios of ozone emitted from the primary

diesel exhaust were calculated from the acetate-CIMS measurements (60 ppm_v). The UV actinic flux was calculated from Figure S18 of Peng et al (2015) which relates the UV flux to lamp voltages if the lamps are similar. The results of these calculations are presented in Figure A1.2.

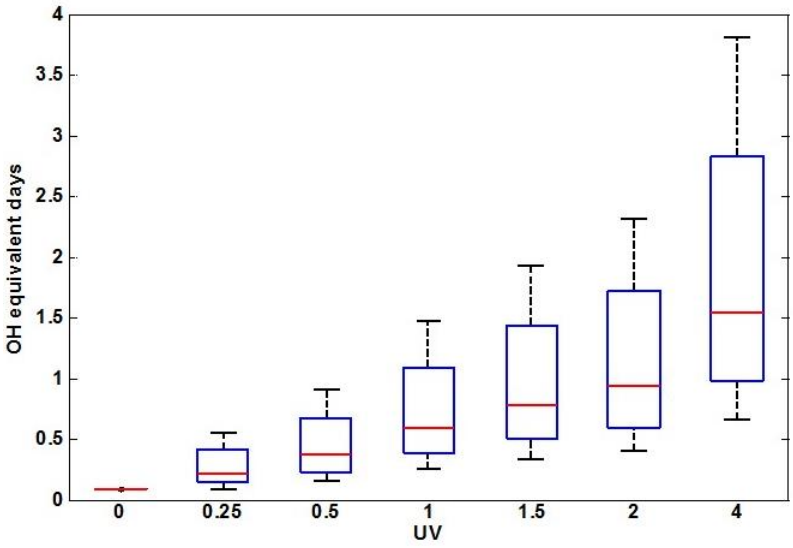

Figure A1.2. Calculated equivalent days of OH exposure as a function of the UV light voltage in the PAM. The 90th and 10th percentiles are represented by the black bars, the 75th and 25th percentiles are represented by the bounds of the blue boxes and the median is show in red. Median equivalent days of OH exposure range from 0.22 days at the lowest voltage settings to 1.5 days at the highest settings.

The median OH_{exp} days resulting from this calculation were used as approximations of OH_{exp} for the results presented in the main article.

A1.3. Calibration of Acetate-CIMS for HNCO

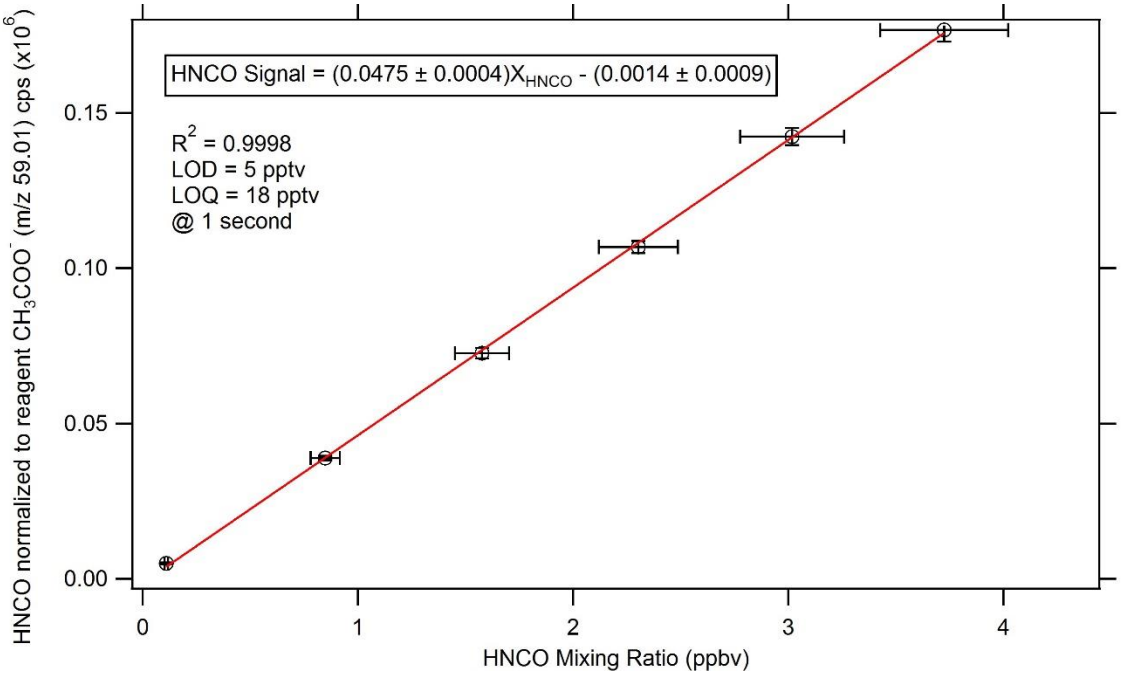

Figure A1.3. Calibration curve for HNCO on the acetate-CIMS. The signal for HNCO (measured as m/z 41.99 on the acetate-CIMS) on the acetate-CIMS is normalized to the reagent ion, acetate (m/z 59.01), and plotted against HNCO mixing ratio from the source. The HNCO ion signal is normalized to account for any changes in the reagent ion concentration.[6] The [a]limit of detection and [b]limit of quantification for 1 second acquisition was 5 and 18 ppt_v, respectively.

[a]The limit of detection for a signal to noise ratio of 3 was calculated by equation A1.2.:

$$\frac{S}{N} = \frac{C_f[X]t}{\sqrt{C_f[X]t+2Bt}} \qquad \text{(A1.2.)}$$

Where S/N is the signal to noise ratio, C_f is the calibration factor for HNCO, [X] is the HNCO concentration, t is the integration time for the measurement and B is the background count rate.[7]

[b]The limit of quantification was calculated similarly to the limit of detection using a signal to noise ratio of 10.

A1.4. Primary HNCO Emissions and Emission Factors

A.1.4.1. Primary HNCO Emission Factors

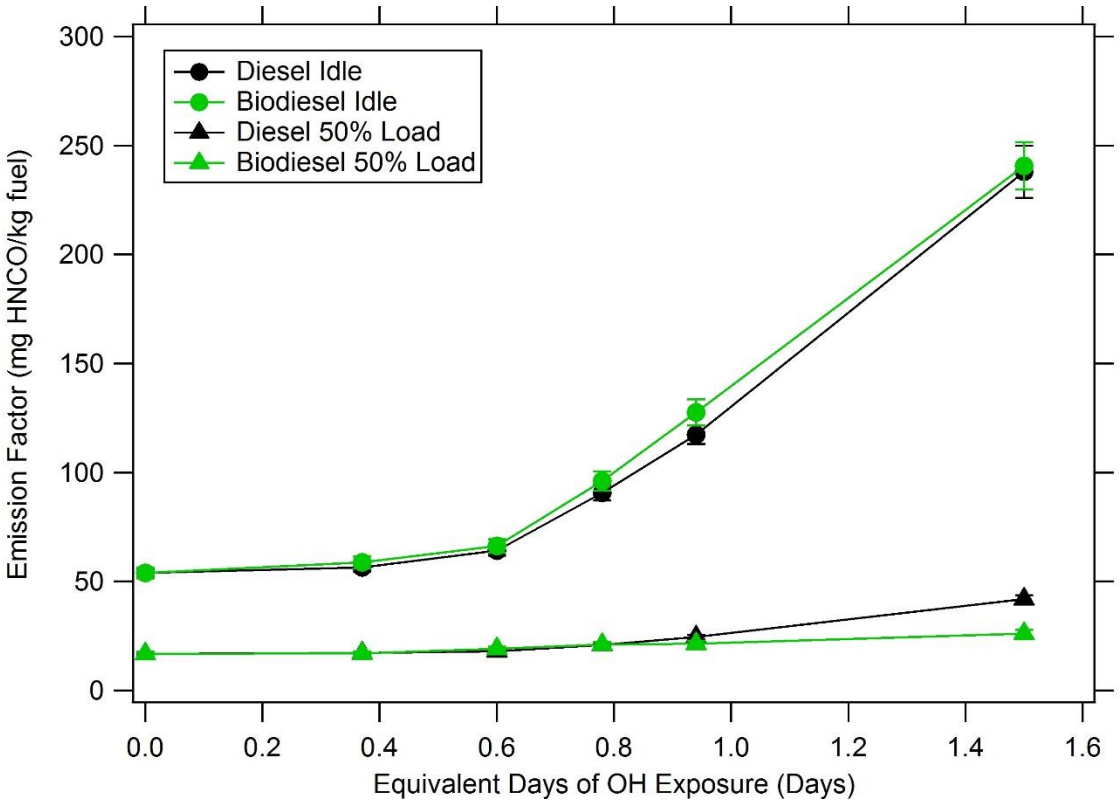

Figure A1.4. HNCO emission factors as calculated from tailpipe HNCO mixing ratios. Tailpipe HNCO mixing ratios represent primary emissions that are corrected for dilution. HNCO emission factors from diesel (black) and biodiesel (green) fuels are plotted under idle (circle) and 50% load (triangle) engine operating conditions. Vertical error bars represent the errors in measured mixing ratios of HNCO, CO_2, and CO propagated throughout the calculations.

A1.4.2. Tailpipe HNCO Emissions Mixing Ratios

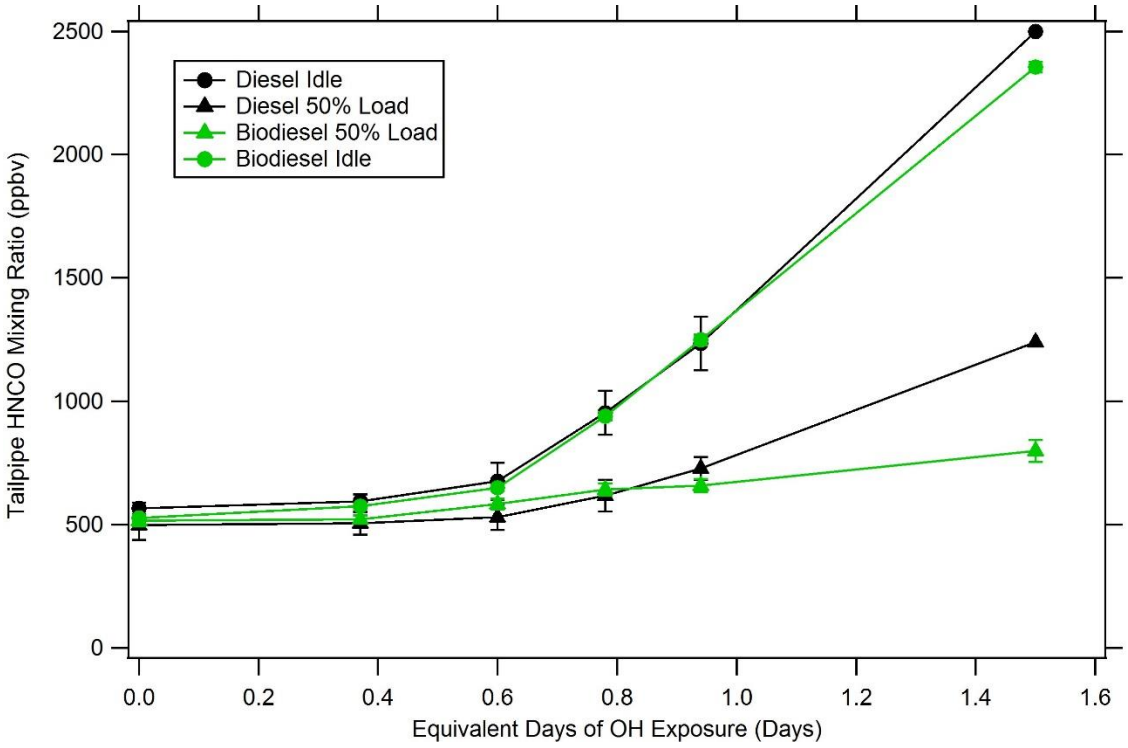

Figure A1.5. Tailpipe HNCO emission mixing ratio (ppb_v) as a function of equivalent days of OH exposure. HNCO mixing ratios from diesel (black) and biodiesel (green) fuels are plotted under idle (circle) and 50% load (triangle) engine operating conditions.

Table A1.2. The ratio of HNCO to CO and the ratio of HNCO to NO_x separated by fuel type and engine load. The top panel shows the emission factors calculated from tailpipe concentrations and the bottom panel shows the emission factors calculated from enhanced concentrations after ~1.5 of atmospheric aging.

Primary Emission Factors				
	Idle HNCO/CO (mmol HNCO mol CO-1)	50% Load HNCO/CO (mmol HNCO mol CO-1)	Idle HNCO/NOx (mmol HNCO mol NOx-1)	50% Load HNCO/NOx (mmol HNCO mol NOx-1)
Diesel	1.0-1.6	3.5-5.6	3.9-4.7	1.2-1.3
Biodiesel	0.1	4.9	2.3	1.0
Enhanced Emission Factors After ~1.5 Days of Atmospheric Aging				
Diesel	4.2	9.2-13.3	12.4	3.2-3.4
Biodiesel	0.5	7.6	11.5	1.6

A1.4.3. Discussion of nitrogen precursor contributions to HNCO secondary production

Precursors to HNCO reported in previous literature, formamide and acetamide, were identified in the CIMS mass spectra during the diesel fuel experiments.[8–10] These two precursors were not identified in the biodiesel fuel experiments. We note that while we were unable to verify their identity with independent standards during the experiment, peak fitting procedures suggest that peaks present at m/z 44.01 and m/z 58.03 correspond to peaks of CH_2NO^- and $C_2H_4NO^-$, consistent with formamide and acetamide, respectively. Both species are known to be secondary products from oxidation of amines by OH and can be seen to increase in concentration in response to photochemical perturbations (Figure A1.6.).[11] This observation suggests secondary production of these nitrogen-containing species, which is consistent with previous research.[9]

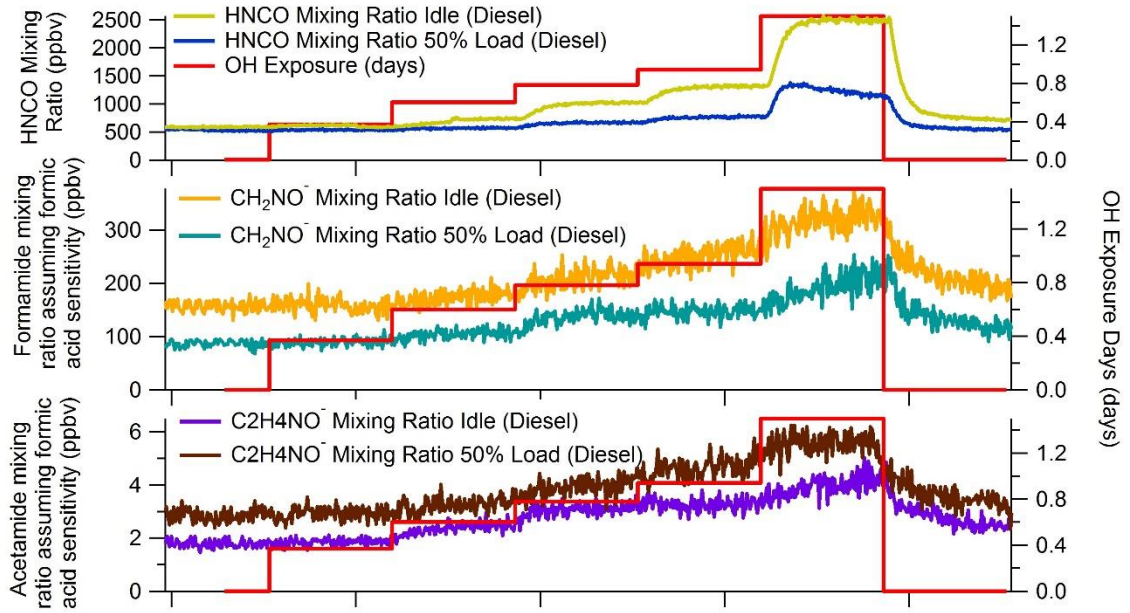

Figure A1.6. Comparison of HNCO production (top panel; idle, gold; 50% load, blue), formamide production (middle panel; idle, gold; 50% load, blue), and acetamide production (bottom panel; idle, brown, 50% load, purple) during a diesel fuel experiment. Formamide (CH_2NO^-; m/z 44.01) and acetamide ($C_2H_4NO^-$; m/z 58.03) mixing ratios were obtained by assuming an equal sensitivity to formic acid of 13 Hz ppt^{-1} [12], though we note below the significant limitations of this assumption. OH exposure (red) is displayed on the right axis to demonstrate chemical signal increases in response to photochemical perturbations.

Calibrations for formamide and acetamide were not performed for the experiments in this study. A lower bound on the concentration of formamide and acetamide mixing ratios can be calculated by assuming an equal sensitivity to formic acid of 13 Hz ppt^{-1} [12]. We consider the formic acid sensitivity to be a maximum sensitivity for these compounds because a proton transfer from the analyte to the acetate reagent ion would have to occur via abstraction from either the amine group or the α-carbon on the carbonyl of formamide and acetamide (or a methyl group on acetamide). This is in contrast to a proton abstraction from the carboxylic acid functional group of formic acid, which is far more favorable. Thus, using the high sensitivity of formic acid for these compounds results in a lower bound on the estimated mixing ratios of formamide and acetamide. We also note that the $C_{1\text{-}2}H_{2\text{-}4}NO^-$ signals observed in the instrument could be the result of fragmentation of larger nitrogen-containing organic compounds.

Assuming 100% yields of HNCO from the oxidation of these nitrogen-containing organic compounds, they would account for a maximum of 10-15% of the observed HNCO. This is obviously a poorly-constrained estimate with large uncertainties, perhaps the most important of which is that the sensitivity of the acetate-CIMS detector is unlikely as high as assumed. This error would suggest that this number is a lower estimate of formamide + acetamide contributions to HNCO. However, we also note that this assumes 100% conversion within the residence time of the chamber under the OH conditions observed, which is unlikely true (i.e. $k_{CH3NO + OH} = 0.4 \times 10^{-11}$ molecules cm^{-3}; $k_{C2H5NO + OH} = 0.35 \times 10^{-11}$ molecules cm^{-3}), and would suggest this calculation is an upper estimate of contributions to HNCO production. Overall, a quantitative understanding of the contribution of formamide and acetamide, originating from diesel exhaust, to secondary HNCO production is highly uncertain.

REFERENCES

(1) Lambe, A. T.; Ahern, A. T.; Williams, L. R.; Slowik, J. G.; Wong, J. P. S.; Abbatt, J. P. D.; Brune, W. H.; Ng, N. L.; Wright, J. P.; Croasdale, D. R.; et al. Characterization of Aerosol Photooxidation Flow Reactors: Heterogeneous Oxidation, Secondary Organic Aerosol Formation and Cloud Condensation Nuclei Activity Measurements. *Atmos Meas Tech* **2011**, *4* (3), 445–461. https://doi.org/10.5194/amt-4-445-2011.

(2) Ortega, A. M.; Day, D. A.; Cubison, M. J.; Brune, W. H.; Bon, D.; de Gouw, J. A.; Jimenez, J. L. Secondary Organic Aerosol Formation and Primary Organic Aerosol Oxidation from Biomass-Burning Smoke in a Flow Reactor during FLAME-3. *Atmos Chem Phys* **2013**, *13* (22), 11551–11571. https://doi.org/10.5194/acp-13-11551-2013.

(3) Tkacik, D. S.; Lambe, A. T.; Jathar, S.; Li, X.; Presto, A. A.; Zhao, Y.; Blake, D.; Meinardi, S.; Jayne, J. T.; Croteau, P. L.; et al. Secondary Organic Aerosol Formation from in-Use Motor Vehicle Emissions Using a Potential Aerosol Mass Reactor. *Environ. Sci. Technol.* **2014**, *48* (19), 11235–11242. https://doi.org/10.1021/es502239v.

(4) Department for Environment, F. and R. A. (Defra) webmaster@defra gsi gov uk. Report: Speciation of UK emissions of non-methane volatile organic compounds - Defra, UK http://naei.defra.gov.uk/reports/reports?report_id=130 (accessed Dec 2, 2015).

(5) Atkinson, R.; Arey, J. Atmospheric Degradation of Volatile Organic Compounds. *Chem. Rev.* **2003**, *103* (12), 4605–4638. https://doi.org/10.1021/cr0206420.

(6) Veres, P.; Roberts, J. M.; Burling, I. R.; Warneke, C.; de Gouw, J.; Yokelson, R. J. Measurements of Gas-Phase Inorganic and Organic Acids from Biomass Fires by Negative-Ion Proton-Transfer Chemical-Ionization Mass Spectrometry. *J. Geophys. Res. Atmospheres* **2010**, *115* (D23), D23302. https://doi.org/10.1029/2010JD014033.

(7) Bertram, T. H.; Kimmel, J. R.; Crisp, T. A.; Ryder, O. S.; Yatavelli, R. L. N.; Thornton, J. A.; Cubison, M. J.; Gonin, M.; Worsnop, D. R. A Field-Deployable, Chemical Ionization Time-of-Flight Mass Spectrometer. *Atmos Meas Tech* **2011**, *4* (7), 1471–1479. https://doi.org/10.5194/amt-4-1471-2011.

(8) Barnes, I.; Solignac, G.; Mellouki, A.; Becker, K. H. Aspects of the Atmospheric Chemistry of Amides. *ChemPhysChem* **2010**, *11* (18), 3844–3857. https://doi.org/10.1002/cphc.201000374.

(9) Borduas, N.; Abbatt, J. P. D.; Murphy, J. G. Gas Phase Oxidation of Monoethanolamine (MEA) with OH Radical and Ozone: Kinetics, Products, and Particles. *Environ. Sci. Technol.* **2013**, *47* (12), 6377–6383. https://doi.org/10.1021/es401282j.

(10) Roberts, J. M.; Veres, P. R.; VandenBoer, T. C.; Warneke, C.; Graus, M.; Williams, E. J.; Lefer, B.; Brock, C. A.; Bahreini, R.; Öztürk, F.; et al. New Insights into Atmospheric Sources and Sinks of Isocyanic Acid, HNCO, from Recent Urban and Regional Observations. *J. Geophys. Res. Atmospheres* **2014**, *119* (2), 2013JD019931. https://doi.org/10.1002/2013JD019931.

(11) Lee, D.; Wexler, A. S. Atmospheric Amines – Part III: Photochemistry and Toxicity. *Atmos. Environ.* **2013**, *71*, 95–103. https://doi.org/10.1016/j.atmosenv.2013.01.058.

(12) Brophy, P.; Farmer, D. K. A Switchable Reagent Ion High Resolution Time-of-Flight Chemical Ionization Mass Spectrometer for Real-Time Measurement of Gas Phase Oxidized Species: Characterization from the 2013 Southern Oxidant and Aerosol Study. *Atmos Meas Tech* **2015**, *8* (7), 2945–2959. https://doi.org/10.5194/amt-8-2945-2015.

APPENDIX 2 - CHAPTER 3 SUPPORTING INFORMATION

A2.1 Supplementary Experimental Methods

A2.1.1 Experimental Design and Oxidation Flow Reactor (OFR) Operation.

Figure A2.1 displays the experimental set up for the vehicle exhaust measurements.

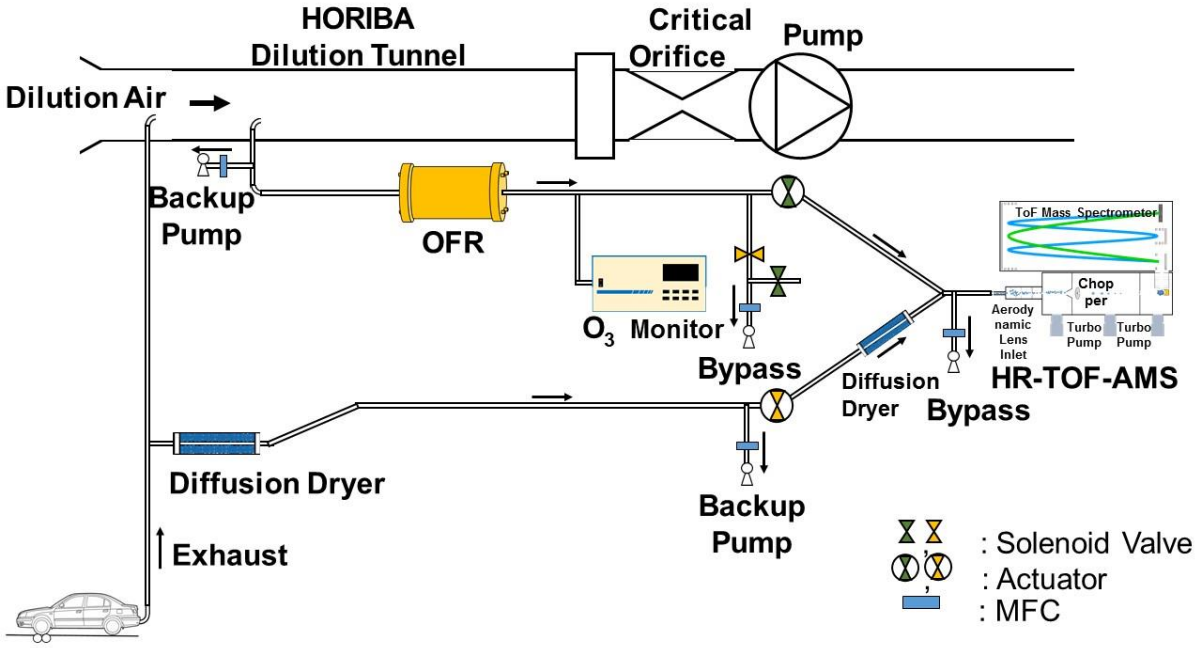

Figure A2.1. Schematic of experimental design including set up of the OFR.
A system of solenoid valves and actuators were used to either direct airflow through the OFR to the sampling instruments, or to a bypass. Setting up sampling in this configuration allowed for air to be constantly flowing through the OFR at 3 standard liters per minute (sLpm). Lights in the OFR were left on, at the lowest possible operating voltage, during the entire day when experiments would be performed so that when measurements were acquired from air sampled from the OFR the oxidized exhaust samples would be fully processed. The relative humidity (RH) in the KNU OFR varied between 40-60%. OH radical generation was performed by the photolysis of ozone by UV light (λ = 254 nm).

$$O_3 + h\nu\ (\lambda\ =\ 254\ \text{nm}) \rightarrow\ O_2 + O(^1D) \qquad \text{(S1)}$$

$$O(^1D) +\ H_2O\ \rightarrow 2OH \qquad \text{(S2)}$$

Ozone externally added to the OFR was generated in a separate chamber mounted to the OFR by exposing oxygen in clean dry air to UV light (λ = 185 nm) produced from lamps in the separate

chamber. OH exposures representative of ~0.5 days of atmospheric aging were targeted by introducing ozone (targeted 600 ppb_v measured at the output of the reactor) to the KNU OFR under the lowest applied light voltage settings representative of the lowest amount of irradiance produced by the UV lamps. This design operates similarly to other published designs.[1,2]

A2.2 Supplementary Results and Discussion

A2.2.1 Discussion of estimation of the OH exposure in the KNU OFR

A total of 84 experiments were performed during the entire exhaust sampling campaign, but only 72 are presented as data in this manuscript because 12 of the experiments consisted of non-constant mode driving cycles. As discussed in the section above, the OH exposure in the KNU OFR was controlled by introducing ozone to the KNU OFR while the UV lights in the OFR were on and measuring a stable 600 ppb_v at the output. The ozone introduction was controlled with a rotometer and, as shown in Figure A2.2, was imprecise for some of the experiments.

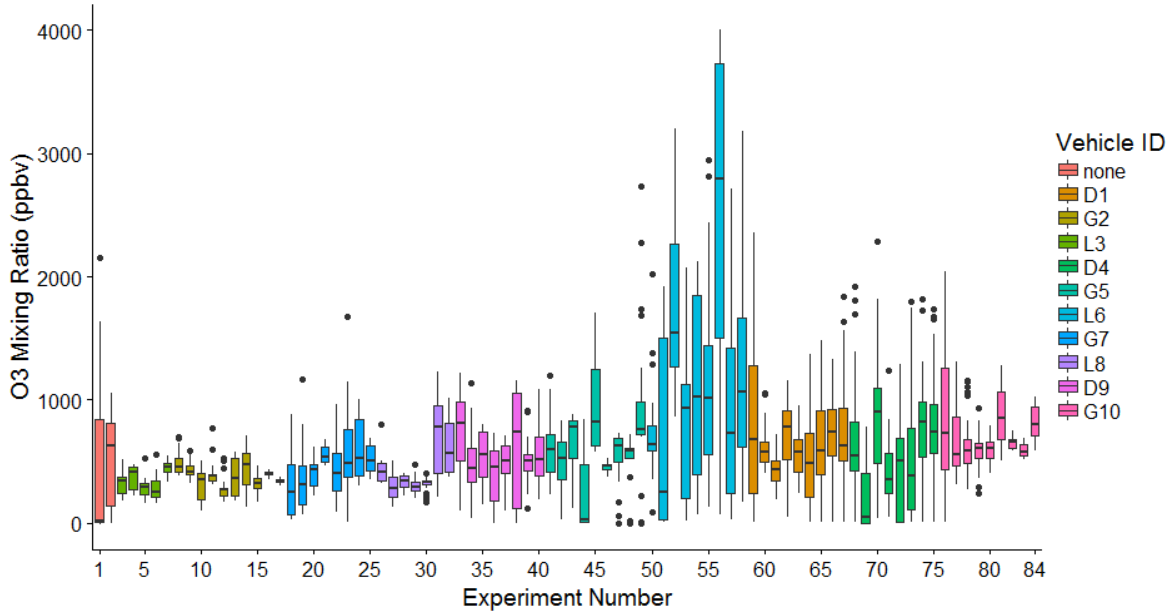

Figure A2.2. Ozone mixing ratio (ppb_v) measured at the output of the KNU OFR as a function of experiment number. The edges of the boxplots represent the 25th and 75th quartiles and the whiskers represent the 10th and 90th quartiles. Black dots are outliers.

In Figure A2.2 the ozone mixing ratio measured at the output of the KNU OFR is shown on the y-axis and is plotted as a function of experiment number. Experiment number is separated by the vehicles that were tested during those experiments as shown by the annotations at the top of the plot. The vehicles subject to the lowest variability in ozone introduction were G2, L3, G7,

L8, D9 and G10. G5 was subject to moderate variability and D1, D4, and L6 were subject to high variability.

Based on some of the general trends of what is observed from the ozone data, we can provide constraints on the magnitude of the OH exposure. In the KNU OFR operation mode, we expect that the more ozone that is put into the KNU OFR, the more OH exposure would result. Based on this principle G2, L3, G7, L8, D9 and G10 should be expect to have similar magnitudes of OH exposure based on the similarity in magnitude and variability of the distributions of measured ozone mixing ratios during these experiments. L6 had a measured ozone distribution with median values biased higher than the rest of the experiments. From this, we expect that the emissions from L6 would have been subjected to the highest OH exposures. For D1 and D4 it should be expected that if the variability in the OH exposure during these experiments had an effect on the secondary production of particles a wide distribution of secondarily produced particles would be observed in the data. Two of the data points for the measured secondary production of nitrate from D4 fall as outliers in the dataset suggesting that this variability may have had a slight influence on the results from D4. As shown in Figure 2, however, these two data points, from two different experiments, are reproducible at the constant speed of 110km, suggesting that these outliers might be real products of the labored emissions of V4 under this higher speed.

A2.2.2 Summary of vehicle emission data

Emission data from the different vehicles tested in this study are summarized in this section. Below in Table A2.1 is shown the average, median and interquartile ranges for aerosol nitrate and aerosol ammonium production values measured in this study.

Table A2.1. Average, median, and interquartile ranges for aerosol nitrate and aerosol ammonium production categorized by vehicle brand. All values reported are in units of μg/km.

		Average (±1σ)	Median	IQR low	IQR high
D1	Nitrate	7 ± 3	6	5	9
	Ammonium	2 ± 1	1	1	2
G2	Nitrate	4587 ± 1643	4503	3782	5775
	Ammonium	1200 ± 416	1163	1028	1537
L3	Nitrate	3114 ± 1397	2650	2148	4125
	Ammonium	813 ± 379	667	563	1118
D4	Nitrate	5 ± 3	4	3	7
	Ammonium	1 ± 1	0	0	1
G5	Nitrate	316 ± 548	79	10	305
	Ammonium	89 ± 145	30	5	85
L6	Nitrate	47 ± 66	17	11	52
	Ammonium	17 ± 25	6	2	14
G7	Nitrate	1778 ± 1218	1229	989	2577
	Ammonium	453 ± 406	302	220	743
L8	Nitrate	261 ± 274	137	106	365
	Ammonium	95 ± 94	51	42	129
D9	Nitrate	371 ± 565	10	7	777
	Ammonium	115 ± 176	1	1	250
G10	Nitrate	297 ± 452	12	7	591
	Ammonium	80 ± 123	2	1	161

Large values for the standard deviations as well as the large distribution for the interquartile ranges generally reflect differences in patterns of secondary production associated with different speeds.

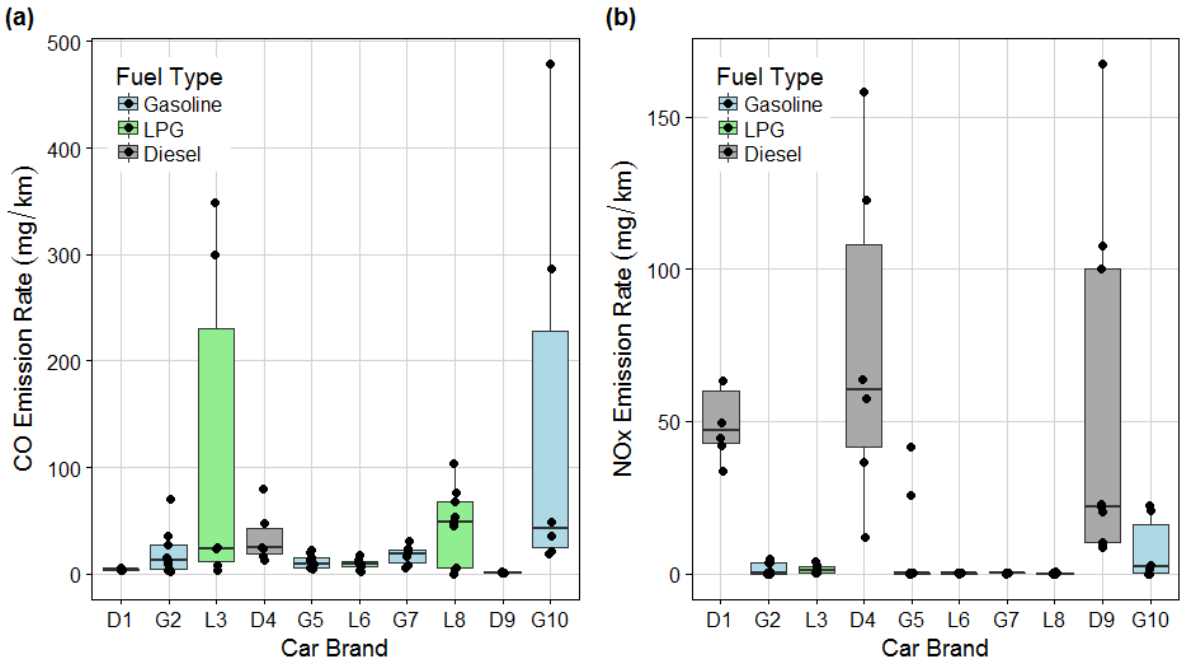

Figure A2.3. (a) CO emission rate (mg/km) and (b) NO_x emission rate (mg/km) as a function of car brand and colored by fuel type. The edges of the boxplots represent the 25th and 75th quartiles and the whiskers represent the 10th and 90th quartiles. The black dots represent the individual measured data points. Points shown outside of the 10th and 90th quartiles are outliers.

A2.2.3 Variation of emissions with speed

The nitrate primary emission and ammonium primary emission and secondary production shown as a function of speed and car brand is shown in the figures below (A2.4-A2.7). Briefly, for the vehicles that had the highest measured production of aerosol ammonium, we observed a slight negative relationship with increasing speed. This relationship was also observed from G7 and L8. Ammonium production was only observed at the highest tested speed for G10 because this vehicle had a smaller engine which operated less efficiently under higher speed conditions.

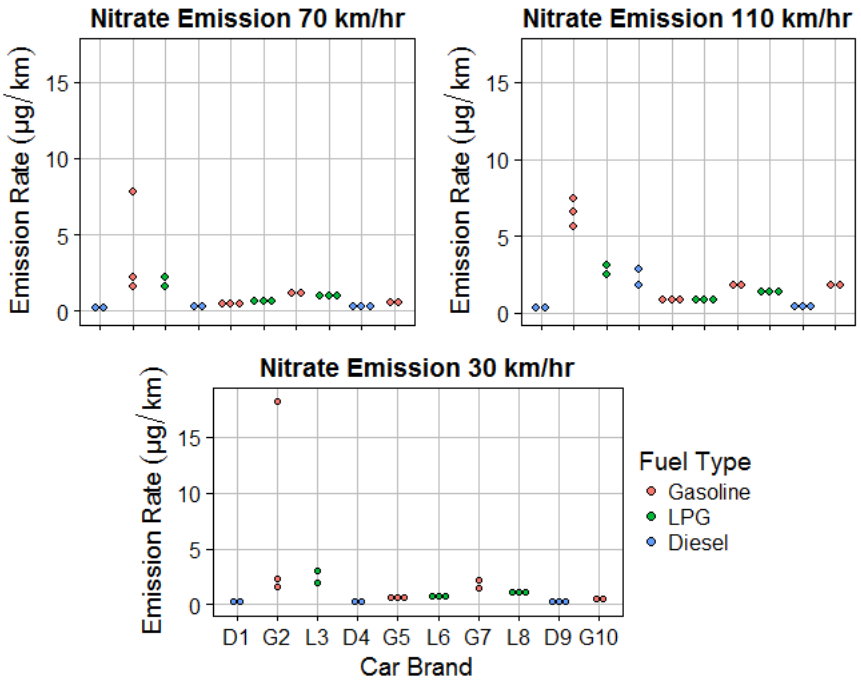

Figure A2.4. Aerosol nitrate primary emission rate (µg/km) as a function of car brand and speed.

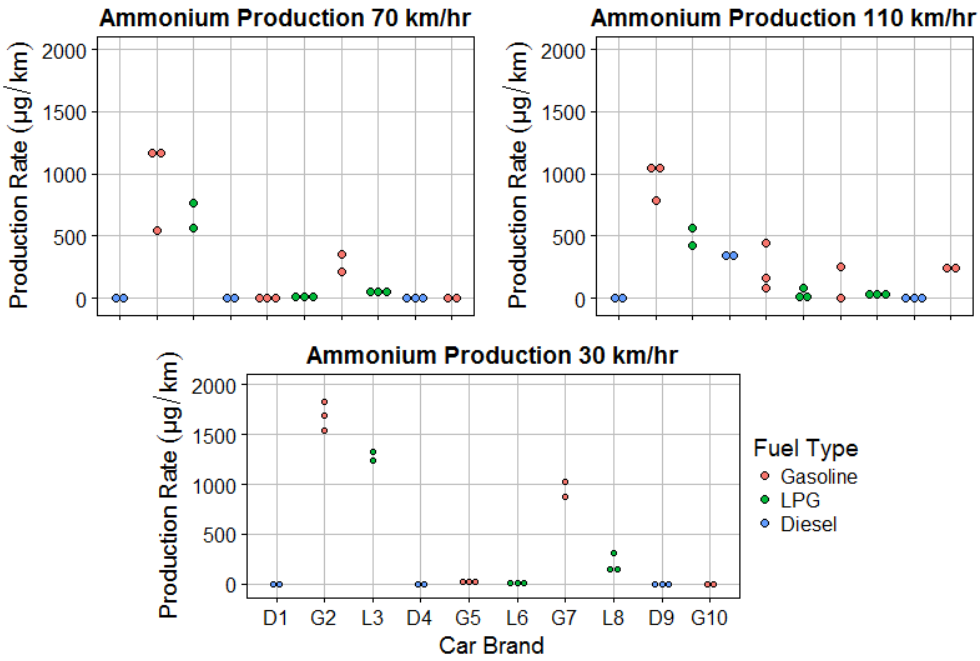

Figure A2.5. Aerosol ammonium secondary production rate (µg/km) as a function of car brand and speed.

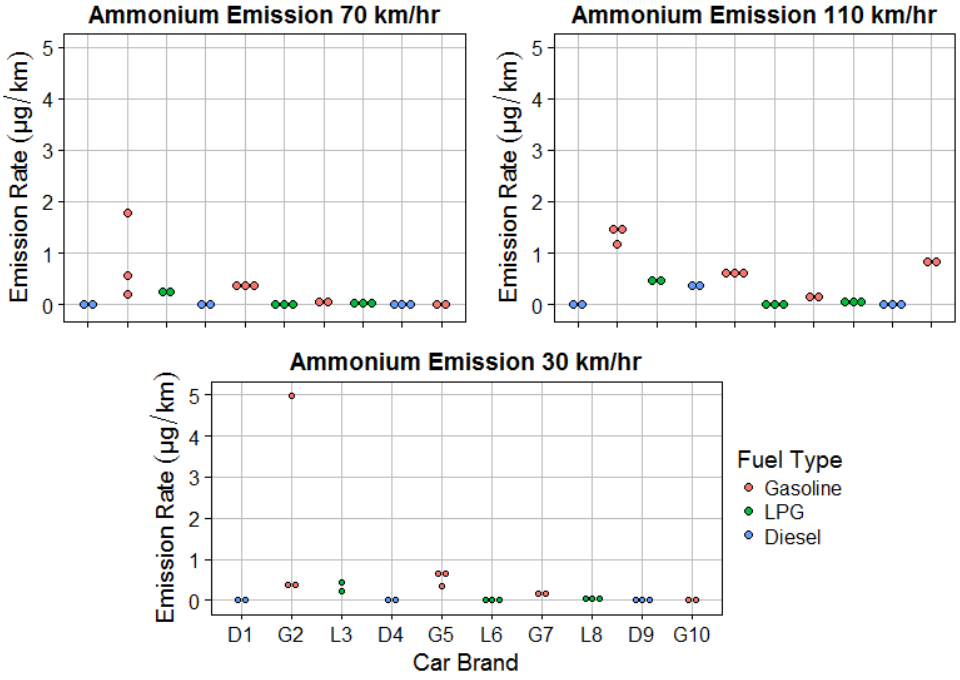

Figure A2.6. Aerosol ammonium primary emission rate (µg/km) as a function of car brand and speed.

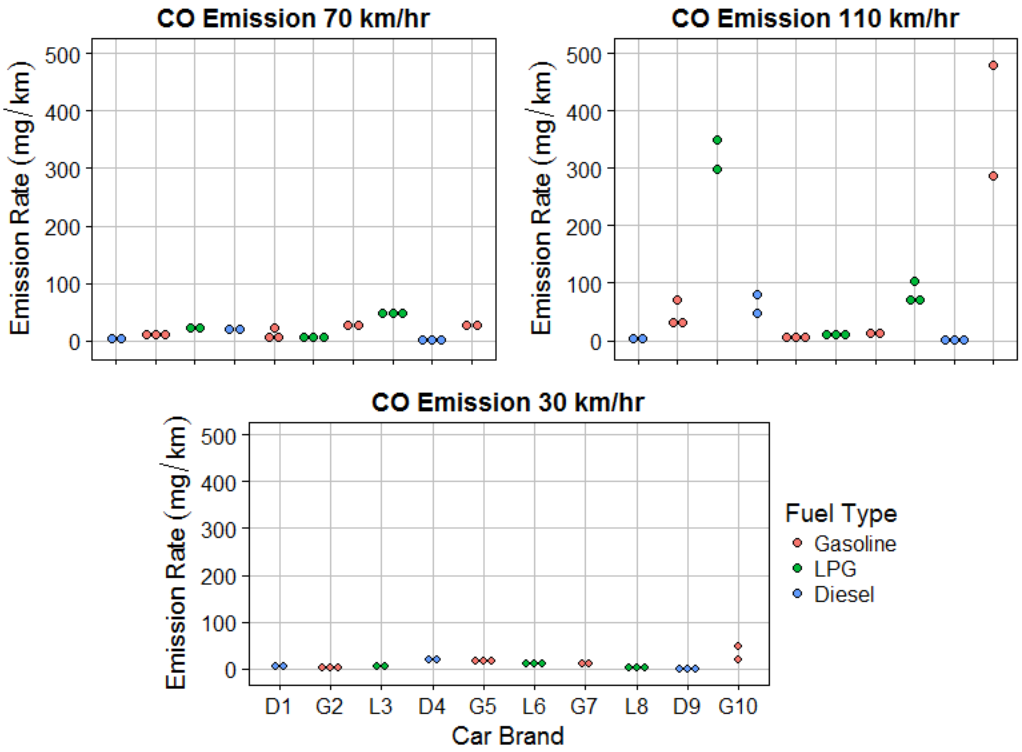

Figure A2.7. CO primary emission rate (mg/km) as a function of car brand and speed.

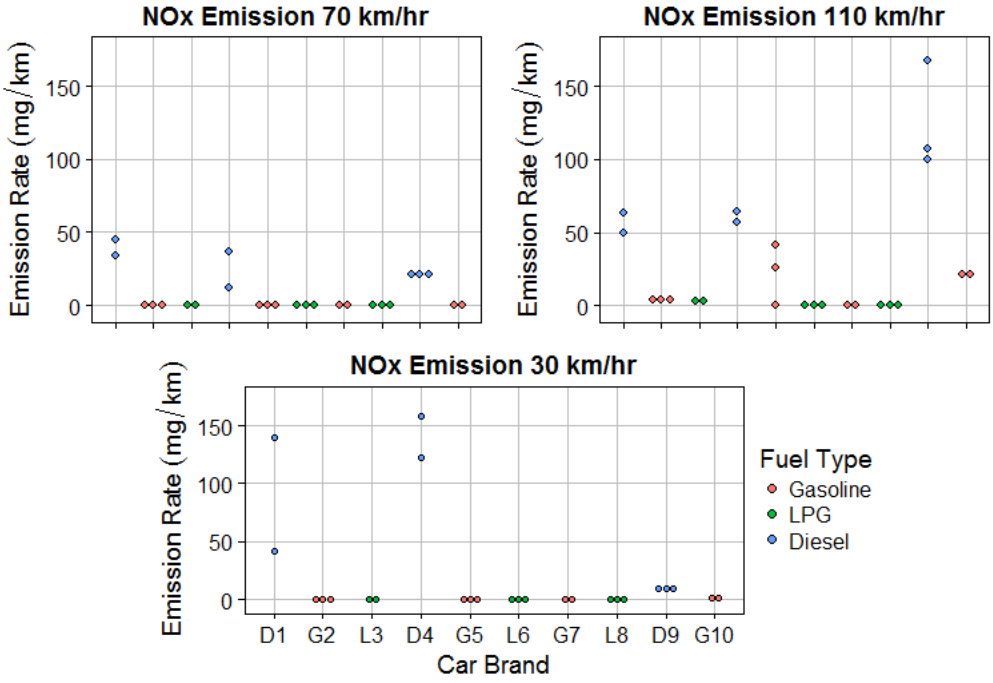

Figure A2.8. NO_x primary emission rate (mg/km) as a function of car brand and speed.

REFERENCES

(1) Kang, E.; Root, M. J.; Toohey, D. W.; Brune, W. H. Introducing the Concept of Potential Aerosol Mass (PAM). *Atmos Chem Phys* **2007**, *7* (22), 5727–5744. https://doi.org/10.5194/acp-7-5727-2007.

(2) Lambe, A. T.; Ahern, A. T.; Williams, L. R.; Slowik, J. G.; Wong, J. P. S.; Abbatt, J. P. D.; Brune, W. H.; Ng, N. L.; Wright, J. P.; Croasdale, D. R.; et al. Characterization of Aerosol Photooxidation Flow Reactors: Heterogeneous Oxidation, Secondary Organic Aerosol Formation and Cloud Condensation Nuclei Activity Measurements. *Atmos Meas Tech* **2011**, *4* (3), 445–461. https://doi.org/10.5194/amt-4-445-2011.

APPENDIX 3 - CHAPTER 3 SUPPORTING INFORMATION

A3.1 Summary of Focused Isoprene Experiments at the California Institute of Technology (FIXCIT) laboratory measurements

Table S1. Summary of FIXCIT experiments analyzed for organic acid production.

Experiment Number	Date	Precursor and conditions	UV light intensity[a]	RH	Background subtraction	Oxidant exposure
2	01.02.14	Isoprene + OH ("low NO")	100%	< 5%	"low NO" OH blank	2.2 x 10^{10} molecules s cm^{-3}
3	01.03.14	Isoprene + OH ("high NO")	50%	< 5%	"high NO" OH blank	2.2 x 10^{10} molecules s cm^{-3}
----	01.04.14	"low NO" OH blank	100%	< 5%	-----	------
----	01.05.14	"high NO" OH blank	50%	< 5%	-----	-------
6	01.06.14	Isoprene + O3	--	< 5%	Pre-hydrocarbon injection	8.1 x 10^{6} ppb_v s
7	01.07.14	slow isoprene oxidation followed by HPALD oxidation	1%, 20%, 100%	< 5%	1% lights on – CH_3ONO blank >20% lights on -- "low NO" OH blank	2.0 x 10^{9} molecules s cm^{-3} 9.1 x 10^{10} molecules s cm^{-3}

9	01.09.14	Isoprene + NO3	--	< 5%	Pre-hydrocarbon injection	--
10	01.10.14	α-pinene + OH ("low NO")	100%	< 5%	"low NO" OH blank	5.3 x 10^{10} molecules s cm^{-3}
11	01.11.14	α-pinene + OH ("high NO")	50%	< 5%	"high NO" OH blank	4.8 x 10^{10} molecules s cm^{-3}
13	01.13.14	a-pinene + NO3/HO2	--	< 5%	Pre-hydrocarbon injection	--
14	01.14.14	Isoprene + O3	--	< 5%	Pre-hydrocarbon injection	9.57 x 10^{6} ppb_v s
16	01.16.14	a-pinene + OH	1%, 20%, 100%	< 5%	1% lights on – CH_3ONO blank >20% lights on ;"low NO" OH blank for photolysis	2.0 x 10^{9} molecules cm^{-3} 6.35 x 10^{10} molecules cm^{-3}
17	01.17.14	ISOPOOH + OH	100%	< 5%	"low NO" OH blank	8.6 x 10^{9} molecules cm^{-3}
19	01.19.14	Isoprene + OH ("low NO")	100%	50%	"low NO" OH blank	1.9 x 10^{10} molecules cm^{-3}
---	01.20.14	CH_3ONO blank	1%	< 5%	------	---
21	01.21.14	Isoprene + OH ("low NO")	100%	< 5%	"low NO" OH blank	2.2 x 10^{10} molecules cm^{-3}

[a]Reported as a percentage of the 320 UV bulbs installed in the chamber

A3.2 Background subtraction

A3.2.1 Background subtraction example for isoprene + OH "high NO" experiment

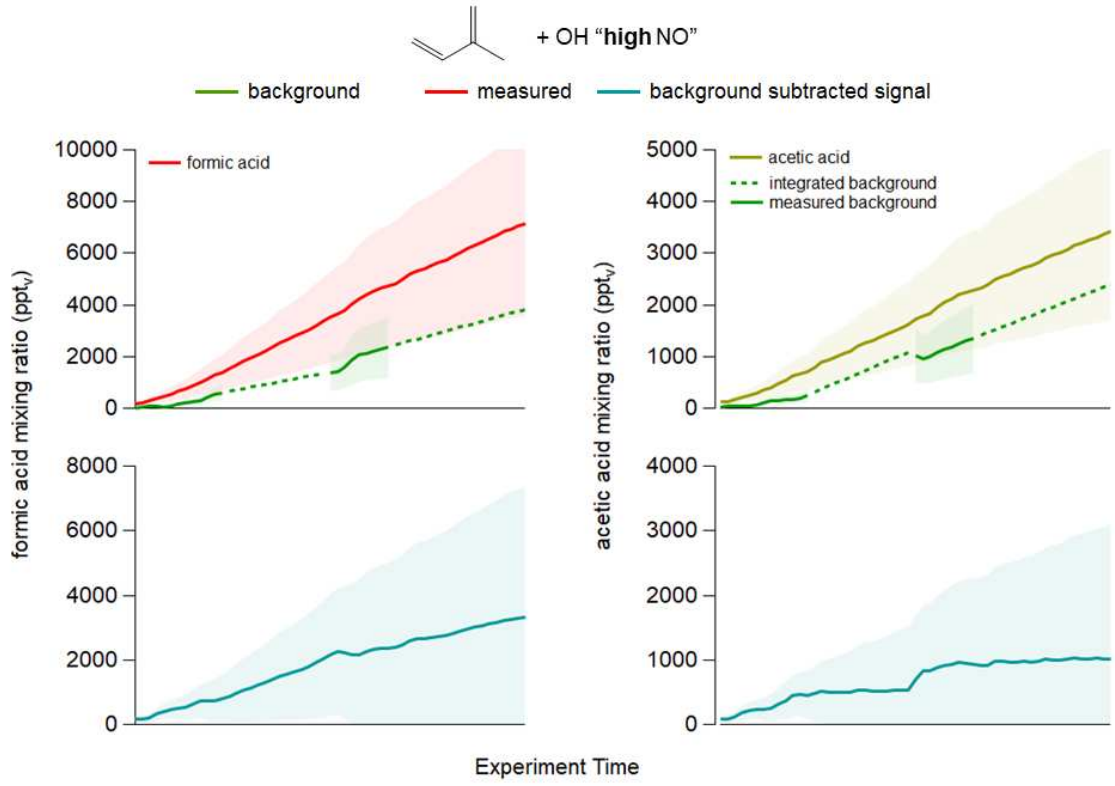

Figure A3.1. An example of background subtraction of formic (panels a and c) and acetic (b and d) acid from isoprene + OH "high NO" experiment. (a) The raw formic acid mixing ratio (red) is shown with the estimated mixing ratio from background (green). The solid portion of the background is the mixing ratio that was measured directly and the dashed portion of the line is the interpolated mixing ratio. The shaded regions represent the uncertainty of measurements (top) and calculated background-subtracted mixing ratio (bottom). (c) Subtracting the green background mixing ratio from the red mixing ratio produces the blue line which is the background-subtracted formic acid mixing ratio for the isoprene + OH "high NO" experiment. (b) Same as panel (a) except acetic, instead of formic, acid is shown. (d) Same as panel (c) except acetic, instead of formic, acid is shown.

A3.2.2 Background subtraction for "slow chemistry" experiments (Experiments 7 and 16; 1% UV light intensity)

The source of the acetic and formic acid backgrounds in the FIXCIT chamber experiments is not known but is suspected to be resulting from oxidation of organic vapors or particles deposited on the walls of the chambers. In order to estimate the background production of formic and acetic acid from the bags during the "slow" part of the Jan. 7 (and Jan. 16) "slow chemistry isoprene + OH" experiment we assumed the rate of production was zeroth order. This means the slope of the formic/acetic acid versus time would provide the estimated rate constant for background production of these acids during those experiments.

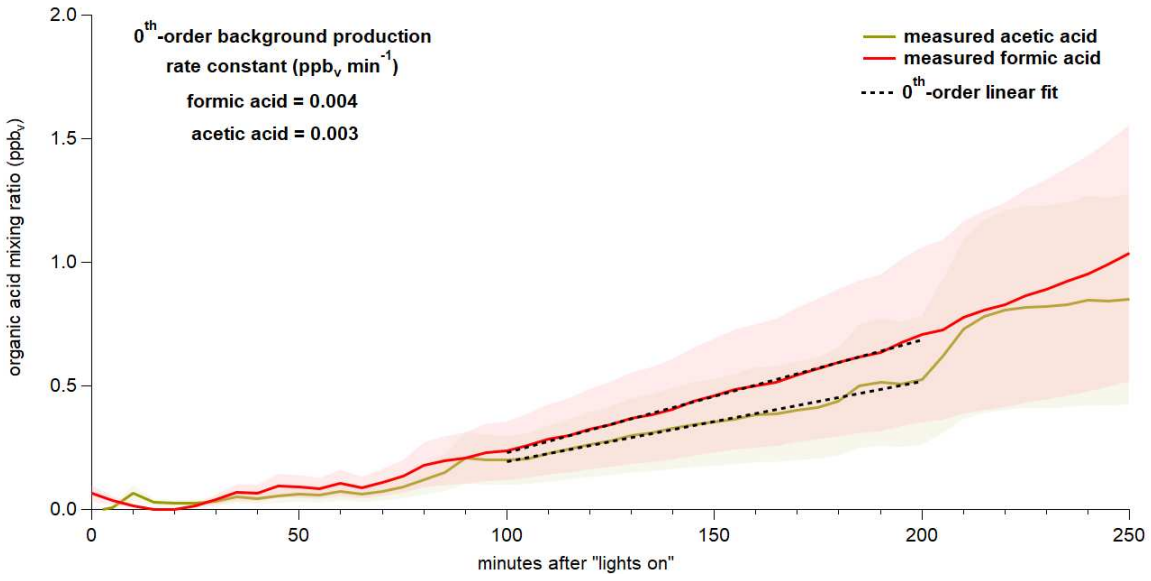

Figure A3.2. Time series of formic (red) and acetic (yellow) acids during the Jan. 20 CH_3ONO blank using 1% of the UV lights on the chamber to produce OH. These conditions are expected to produce a representative background for the "slow chemistry" experiments on Jan. 7 (isoprene) and Jan. 16 (α-pinene). Acid measurements from a 100-minute portion of this background experiment had a linear fit applied to them (dashed lines) to obtain rate constants for the assumed 0^{th}-order production rate. The obtained constants for formic and acetic acid were 0.004 and 0.003 ppb_v min^{-1}, respectively. Shaded areas show +/- 50% uncertainty.

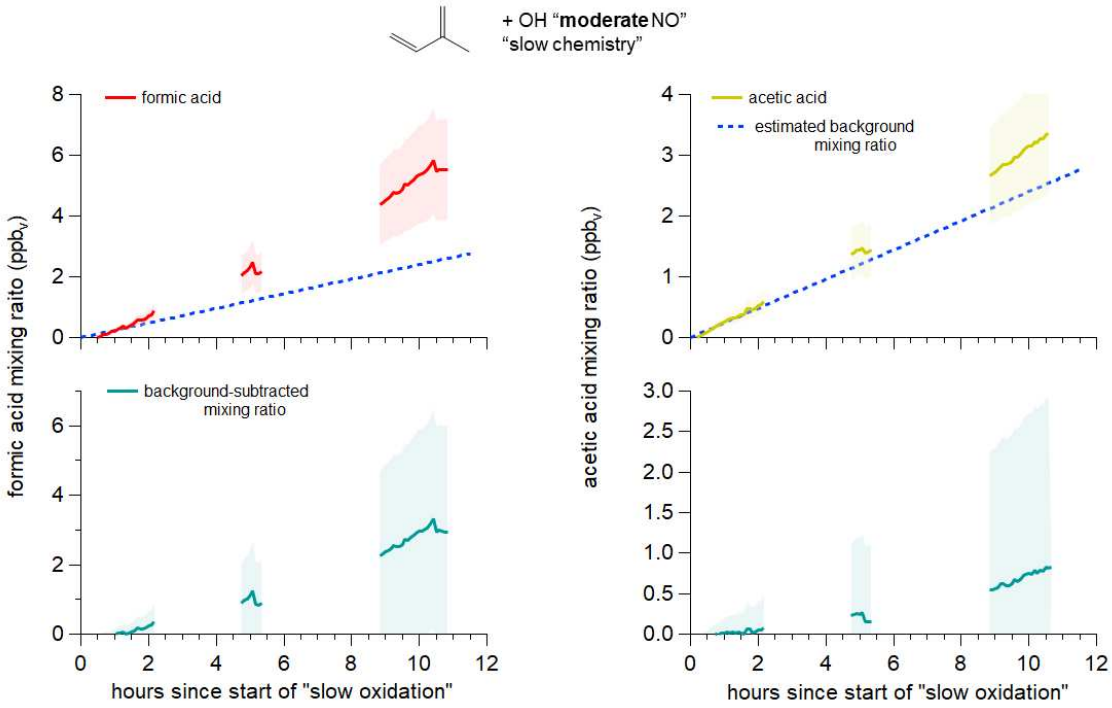

Figure A3.3. Example application of background subtraction used for experiment 7; isoprene + OH "slow chemistry". This same method was applied to measurements from the Jan. 16 α-pinene "slow chemistry" experiment. Raw signals from formic and acetic acid are shown in the top panels as measured during experiment 7. The blue dashed line is the estimated background mixing ratio of the acids calculated from the regression shown in Figure S2. The bottom panels show the background-subtracted mixing ratios for experiment 7. The shaded regions represent the uncertainty of measurements (top) and calculated background-subtracted mixing ratio (bottom; assuming an error of +/- 50% on estimated background).

A3.3. Additional analyses of chamber measurements

3.1 "Slow chemistry" oxidation experiment yields from isoprene and α-pinene

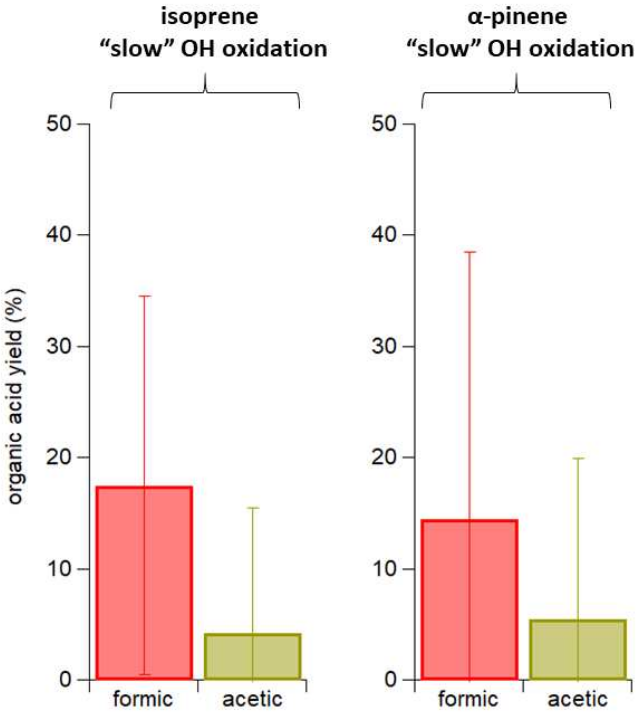

Figure A3.4. Formic and acetic acid yields measured from the "slow" OH oxidation experiments. Yields from the isoprene oxidation experiment are shown on the left and α-pinene is shown on the right. Yields from the experiments were calculated from mixing ratios background subtracted with a background measured from the Jan. 20 CH_3ONO blank experiment.

A3.3.2 Isoprene + NO_3 oxidation

Approximately 40 ppb_v of O_3 was present in the "isoprene + NO_3" experiment to promote the formation of NO_3 radicals. The formic and acetic acid that was produced was likely a result of combined NO_3 and O_3 oxidation chemistry. To place an upper bound on the contribution of O_3 to the formic and acetic acid yields we subtract the molar yields determined from the "isoprene + OH <5% RH" (including the cyclohexane scavenger) experiment from the yields observed in the "isoprene + NO_3" experiment. Modeling of the "isoprene + NO_3" experiment showed that 77% of isoprene was lost to NO_3 oxidation while 22% and 1% were lost to O_3 and OH oxidation, respectively (Figure A3.5).

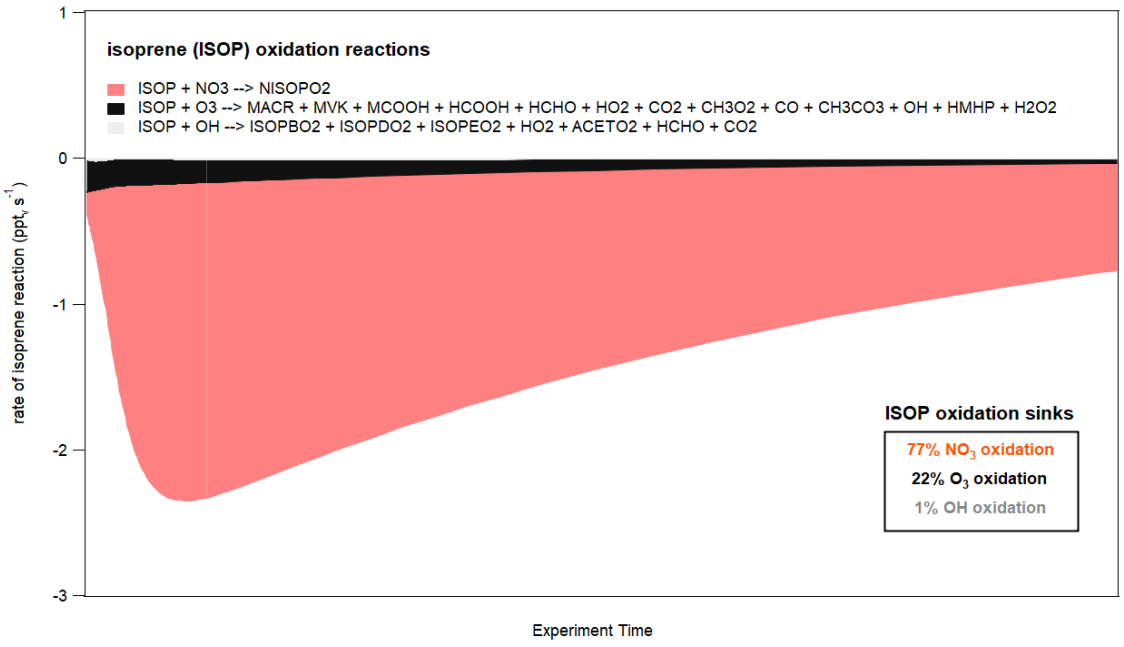

Figure A3.5. Modeled rate of isoprene reaction (ppt_v s^{-1}) with O_3, NO_3, and OH from the "isoprene + NO_3" oxidation experiment. OH acts as a minor (1%) sink for isoprene whereas O_3 is a more substantial chemical sink (22%). Most of the isoprene oxidation can be attributed to NO_3 oxidation (77%).

A3.3.3 α-pinene + OH "slow oxidation" then combined photolysis and OH reaction of α-pinene oxidation products

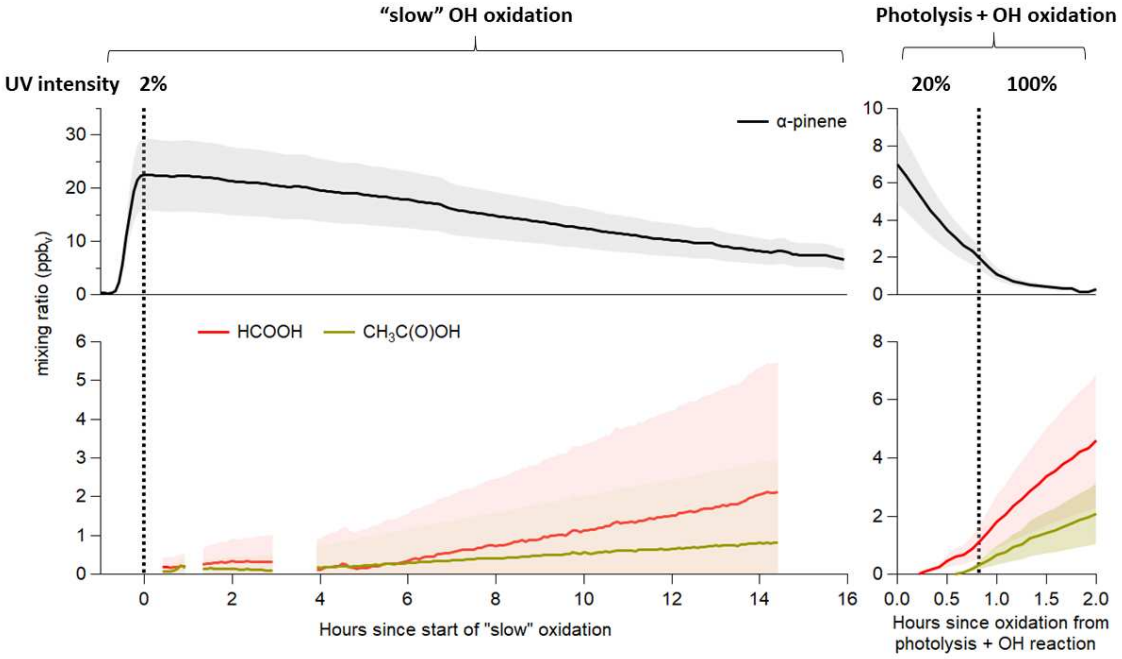

Figure A3.6. The oxidation of α-pinene (top panels; black trace) by OH carried out in experiment 16 under very low UV light intensity (2%) to extend RO_2 lifetimes. The "slow" oxidation of α-pinene occurred over 16 hours (left panels). At the end of the 16 hours the lights were turned off for ~30 minutes, then the lights were turned on for 45 minutes to 20% intensity and 100% intensity for 75 minutes (right panels). High mixing ratios of formic (red trace) and acetic (yellow trace) acids from both parts of the oxidation experiment were observed. Shaded areas show +/- 50% uncertainty for the acids. α-pinene has a 30% uncertainty.

A3.3.4 Influence of seed aerosol on organic acid production: Experiment 19 (Isoprene and ISOPOOH + OH "low NO" with deliquesced $(NH_4)_2SO_4$ seed aerosol

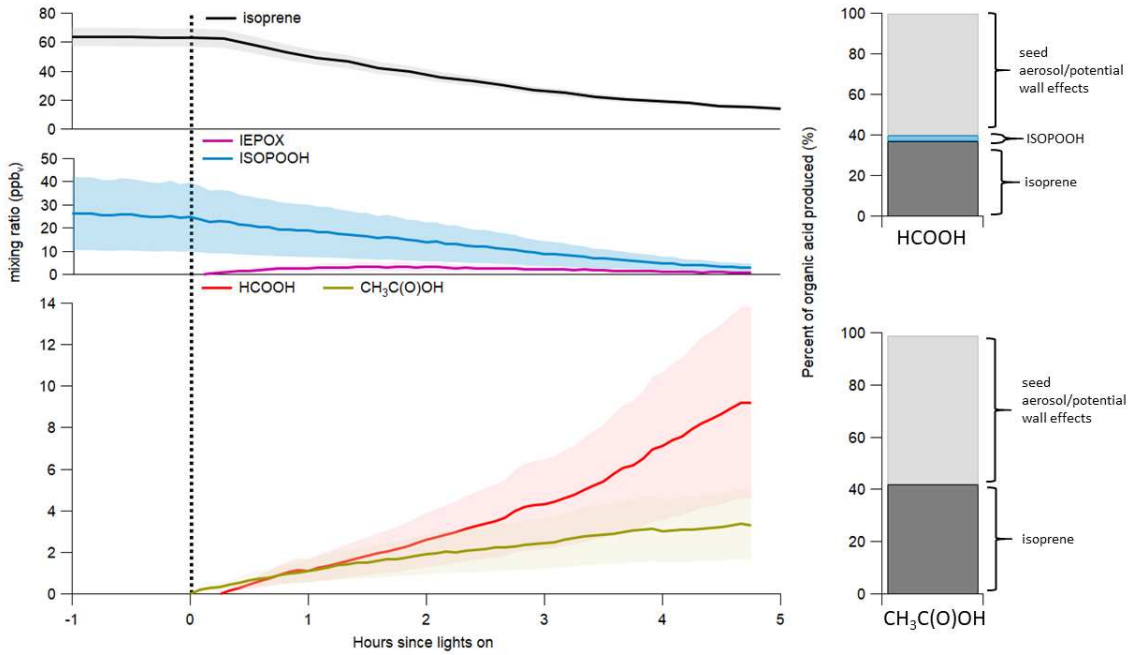

Figure A3.7. Experiment 19 was meant to be an OH oxidation experiment, like experiment 2, under "low NO" conditions in the presence of deliquesced $(NH_4)_2SO_4$ seed aerosol, but nearly 30 ppb_v of ISOPOOH (middle panel; blue trace) was also injected with isoprene (top panel; black trace). When the lights were turned on in this experiment (black dotted line) isoprene and ISOPOOH were both simultaneously oxidized by OH. Low levels of IEPOX were formed (middle panel; purple trace). High mixing ratios of formic (bottom panel; red trace) and acetic (bottom panel; yellow trace) acids were produced. High humidity and/or the presence of seed aerosol was estimated to contribute to ~60% of both organic acids produced (gray bars). Gas-phase OH oxidation of isoprene (black bars), and to a lesser extent ISOPOOH (blue bar), was estimated to contribute ~40% to the observed organic acid mixing ratios. Shaded areas show +/- 50% uncertainty for the acids. Shaded areas for ISOPOOH and IEPOX show +/- 60% uncertainty. The isoprene measurement has a 10% uncertainty. Organic acid mixing ratios are background subtracted.

A3.4. Differences in model treatment of isoprene oxidation and isoprene oxidation products

A3.4.1 Methacrolein (MACR) + OH mechanism

Methacrolein reacts with OH (lifetime ~9 hours; T = 298K; [OH] = 10^6 molecules cm^{-3}) either through addition at the external olefinic carbon or through H-abstraction of the aldehydic hydrogen atom. Two major RO_2 species are produced from reaction with OH.

A3.4.1.1 WR+

Initial RO_2 (OH addition: MCROHOO and H-abstraction: MACR1OO)

- Explicitly treats initial RO_2 branching for OH-add (~55%) for H-abs (~45%)

MACR1OO (methacrolein 1-peroxyl radical)

- MACR1OO + NO uses same rate constant as MCM and predicts the same products as the MCM
- MACR1OO + HO_2 is modeled after the $CH_3C(O)O_2$ + HO_2 reaction and produces methacrylic acid, peroxymethacrylic acid, and an alkoxy radical (branching equal to 0.13, 0.37 and 0.5) that rapidly decomposes to form CH_3O_2 and $C_2H_3O_3$ radicals.

MCROHOO (3-hydroxy 2-peroxyl 2-methyl propanal radical)

- When terminated by NO and HO_2 this RO_2 produces an RO radical that mostly decomposes to form hydroxyacetone.
- This RO_2 + HO_2 also produces an isoprene hydroxy peroxide carbonyl (~0.4 yield).
- A rapid 1,4-H shift isomerization is included as a major sink (~0.5 s^{-1}) to form hydroxyacetone.

A3.4.1.2 MCM v3.3.1

Initial RO_2 (OH addition: (beta) MACRO2, (gamma) MACROHO2 and H-abstraction: MACO3)

- Three RO_2s are formed from MACR + OH with branching for OH-addition to the β-carbon (47%), the γ-carbon (8%), and H-abstraction (45%).

MACO3 (methacrolein 1-peroxyl radical)

- MACO3 + NO produces an RO intermediate ($CH_3C_2H_2O_2$) that rapidly decays (1e6 s^{-1}) with branching of 0.35 to $C_2H_3O_3$ and 0.65 CH_3O_2 with unity production of HCHO and CO.
- MACO3 + HO_2 produces the same three products as described in the WR+ mechanism with slightly different branching ratios (branching equal to 0.15, 0.41 and 0.44 for methacrylic acid, peroxymethacrylic acid, and the alkoxy radical).
- RO_2 self-reactions are included in this mechanism and produce the RO intermediate described in the MACO3 + NO reaction with 0.7 yield and methacrylic acid with 0.3 yield. This sink becomes important with higher RO_2 mixing ratios (i.e. chamber experiments).
- Reaction of RO_2 with NO_3 is included.

MACRO2 (3-hydroxy 2-peroxyl 2-methyl propanal radical)

- RO_2 self-reactions are included as a fate for $MACRO_2$ in the MCM; however, this termination pathway is mostly negligible compared to $MACRO_2$+ HO_2 and isomerization.

MACROHO2 (3-peroxyl 2-hydroxy 2-methyl propanal radical)

- This RO_2 is assumed to isomerize to form hydroperoxyacetone in high yield.

A3.4.1.3 MAGRITTE v1.1

Initial RO_2 (H-abstraction: MCO3)

- Assumes rapid isomerization of the RO_2 produced from OH addition to form hydroperoxyacetone (HPACET), hydroxyacetone (HYAC), HO_2 and OH.

MCO3 (methacrolein 1-peroxyl radical)

- Reaction of RO_2 with NO_3 is included.
- MCO3 + HO_2 produces same species as predicted by MCM and WR+.
- Four unique reactions have MCO3 reacting with ISOPDO2, ISOPBO2, $C_2H_3O_3$ and CH_3O_2 to form a variety of small molecules like HCHO and CO as well as small radicals. Peroxides and carbonyls are produced from these reactions. The most important reaction from this set is MCO3 + CH_3O_2.

A3.4.2 trans-β- Isoprene epoxydiol (IEPOX) + OH mechanism

IEPOX reacts with OH by H-abstraction (lifetime ~24 hours; T= 298K; [OH] = 10^6 molecules cm^{-3}) to produce one of three different alkyl radicals. Through a minor (~10-20%) product channel, oxygen can add to the radical to form RO_2 that subsequently react with HO_2 producing isoprene carbonyl hydroxy epoxides. Through major product channels (~80-90%), the alkyl radicals isomerize, breaking open the epoxide ring to form dihydroxy carbonyl RO_2.

A3.4.2.1 WR+

- The products resulting from NO or HO_2 termination of the minor channel epoxide ring-opening initial RO_2 (4-hydroxy 3-peroxyl 2-methyl 1-hydroxy propanal) are grouped into the product yields from termination of one of the other major yield RO_2, IEPOXAOO (3,4-dihydroxy 2-peroxyl 2-methyl butanal). Yields from NO or HO_2 termination of the other major yield RO_2, IEPOXBOO (3,4-dihydroxy 3-methyl 2-peroxyl butanal), are lower (~0.33) compared to MCM and so yields of IEPOXAOO are increased (~0.67) in this mechanism.
- The 1,5 H-shift isomerization process are included and produce dicarbonyl hydroxy hydroperoxide compounds. Oxidation of these C_5 compounds generally produce C_4 hydroxy carbonyl compounds.
- IEPOXAOO and IEPOXBOO reaction with RO_2 is not included.
- IEPOXAOO produces 3,4-dihydroxy-2-butanone (called MVK3OH4OH) after 1,4 H-shift isomerization, like the MCM, but when this product reacts with OH, two products are possible, with 1-hydroxy 2,3-butanedione (BIACETOH) being the major yield product (~0.61).

A3.4.2.2 MCM v3.3.1

- All three RO_2 produced in the ring-opening channel are treated explicitly.
- Only 1,4 H-shifts are considered as important isomerization processes for the 3,4-dihydroxy 2-peroxyl 2-methyl butanal (C57O2) and 3,4-dihydroxy 3-methyl 2-peroxyl butanal (C58AO2) peroxy radicals. The 3,4-dihydroxy-2-butanone product from C57O2

isomerization can either photolyze or react with OH to produce glycoaldehyde and BIACETOH.

- Termination by NO_3 and RO_2 is included in the C57O2 and C58AO2 reactions.
- HO_2 termination reactions are generally producing multi-functional peroxides.

A3.4.2.3 MAGRITTE v1.1

- Lumps cis- and trans- isomers of β-IEPOX and the branching between the initial RO_2 (i.e. IEPOXAO2 and IEPOXBO2) is combined to represent the distribution produced from both isomers. This is also considered when providing yields for the isoprene hydroxy carbonyl species (minor channel).
- Fast photolysis of the 1,5 H-shift isomerization products is assumed and largely produces methylglyoxal.

A3.4.3 4,3-ISOPOOH + OH mechanism

ISOPOOH reacts with OH (lifetime ~3 hours; T = 298K; [OH] = 10^6 molecules cm^{-3}) through a major OH-addition channel and a minor H-abstraction channel. The major product of the OH-addition channel is IEPOX. An important minor product resulting from 1,5 H-shift isomerization of the resulting RO_2 is a dihydroxyhydroperoxy epoxide.

A3.4.3.1 WR+

- The trans- and cis- isomers of IEPOX (i.e. 0.68:0.32 yield) are explicitly treated. The consequence of this shouldn't be major because the resulting peroxy radicals from reaction of OH with the cis- isomer are the same as the ones produced from OH oxidation of the trans- IEPOX isomer.

- Minor OH-addition channel is modeled to produce two RO_2 that are in equilibrium with one another, but an estimated yield distribution is applied. The major product from reactions of these two RO_2 is dihydroxyhydroperoxy epoxide. Other minor products include glycoaldehyde, formaldehyde, and hydroperoxyacetone.
- The H-abstraction channels are explicitly treated, but this reaction occurs relatively slowly (lifetime ~35 hours). The products of this reaction include multi-function hydroxy carbonyl species and peroxides. Additionally, an ISOPOO radical is produced in high yield to be recycled into the isoprene oxidation ladder.

A3.4.3.2 MCM v3.3.1

- The MCM assumes all the IEPOX formed from this ISOPOOH + OH takes the form of the trans- isomer with a yield from the OH-addition channel of 75%. Isoprene hydroxy carbonyl is the other product assumed to be produced with a 22% yield.
- The H-abstraction channel is represented by a 3% yield of ISOPOO that feeds back into the isoprene oxidation ladder.

A3.4.3.3 MAGRITTE v1.1

- The OH-addition channel is treated similarly to how the MCM and WR+ treat it. IEPOX and dihydroxyhydroperoxy epoxide are major products with 85% and 15% yields, respectively.
- Most of the yield from the H-abstraction channels is the ISOPOO radical that goes on to be recycled into the isoprene oxidation cascade. The major difference for this channel is the creation of unsaturated hydroperoxyl aldehydes that photolyze to enols. The enols then react with OH to produce small molecule products, including formic acid.

A3.4.4 Fate of CH_3CO_3 and CH_3O_2

A3.4.4.1 WR+

- CH_3CO_3 + HO_2 follows the same kinetics and products suggested in the MCM and is source of acetic acid.
- CH_3CO_3 + NO same for all mechanisms with CH_3CO_2 as a major product.
- CH_3CO_3 + MO_2 is a source of acetic acid and the rate constant is somewhat different from MCM.
- Same NO_3 fate as MCM
- CH_3COO reacts specifically with different RO_2 to produce different products. Major product of these reactions is HCHO.

A3.4.4.2 MCM v3.3.1

- CH_3CO_3 + HO_2 produces peroxyacetic, acetic and CH_3CO_2 as major products.
- CH_3CO_3 + NO is the same for all mechanisms.
- CH_3CO_3 + RO_2 is a source of acetic acid and a source of CH_3CO_2.
- NO_3 fate included
- CH_3O_2 mostly goes to HCHO

A3.4.4.3 MAGRITTE v1.1

- CH_3CO_3 + HO_2 produces peroxyacetic, acetic and CH_3CO_2 as major products.
- CH_3CO_3 + NO same for all mechanisms.
- Reacts with CH_3CO_3 (self-RO_2 reaction) and CH_3CO_2 to produce some acetic and CH_3CO_2.

A3.5. "Base case" results modeling FIXCIT experiments

Table A3.2. Predicted and actual organic acid yields for modeled FIXCIT experiments.

Experiment name	Formic acid yield (%)				Acetic acid yield (%)			
	MCM	WR +	MAG	Actual	MCM	WR +	MAG	Actual
Isoprene + OH "low NO"	0.4	0.4	1.7	7.0	0.3	0.7	1.7	2.9
Isoprene + OH "high NO"	0.3	0.2	0.1	4.0	0	0	0.2	1.0
Isoprene + OH "low HC, low NO"	0.4	0.5	2.0	12.0	0.3	0.8	1.9	< DL
Isoprene + NO3	1.3	1.0	0.2	35.5	< 0.1	< 0.1	< 0.1	7.1
Isoprene + O3 w/o scavenger	14.2	7.7	3. 3	19.2	3.6	1.5	1.0	5.2
Isoprene + O3 w/ scavenger	20.0	10.3	3.4	10.3	3.9	1.2	0.9	1.7
Isoprene + O3 w/o scavenger 50% RH	13.9	16.2	3.1	119.7	3.5	1.5	0.9	8.1
Isoprene + O3 w/ scavenger 50% RH	20.0	22.5	3.6	70.0	3.9	1.3	0.9	4.8
ISOPOOH + OH "low NO"	< 0.1	< 0.1	2.1	1.7	< 0.1	< 0.1	0.1	< DL
IEPOX + OH "moderate NO"	< 0.1	< 0.1	< 0.1	12.5	< 0.1	< 0.1	0.2	< DL
MACR + OH "low NO"	< 0.1	< 0.1	< 0.1	10.9	1.8	1.6	2.2	8.8
MACR + OH "high NO"	1.7	2.3	< 0.1	3.4	< 0.1	< 0.1	1.8	< DL

6. Modifications to improve model prediction of organic acid production with measurements

Table S3. Summary of modifications made to mechanisms to bring organic acid model prediction into agreement with observations from FIXCIT experiments.

Experiment Modified	Organic acid	Mechanism	Reaction modified	Rate constant
MACR + OH "low NO"	formic acid	MCM v3.3.1	MACO3 + HO2 = CH3C2H2O2 + OH + **0.5 HCOOH** + 0.32 CH3CO2H	[a]KAPHO2*0.44
		WR+	MACR1OO + HO2 = 0.37MACR1OOH + 0.5HCHO + 0.325CO + 0.325CH3OO + 0.175CH3CO3 + 0.5CO2 + 0.5OH + 0.13O3 + 0.13MACR1OH + **0.25 HCOOH** + 0.15 CH3CO2H	3.14e-12*exp(580/T)
		MAGRITTE v1.1	MCO3 + HO2 = CO2 + HCHO + OH + CH3O2 + CO + **0.8 HCOOH** + 0.5 CH3COOH	4.155e-13*exp(980/T)
	acetic acid	MCM v3.3.1	MACO3 + HO2 = CH3C2H2O2 + OH + 0.5 HCOOH + **0.32 CH3CO2H**	[a]KAPHO2*0.44
		WR+	MACR1OO + HO2 = 0.37MACR1OOH + 0.5HCHO + 0.325CO + 0.325CH3OO + 0.175CH3CO3 + 0.5CO2 + 0.5OH + 0.13O3 + 0.13MACR1OH + 0.25 HCOOH + **0.15 CH3CO2H**	3.14e-12*exp(580/T)
		MAGRITTE v1.1	MCO3 + HO2 = CO2 + HCHO + OH + CH3O2 + CO + 0.8 HCOOH + **0.5 CH3COOH**	4.155e-13*exp(980/T)
MACR + OH "high NO"	formic acid	MCM v3.3.1	MACRO = ACETOL + CO + HO2 + **0.1 HCOOH**	[b]KDEC
		WR+	MCROHOO + NO = 0.86HAC + 0.86CO + 0.86HO2 + NO2 +	[c]8.3612e-12

			0.14MGLY + 0.14HCHO + **0.01 HCOOH**	
		MAGRITTE v1.1	MACR + OH = CO + 0.036 HPACET + 0.036 HO2 + 0.964 HYAC + OH + **0.03 HCOOH**	4.4E-12*exp(380/T)
IEPOX + OH "moderate NO"	formic acid	MCM v3.3.1	C58AO2 + NO = C58AO + NO2 + **0.2 HCOOH**	KRO2NO.*0.935
		WR+	IEPOXAOO + NO = 0.2MVK3OH4OH + HO2 + NO2 + 0.2CO + 0.8GLYC + 0.8MGLY + **0.2 HCOOH**	[c]8.5534e-12
		MAGRITTE v1.1	IEPOXAO2 + NO = NO2 + HO2 + 0.8 MGLY + 0.8 GLYALD + 0.2 DHBO + 0.2 CO + **0.2 HCOOH**	2.7e-12*exp(350/T)
ISOPOOH + OH "low NO"	formic acid	MCM v3.3.1	OH + ISOPDOOH = HCOC5 + OH + **0.07 HCOOH**	1.15e-10*0.22
		WR+	ISOP3OOH4OH + OH = 0.655IHPOO3 + 0.345IHPOO2 + **0.12 HCOOH**	4.35e-12*exp(390/T)
		MAGRITTE v1.1	[e]	[e]
Isoprene + OH "low NO"	formic and acetic acid	MAGRITTE v1.1	HPALD2 = OH + 1.15 HO2 + 1.35 CO2 + 0.55 HCHO + 0.65 CH3CO3 + 0.2 MMAL +0.15 MGLY + 0.15 CO + 0.1 GLY + **3 HCOOH + 1 CH3COOH**	[f]6.4e-05

[a]KAPHO2 = 5.2e-13*exp(980/T)

[b]KDEC = 1e6

[c]Reported for 298K and 1000mbar

[d]KRO2NO = 2.7e-12*exp(360/T)

[e]no modification

[f]Calculated with absorption cross sections and quantum yields for HPALD reported in Muller et al.[1] Calculated with chamber spectrum recorded with 100% UV lights on.

A3.6.1 MACR + OH “low NO”

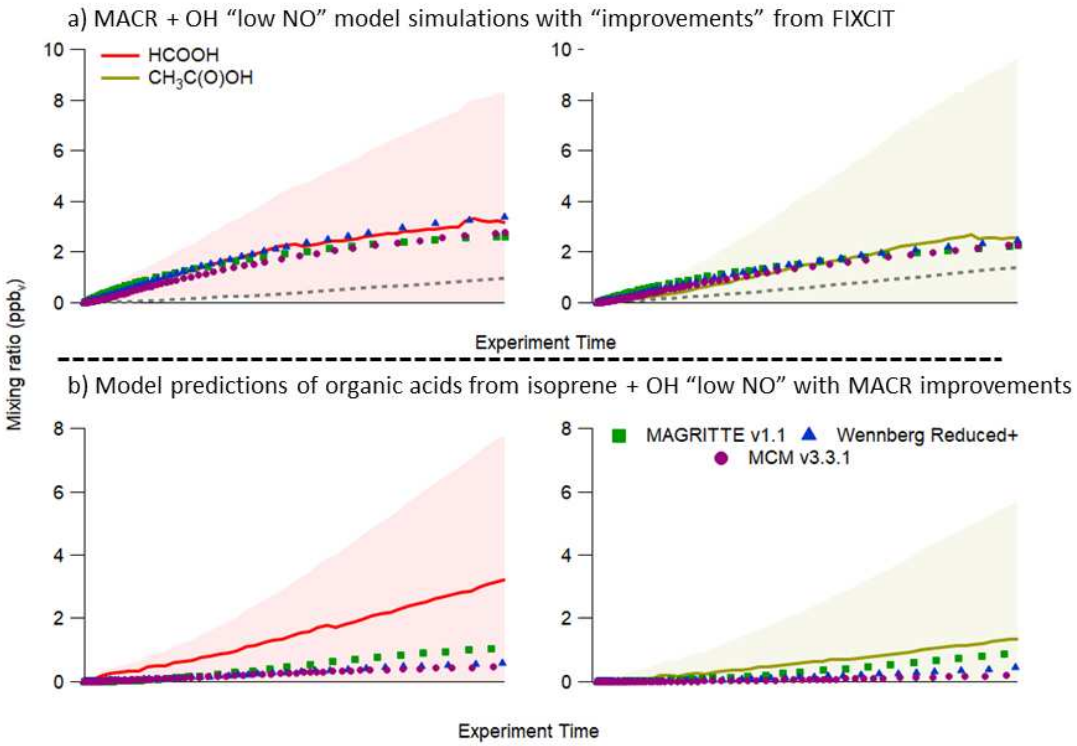

Figure A3.8. (a) Formic (red) and acetic (yellow) acid mixing ratios observed during the OH oxidation of MACR under conditions of “low NO”. Yields were applied to the MACO3 + HO2 termination pathway in the isoprene oxidation mechanisms to bring predictions of organic acid production (markers) into agreement with measured values (solid lines). Unadulterated mechanisms were run with modifications (dashed lines) to include oxidation of hydroxyacetone (HAC) and glycolaldehyde (GLY) to test the sensitivity of organic acid production to these primary sources. (b) Model predictions of organic acid production from the isoprene + OH “low NO” experiment with modifications to the mechanism exclusively informed by the MACR + OH “low NO” experiment. Shaded areas show uncertainty propagated from background-subtracted mixing ratios.

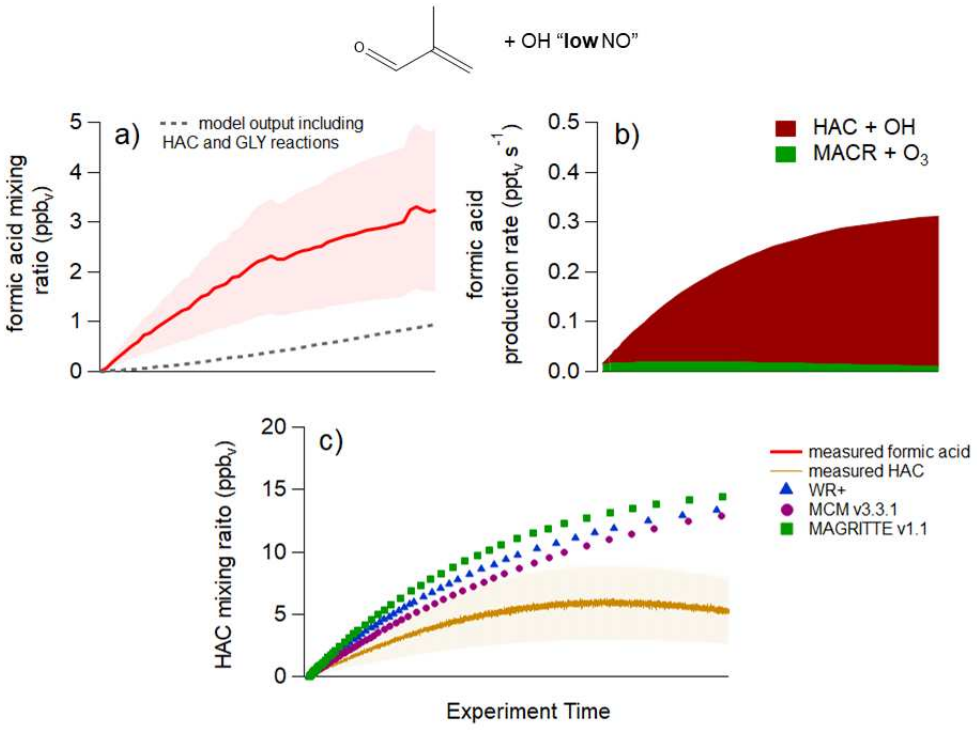

Figure A3.9. (a) Formic acid mixing ratio measured (solid line) from the MACR + OH "low NO" experiment and the predicted formic acid production (dashed line) from the MAGRITTE mechanism modified to only include production routes from hydroxyacetone (HAC) and glycolaldehyde. (b) Formic acid production rates from the HAC and GLY mechanism prediction. (c) HAC measured during the MACR + OH "low NO" experiment (solid line) and the predictions of HAC production from the three isoprene oxidation mechanisms tested (markers). Shaded areas show +/- 50% uncertainty.

A3.6.2 MACR + OH “high NO”

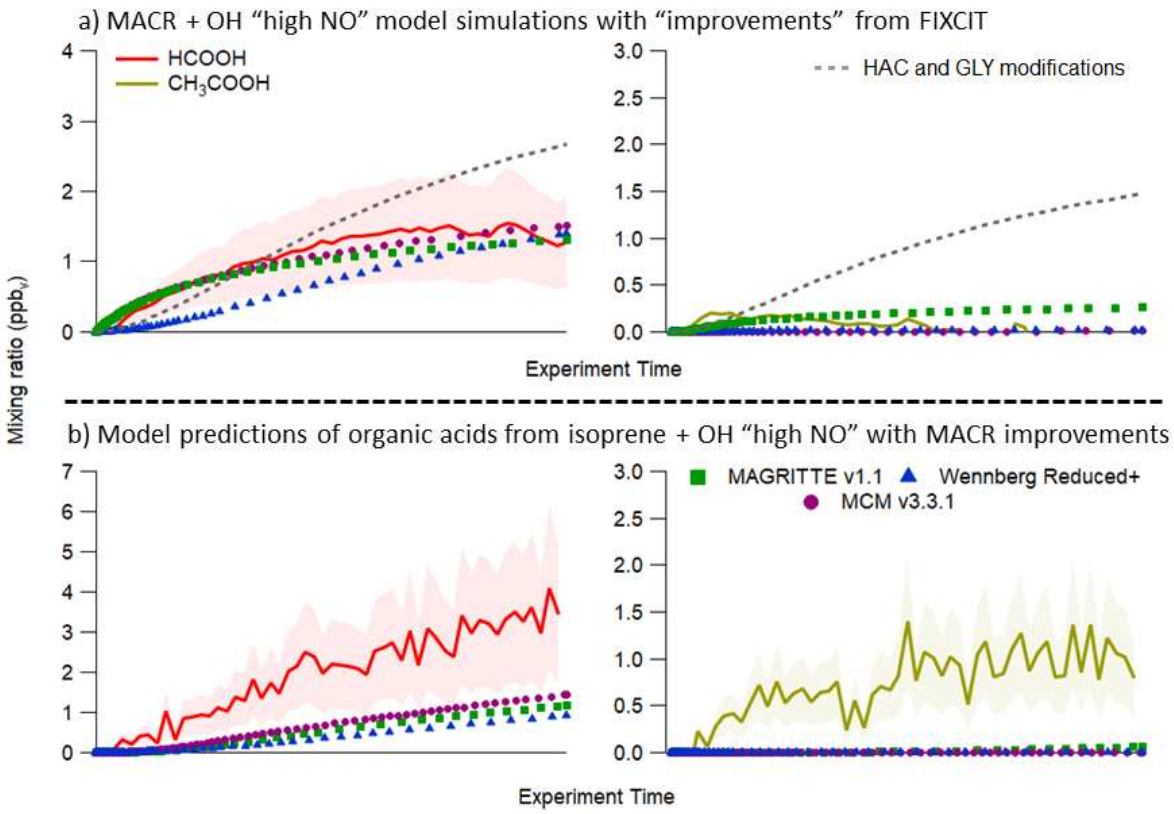

Figure A3.10. (a) Formic (red) and acetic (yellow) acid mixing ratios observed during the OH oxidation of MACR under conditions of “high NO”. Yields were applied to the MACRO2 + NO termination pathway in the isoprene oxidation mechanisms to bring predictions of organic acid production (markers) into agreement with measured values (solid lines). Unadulterated mechanisms were run with modifications (dashed lines) to include oxidation of hydroxyacetone (HAC) and glycolaldehyde (GLY) to test the sensitivity of organic acid production to these primary sources. (b) Model predictions of organic acid production from the isoprene + OH “high NO” experiment with modifications to the mechanism exclusively informed by the MACR + OH “low NO” and “high NO” experiments.

A3.6.3 IEPOX + OH "moderate NO"

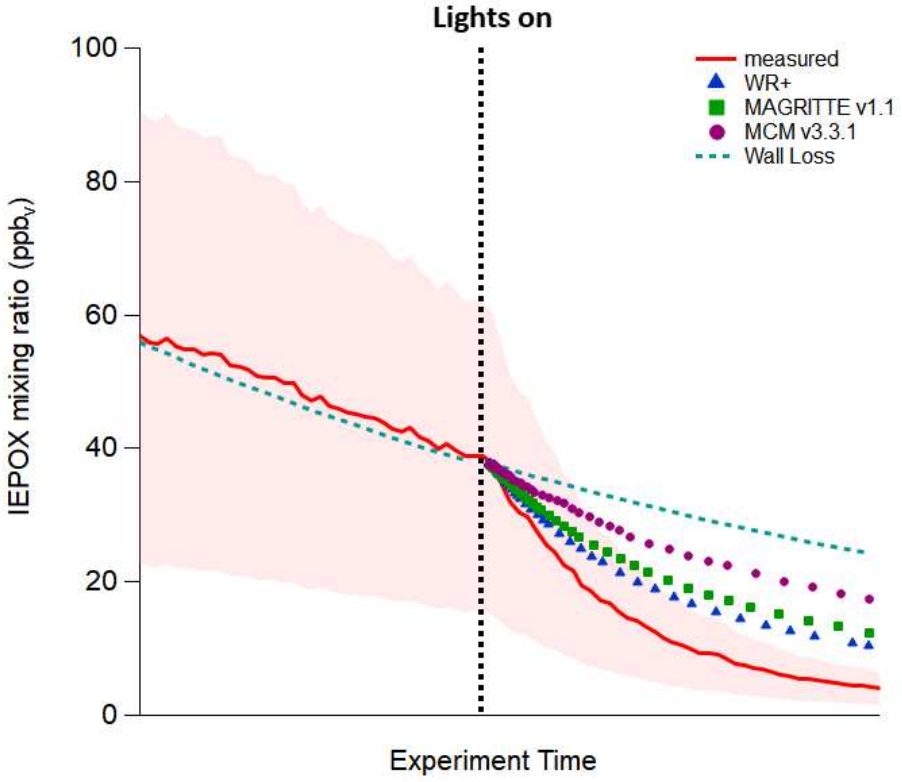

Figure A3.11. Trans-β-IEPOX mixing ratios measured (solid line) and model predicted (markers). The dashed line indicates where UV lights were turned on and oxidation of IEPOX was initiated by OH. Decrease in the IEPOX mixing ratio prior to turning lights on is attributed to vapor wall loss. Wall loss is parameterized in the mechanisms and shown by the blue dashed line.

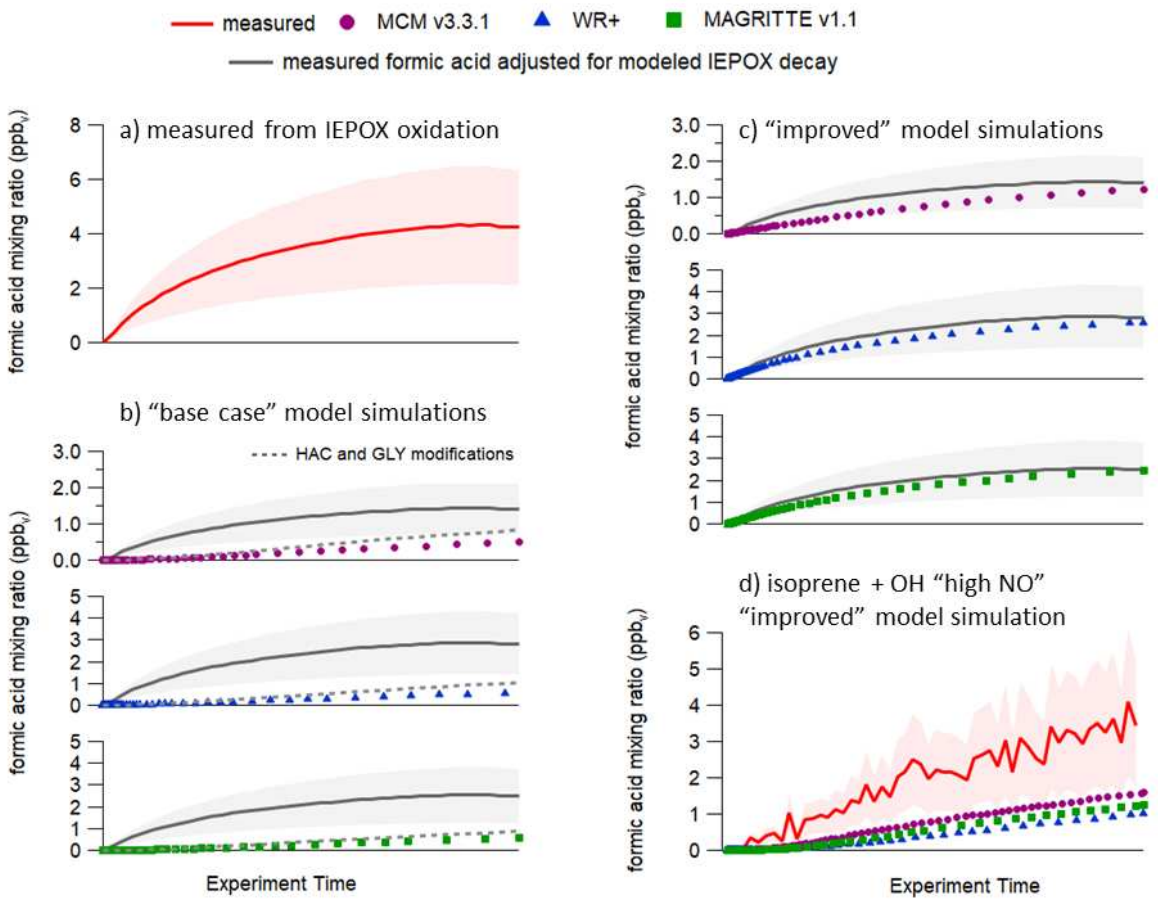

Figure A3.12. (a) Formic acid mixing ratio measured from IEPOX oxidation. (b) Formic acid mixing ratios were predicted for each mechanism based on the yield of formic acid measured in the experiment and the amount of IEPOX consumed as predicted by the model. Each of the mechanisms was run in their unaltered form to see the "base case" predictions of formic acid. Unadulterated mechanisms were also run with modifications (dashed lines) to include oxidation of hydroxyacetone (HAC) and glycolaldehyde (GLY) to test the sensitivity of organic acid production to these primary sources. (c) Yields of formic acid were applied to the IEPOX + OH mechanism to bring model prediction into agreement with measured formic acid mixing ratios (adjusted for predicted IEPOX consumption by model). (d) Model predictions of organic acid production from the isoprene + OH "high NO" experiment with modifications to the mechanism exclusively informed by the MACR + OH "low NO" and "high NO" and IEPOX + OH experiments.

A3.6.4 ISOPOOH + OH “low NO”

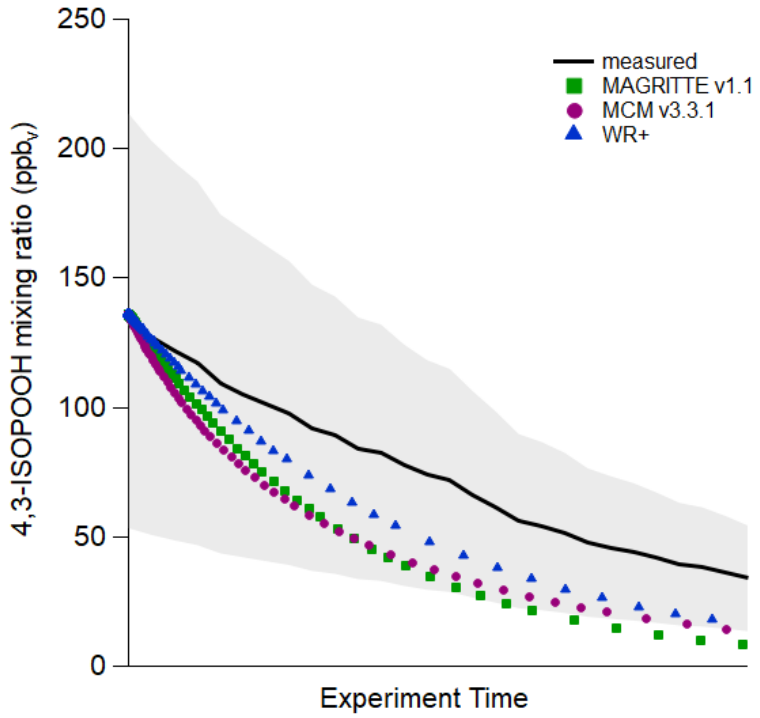

Figure A3.13. 4,3-ISOPOOH mixing ratios measured (solid line) and model predicted (markers).

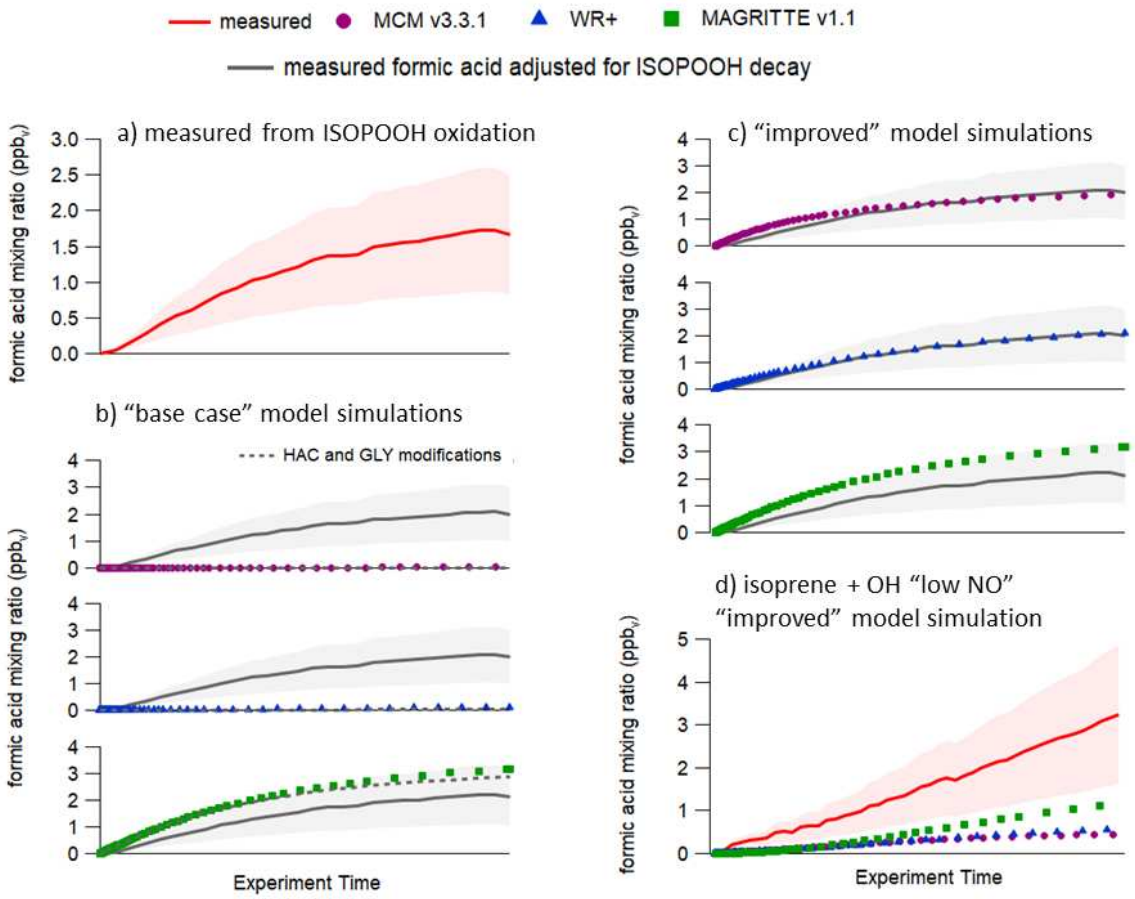

Figure A3.14. (a) Formic acid mixing ratio measured from ISOPOOH oxidation. (b) Formic acid mixing ratios were predicted for each mechanism based on the yield of formic acid measured in the experiment and the amount of ISOPOOH consumed as predicted by the model. Each of the mechanisms was run in their unaltered form to see the "base case" predictions of formic acid. Unadulterated mechanisms were also run with modifications (dashed lines) to include oxidation of hydroxyacetone (HAC, and glycolaldehyde (GLY) to test the sensitivity of organic acid production to these primary sources. (c) Yields of formic acid were applied to the ISOPOOH + OH mechanism to bring model prediction into agreement with measured formic acid mixing ratios (adjusted for predicted ISOPOOH consumption by model). (d) Model predictions of organic acid production from the isoprene + OH "low NO" experiment with modifications to the mechanism exclusively informed by the MACR + OH "low NO" and "high NO", IEPOX + OH, and ISOPOOH + OH experiments.

A3.6.5 Isoprene + OH

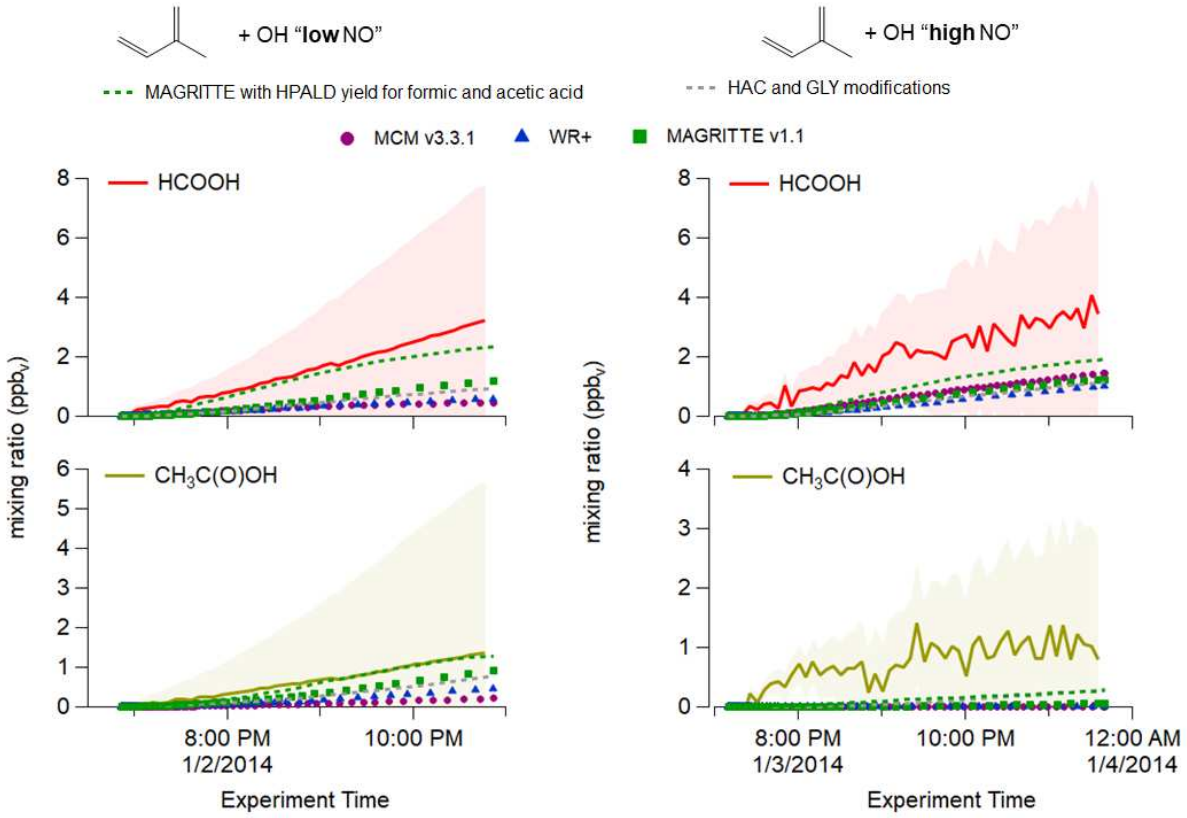

Figure A3.15. The ability of the FIXCIT-modified models, including the additional HPALD photolysis modification for MAGRITTE, to predict formic (red) and acetic (yellow) acid mixing ratios during the isoprene + OH "low NO" (left) and isoprene + OH "high NO" (left) experiments.

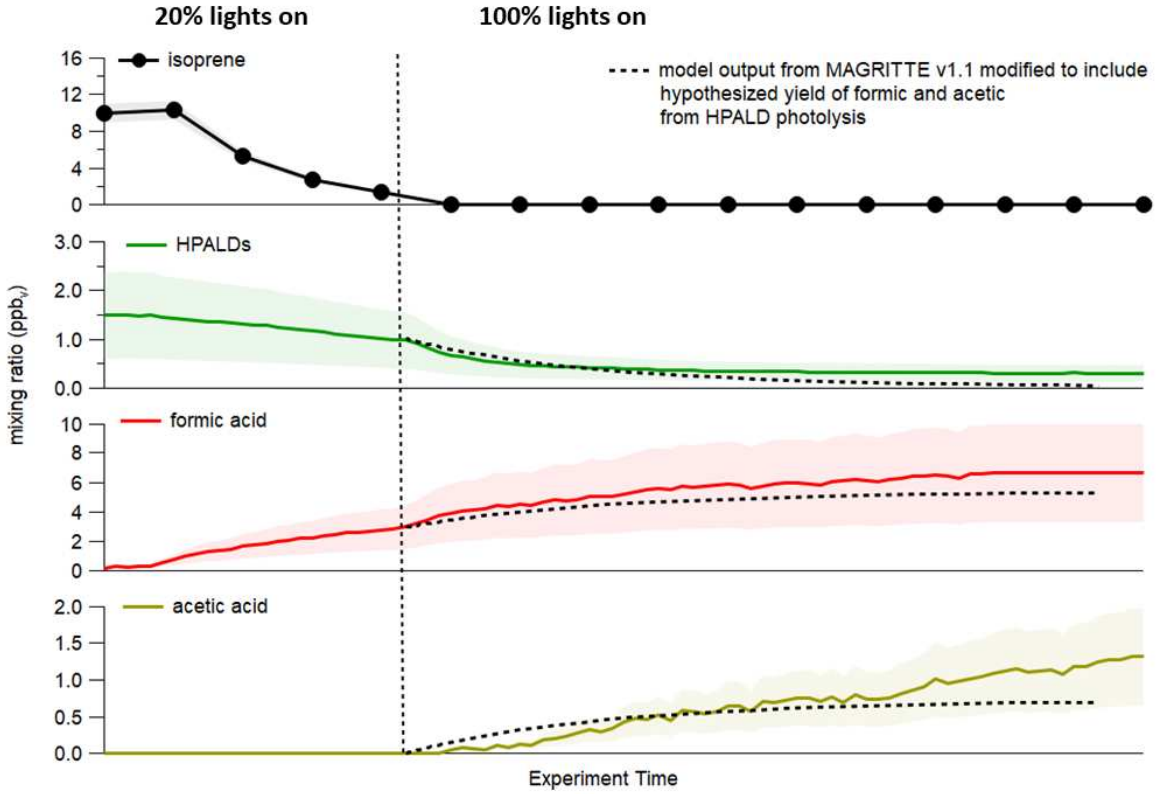

Figure A3.16. The right panels isolated from Figure 3.3 showing the portion of the January 7th experiment that targeted combined photolysis and OH oxidation of HPALD compounds. For the first part of this experiment 20% of the UV lights were turned on to initiate photolysis and OH oxidation (left of the vertical dashed line). The UV lights were then turned up to 100% to enhance photolysis and OH oxidation (left of the vertical dashed line). To close the gap between measured and modeled formic acid in the "low NO" isoprene + OH oxidation experiment a molar yield of 300% for formic acid was applied to the photolysis reaction of HPALD2 in the MAGRITTE mechanism. The model results using this updated MAGRITTE mechanism are shown by the dashed line traces in the time series for HPALDs, formic acid, and acetic acid. A molar yield of 100% was also applied for acetic acid. This figure shows that even with the updated mechanism formic and acetic acid mixing ratios are not captured in this photolysis experiment suggesting HPALD photolysis is likely not the exclusive 'missing' chemical source of formic and acetic acid in these isoprene oxidation experiments.

A3.7. Modeling of organic acid production during SOAS

Ambient modeling of organic acid production during SOAS was performed for six simulated days to allow diurnal steady-state to be established. Many organic and inorganic species measured during SOAS were constrained to their measured diel profiles for the model runs as described in We converted all the species names in the MAGRITTE v1.1 mechanism to MCM species names to ensure compatibility in running the combined MCM and MAGRITTE mechanisms.

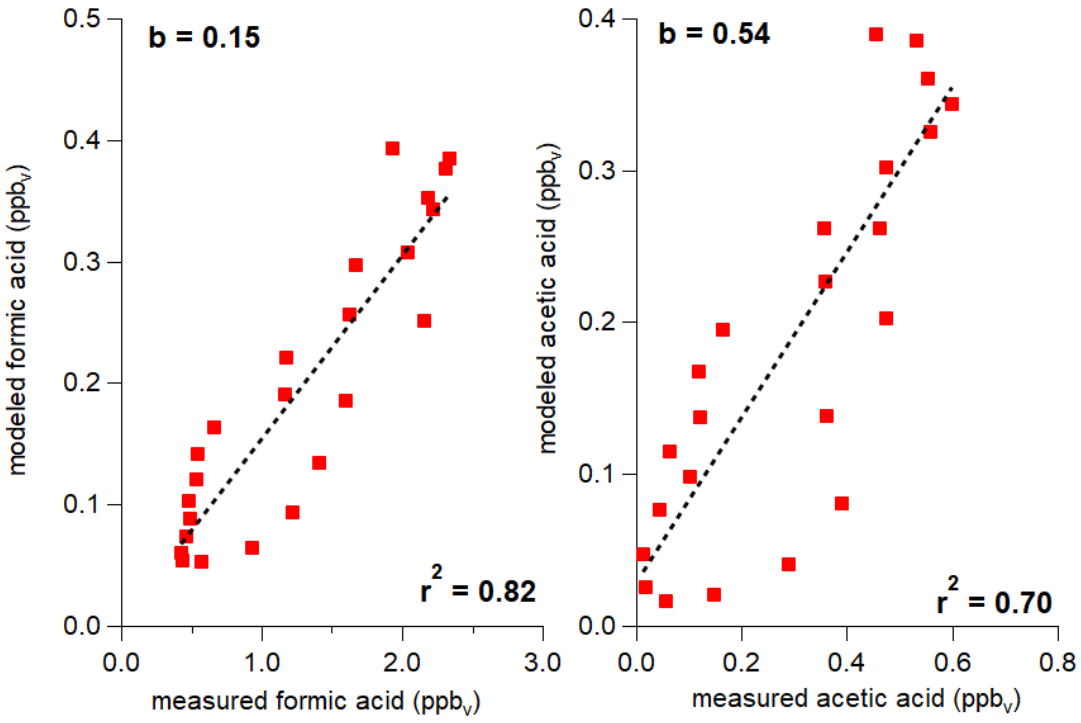

Figure A3.17. Comparison of modeled versus measured formic (left) and acetic (right) acid. Modeled versus measured formic acid exhibits greater temporal agreement than acetic acid, however the magnitude of the acetic acid mixing ratio is better predicted than formic.

A3.8. Sensitivity analysis of model dilution scheme on ambient organic acids

Kaiser et al.[2] experimented with three different dilution schemes and found that applying a constant dilution rate of 4 day^{-1} of VOC-free background air best reproduced measured mixing ratios of glyoxal, HCHO, glycolaldehyde and PAN. The authors also found that the results of their study, focusing on OH reactivity, were mostly insensitive to the planetary boundary layer dilution scheme used. We replicate the sensitivity test performed in that study and apply it to the modeling of formic and acetic acid in this study (Figure A3.14). Following the methods of Kaiser et al (2016) were tested three constant dilution ratios (2, 4, and 40 day^{-1}) and two dilution rates calculated from the planetary boundary layer height measurement; one from a calculated entrainment rate and another scaled by the boundary layer measurement. The underestimation of formic acid by the model ranged from 84, 85, and 84% between the bounds of the 2, 4, and 40 day^{-1} dilution rate. The best agreement ($r^2 = 0.82$) between modeled output and measurements for these dilution schemes was when using the value of 4 day^{-1}. Similar results were obtained for acetic acid. When comparing the PBL-scaled dilution estimate to the constant 4 day^{-1} estimate the agreement between modeled and measured diel profiles increase slightly, but the underestimates of the models also increase slightly (Figure A3.15). For consistency with previous literature we use the constant 4 day^{-1} estimate of dilution acknowledging that the differences between results from this and the PBL-scaled model case are minor. Similar to the findings of Kaiser et al, the entrainment-based dilution scheme produced diel profiles that were in poor agreement with measured OVOC profiles.

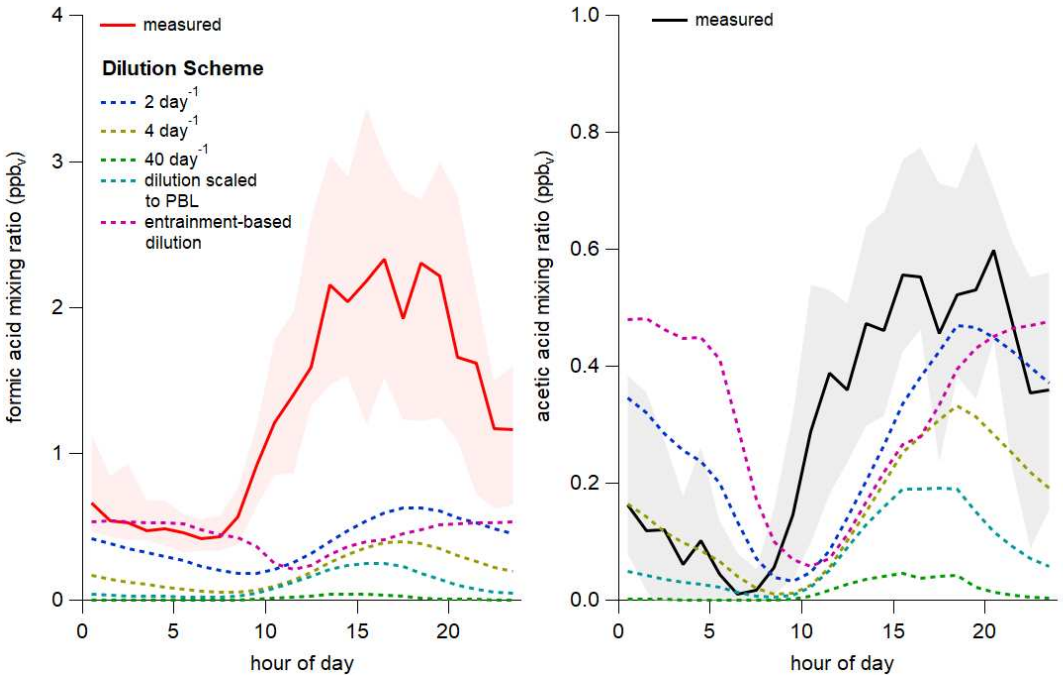

Figure A3.18. Modeled formic and acetic acid mixing ratios during SOAS (dashed lines) using different parameterizations for simulated planetary boundary layer dilution.

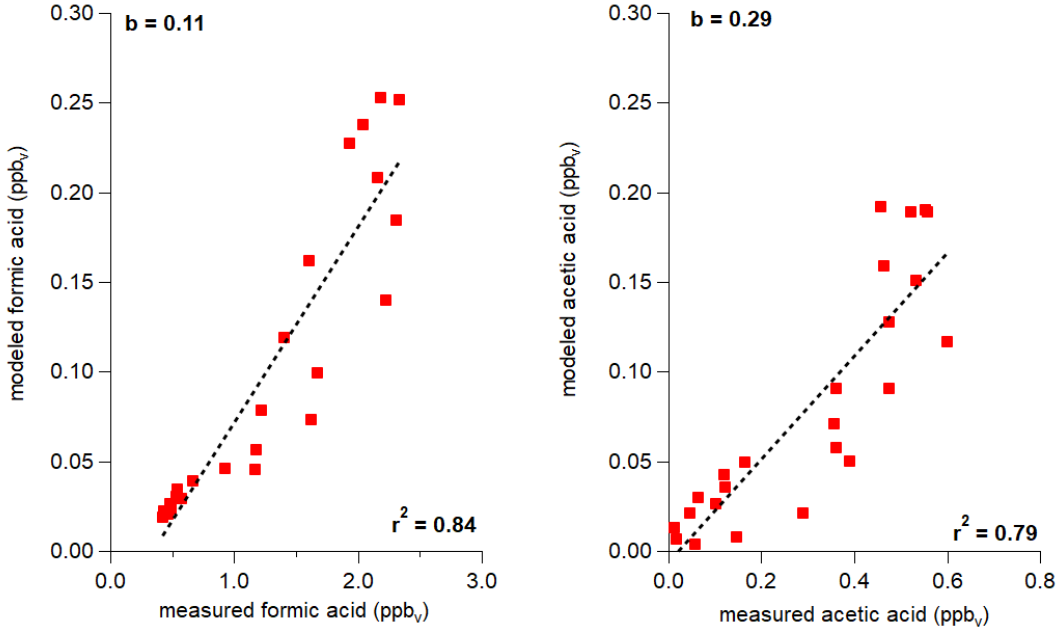

Figure A3.19. Comparison of modeled to measured organic acids using the PBL-scaled dilution scheme for modeled mixing ratios.

A3.9. Estimate of global contribution of isoprene oxidation to formic and acetic acid production

We provide a rough estimate of formic and acetic acid production from isoprene based on the distribution of average global oxidative fate of isoprene presented in Bates and Jacob (2019).[3] We first multiplied the fractional contribution to isoprene oxidative fate (column 2 of Table A3.4) by the estimate of annual isoprene emission described in Bates and Jacob of 535 Tg a^{-1} to get the moles of isoprene reacted by that corresponding pathway (column 1 of Table A3.4). We then multiplied these moles of isoprene by the yield of organic acid and converted that value to Tg of organic acid. The various contributions of isoprene oxidation to estimated organic acid global production rates are presented below in Table A3.4.

Table A3.4. Details of the estimates of formic and acetic acid production from isoprene oxidation.

GOES-Chem chemical Source	GEOS-Chem Bates distribution (fraction)	FIXCIT formic yield (fraction)	FIXCIT acetic yield (fraction)	FIXCIT experiment source	formic global source (Tg a^{-1})	acetic global source (Tg a^{-1})
ISOP + NO3	0.02	0	0.019	ISOP + NO3; experiment 9	0	0.18
ISOP + O3	0.1	1.19	0.08	ISOP + O3 with scavenger 50% RH; experiment 29	43.0	3.8
Isoprene + OH + O2 + HO2	0.36	0.07	0.03	ISOP + OH "low NO"; experiment 2	9.1	5.1
Isoprene + OH + O2 + NO	0.25	0.04	0.01	ISOP + OH "high NO"; experiment 3	3.6	1.2

Isoprene + OH + O2 then H-shift	0.19	0.27	0.05	experiment 7	18.5	4.5
Isoprene + OH + O2 + RO2	---	---	---	n/a	---	---

REFERENCES

(1) Müller, J.-F.; Stavrakou, T.; Peeters, J. Chemistry and Deposition in the Model of Atmospheric Composition at Global and Regional Scales Using Inversion Techniques for Trace Gas Emissions (MAGRITTE v1.1) – Part 1: Chemical Mechanism. *Geosci. Model Dev.* **2019**, *12* (6), 2307–2356. https://doi.org/https://doi.org/10.5194/gmd-12-2307-2019.

(2) Kaiser, J.; Skog, K. M.; Baumann, K.; Bertman, S. B.; Brown, S. B.; Brune, W. H.; Crounse, J. D.; de Gouw, J. A.; Edgerton, E. S.; Feiner, P. A.; et al. Speciation of OH Reactivity above the Canopy of an Isoprene-Dominated Forest. *Atmos Chem Phys* **2016**, *16* (14), 9349–9359. https://doi.org/10.5194/acp-16-9349-2016.

(3) Bates, K. H.; Jacob, D. J. A New Model Mechanism for Atmospheric Oxidation of Isoprene: Global Effects on Oxidants, Nitrogen Oxides, Organic Products, and Secondary Organic Aerosol. *Atmospheric Chem. Phys.* **2019**, *19* (14), 9613–9640. https://doi.org/https://doi.org/10.5194/acp-19-9613-2019.

APPENDIX 4 - CHAPTER 4 SUPPORTING INFORMATION

A4.1 Supplemental site description

A4.1.1 SOAS

Median daytime temperatures during SOAS were around 29°C while temperatures in the evening dropped to around 21°C. Relative humidity (RH) was lowest during the day (~60%) and increased in the evening often above 90%. A period of cloud cover (i.e. decreased solar radiation) was observed from July 3rd to the 7th. This resulted in decreased photochemistry as evidenced by low HO2 and O3 mixing ratios. Coincident with the measurements of organic acids, the most precipitation was observed between July 3-7 totaling 51.7 mm with an additional 18.5 mm of precipitation observed at different times during the three-week measurement period. Occasional influence of anthropogenic emissions on the site was observed as evidenced by spikes in SO2 mixing ratios.

A4.1.2 SPiFFY

Monoterpenes were not measured during SPiFFY, but it's estimated that monoterpene mixing ratios were similar to mixing ratios observed from other years. Figure A4.1 presents the diel variation of monoterpenes observed from the years 2008 (Kim et al., 2010), 2010 (Kaser et al., 2013), and 2015 at Manitou Experimental Forest. The diel plots suggest the mixing ratios of monoterpenes from year to year are fairly similar with nighttime mixing ratios around 1 ppbv and daytime mixing ratios below 0.5 ppbv. This is similar to what was observed during SOAS (Figure A4.1; bottom right panel).

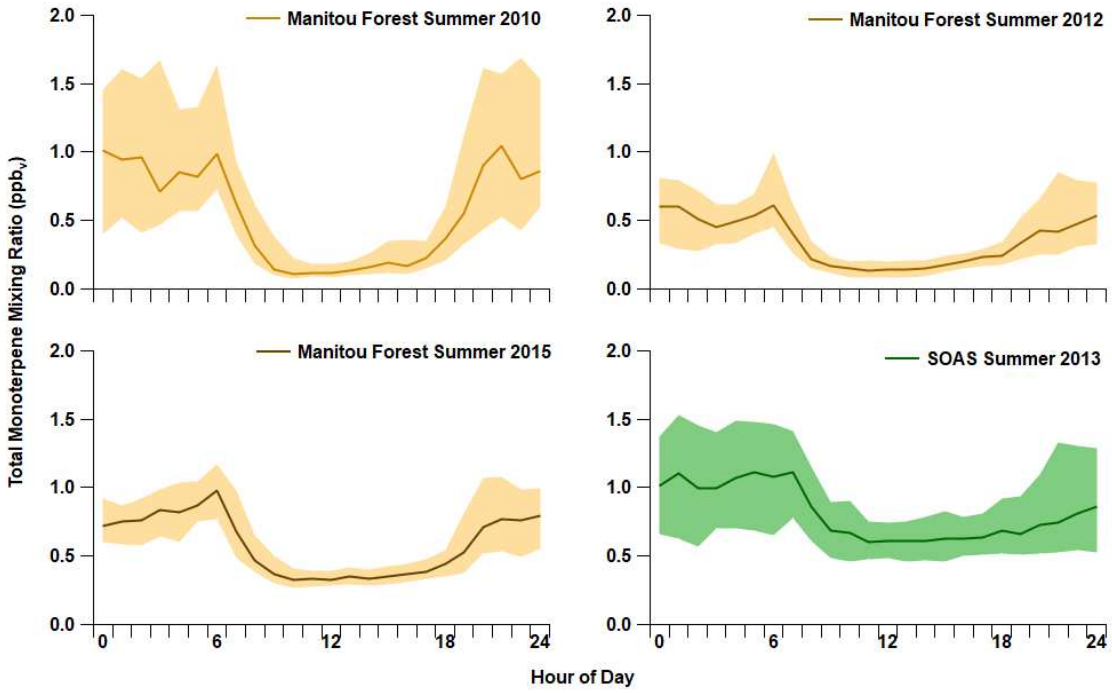

Figure A4.1. Diel plots of monoterpene mixing ratios measured at Manitou Experimental Forest (SPiFFY campaign location) from the years 2008 (beige; top left), 2012 (beige; top right) and 2015 (beige; bottom left) and SOAS (green; bottom right).

A4.1.4 FIXCIT experiment summary

Organic acids were quantified from eight experiments from FIXCIT. Important conditions for each of the experiments are shown below in Table A4.1.

Table A4.1. Summary of FIXCIT experiments analyzed.

Experiment Number	Date of experiment	Precursor and conditions	Background subtraction	Oxidant exposure
2	01.02.14	Isoprene + OH ("low NO")	"low NO" OH blank	2.2 x 10^{10} molecules s cm^{-3}
3	01.03.14	Isoprene + OH ("high NO")	"high NO" OH blank	2.2 x 10^{10} molecules s cm^{-3}
6	01.06.14	Isoprene + O3	Pre-hydrocarbon injection	8.1 x 10^{6} ppb_v s
9	01.09.14	Isoprene + NO3	Pre-hydrocarbon injection	--
10	01.10.14	α-pinene + OH ("low NO")	"low NO" OH blank	5.3 x 10^{10} molecules s cm^{-3}
11	01.11.14	α-pinene + OH ("high NO")	"high NO" OH blank	4.8 x 10^{10} molecules s cm^{-3}
14	01.14.14	Isoprene + O3	Pre-hydrocarbon injection	9.57 x 10^{6} ppb_v s
29	01.29.14	Isoprene + O3	Pre-hydrocarbon injection	7.57 x 10^{6} ppb_v s

[a]Reported as a percentage of the 320 UV bulbs installed in the chamber

A4.2. Acetate CIMS data treatment

A4.2.1 Data processing and mass calibration

All CIMS data were processed using Tofware v2.5.12 in Igor Pro 7. Mass calibrants varied slightly between all campaigns and lab experiments but common calibrants included O_2^- (m/z 31.99), NO_3^- (m/z 61.99), CHO_2^- (m/z 45.00), $C_4H_7O_4^-$ (m/z 119.03), $C_2H_3O_2^-$ (m/z 59.01)

and CF_3^- (m/z 68.99). A calibrant that was used unique to SOAS was $C_{12}H_{20}NO_7^-$ (m/z 290.12), presumably a sesquiterpene hydroxynitrate. During SPiFFY $C_{18}H_{35}O_2^-$ (m/z 288.26) was used as a mass calibrant.

A4.2.2 Background subtraction methods

A4.2.2.1 Ambient measurements

Instrumental backgrounds we measured for one minute every hour during SOAS and SPiFFY. Backgrounds were performed by introducing purified air upstream of the inlet to the instrument. Many species exhibited a first-order decay in signal during the background measurement as a result of gas-wall partitioning equilibrium effects on tubing leading to the instrument and on the surface of the ion-molecule reactor.[1,2] These wall effects complicate measurement of a "true" instrumental background and methods employing short-duration (<5 s) background determination have been shown to be successful for plume-like sampling conditions.[3] For the "long" backgrounds employed here we are likely over-estimating the background for species with sufficiently low vapor pressures. For the 10 second averaged data we take the final three signal points during the background measurement, average them, then subtract that value from the time series for a given species corresponding to that hour of measurement.

A4.2.2.2 FIXCIT measurements

Two background experiments were performed to capture the method backgrounds for experiments involving OH oxidation of isoprene and α-pinene under conditions of "low NO" or "high NO" during FIXCIT. Details about the blank experiments are provided in Nguyen et al.[4] (2014). To account for background, we take the signal from all species in the mass spectrum and

subtract from it the signal acquired, after an equivalent amount of time, from the corresponding blank experiment (i.e. for the isoprene + OH "low NO" experiment that lasted five hours we subtract the corresponding signal after five hours from the blank OH "low NO" experiment). We recommend improving the understanding of how backgrounds impact organic acid production during chamber experiments by acquiring measurements of experiment-simulated backgrounds before and after an experiment involving a precursor in the future. The signal from species prior to injection of the hydrocarbon precursor was defined as the background for ozonolysis and the nitrate radical oxidation experiments.

A4.2.3 Detection limit filtering

Following a previously published method, ion signals were determined to be quantifiable if the average ion signal was above the signal detection limit.[5] For each file of 10 second data collected during the SOAS campaign, the signal for each high resolution identified species was averaged during a 30-minute time period in the middle of the file (i.e. 15 minutes from the start and 15 before the end of file collection) and was defined as the average signal for that file. A short three second period from the zero period that occurred during each file was also averaged for each HR species and that was defined as the background signal average. The detection limit for the averaged signal was then calculated by equation 1:

$$DL_{\bar{S}} = (3\sigma_{back} + Sig_{back})\, x \sqrt{\frac{t_{back}}{t_{signal}}} \quad (1)$$

Where DL_s is the average signal detection limit, σ_{back} is the standard deviation of the signal during the background measurement, Sig_{back} is the average signal during the background measurement, t_{back} is the duration of the average for the background measurement and t_{signal} is the duration of the average for measurement of the signal during ambient sampling.

A4.2.4 Determination of clustered species in acetate CIMS spectra

Manual peak assignment was performed on the mass spectra for FIXCIT. During FIXCIT the acetate CIMS was operated as to optimize the transmission of [acetate+M]$^-$ clusters. Operating the acetate CIMS in a "clustering" mode results in ambiguity when identifying deprotonated M$^-$ species from species clustered with acetate in the mass spectrum.[6] A recent review of isoprene oxidation chemistry was used to help identify potential species that most likely appeared as clusters with the acetate reagent ion in the mass spectrum.[7] Identification of the isoprene and monoterpene oxidation product clusters was verified by observing the presence of the [M+I]- clusters in the mass spectra acquired during the same experiments by the iodide reagent. Other species, such as $C_5H_{10}O_3$ and $C_{10}H_{17}NO_5$, were also verified by co-identification with the CF3O$^-$ CIMS. Specific experiments were not performed during FIXCIT to determine if species identified as clusters with acetate in the mass spectrum were in fact clusters so if an elemental formula identified in the mass spectrum could feasibly be an acetate ion clustered with a neutral species than the peak was assigned as an acetate cluster. It was observed from the experiments that acetate clusters with appreciable sensitivity with organic nitrate species as well as peroxides. This chemical information was considered when assigning identities to peaks in the mass spectrum. Species filtering procedures described below were used to exclude potential fragments or clustered species from quantification.

A4.2.4.1 Clustered species identified in the FIXCIT chamber study

A total of 15 isoprene and terpene oxidation products were identified as clusters with acetate in the FIXCIT experiments. These compounds were uniquely associated with the precursor oxidation and different from background signals.

Table A4.2. Species identified as clusters with the acetate reagent from the FIXCIT experiments.

Precursor	observed formula	identification	Experiment observed	Observed at SOAS
isoprene	$C_4H_8O_3 \cdot (C_2H_3O_2)^-$	Dihydroxy butanone/C_4 dihydroxycarbonyl	Low NO isoprene	yes
isoprene	$C_5H_{10}O_3 \cdot (C_2H_3O_2)^-$	IEPOX/ISOPOOH	Low NO isoprene	yes
isoprene	$C_5H_{12}O_4 \cdot (C_2H_3O_2)^-$	Pentaerythritol ?	Low NO isoprene	yes
isoprene	$C_5H_{10}O_5 \cdot (C_2H_3O_2)^-$	C_5 HOM	Low NO isoprene	yes
isoprene	$C_4H_8O_5 \cdot (C_2H_3O_2)^-$	C_4 HOM	Low NO isoprene	yes
isoprene	$C_4H_7NO_5 \cdot (C_2H_3O_2)^-$	MVK/MACR hydroxynitrate	High NO isoprene	yes
isoprene	$C_5H_{11}NO_4 \cdot (C_2H_3O_2)^-$	Unreported saturated hydroxynitrate ?	High NO isoprene	no
isoprene	$C_4H_8O_6 \cdot (C_2H_3O_2)^-$	C_4 HOM	High NO isoprene	no
isoprene	$CH_4O_3 \cdot (C_2H_3O_2)^-$	sCI product?	Ozone no scavenger	no

isoprene	$CH_4O_4 \cdot (C_2H_3O_2)^-$	sCI product?	Ozone no scavenger	no
isoprene	$C_5H_9NO_5 \cdot (C_2H_3O_2)^-$	Major isoprene + NO_3 product prev. reported	NO_3 and formaldehyde	yes
isoprene	$C_5H_9NO_6 \cdot (C_2H_3O_2)^-$	C_5 hydroxynitrate ?	NO_3 and formaldehyde	yes
isoprene	$C_4H_5NO_7 \cdot (C_2H_3O_2)^-$	C_4 hydroxynitrate ?	NO_3 and formaldehyde	yes
α-pinene	$C_{10}H_{17}NO_5 \cdot (C_2H_3O_2)^-$	pinene nitrooxyhydro peroxide	high NO α-pinene + OH	yes
α-pinene	$C_9H_{13}O_6 \cdot (C_2H_3O_2)^-$	C_9 HOM	high NO α-pinene + OH	no

A4.2.4.2 Clustered species identified at SOAS

A total of 53 compounds in the mass spectrum were identified as clusters with acetate. Previous studies have observed that organic peroxides and carboxylic acids cluster favorably with acetate, but we also observe favorable clustering with organonitrate compounds.[6,8,9] The identity of many of the species identified as clusters with the acetate reagent were validated by confirming their presence in spectra collected using the iodide reagent during the campaign.

Table A4.3. Species identified as clusters with the acetate reagent observed during SOAS.

Precursor	**observed formula**	**m/z (acetate + M)**	**Identification[a]**	**Observed with iodide**
	$C_2H_6O_4 \cdot (C_2H_3O_2)^-$	153.04	polyol?	yes
isoprene	$C_5H_9O_2 \cdot (C_2H_3O_2)^-$	160.07	Isoprene hydroxy carbonyl	no
isoprene	$C_4H_6O_3 \cdot (C_2H_3O_2)^-$	161.05	methacrylic acid epoxide	yes
	$C_4H_7O_3 \cdot (C_2H_3O_2)^-$	162.04		yes
	$C_4H_8O_3 \cdot (C_2H_3O_2)^-$	163.06	hydroxybutyric acid?	yes
	$C_3H_4O_4 \cdot (C_2H_3O_2)^-$	163.02	malonic acid?	yes
isoprene	$C_5H_8O_3 \cdot (C_2H_3O_2)^-$	175.06	HPALD	yes
	$C_4H_4O_4 \cdot (C_2H_3O_2)^-$	175.02	maleic acid?	yes
isoprene	$C_5H_{10}O_3 \cdot (C_2H_3O_2)^-$	177.08	IEPOX/ISOPOOH	yes

isoprene	$C_4H_6O_4 \cdot (C_2H_3O_2)^-$	177.04	ISOPOOH + OH product	yes
isoprene	$C_4H_8O_4 \cdot (C_2H_3O_2)^-$	179.06	2-methylglyceric acid	yes
	$C_5H_{12}O_3 \cdot (C_2H_3O_2)^-$	179.09		no
	$C_5H_8O_4 \cdot (C_2H_3O_2)^-$	191.06	glutaric acid?	yes
	$C_4H_4O_5 \cdot (C_2H_3O_2)^-$	191.02	diacid?	yes
isoprene	$C_5H_{10}O_4 \cdot (C_2H_3O_2)^-$	193.07	ISOPOOH + OH product	yes
	$C_4H_6O_5 \cdot (C_2H_3O_2)^-$	193.04	diacid?	yes
	$C_5H_{12}O_4 \cdot (C_2H_3O_2)^-$	195.09	polyol?	yes
	$C_4H_8O_5 \cdot (C_2H_3O_2)^-$	195.05	hydroxyacid?	yes
isoprene	$C_5H_9NO_4 \cdot (C_2H_3O_2)^-$	206.07	1st generation isoprene nitrate	yes
	$C_4H_5NO_5 \cdot (C_2H_3O_2)^-$	206.03	Isoprene nitrate?	yes
	$C_5H_8O_5 \cdot (C_2H_3O_2)^-$	207.05	diacid?	yes
	$C_4H_7NO_5 \cdot (C_2H_3O_2)^-$	208.05	Isoprene nitrate?	yes
	$C_5H_{10}O_5 \cdot (C_2H_3O_2)^-$	209.07	C_5 isoprene HOM	yes
	$C_4H_6O_4S \cdot (C_2H_3O_2)^-$	209.01	C_4 organosulfate?	yes
	$C_7H_{12}O_4 \cdot (C_2H_3O_2)^-$	219.09	diacid?	yes

	$C_5H_9NO_5 \cdot (C_2H_3O_2)^-$	222.06	Isoprene nitrate?	yes
	$C_5H_{11}NO_5 \cdot (C_2H_3O_2)^-$	224.08	Isoprene hydroxy nitrate?	yes
	$C_5H_9O_6 \cdot (C_2H_3O_2)^-$	224.05		yes
isoprene	$C_5H_{10}O_6 \cdot (C_2H_3O_2)^-$	225.06	ISOPOOH + OH product	yes
isoprene	$C_5H_9NO_6 \cdot (C_2H_3O_2)^-$	238.06	C_5 hydroxynitrate?	yes
	$C_4H_5NO_7 \cdot (C_2H_3O_2)^-$	238.02	C_4 hydroxynitrate?	yes
	$C_4H_6NO_7 \cdot (C_2H_3O_2)^-$	239.03		yes
	$C_5H_{10}NO_6 \cdot (C_2H_3O_2)^-$	239.06		no
	$C_5H_9O_7 \cdot (C_2H_3O_2)^-$	240.05	C_5 HOM	yes
terpene	$C_{10}H_{16}O_3 \cdot (C_2H_3O_2)^-$	243.12	pinonic acid or related isomer	yes
	$C_9H_{12}O_4 \cdot (C_2H_3O_2)^-$	243.09	Terpene oxidation product?	yes
	$C_9H_{14}O_4 \cdot (C_2H_3O_2)^-$	245.1	Terpene oxidation product?	yes
	$C_6H_6O_7 \cdot (C_2H_3O_2)^-$	249.03	C_6 HOM	yes
	$C_9H_{18}O_4 \cdot (C_2H_3O_2)^-$	249.13		yes
	$C_9H_{10}O_5 \cdot (C_2H_3O_2)^-$	257.07	Terpene oxidation product?	yes
	$C_9H_{14}NO_4 \cdot (C_2H_3O_2)^-$	259.11	Terpene nitrate?	yes

	$C_8H_8O_6 \cdot (C_2H_3O_2)^-$	259.05	C_8 HOM	yes
	$C_7H_6O_7 \cdot (C_2H_3O_2)^-$	261.03	C_7 HOM	yes
	$C_9H_{16}O_5 \cdot (C_2H_3O_2)^-$	263.11	Terpene oxidation product?	yes
	$C_9H_6O_9 \cdot (C_2H_3O_2)^-$	269.03		yes
	$C_5H_{10}O_9 \cdot (C_2H_3O_2)^-$	273.05	C_5 isoprene oxidation HOM	yes
	$C_{10}H_{14}O_5 \cdot (C_2H_3O_2)^-$	273.10	Terpene oxidation product?	yes
	$C_{10}H_{16}O_5 \cdot (C_2H_3O_2)^-$	275.11	Terpene oxidation product?	yes
α-pinene	$C_{10}H_{17}NO_5 \cdot (C_2H_3O_2)^-$	290.13	pinene nitrooxyhydroperoxide	no
	$C_9H_{15}NO_6 \cdot (C_2H_3O_2)^-$	292.10	Terpene nitrate?	yes
	$C_{10}H_{19}NO_5 \cdot (C_2H_3O_2)^-$	292.14	Terpene nitrate?	yes
	$C_{10}H_{15}NO_7 \cdot (C_2H_3O_2)^-$	320.10	Terpene nitrate?	yes

[a]Species identifications marked with "?" indicate uncertain significant uncertainty. Assignment of identification based on consideration of selectivity towards clustering, likelihood of appearing in the atmosphere, and/or informed from FIXCIT experiments or published literature.

A4.2.4.3 Common measurement artifacts observed using acetate CIMS

Listed below are common artifacts observed in our field measurements using acetate CIMS. Depending on the "clustering" regime the mass spectrometer is configured to operate under some artifacts are going to be less relevant.

Table A4.4 Common measurement artifacts observed in acetate CIMS mass spectrum.

Common acetate CIMS interferences			
Source			
Teflon Tubing	**m/z**	**formula of artifact**	
	69	CF_3^-	
	113	$C_2F_3O_2^-$	
	169	$C_3F_7^-$	
	119	$C_2F_5^-$	
	163	$C_3F_5O_2^-$	
	213	$C_4F_7O_2^-$	
	219	$C_4F_9^-$	
	269	$C_5F_{11}^-$	
	263	$C_5F_9O_2^-$	
	313	$C_6F_{11}O_2^-$	
	319	$C_6F_{13}^-$	
Reactions	**m/z**	**Formula of artifact**	**reaction**
	60	CO_3^-	$O_2^- + O_3 \rightarrow O_3^- + O_2$ $O_3^- + CO_2 \rightarrow CO_3^- + O_2$

	112	SO_5^-	$CO_3^- + SO_2 \rightarrow SO_3^- + CO_2$ $SO_3^- + O_2 + N_2 \rightarrow SO_5^- + N_2$
	76	CO_4^-	
Common clusters	**m/z**	**Formula of artifact**	**identity**
	92	$(C_2H_3O_2)HO_2^-$	HO_2 cluster
	93	$(C_2H_3O_2)H_2O_2^-$	H_2O_2 cluster
	77	$(C_2H_3O_2)H_2O^-$	water cluster
	119	$(C_2H_3O_2)C_2H_4O_2^-$	acetic acid cluster
	166	$(C_2H_3O_2)C_2H_3O_5^-$	acetic acid autoxidation product cluster
	179	$[C_2H_3O_2 + C_2H_4O_2 + C_2H_4O_2]^-$	acetic acid double cluster
	125	$(HNO_3)NO_3^-$	nitric acid nitrate cluster
	112	$CO_4(H_2O)_2^-$	CO4 dihydrate
	78	$CO_3(H_2O)^-$	CO3 water cluster
	91	$(C_2H_3O_2)O_2^-$	acetate oxygen cluster
	102	$(C_2H_3O_2)HNCO^-$	isocyanic acid acetate cluster
	102	$(C_2H_3O_2)C_2H_3O^-$	acetate cluster
	105	$(C_2H_3O_2)CH_2O_2^-$	formic acid cluster
	122	$(C_2H_3O_2)HNO_3^-$	acetate nitric acid cluster
	149	$(C_2H_3O_2)C_2H_2O_4^-$	oxalic acid cluster

	94	$(C_2H_3O_2)H_3O_2^-$	water cluster
Fragments	**m/z**	**Formula of artifact**	**Fragment of…**
	43	$C_2H_3O^-$	lactic acid

3. Spectra with speciation from FIXCIT

Figures A4.2-A4.8 show average mass spectra for each experiment listed in Table A4.1. Shown in red is total ion signal from the experiment. The black trace is the average mass spectrum from the background and the green inset figure shows the difference between the average mass spectrum during the experiment and the background. Many species were not confidently identified in the mass spectrum likely due to clustering processes that were not completely understood.

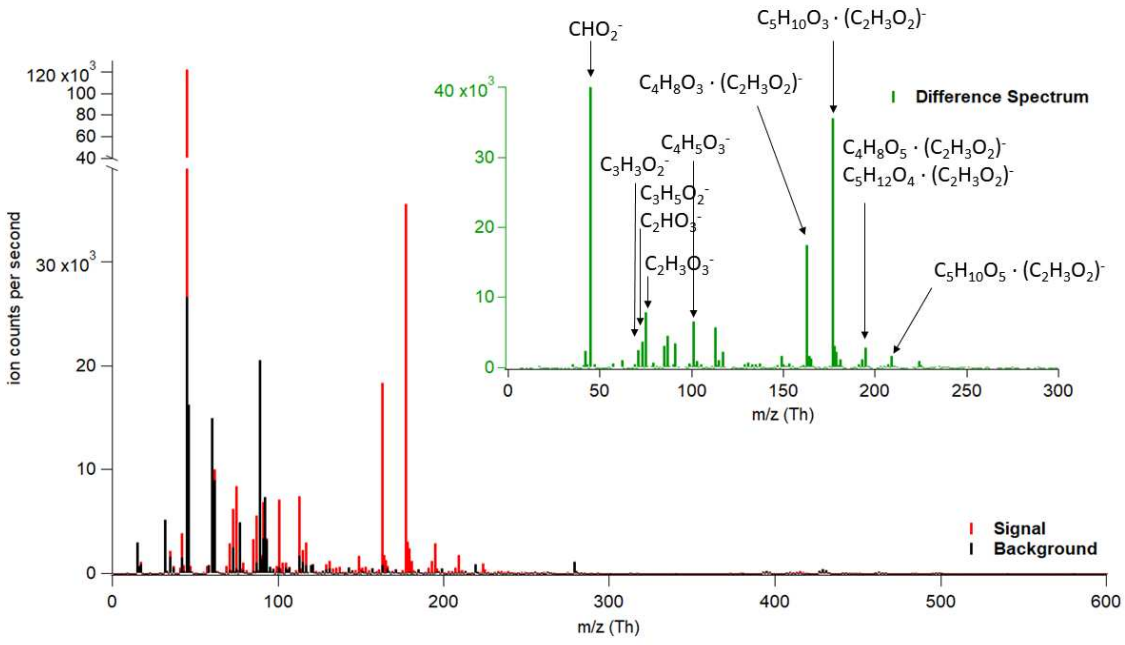

Figure A4.2. Average mass spectra from "low NO" isoprene + OH experiment.

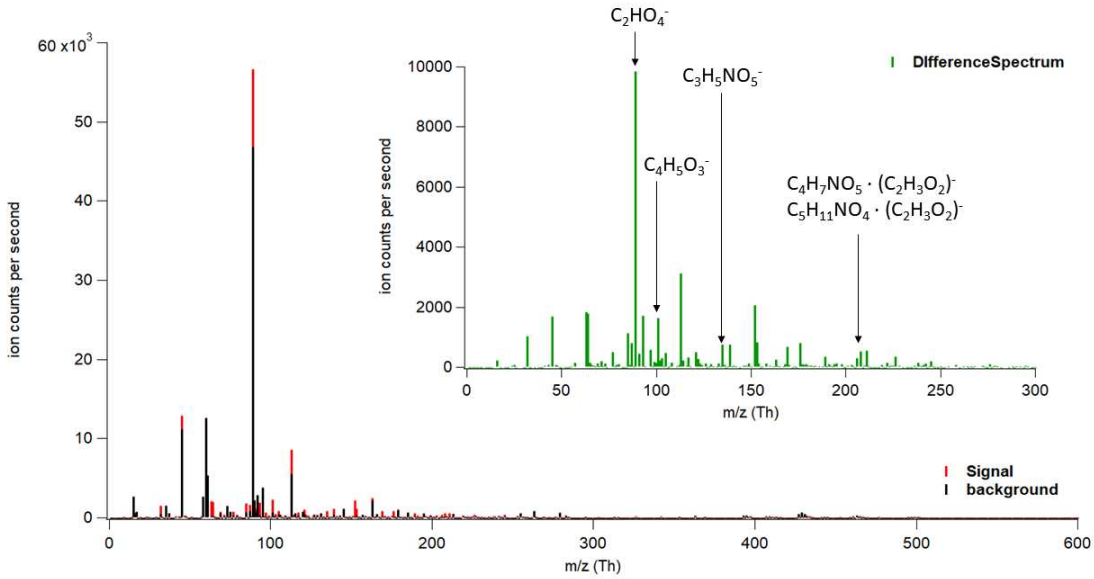

Figure A4.3. Average mass spectra from "high NO" isoprene + OH experiment.

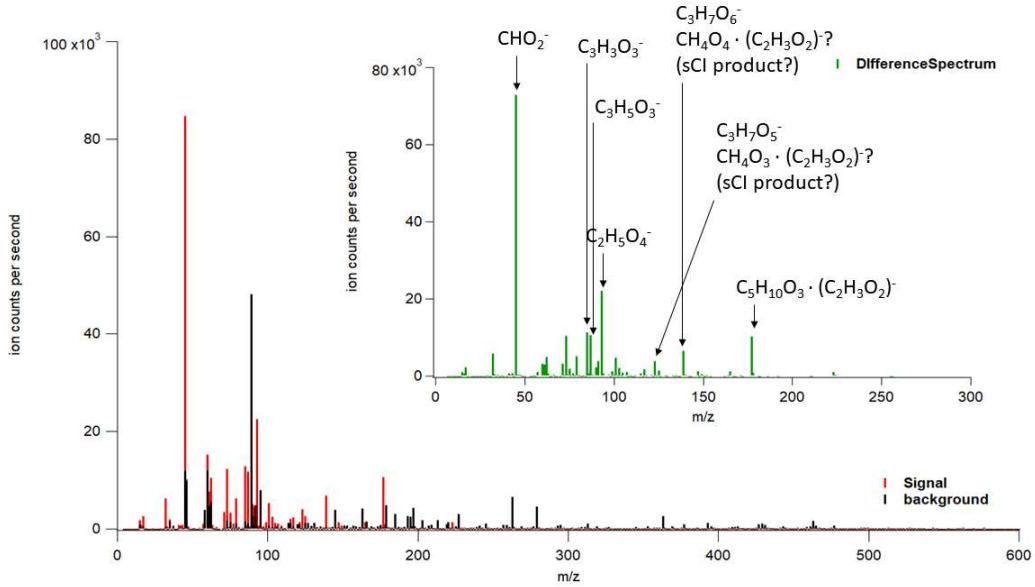

Figure A4.4. Average mass spectra from O_3 + isoprene (no scavenger) experiment.

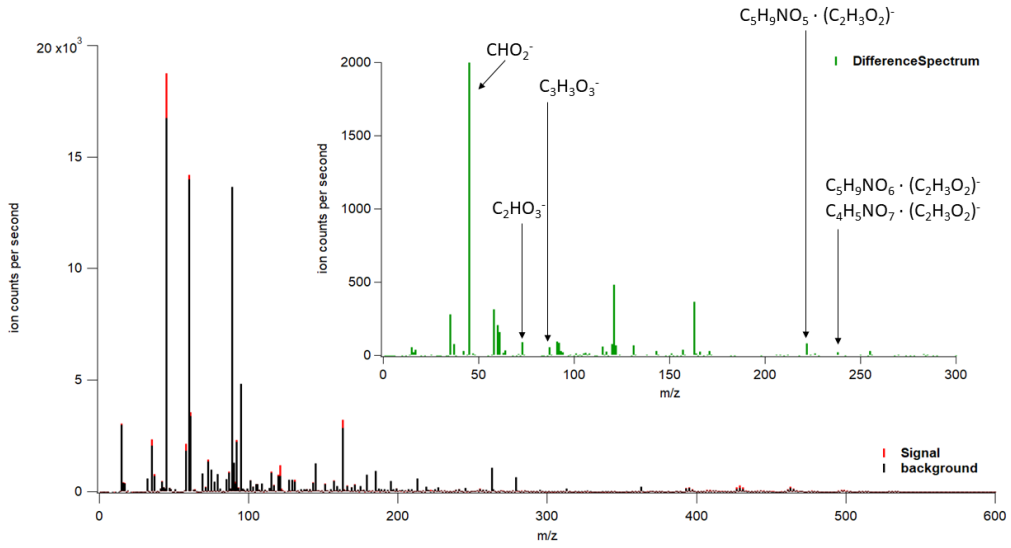

Figure A4.5. Average mass spectra from isoprene + NO_3 experiment.

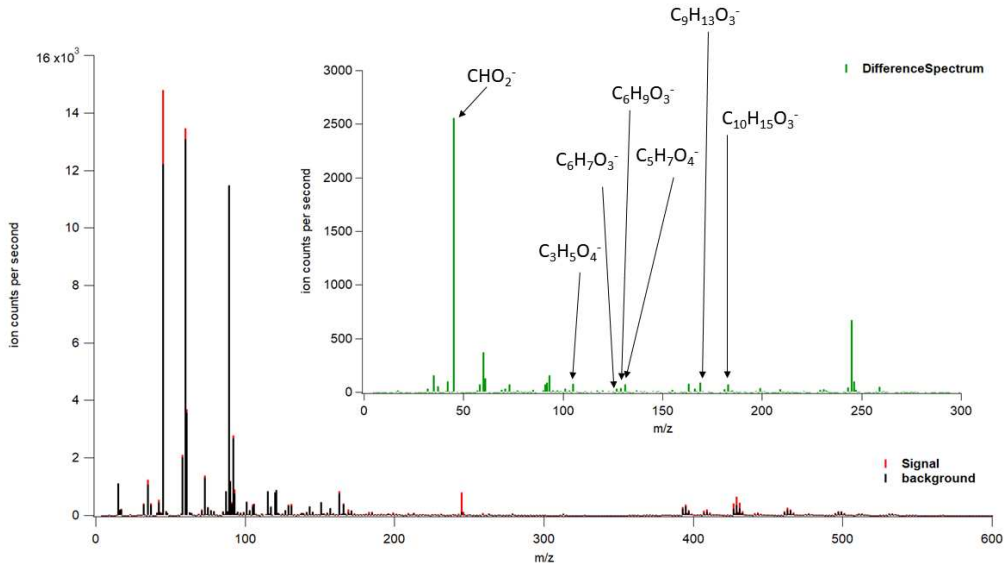

Figure A4.6. Average mass spectra from α-pinene + OH "low-NO" experiment.

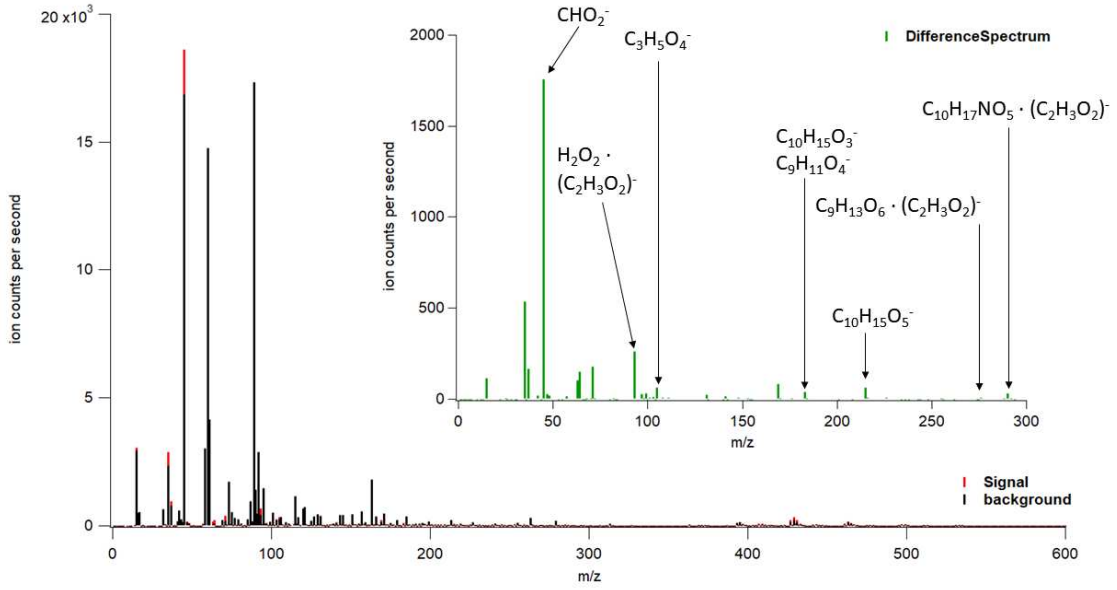

Figure A4.7. Average mass spectra from α-pinene + OH "high NO" experiment.

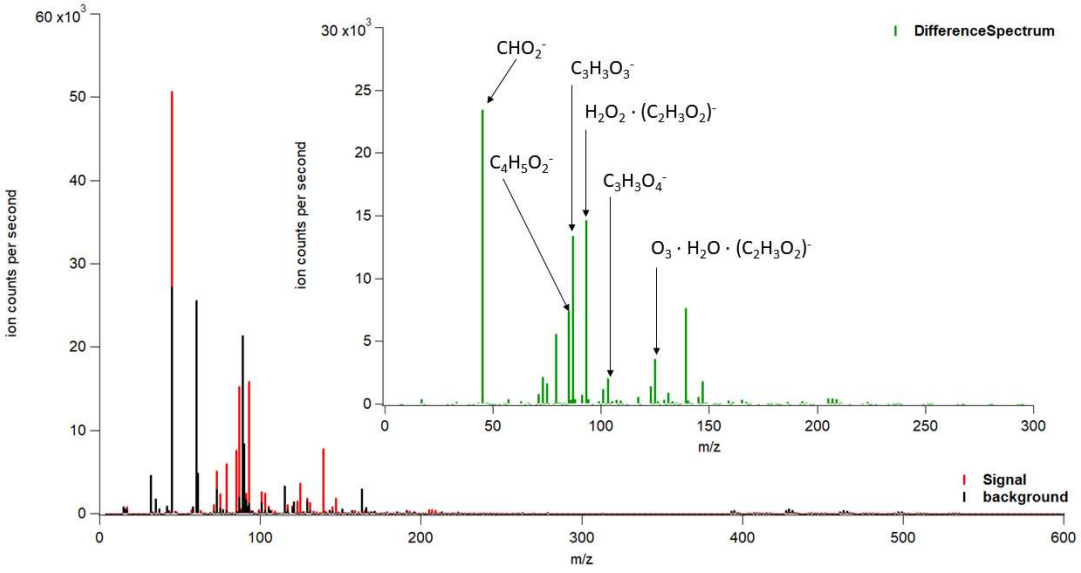

Figure A4.8. Average mass spectra from Isoprene + O_3 (cyclohexane scavenger) experiment.

A4.4. Bulk quantification of the mass spectrum

A4.4.1 Parameterization of sensitivity and calibrations for acetate CIMS

A previously published parameterization of sensitivity as a function of average carbon oxidation state (OSc) and carbon number was investigated and employed for quantification of organic acids in this study.[5] Measured sensitivities were used in place of parameterized sensitivities when possible. A series of heated liquid injection calibrations were performed and sensitivities were measured for a wide variety of organic acids with different additional functional groups such as hydroxy, carbonyl and aromatic moieties.[10] Liquid calibrant solutions were prepared in HPLC grade methanol and sonicated to ensure mixing. Injections of analytes were on the order of 10^{13}-10^{14} total molecules injected. A constant 10 uL injection volume was used for all calibrations and was applied to a quartz filter enclosed in a PFA injection apparatus. Heating was applied with a heat gun over the PFA injection apparatus to ensure liquid analyte evaporation. When possible injections of calibrants were compared to permeation tube calibration sources and compared well. Calibrants that did not have permeation tube sources for comparison generally were in the condensed phase at room temperature and thus had corresponding low volatilities. Prolonged heating was necessary to get the lower volatility calibrants into the instrument. Previous studies have observed significant thermal decomposition of carboxylic acids when heated.[11,12] Analysis of expected decarboxylation or dehydration products of the parent carboxylic acid suggest that thermal decomposition did not play a major role in determining signal intensity during the calibrations however this influence can't be ruled out, so the sensitivities of the lower volatility compounds (i.e. pinonic, myristic and palmitic acids) measured here may represent a lower bound.

Calibrations were performed under "declustered" and "clustered" ion transmission regimes to capture the effects of instrument operating conditions on sensitivity for the SPiFFY and SOAS/FIXCIT campaigns, respectively. The campaign averaged ratio of the reagent self-cluster ($[C_2H_3O_2^- + C_2H_4O_2]$; m/z 119.03; acetate cluster) signal to the reagent ($C_2H_3O_2^-$; m/z 59.01; acetate) signal was used to determine if the voltage settings were configured such that the mass spectra would reflect "clustered' (i.e. high acetate cluster to acetate ratio) or "declustered" settings (i.e. low acetate cluster to acetate cluster ratio). It was demonstrated by Brophy and Farmer (2016) that tuning of the ion optics in the instrument can result in transmission where collisions are preferentially favored or limited resulting in mass spectra that contain either deprotonated species or clusters, respectively. The ratio of the signal of the acetate cluster to acetate should be the best indicator of the electric fields established in the ion optics under a particular set of voltage settings. Here we define "declustered" settings as ion optic voltage settings that produce an acetate cluster to acetate ratio of 0.004 and "clustered" as settings that produce a ratio of 0.04 (the ratio observed at SOAS was 0.02).

Using the relationship between sensitivity and extraction frequency—combined with the relative sensitivities observed under different voltage settings—the following equation was derived to convert sensitivities measured in lab to sensitivities that theoretically would have been observed at SOAS:

$$SOAS\ sensitivities = \frac{Lab\ sensitiviites\ x\ 0.716}{0.444} \quad (2)$$

The value of 0.716 in equation 2 comes from the extraction frequency calibration and shows the relative drop in sensitivity going from an extraction frequency of 24 kHz (used in lab) to 17 kHz (used at SOAS). The value of 0.444 in equation 2 comes from the voltage settings calibration and

shows the relative increase in sensitivity when operating under “clustered” voltage settings compared to “declustered” settings.

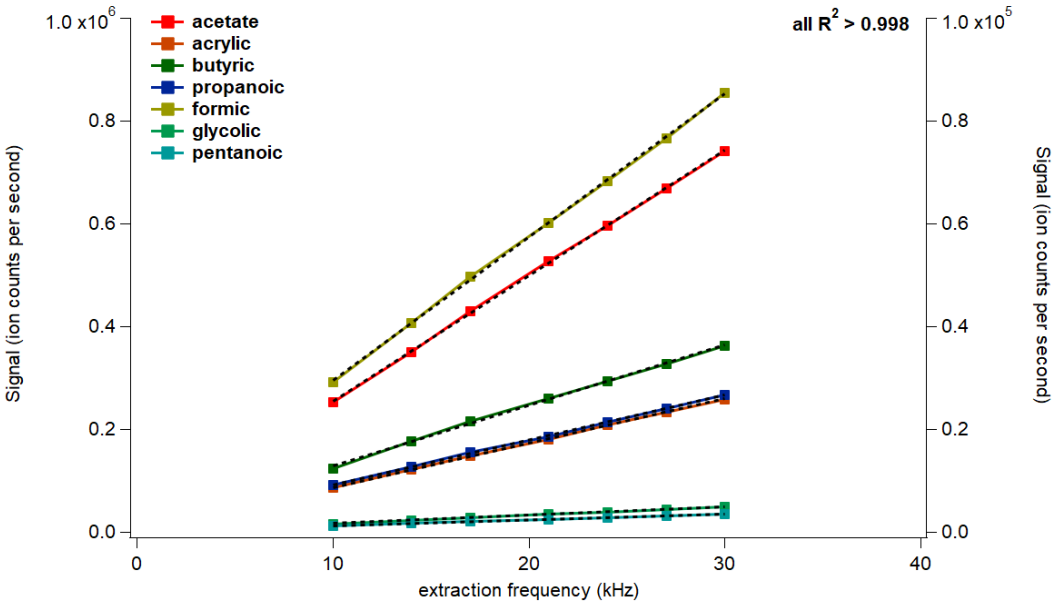

Figure A4.9. Signal as a function of ToF extraction frequency for select acids.

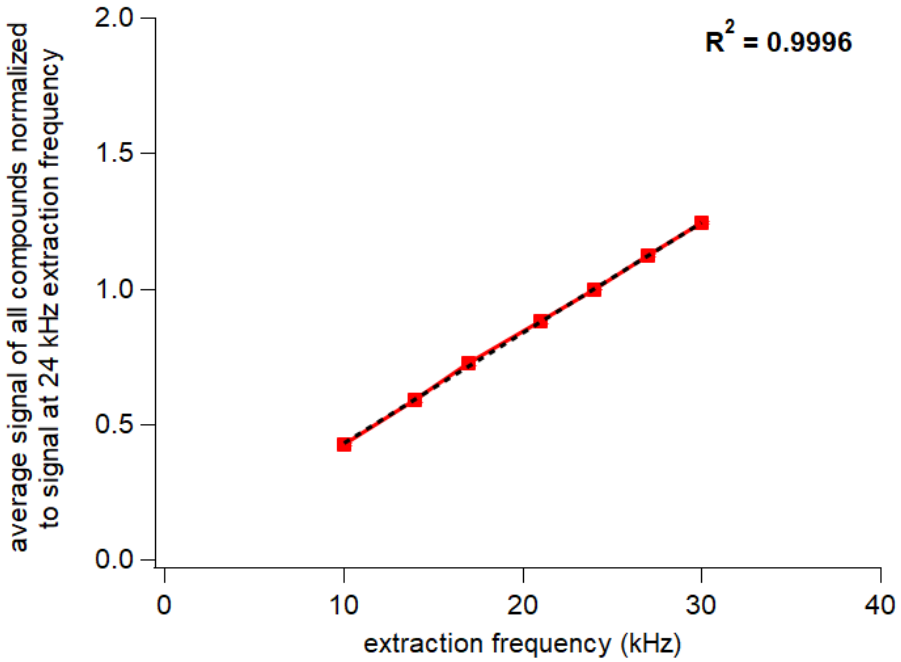

Figure A4.10. Average of all the signals in Figure A4.9 normalized to their signal at 24 kHz and plotted as a function of ToF extraction frequency.

Evidence that the method employed here to adjust sensitivities measured in lab to what the sensitivities would be when measured during the field campaigns is shown in the example of formic acid (Figure A4.11). Hourly calibrations of formic acid were performed during SOAS resulting in a campaign averaged sensitivity of 13 ± 5 Hz ppt_v^{-1}.[13] Under the conditions that the instrument was operated in the lab a sensitivity to formic acid of 6.9 ± 1 Hz ppt_v^{-1} was measured. When this sensitivity was corrected for voltage settings (as determined by the average $[C_2H_3O_2^- + C_2H_4O_2]/[C_2H_3O_2^-]$ ratio measured during SOAS) and extraction frequency the "corrected" formic acid sensitivity expected at SOAS was calculated to be 10.9 ± 3 Hz ppt_v^{-1} falling well within error for the formic acid sensitivity measured at SOAS.

A factor influencing the sensitivity of the CIMS during the SPiFFY campaign was the flowrate into the instrument. A larger orifice for the entrance of the IMR region was used during SPiFFY to maintain IMR pressure in-line with the low-pressure inlet. Calibrations were performed in lab to look at the relative change in sensitivity for select organic acids using the standard orifice inlet provided with delivery of the instrument, that produces a flowrate into the instrument of 2 sLpm, versus using the larger orifice.

An equation to convert sensitivities measured in lab to sensitivities that would have been measured during SPiFFY was derived as:

$$SPiFFY\ sensitivities = Lab\ sensitivities\ x\ 0.9\ x\ 1.86 \quad (3)$$

The value of 0.9 in equation 3 comes from Figure A4.10 showing the relative drop in sensitivity going from an extraction frequency of 24 kHz (used in lab) to 22 kHz (used during SPiFFY). The value of 1.86 is the relative change in sensitivity when using the inlet with the larger orifice versus the standard orifice.

A4.4.2 Quantification of all measured organic acids in mass spectrum

A multiple linear regression between the properties of average carbon oxidation state (OSc; OSc ≈ 2 x O/C – H/C), number of carbons (nC) and sensitivity for 12 different organic acid calibrants was used to parameterize sensitivity for all the organic acids measured by the acetate CIMS during SOAS/FIXCIT and SPiFFY. Two separate multiple linear regressions were performed; one using the corrected sensitivities for SOAS/FIXCIT as inputs to the regression and the other using the corrected sensitivities for SPiFFY as inputs to the regression. The parameterizations for sensitivity for measured organic acids from the two campaigns are listed below in equations 4 and 5.

SOAS/FIXCIT campaign:

$$\log_{10}(sensitivity) = (0.205\ x\ OSc) + (0.135\ x\ nC) + 0.495 \quad (4)$$

SPiFFY campaign:

$$\log_{10}(sensitivity) = (0.205\ x\ OSc) + (0.135\ x\ nC) + 0.511 \quad (5)$$

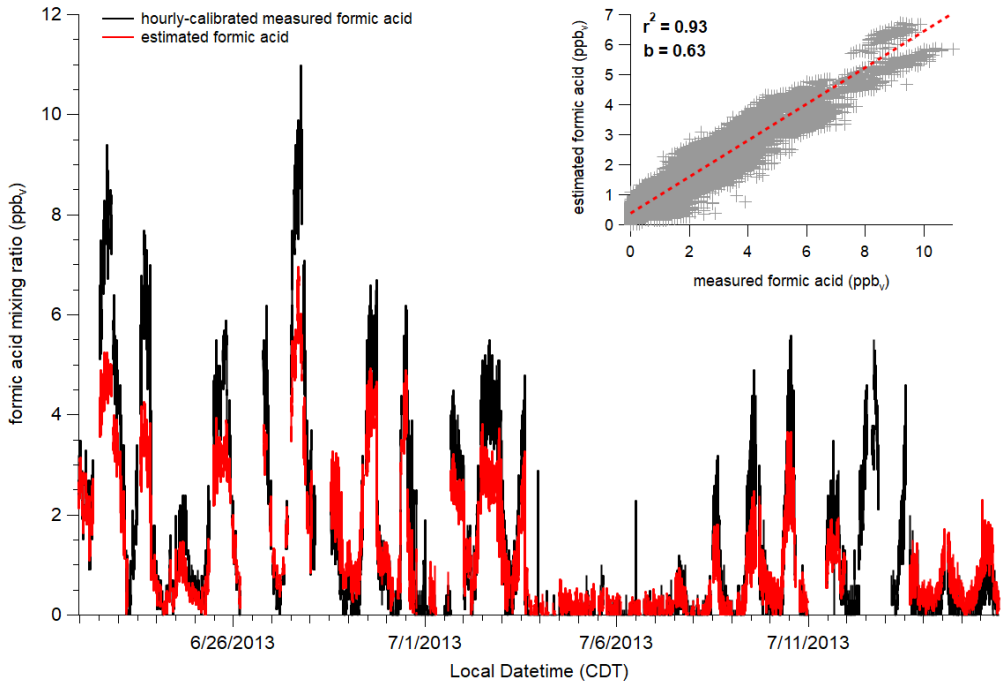

Figure A4.11. Comparison of formic acid mixing ratios calculated with sensitivities derived from using on-line hourly calibrations (black trace) versus estimation from the sensitivity parameterization (red trace).

A4.4.3 Bulk analysis of mass spectrum

Omission of species from bulk analysis were decided based on violations of rules based on double bond equivalency (DBE) or elemental composition.[14,15] Because the primary mechanism for ionization in acetate CIMS is proton transfer from the analyte to the reagent elemental formulae from the high-resolution peak list were analyzed by adding a hydrogen atom to the formula (i.e. formic acid is observed as CHO_2^- in the mass spectrum; here we modified the formula in the peak list to show CH_2O_2).[13,16] All quantifiable species were assumed to contain a carboxylic acid moiety and so elemental formulae containing less than two oxygen atoms were excluded from bulk analysis. If the DBE was calculated to be a positive non-integer value, then the species was excluded from bulk analysis. Additionally, the elemental composition was

constrained to H/C and O/C ratios of 0.3-3 and 0-3.[15] In the data processing procedures elemental formulae that violated these rules were flagged. Tentative explanations for flagged species are that these detected compounds are either clusters or fragments of molecules formed from unstable transmission through the instrument or reactions in the IMR.[6] Table A4.4 presents many of the artifacts of the acetate CIMS measurement observed in the studies covered here. Despite all this knowledge and analysis, it is likely that some species identified in the mass spectrum as deprotonated neutral molecules are potentially clusters with the acetate reagent ion, or products of ion-molecule chemistry unique to the IMR, and thus measurement artifacts. However, if a species was identified as a cluster during the construction of the peak list that species was omitted from the bulk analysis. Elemental formulae in the peak list were also categorized into groups of organic acids with different functional groups per the method described in a previous publication.[5] Briefly, the calculated degrees of unsaturation and the number of oxygens in the elemental formula were used as criteria to classify an elemental formula into an organic acid group (i.e. monosaturated acids, diacids/hydroxycarbonyl acids, hydroxyacids, ect.). If the formula did not satisfy the criteria placing it into a specific organic acid group that formula was classified as "ungrouped" and was not included in the bulk analysis.

A4.4.3.1 SOAS bulk analysis details

An initial peak list was manually (i.e. no use of automated peak fitting procedures) constructed consisting of 660 high-resolution identified ions spanning m/z 32-463. Very low signal above this (i.e. m/z 463) unit mass suggested that peaks above m/z 463 would make negligible contributions to the bulk analysis. In fact, integrated unit masses between m/z 463-1047 contributed less than 1% to the total UMR signal (omitting the reagent m/z 59) for the entire campaign. From the initial list of 660 ions 416 contained only C, H and O. A total of 120

out of this set of 416 formulae were flagged for removal from the bulk analysis calculations. A total of 42 formulae were omitted from bulk analysis because they were identified as clusters. A total of 173 HR assignments were classified as ungrouped and were not included in the bulk analysis. Some compounds met multiple exclusion criteria. After these exclusion criteria were applied to the peak list a total of 100 out 416 compounds containing C, H and O were used in the bulk analysis.

A4.4.3.2 SPiFFY bulk analysis details

An initial peak list was manually constructed consisting of 583 high-resolution identified ions spanning m/z 32-304. Very low signal above this unit mass suggested that peaks above m/z 304 would make negligible contributions to the bulk analysis. From the initial list of 583 ions 337 contained only C, H and O. A total of 91 out of this set of 337 formulae were flagged for removal from the bulk analysis calculations. Because the declustering voltage settings were optimally tuned during this campaign no HR assignments were identified as clusters. A total of 146 HR assignments were classified as ungrouped and were not included in the bulk analysis. Some compounds met multiple exclusion criteria. After these exclusion criteria were applied to the peak list a total of 100 out 337 compounds containing C, H and O were used in the bulk analysis.

A4.5. Quantification of carbon yields from the FIXCIT experiments

In Figure 4.4 in Chapter 4 the total carbon present in eight of the FIXCIT oxidation experiments is quantified and categorized. The three reservoirs for reacted carbon in the experiments are organic acid carbon, secondary organic aerosol (SOA) carbon and un-speciated carbon from other oxidation products (i.e. aldehydes, ketones, alcohols, ect.) not measured by the

acetate CIMS. The total carbon in each experiment is determined by the carbon-equivalent (C_{eq}) mixing ratio of the parent VOC consumed during the experiment. For instance, the C_{eq} mixing ratio of 100 ppb_v of isoprene is 500 ppbC. The pie charts to the left of the bar plots in Figure 4.4 represent a snapshot of the distribution of carbon at some time near the end of each experiment. The parent VOC consumed is determined by subtracting the initial mixing ratio of VOC introduced into the chamber by the mixing ratio of VOC remaining at the time of the determination of the yield calculation. The mixing ratio of isoprene was determined by a co-located GC-FID [17] and the mixing ratio of α-pinene was determined from PTF-ToF measurements. The yield of SOA carbon was determined by dividing the concentration of OA, measured by a co-located HR-AMS, by an OM:OC ratio of 1.8 for α-pinene SOA and 1.95 for isoprene SOA and converting the carbon-equivalent mass to a mixing ratio.[18,19]

Organic acid carbon yield was determined in the following way; (1) high-resolution peak fits were assigned to peaks from a list of species identified from the SOAS campaign, (2)the final signal for all HR species was determined at some point near the end of an experiment, (3) all species were normalized by the reagent and only organic acid species were considered for quantification, (4) mixing ratios for all organic acids were calculated based off the sensitivity parameterization described in section A4.4, (5) a background chamber measurement was made for the "low NO" and "high NO" + OH oxidation experiments, and HR signals from these background chambers experiments were converted to mixing ratios, averaged and subtracted from the VOC oxidation experiment mixing ratios to get background subtracted experiment mixing ratios, (7) carbon equivalent mixing ratios were determined by multiplying the HR species mixing ratio by the number of moles of carbon in the elemental formula. HR species were then lumped into C1, C2, C3, ect. grouped C_{eq} mixing ratios. Acetic acid, as measured by

the Caltech ToF-CIMS was converted to a C_{eq} mixing ratio and added to the C2 group of organic acids. Acetic acid was background subtracted using the mixing ratios observed during the chamber blank experiments. Organic acid yields were calculated from the isoprene oxidation experiments by only including mixing ratios of organic acids with five carbons or less and yields were calculated from the a-pinene experiments using species with ten carbons or less.

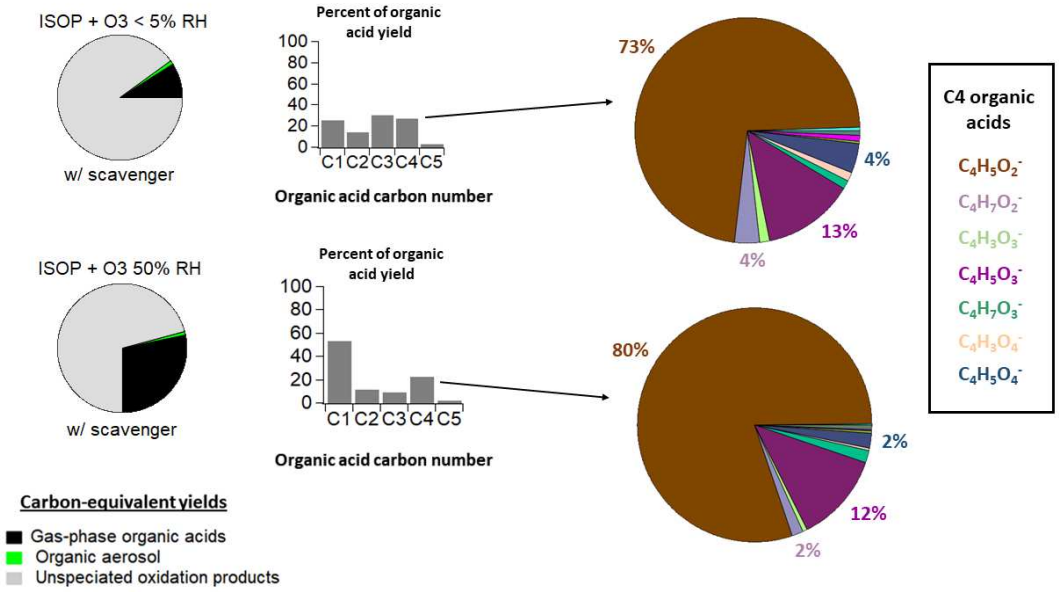

Figure A4.12. The pie charts on the right are taken from Figure 4.4 in Chapter 4 showing the contribution of organic acid carbon (black slice) to the total amount of isoprene carbon consumed in the "isoprene + O_3 <5% RH (with cyclohexane scavenger)" experiment (top) compared to the "isoprene + O_3 50% RH (with cyclohexane scavenger)" experiment (bottom). The bar charts to the right of the pie charts show the C_{eq} yields of organic acids, organized by carbon number. The pie charts to the right of the bar charts showing the fractional contribution of C4 organic acids to the measured C_{eq} yields associated with C4 acids from the ozonolysis experiments.

A4.5.1 Estimation of O_3 oxidation contribution to "isoprene + NO_3" experiment yields

Approximately 40 ppb_v of O_3 was present in the "isoprene + NO_3" experiment to promote the formation of NO_3 radicals. The observed organic acids produced were likely a result of combined NO_3 and O_3 oxidation chemistry. To place an upper bound on the contribution of O_3 to the observed organic acid distribution we subtract the C_{eq} yields, as a function of carbon number, determined from the "isoprene + OH <5% RH" (including the cyclohexane scavenger) experiment from the yields observed in the "isoprene + NO_3" experiment. We note the ozonolysis experiment has higher yields than the NO_3 oxidation experiment of C3 and C4 acids suggesting this is in fact putting a lower bound on contribution of NO_3 oxidation to organic acids. After accounting for potential O_3 chemistry the total C_{eq} organic acid yield from the NO_3 oxidation experiment was reduced from ~16% to ~11%. Box-modeling of the "isoprene + NO_3" experiment showed that 77% of isoprene was lost to NO_3 oxidation while 22% and 1% were lost to O_3 and OH oxidation, respectively.

A4.6. Treatment of CIMS data for PMF

A4.6.1 Data preparation

Unit mass resolution (UMR) data were produced from Tofware v5.12 (via PMF analysis tools), calibration periods were removed, data were normalized to the reagent and background subtracted. For SOAS, time periods of precipitation or significant cloud cover were removed. Only m/z from 38 to 400 were included in the analysis. These UMR matrices were then averaged to a 5-minute time base. Some UMR peaks were removed to help PMF analyze only UMRs not affected by some known form of interference. Some UMR peaks (such as m/z 45 for formic acid) were removed to aid in interpretability of PMF factors.

- m/z removed for the SOAS PMF analysis: 32 (O_2^-), 35 (Cl^-) , 37 ($^{37}Cl^-$), 42 (CNO^-), 45 (CHO_2^-), 46 (NO_2^-), 59 ($C_2H_3O_2^-$; reagent), 60 (CO_3^-), 61, 62 (NO_3^-), 69 (CF_3^-), 77 (water cluster), 78 (CO_3 water cluster), 89 ($C_3H_5O_3^-$; mostly lactic acid), 90 ($C_2H_2O_4^-$), 91 (O_2 cluster) , 94, 113, and 114 ($C_2F_3O_2^-$; tubing), 119 (reagent cluster), 166 (reagent autoxidation product cluster), 179 (acetic acid double cluster); 163, 169, 213, 219, 263, 269, 313, and 319 (tubing artifacts).
- m/z removed for the SPiFFY analysis: 32 (O_2^-), 35 (Cl^-) , 37 ($^{37}Cl^-$), 42 (CNO^-), 45 (CHO_2^-), 46 (NO_2^-), 59 ($C_2H_3O_2^-$; reagent), 60 (CO_3^-), 61, 62 (NO_3^-), 69 (CF_3^-), 113, and 114 ($C_2F_3O_2^-$; tubing); 163, 169, 213, 219, 263, 269, 313, and 319 (tubing artifacts).

A4.7. Comparison of formic acid C_{eq} yields measured by different chemical ionization methods

We use measurements of acetic acid from a co-located CF_3O^- CIMS during FIXCIT to help quantify the contribution of organic acids to total carbon yields from isoprene and α-pinene oxidation. We use acetic acid measurements from the CF_3O^- CIMS also to quantify total C_{eq} mixing ratios observed during SOAS. Iodide CIMS (I^-) measurements were used to help identify clusters observed from acetate CIMS measurements during SOAS and FIXCIT. To validate comparisons and cross-application of measurements across ionization techniques we compared formic acid C_{eq} yields calculated from the FIXCIT experiments by CF_3O^-, I^-, and acetate CIMS. Absolute values of yields agree well compared to one another, but, more importantly, all the measured yields fall within error of one another with the exception of the “high NO” experiments were organic acid yields overall were very low.

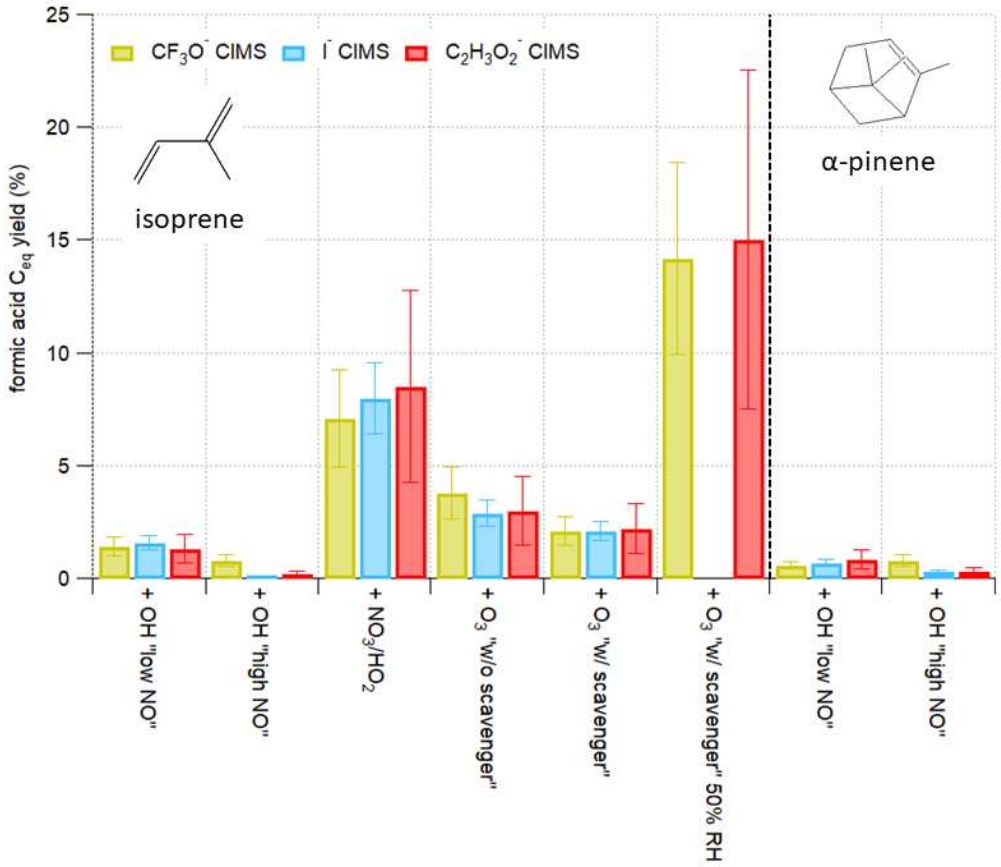

Figure A4.13. Formic acid C_{eq} yields from isoprene (left of dashed black line) and α-pinene (right of dashed black line) experiments as determined by measurements from CF_3O^- (yellow), I^- (blue), and acetate (red) CIMS. Error associated with CF_3O^-, I^-, and acetate is 30, 20, and 50%, respectively.

A4.8. Diagnosis of temperature-driven signal artifact observed during SOAS

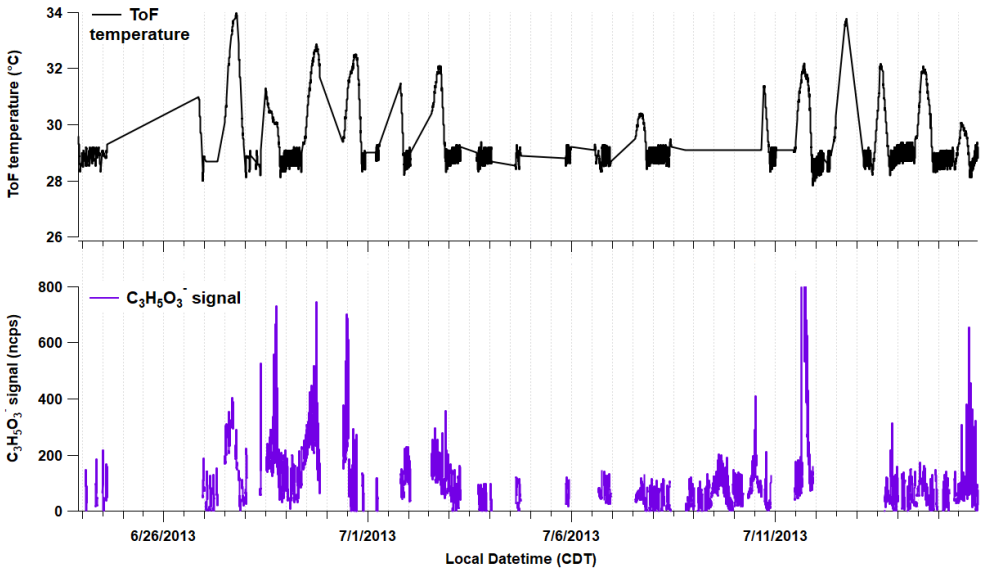

Figure A4.14. Time series of ToF temperature (top panel; black) and an example ion, $C_3H_5O_3^-$ (bottom panel; purple). Fine oscillations in the ToF temperature, caused by changes in the temperature of the trailer where the acetate CIMS was located, created oscillations in the signal of many measured organic acids such as $C_3H_5O_3^-$.

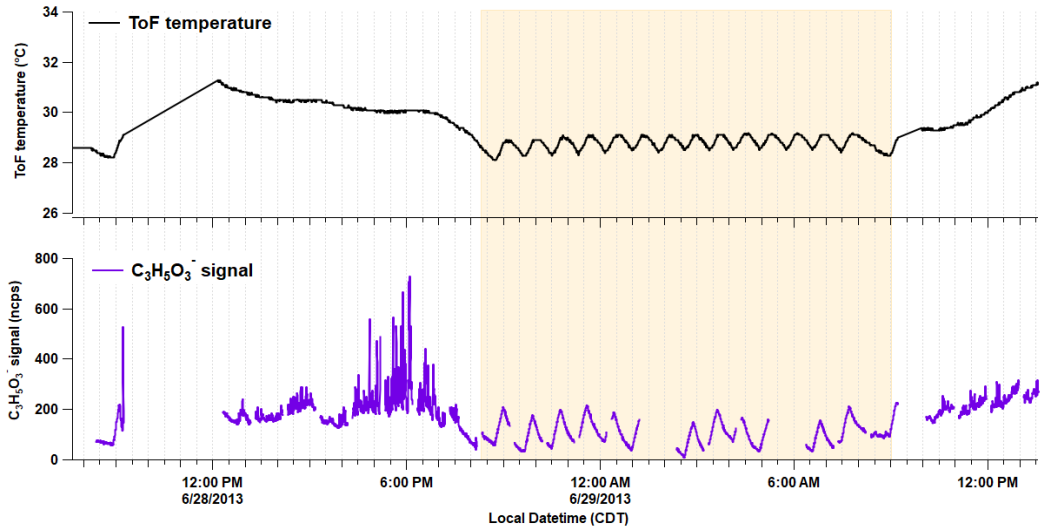

Figure A4.15. The time series in Figure A4.14 are zoomed in to a period on the 29th to show greater detail in the structure of the interference. The shaded area indicates period of time where the temperature-driven artifact was active.

A4.9 Determination of PMF solutions for SOAS and SPIFFY

We performed two types of analyses to determine the stability of PMF factors and find evidence for factor-splitting; (1) PMF factor signal allocation analysis and (2) correlation of PMF factor diel profiles with high-resolution identified species diel profiles from the acetate CIMS.

For the first analysis, we took the campaign-integrated signal from the time series of each PMF factor and divided it by the total measured UMR signal to get a PMF factor fractional contribution to the total UMR signal for each PMF solution (Figures A4.16 and A4.17). This analysis shows how the total UMR signal is allocated to each factor as a function of PMF solution.

To perform the second analysis, we calculated diel profile campaign medians for both PMF factors and high-resolution identified species (659 unique species for SOAS and 579 for SPiFFY). We then determined which factors diel profile a given high-resolution species diel profile had the highest correlation with above a minimum correlation value ($r = 0.80$). If the high-resolution species did not correlate with any PMF factor above the minimum value, it was categorized as correlated with "no factor". This analysis provided information on how much additional correlation with high-resolution species was obtained as a function of PMF solution.

A4.9.1 UMF time series signal allocation to PMF factor analysis

Barplots showing the percent contribution of time series signal from PMF factors from each PMF solution are shown in Figures A4.16 (SOAS) and A4.17 (SPiFFY).

Going from a five to six factor solution a portion of the signal allocated to the isoprene RO_2 + HO_2 factor gets allocated to the isoprene RO_2 + NO factor. This is a stable change because, going from the six to seven factor solution, the relative amount of signal allocated to the two isoprene factors is similar. Because the amount of signal that is allocated to the tubing and A/C unit factors is relatively constant through all solutions these factors are stable. Going from the six to the seven factor solution part of the signal from the A/C unit factor and the isoprene RO_2 + NO factor is allocated to a new factor that is likely a split from these two factors. The diel profile of this new factor is most similar to the A/C unit factor and decreases the overall interpretability of the six factor solution. This analysis also shows that the biogenic factor comprises a significant portion of the total UMR signal and is stable across all the solutions shown here.

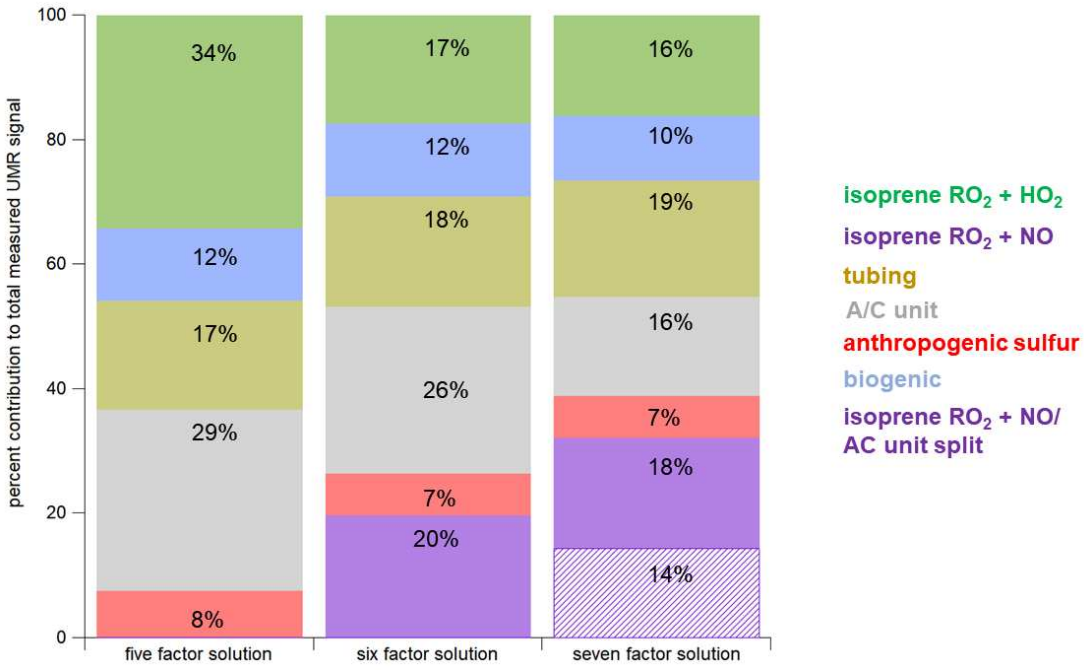

Figure A4.16. Percent contribution of each SOAS PMF factor signal—from campaign-integrated time series signal from the five, six and seven factor solutions—to the total measured UMR signal. The boxes with the dashes indicate contributions from splits of factors in previous solutions.

Factor splitting is observed for the SPiFFY PMF solutions going from a five to a six factor solution. The new factor that appears in the six factor solution has diel characteristics taken from all the daytime factors and does not increase the interpretability of the PMF results.

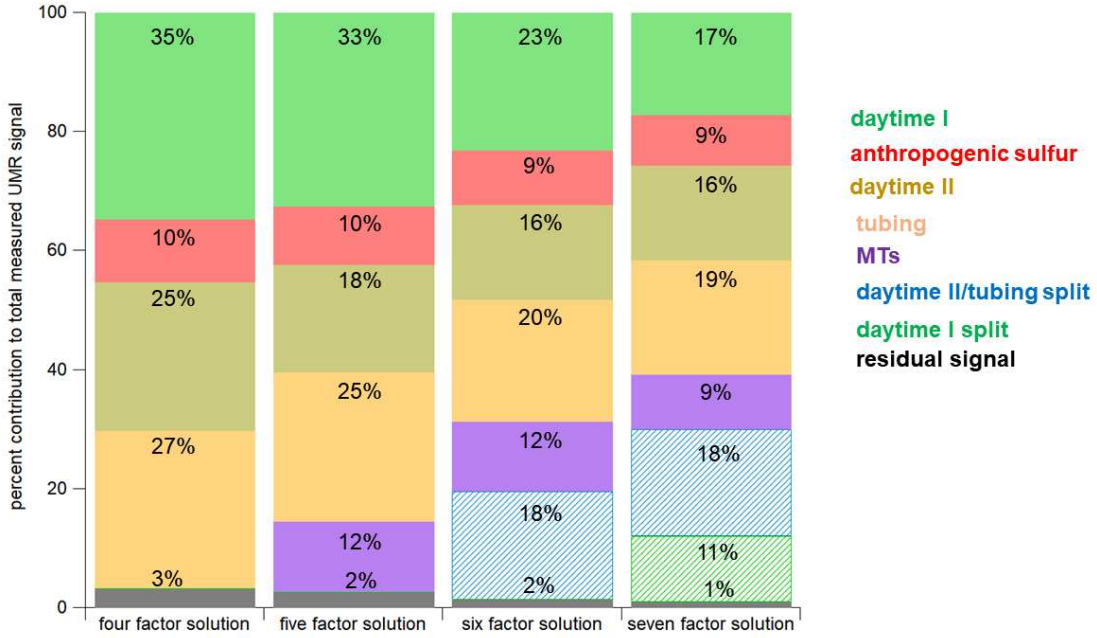

Figure A4.17. Percent contribution of each SPiFFY PMF factor signal—from campaign-integrated time series signal from the four, five, six and seven factor solutions—to the total measured UMR signal. The boxes with the dashes indicate contributions from splits of factors in previous solutions.

A4.9.2 High-resolution species diel profile correlation analysis with PMF factors

Pie charts showing the number of HR species whose diel profile correlated with PMF factor diel profiles (expressed as a percentage), above a value of r = 0.80, are shown in Figures A4.18 (SOAS) and A4.19 (SPiFFY).

Though the two isoprene factors have similar signature of daytime photochemical production, the HR analysis suggests going from a five to a six factor solution increases the interpretability of the PMF factors. In the six factor solution the "isoprene RO_2 + NO" factor is created from signal originally allocated to the "isoprene RO_2 + HO_2" factor. Because many of the HR species that originally correlated with the "RO_2 + HO_2" factor from the five factor solution correlate with the "RO_2 + NO" factor without an increase in the contribution to the number of species that are classified as "no factor" we determine that the six factor solution is stable. Increasing to a seven factor solution does not increase the interpretability of the PMF factors and results in splitting of the "RO_2 + NO" factor.

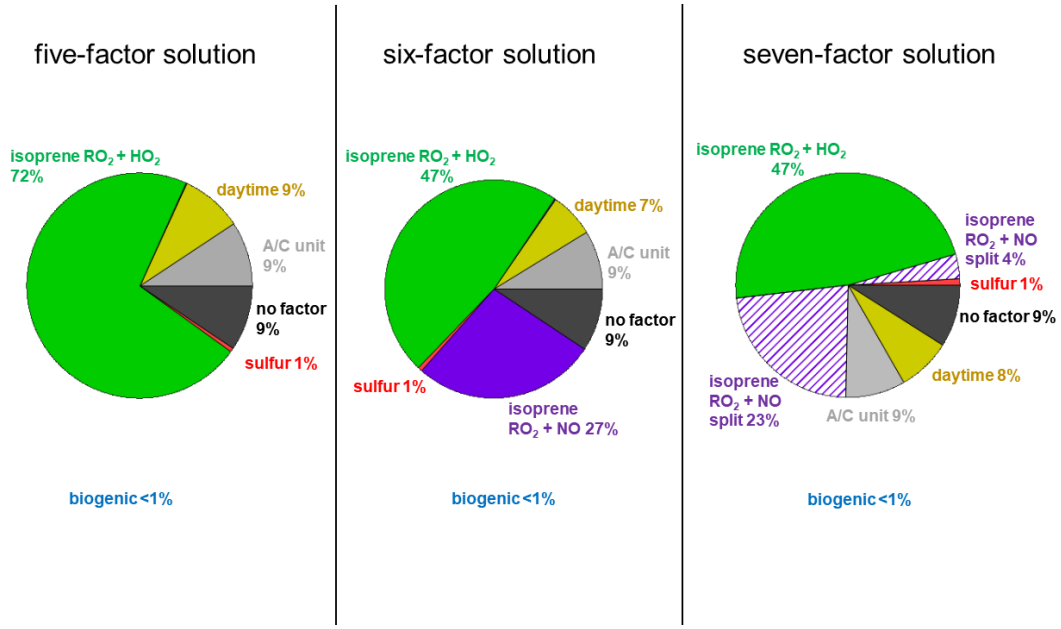

Figure A4.18. High-resolution comparison with UMR-based PMF factors corresponding to five to seven factor solution. The total number of HR species correlated to PMF factors for this analysis was 659. Dashed areas show factors that have split as solution factor number increases.

Going from a five to six factor solution, the additional factor that is added does not correlate well with many HR species and does not add to the interpretability of the five factor solution.

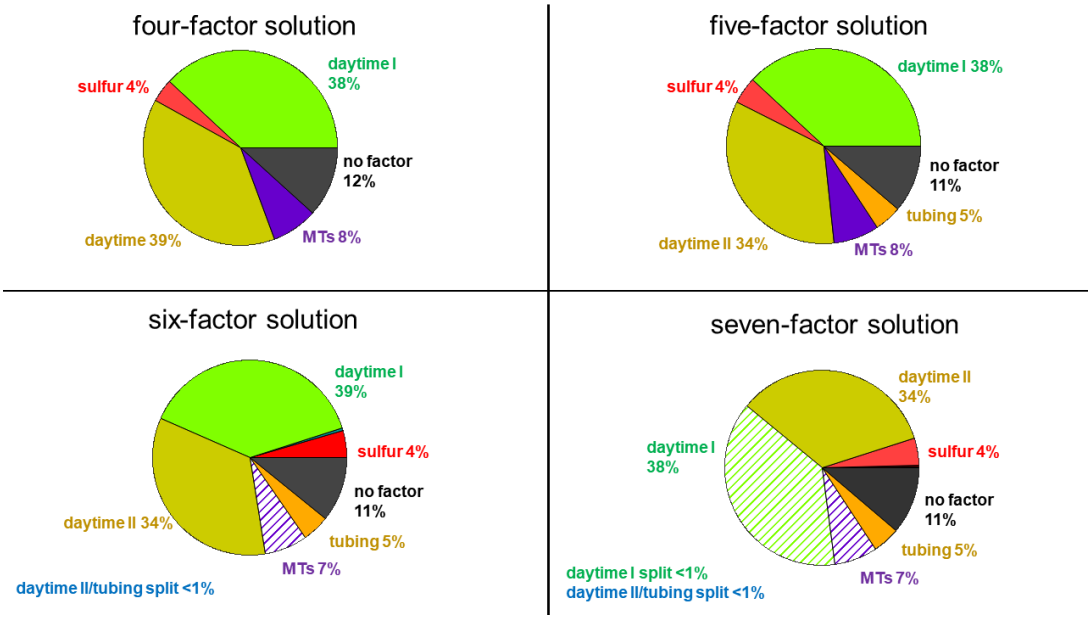

Figure A4.19. Same as Figure A4.18 shown for the four to seven factor solutions. The total number of HR species correlated to PMF factors for this analysis was 579. Dashed areas show factors that have split as solution factor number increases.

REFERENCES

(1) Deming, B.; Pagonis, D.; Liu, X.; Day, D.; Talukdar, R.; Krechmer, J.; Gouw, J. A. de; Jimenez, J. L.; Ziemann, P. J. Measurements of Delays of Gas-Phase Compounds in a Wide Variety of Tubing Materials due to Gas-Wall Interactions. *Atmospheric Meas. Tech. Discuss.* **2019**, 1–19. https://doi.org/https://doi.org/10.5194/amt-2019-25.

(2) Krechmer, J. E.; Pagonis, D.; Ziemann, P. J.; Jimenez, J. L. L. Quantification of Gas-Wall Partitioning in Teflon Environmental Chambers Using Rapid Bursts of Low-Volatility Oxidized Species Generated in-Situ. *Environ. Sci. Technol.* **2016**.

(3) Lee, B. H.; Lopez-Hilfiker, F. D.; Veres, P. R.; McDuffie, E. E.; Fibiger, D. L.; Sparks, T. L.; Ebben, C. J.; Green, J. R.; Schroder, J. C.; Campuzano-Jost, P.; et al. Flight Deployment of a High-Resolution Time-of-Flight Chemical Ionization Mass Spectrometer: Observations of Reactive Halogen and Nitrogen Oxide Species. *J. Geophys. Res. Atmospheres* **2018**, *123* (14), 7670–7686. https://doi.org/10.1029/2017JD028082.

(4) Nguyen, T. B.; Crounse, J. D.; Schwantes, R. H.; Teng, A. P.; Bates, K. H.; Zhang, X.; St. Clair, J. M.; Brune, W. H.; Tyndall, G. S.; Keutsch, F. N.; et al. Overview of the Focused Isoprene eXperiment at the California Institute of Technology (FIXCIT): Mechanistic Chamber Studies on the Oxidation of Biogenic Compounds. *Atmos Chem Phys* **2014**, *14* (24), 13531–13549. https://doi.org/10.5194/acp-14-13531-2014.

(5) Liu, S.; Thompson, S. L.; Stark, H.; Ziemann, P. J.; Jimenez, J. L. Gas-Phase Carboxylic Acids in a University Classroom: Abundance, Variability, and Sources. *Environ. Sci. Technol.* **2017**, *51* (10), 5454–5463. https://doi.org/10.1021/acs.est.7b01358.

(6) Brophy, P.; Farmer, D. K. Clustering, Methodology, and Mechanistic Insights into Acetate Chemical Ionization Using High-Resolution Time-of-Flight Mass Spectrometry. *Atmos Meas Tech* **2016**, *9* (8), 3969–3986. https://doi.org/10.5194/amt-9-3969-2016.

(7) Wennberg, P. O.; Bates, K. H.; Crounse, J. D.; Dodson, L. G.; McVay, R. C.; Mertens, L. A.; Nguyen, T. B.; Praske, E.; Schwantes, R. H.; Smarte, M. D.; et al. Gas-Phase Reactions of Isoprene and Its Major Oxidation Products. *Chem. Rev.* **2018**. https://doi.org/10.1021/acs.chemrev.7b00439.

(8) Budisulistiorini, S. H.; Li, X.; Bairai, S. T.; Renfro, J.; Liu, Y.; Liu, Y. J.; McKinney, K. A.; Martin, S. T.; McNeill, V. F.; Pye, H. O. T.; et al. Examining the Effects of Anthropogenic Emissions on Isoprene-Derived Secondary Organic Aerosol Formation during the 2013 Southern Oxidant and Aerosol Study (SOAS) at the Look Rock, Tennessee Ground Site. *Atmos Chem Phys* **2015**, *15* (15), 8871–8888. https://doi.org/10.5194/acp-15-8871-2015.

(9) Inomata, S.; Hirokawa, J. Non-Radioactive Chemical Ionization Mass Spectrometry Using Acetic Acid–Acetate Cluster as a Reagent Ion for the Real-Time Measurement of Acids and Hydroperoxides. *Chem. Lett.* **2016**, *46* (1), 38–41. https://doi.org/10.1246/cl.160828.

(10) Murschell, T.; Fulgham, S. R.; Farmer, D. K. Gas-Phase Pesticide Measurement Using Iodide Ionization Time-of-Flight Mass Spectrometry. *Atmos Meas Tech* **2017**, *10* (6), 2117–2127. https://doi.org/10.5194/amt-10-2117-2017.

(11) Lopez-Hilfiker, F. D.; Mohr, C.; Ehn, M.; Rubach, F.; Kleist, E.; Wildt, J.; Mentel, T. F.; Lutz, A.; Hallquist, M.; Worsnop, D.; et al. A Novel Method for Online Analysis of Gas and Particle Composition: Description and Evaluation of a Filter Inlet for Gases and AEROsols (FIGAERO). *Atmos Meas Tech* **2014**, *7* (4), 983–1001. https://doi.org/10.5194/amt-7-983-2014.

(12) Stark, H.; Yatavelli, R. L. N.; Thompson, S. L.; Kang, H.; Krechmer, J. E.; Kimmel, J. R.; Palm, B. B.; Hu, W.; Hayes, P. L.; Day, D. A.; et al. Impact of Thermal Decomposition on Thermal Desorption Instruments: Advantage of Thermogram Analysis for Quantifying Volatility Distributions of Organic Species. *Environ. Sci. Technol.* **2017**, *51* (15), 8491–8500. https://doi.org/10.1021/acs.est.7b00160.

(13) Brophy, P.; Farmer, D. K. A Switchable Reagent Ion High Resolution Time-of-Flight Chemical Ionization Mass Spectrometer for Real-Time Measurement of Gas Phase Oxidized Species: Characterization from the 2013 Southern Oxidant and Aerosol Study. *Atmos Meas Tech* **2015**, *8* (7), 2945–2959. https://doi.org/10.5194/amt-8-2945-2015.

(14) Kind, T.; Fiehn, O. Seven Golden Rules for Heuristic Filtering of Molecular Formulas Obtained by Accurate Mass Spectrometry. *BMC Bioinformatics* **2007**, *8*, 105. https://doi.org/10.1186/1471-2105-8-105.

(15) Wang, X. K.; Rossignol, S.; Ma, Y.; Yao, L.; Wang, M. Y.; Chen, J. M.; George, C.; Wang, L. Molecular Characterization of Atmospheric Particulate Organosulfates in Three Megacities at the Middle and Lower Reaches of the Yangtze River. *Atmospheric Chem. Phys.* **2016**, *16* (4), 2285–2298. https://doi.org/https://doi.org/10.5194/acp-16-2285-2016.

(16) Veres, P.; Roberts, J. M.; Warneke, C.; Welsh-Bon, D.; Zahniser, M.; Herndon, S.; Fall, R.; de Gouw, J. Development of Negative-Ion Proton-Transfer Chemical-Ionization Mass Spectrometry (NI-PT-CIMS) for the Measurement of Gas-Phase Organic Acids in the Atmosphere. *Int. J. Mass Spectrom.* **2008**, *274* (1–3), 48–55.

(17) Rivera-Rios, J. C.; Nguyen, T. B.; Crounse, J. D.; Jud, W.; St. Clair, J. M.; Mikoviny, T.; Gilman, J. B.; Lerner, B. M.; Kaiser, J. B.; de Gouw, J.; et al. Conversion of Hydroperoxides to Carbonyls in Field and Laboratory Instrumentation: Observational Bias in Diagnosing Pristine versus Anthropogenically Controlled Atmospheric Chemistry. *Geophys. Res. Lett.* **2014**, *41* (23), 2014GL061919. https://doi.org/10.1002/2014GL061919.

(18) Chhabra, P. S.; Flagan, R. C.; Seinfeld, J. H. Elemental Analysis of Chamber Organic Aerosol Using an Aerodyne High-Resolution Aerosol Mass Spectrometer. *Atmospheric Chem. Phys.* **2010**, *10* (9), 4111–4131. https://doi.org/https://doi.org/10.5194/acp-10-4111-2010.

(19) Nguyen, T. B.; Bateman, A. P.; Bones, D. L.; Nizkorodov, S. A.; Laskin, J.; Laskin, A. High-Resolution Mass Spectrometry Analysis of Secondary Organic Aerosol Generated by Ozonolysis of Isoprene. *Atmos. Environ.* **2010**, *44* (8), 1032–1042. https://doi.org/10.1016/j.atmosenv.2009.12.019.